

---

Dissertation zur Erlangung des Doktorgrades der  
Fakultät für Chemie und Pharmazie der  
Ludwig-Maximilians-Universität München

# The inner kinetochore architecture and its role in error correction

Josef Fischböck-Halwachs (geb. Fischböck)

aus

Vöcklabruck, Österreich

2020

---

## Erklärung

Diese Dissertation wurde im Sinne von § 7 der Promotionsordnung vom 28. November 2011 von Herrn Dr. Franz Herzog betreut.

## Eidesstattliche Versicherung

Diese Dissertation wurde eigenständig und ohne unerlaubte Hilfe erarbeitet.

München, 24.02.2020

...Josef Fischböck-Halwachs.....

Dissertation eingereicht am	30.03.2020
1. Gutachterin / 1. Gutachter:	Dr. Franz Herzog
2. Gutachterin / 2. Gutachter:	Prof. Dr. Stefan Westermann
Mündliche Prüfung am	21.04.2020

## Contribution statement

The work described in this thesis was conducted during my PhD research from October 2014 to March 2019 in the laboratory of Dr. Franz Herzog at the Gene Center of the Ludwig-Maximilians University in Munich. The results on the COMA complex and its implications on the recruitment of Sli15/Ipl1 to centromeric nucleosomes were published in eLife (see appendix).

Several collaborative projects were performed with scientists from the laboratory of Prof. Andrea Musacchio (Dortmund, Germany). These projects are not part of this thesis.

## Publication

Fischböck-Halwachs J, Singh S, Potocnjak ., Hagemann G, Solis-Mezarino V, Woike S, Ghodgaonkar-Steger M, Weissmann F, Gallego LD, Rojas J, Andreani J, Köhler A, Herzog F.(2019) The COMA complex interacts with Cse4 and positions Sli15/Ipl1 at the budding yeast inner kinetochore. *eLife* 2019;8:e42879 10.7554/eLife.42879

## Publications of collaborations

### Publication 1

Weir JR, Faesen AC, Klare K, Petrovic A, Basilico F, **Fischböck J**, Pentakota S, Keller J, Pesenti ME, Pan D, Vogt D, Wohlgemuth S, Herzog F, Musacchio A. (2016) Insights from biochemical reconstitution into the architecture of human kinetochores. *Nature*. 537:249-253 10.1038/nature19333

### Publication 2

Friese A, Faesen AC, Huis in 't Veld PJ, **Fischböck J**, Prumbaum D, Petrovic A, Raunser S, Herzog F, Musacchio A. (2016) Molecular requirements for the inter-subunit interaction and kinetochore recruitment of SKAP and Astrin. *Nat Commun*. 7:11407 10.1038/ncomms11407

## Table of contents

1. Abstract .....	1
2. Introduction.....	3
2.1. The eukaryotic cell cycle.....	3
2.2. The kinetochore .....	4
2.2.1. Composition of the inner kinetochore .....	5
2.2.1.1. Mif2 homodimer .....	5
2.2.1.2. The Chl4/Iml3 heterodimer .....	6
2.2.1.3. The CTF3 complex.....	6
2.2.1.4. The Cnn1/Wip1/Mhf1/Mhf2 complex .....	7
2.2.1.5. The Nkp1/Nkp2 heterodimer .....	7
2.2.1.6. The CBF3 complex .....	7
2.2.1.7. The Ctf19/Mcm21/Ame1/Okp1 (COMA) complex.....	8
2.2.2. The outer kinetochore KNL1/MIS12/NDC80 (KMN) network .....	9
2.3. Regulation of kinetochore microtubule attachments.....	11
2.3.1. The chromosomal passenger complex (CPC) .....	13
2.3.2. The spindle assembly checkpoint (SAC) .....	16
2.4. Aim of this work .....	19
3. Results .....	21
3.1. Mass spectrometric analysis of native yeast kinetochores.....	21
3.1.1. Quantitative mass spectrometry identified the protein composition of native yeast kinetochore complexes .....	21
3.1.1.1. Ame1 associated complexes .....	22
3.1.1.2. Cnn1/Wip1 associated complexes .....	23
3.1.1.3. CTF3c associated complexes .....	23
3.1.1.4. Chl4/Iml3 associated proteins.....	24
3.1.1.5. MS analysis of Mif2 associated proteins .....	24
3.1.2. Optimization of the purification protocol to enrich for kinetochore associated regulatory complexes.....	26
3.1.3. Chemical crosslinking and mass spectrometry (XLMS) analysis of native yeast kinetochore complexes.....	28
3.2. The chromosomal passenger complex directly associates with native kinetochore complexes.....	30
3.3. <i>In vitro</i> reconstitution of inner kinetochore subcomplexes interacting with the chromosomal passenger complex.....	33
3.3.1. The core CPC directly interacts with the COMA complex .....	33
3.3.2. The core of the chromosomal passenger complex directly interacts with Mif2, but not with the CTF3c <i>in vitro</i> .....	38

3.3.3.	The COMA complex mediates the spatial positioning of Sli15/Ipl1 at the inner kinetochore .....	39
3.3.4.	Cohesin loading defects do not provide a valid explanation for the synthetic lethality of the <i>ctf19Δ/sli15ΔN</i> double mutant .....	40
3.3.5.	The synthetic lethality of <i>ctf19Δ/sli15ΔN</i> can be rescued by artificial and selective tethering of Sli15 to inner kinetochore proteins.....	40
3.3.6.	A functional chromosomal passenger complex tethered at inner kinetochores requires Ipl1 kinase activity .....	41
3.3.7.	The Ctf19 C-terminal RWD domain mediates the recruitment of Sli15 to inner kinetochores.....	42
3.4.	<i>In vitro</i> reconstituted KMN interacts with the chromosomal passenger complex .....	44
3.5.	The Ame1/Okp1 heterodimer selectively binds Cse4 containing nucleosomes .....	47
3.5.1.	The Ame1/Okp1 heterodimer links other kinetochore proteins directly to Cse4 containing nucleosomes.....	50
3.5.2.	A small, essential, N-terminal region in Cse4 is required for binding the Ame1/Okp1 heterodimer .....	51
3.5.3.	The small N-terminal region in Cse4, required for binding the Ame1/Okp1 heterodimer <i>in vitro</i> , is essential for viability.....	55
3.5.4.	The Okp1 core domain is required for Cse4 binding.....	55
3.5.5.	The Okp1 core domain required for Cse4 binding is essential for cell growth .....	56
4.	Discussion.....	59
4.1.	The Cnn1/Wip1:CTF3c complex links COMA complex to the NDC80c.....	59
4.2.	The Ame1/Okp1 heterodimer selectively binds Cse4 containing nucleosomes .....	61
4.3.	Ame1/Okp1 represent a centerpiece of kinetochore assembly in budding yeast.....	62
4.4.	Inner kinetochore subcomplexes support Sli15/Ipl1 localization .....	63
4.5.	The interaction of KMN with Sli15/Ipl1 and its putative functional relevance.....	66
4.6.	Summary scheme of the findings .....	67
5.	Material and Methods.....	69
5.1.	Cloning of baculoviral transfer vectors .....	69
5.2.	Generation of recombinant baculoviruses.....	69
5.3.	Expression of recombinant protein complexes from insect cells .....	70
5.4.	Purification of recombinant protein complexes from insect cells .....	70
5.4.1.	Purification of proteins via FLAG-tag.....	70
5.4.2.	Purification of proteins via Strep-tag .....	71
5.4.3.	Purification of Mps1-GST.....	71
5.5.	Ame1-6xHis/Okp1 expression and purification.....	72
5.6.	Preparative size exclusion chromatography (SEC) .....	72
5.6.1.	Preparative SEC of Ame1/Okp1.....	72

5.6.2.	Preparative SEC of Sli15/Ipl1 .....	73
5.7.	<i>In vitro</i> reconstitution of Cse4- and H3-NCPs.....	73
5.8.	Interaction studies using size exclusion chromatography (SEC) .....	73
5.9.	Yeast genetics.....	73
5.10.	Growth assays .....	74
5.11.	Pulldown of native yeast complexes for Mass spectrometry .....	74
5.12.	Chemical crosslinking and mass spectrometry of kinetochore complexes.....	75
5.13.	Mass spectrometry - analysis and settings.....	76
5.14.	<i>In vitro</i> protein binding assay of Sli15/Ipl1 to inner kinetochore proteins .....	77
5.15.	<i>In vitro</i> protein binding assay of KMN to Sli15/Ipl1 .....	77
5.16.	Electrophoretic mobility shift assay .....	78
5.17.	<i>In vitro</i> binding assay using Sli15/Ipl1 and native kinetochore complexes.....	78
5.18.	<i>In vitro</i> binding assay using whole cell lysates .....	79
5.19.	Enrichment of phosphorylated peptides.....	79
5.20.	SDS page analysis.....	79
5.21.	Immunoblotting.....	80
5.22.	Lists and Tables.....	81
5.22.1.	Plasmids list .....	81
5.22.2.	Yeast strains.....	82
5.22.3.	Predicted and experimentally annotated protein domains and motifs depicted in protein crosslink networks.....	85
6.	References.....	87
7.	Appendix.....	95
8.	Curriculum Vitae.....	124
9.	Acknowledgement.....	125

# 1. Abstract

The propagation of all organisms is dependent on the accurate inheritance of the genetic material over generations. Consequently, the elaborate process of chromosome segregation is tightly regulated, and includes several feedback control mechanisms. A key structure driving chromosome segregation is the kinetochore. It forms the physical link between the replicated DNA molecules and spindle microtubules. This evolutionary conserved, multi-protein complex assembles at defined chromosomal regions, referred to as centromeres, which are specified by the presence of the histone H3 variant CENP-A or Cse4 in budding yeast. The hierarchy of kinetochore assembly from the centromere DNA to the microtubule binding interface is largely conserved between human and yeast, with the inner kinetochore or constitutive centromere associated network (CCAN) and the outer kinetochore establishing the microtubule binding interface. In the past years, major efforts have been undertaken to investigate the building plan of the kinetochore and a molecular description of the structure and the biochemical activities of its proteins was revealed. However, a comprehensive understanding of the architecture and the protein interactions establishing the structural framework and the cell cycle surveillance machinery is still missing.

In this work, I applied a structural proteomics approach and used chemical crosslinking combined with mass spectrometry (XLMS) to elucidate the protein connectivity and topology of budding yeast kinetochore complexes at the domain level. To gain insights into the architecture of the inner kinetochore and its assembly on Cse4 containing nucleosomes, I *in vitro* reconstituted various inner kinetochore subcomplexes starting with the four subunit Ctf19/Mcm21/Ame1/Okp1 (COMA) complex. Biochemical interaction studies revealed that the heterodimer Ame1/Okp1 bound Cse4 through its essential N-terminal domain, thereby providing a direct link from the centromeric nucleosome to the outer kinetochore MTW1 complex.

The kinetochore serves also as a hub for the regulatory feedback control mechanisms that ensure high fidelity of chromosome segregation by temporally aligning the microtubule attachment state to cell cycle progression. A major regulatory module is the chromosomal passenger complex (CPC), which is essential for establishing chromosome biorientation. A central question is, whether and how an interaction between kinetochore proteins and the CPC is required for faithful chromosome segregation. Recent studies implicated the COMA

complex in the recruitment process of the CPC. I *in vitro* reconstituted the CPC and performed a crosslink-guided mutational analysis of potential interactions.

The CPC interacted with COMA *in vitro* through the Ctf19 C-terminus, which is required for viability in a Sli15 centromere-targeting deficient mutant. Fusing Sli15 to Ame1/Okp1 bypassed the requirement of Ctf19 in a Sli15 centromere-targeting deficient mutant. Taken together, my work identifies molecular characteristics of the budding yeast inner kinetochore architecture and suggests a role for the Ctf19 C-terminus in mediating CPC-binding and chromosome biorientation.



## **2. Introduction**

### **2.1. The eukaryotic cell cycle**

The eukaryotic cell cycle consists of four distinct stages G1-, S- and G2-phase followed by mitosis (1). The central components that drive progression through the cell cycle are cyclins which form a complex with and activate cyclin-dependent kinases (CDKs) (2). Oscillating cyclin levels determined via gene expression and destruction by the ubiquitin mediated proteasome pathway, result in oscillating CDKs activities, thereby initiating and coordinating the different cell cycle events. During G1 the cell grows and is preparing for S-phase by synthesising precursors required for DNA synthesis. After G1 the cell either enters G0, which represents an arrest state, characterized by no further growth or division, or the cell progresses into S-phase. In S-phase the chromosomes are duplicated by the replication machinery. The completion of DNA duplication is followed by a short phase of rapid growth and protein synthesis, termed G2. In mitosis, which is initiated through Cdk1 associated with cyclin B, a complex also referred to as the mitosis promoting factor, chromosome segregation is taking place. Mitosis can be further sub-divided as prophase, pro-metaphase, metaphase, anaphase and telophase. At the entry of mitosis (during pro- and prometaphase) the replicated DNA condenses into tightly coiled chromosomes, with two sister chromatids held together by a ring-shaped complex called cohesin (3). Only after all sister chromatids are successfully attached to microtubules, originating from the opposing spindle poles, and are being aligned along the metaphase plate through the resulting tension do cells transition from metaphase to anaphase. Mitotic cyclin B and securin are marked by the anaphase promoting complex (APC), an E3 ubiquitin ligase, for degradation by the 26S proteasome (4, 5). The degradation of securin releases the protease separase, which subsequently cleaves cohesin. Consequently, the shortening spindle microtubules draw the chromatids to opposite sides of the cell, where they decondense. Finally, after successful separation of the genetic material the division of cytoplasm called cytokinesis takes place. An important module in this elaborate system is a large proteinaceous assembly called the kinetochore, which forms the physical connection between chromosomes (or DNA) and microtubules, thereby mediating the processive binding of the depolymerizing microtubules to drive the sister chromatids apart (6, 7).

## 2.2. The kinetochore

The kinetochore is the macromolecular protein complex, that anchors chromosomes to spindle microtubules. Functionally, the kinetochore proteins can be grouped into four categories, the first of which is proteins that establish the link to the centromeric DNA (8). Second, are proteins that connect to the spindle microtubules (8). The third group of kinetochore proteins is involved in establishing correct kinetochore-microtubule attachments by stabilizing correct or destabilizing incorrect interactions, respectively (8). The fourth group of proteins functions in aligning the microtubule kinetochore-attachment state with cell cycle progression by the spindle assembly checkpoint (SAC) in order to prevent precocious anaphase onset and mitotic exit (8).

The assembly of the kinetochore is restricted to centromeres, chromosomal domains that are epigenetically marked by the presence of the histone H3 variant CENP-A (9) (Figure 1A). While human regional centromeres span megabases of DNA, where up to 200 CENP-A containing nucleosomes are positioned (10), the model organism *Saccharomyces cerevisiae* (budding yeast) possesses a point centromere, whose identity is specified by the presence of a single Cse4<sup>CENP-A</sup> (the name of human orthologues names will be superscripted if appropriate) containing nucleosomal core particle (NCP). A conserved sequence-specific DNA stretch of 125 bp length is wrapped around the single Cse4 containing histone octamer, with regularly spaced canonical histone H3 containing nucleosomes positioned on either side (11, 12). This functional DNA segment in yeast is composed of three conserved centromere determining elements (CDEs). While CDEI and CDEIII bind to the respective proteins Cbf1(13) and Cbf3 (14), the AT rich CDEII is wrapped around Cse4-NCP (6). Regardless of the presence of a sequence-specific centromere in yeast, Cse4 is not only required for kinetochore assembly, but when targeted artificially to non-centromere locations, is also sufficient to initiate kinetochore assembly (15). In contrast to humans, where an array of identical kinetochore units is supposed to be spread along regional centromeres, each providing an attachment site for multiple microtubules (16), in budding yeast a single kinetochore unit links a single Cse4<sup>CENP-A</sup>-NCP to a single microtubule. Despite the higher complexity, it is thought that the multiply attached kinetochores of humans represent repetitions of the single budding yeast kinetochore unit (17, 18). Budding yeast kinetochores are assembled by approximately 45 core proteins organized into different stable subcomplexes (19) (Figure 1B), several of which are present in multiple copies (17). Most of the fundamental building blocks and centromere-binding proteins exhibit a close evolutionary relationship between budding yeast and humans (20) and similarly share a highly conserved hierarchical assembly from inner to outer layers

(8). The DNA proximal region is formed by proteins of the constitutive centromere-associated network (CCAN) (21). In contrast to the outer kinetochore proteins the members of the CCAN have less evolutionary conservation and are even absent in some lineages such as *C. elegans* and *D. melanogaster* (22). In budding yeast, the CCAN is also termed CTF19 complex, and consists of the subcomplexes/proteins displayed in Figure 1B (6, 7).

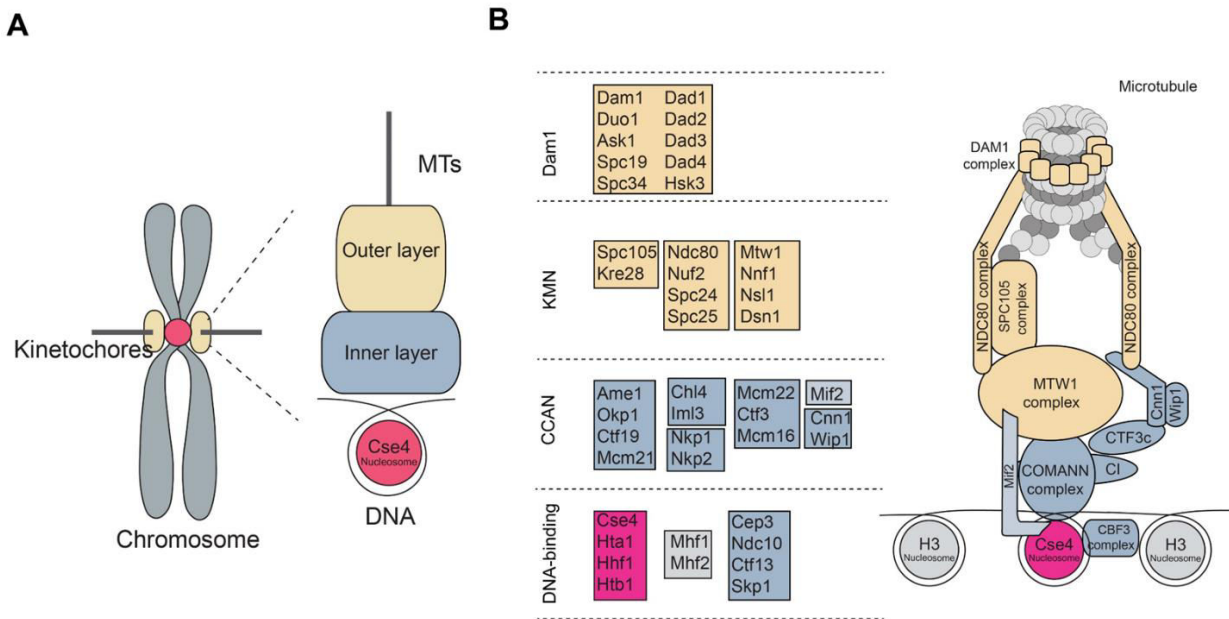


**Figure 1. Hierarchical building plan of the budding yeast kinetochore.** (A) Inner kinetochore assembles on a point centromere that is specified by the presence of a single Cse4 containing nucleosome. The inner kinetochore provides a binding platform for outer kinetochore proteins that establish the linkages to a single microtubule (MT). (B) The kinetochore is composed of different stable subcomplexes. Subcomplexes within the CCAN establish the association with chromosomal DNA, while members of the KMN and the DAM1 complex are forming the outer layer and constitute the microtubule binding interface.

## 2.2.1. Composition of the inner kinetochore

### 2.2.1.1. Mif2 homodimer

Mif2<sup>CENP-C</sup> localizes at the centromere and is essential for viability in all organisms. Acting as a key component of the CCAN, it links outer kinetochore proteins directly to Cse4<sup>CENP-A</sup>-NCP (23). The direct association to the Cse4<sup>CENP-A</sup>-NCP is mainly mediated via the DNA- and histone-binding domain (DHBD), which harbors the “CENP-C signature motif” that interacts with C-terminal hydrophobic residues of CENP-A (24). Additionally, recognition of the AT-rich CDEII by the AT hook motifs and RK clusters (clusters enriched for arginine–lysine residues) and two additional regions in the Mif2 DHBD contribute to centromere

association (23). Essential for Cse4<sup>CENP-A</sup> recognition, the Mif2 N-terminus also associates with the Mtw1p Including Nnf1p-Nsl1p-Dsn1p complex (MIND complex or MTW1c), thereby supporting outer kinetochore assembly (25-27). Meanwhile, the C-terminus mediates homodimerization via the cupin fold domain (28).

### **2.2.1.2. The Chl4/Iml3 heterodimer**

Besides being implicated in kinetochore assembly (29), yeast Chl4 and Iml3 (CI) are involved in pericentromeric cohesin loading during mitosis (30, 31) and deletion mutants display mitotic instability (32). Chl4 and Iml3 form a stable heterodimer, which has been shown to interact directly with Sgo1, highlighting its function in establishing normal levels of cohesin (29). The centromere localization of Chl4 and Iml3 was shown to depend on CTF3c (33). Presumably, Chl4 interacts with Ctf19/Mcm21 and with Mif2, both being required for proper kinetochore targeting of Chl4/Iml3 *in vivo* (34). In agreement, a recent electron microscopy (EM) structure showed multiple contact sites of Chl4/Iml3 with other CTF3c proteins: Chl4 - Ctf19/Mcm21; Chl4 – Ame1/Okp1; Iml3 – CTF3c (35).

For the human orthologues of Chl4 and Iml3 CENP-N/L, respectively, selective association with CENP-A-NCP over H3-NCP has been demonstrated (36-40). Within the heterodimer the larger protein CENP-N mediates this interaction (41). The binding interface within the NCP comprises the histone H2B  $\alpha$ -helix, nucleosomal DNA and the RG loop, a region within the centromere targeting domain (CATD) of CENP-A. The later domain, being a specific feature that discriminates CENP-A- from H3-NCP. However, up to now in budding yeast, specific binding to Cse4-NCP has only been reported for Mif2 and not Chl4/Iml3 (23, 42).

### **2.2.1.3. The CTF3 complex**

In budding yeast the CTF3c, also referred to as HIK complex, is composed of Mcm16/Ctf3/Mcm22<sup>CENP-H/I/K</sup>, while the human orthologue comprises CENP-HIKM. Together with CENP-LN and CENP-C CENP-HIKM forms a tight 7-subunit complex, termed the CENP-CHIKMLN complex (41). In addition to CENP-C and CENP-N, also the CENP-HIKM complex directly interacts with CENP-A, but does not selectively discriminate between CENP-A and H3 nucleosomes. Furthermore, the complex also associates solely with linear DNA (41). Being directly bound to the centromeric nucleosomes indicates that CENP-HIKM is upstream of CENP-OPQUR in the hierarchical assembly of the human kinetochore and is required for its recruitment (43). The direct interaction between these two complexes is

through a composite interface created by CENP-HIK and CENP-LN binding CENP-OP (44). In budding yeast the functional role of the complex is less clear, as Ame1<sup>CENP-U</sup>/Okp1<sup>CENP-Q</sup> localize to centromeres independently of Mcm16/Ctf3/Mcm22. Moreover, correct localization of CTF3c relies on Ctf19 and the Mcm21 N-terminus (35). This suggests a different kinetochore assembly in budding yeast.

#### **2.2.1.4. The Cnn1/Wip1/Mhf1/Mhf2 complex**

Cnn1 together with Wip1 forms a stable five subunit assembly with Mcm16/Ctf3/Mcm22 that is required for targeting Cnn1 to the *Saccharomyces cerevisiae* centromere (32). Presumably, a combination of protein-protein and protein-DNA interactions establishes the centromere recruitment. As Cnn1, Wip1 and Mhf1/2 contain histone fold domains, it has been suggested that these four proteins form a nucleosome like particle comparable to their human orthologues (CENP-TWSX) (45). In contrast, no direct interaction between Cnn1/Wip1 and Mhf1/Mhf2 was detected by *in vitro* binding experiments (32). Cnn1 is a direct receptor for the NDC80 complex, which provides the key microtubule-binding activity of the kinetochore (the function of the NDC80c will be explained in detail later) (46).

Cnn1 has an essential function in budding yeast when the assembly of MTW1c, the main NDC80c recruiting complex in the kinetochore, is perturbed by inhibition of Ipl1 mediated Dsn1 phosphorylation (molecular mechanism will be explained in more detail in later sections) (47). This finding can be explained by the fact that Cnn1 as well as MTW1c are able to recruit the NDC80c to centromere associated kinetochores in a mutually exclusive manner. The Cnn1 binding interface consists of an alpha helical peptide motif at the N-terminal tail, which is encompassed in a hydrophobic cleft formed by the NDC80c proteins Spc24/Spc25 (48). Interestingly, the same peptide motif is present in the MTW1c protein Dsn1, targeting the same binding site in Spc24/25 (49), thereby providing the essential link between MTW1c and NDC80c (48) and explaining the exclusive binding mode.

#### **2.2.1.5. The Nkp1/Nkp2 heterodimer**

Although for most budding yeast kinetochore proteins human orthologues have been identified, there are yeast-specific complexes like the Nkp1/Nkp2 heterodimer. This complex stably associates with Ctf19/Okp1/Mcm21/Ame1<sup>CENP-P/Q/O/U</sup> (COMA) by direct interaction with Ame1/Okp1, presumably increasing inner kinetochore stability (34).

### 2.2.1.6. The CBF3 complex

Another budding yeast specific and essential complex is CBF3c (Ndc10/Cep3/Ctf13/Skp1). This complex directly binds to a centromeric DNA region, termed CDEIII, and associates with the Cse4-NCP (14). The CBF3c represents one of the most upstream factors for nucleating kinetochore assembly (6). Its role in recruiting kinetochore proteins to the centromere remains to be determined.

### 2.2.1.7. The Ctf19/Mcm21/Ame1/Okp1 (COMA) complex

In budding yeast the tetrameric complex consists of two stable heterodimers Ame1/Okp1 and Ctf19/Mcm21. Ctf19 and Mcm21 contain tandem-RWD (RING finger and WD repeat containing proteins and DEAD-like helicases) domains forming a rigid heterodimeric Y-shaped scaffold with flexible N-terminal extensions as revealed by a recent crystal structure of the *K. lactis* complex (50). A hydrophobic groove, formed by the Ctf19 C-terminal RWD domain and the Mcm21  $\alpha 2$  and  $\alpha 3$  helices, serves as the principle binding site for a C-terminal binding motif in Okp1, establishing a stable interaction between Ame1/Okp1 (AO) and Ctf19/Mcm21 (CM) (34). Ame1/Okp1 localizes at mitotic centromeres independently of Ctf19/Mcm21, demonstrated by *ctf19 $\Delta$*  and *mcm21 $\Delta$*  cells not showing reduced Ame1-GFP or Okp1-GFP signals at kinetochores (19). However, temperature sensitive mutants *ame1-4* and *okp1-5* display mis-localization of Ctf19 and Mcm21, suggesting that Ame1/Okp1 is upstream in the kinetochore assembly pathway (51). Interestingly, in humans the recruitment of the CENP-OPQRU complex to kinetochores requires a joint interface formed by CENP-HIKM and CENP-LN (44, 52, 53) and loss of the complex does not affect localization of other inner kinetochore proteins. However, in budding yeast Ame1/Okp1 are essential and their localization is independent of Chl4/Iml3 (34). The COMA complex provides a docking site for the outer kinetochore network via the Ame1 N-terminus which binds to head domain I of MTW1c (25, 49), whereas for human CENP-OPQR no direct interaction with the KMN network (KNL1<sup>SPC105</sup>-/MIS12<sup>MTW1</sup>-/NDC80<sup>NDC80</sup>-complexes) has been detected *in vitro* (44). The distinct recruitment mechanisms of vertebrate and budding yeast inner kinetochores are reflected by the physiological importance of the involved proteins. Besides Mif2, Ame1/Okp1 are the only essential proteins of the CTF19 complex in budding yeast (19, 54, 55). Knockouts of CENP-U/Q and CENP-O/P/R in DT40 cells are viable and display relatively mild effects like slower proliferation and mitotic defects, respectively (21). The requirement for viability in mammalian systems has been only reported for CENP-U in mouse

embryonic stem cells, however not in mouse fibroblasts (56). Taken together, this suggests different roles of COMA proteins, especially of Ame1 and Okp1 in budding yeast kinetochore assembly or function compared to their respective mammalian orthologues CENP-U and -Q, which are not present in the last eukaryotic common ancestor and originated more recently (22).

Despite considerable advances in elucidating the structure, biochemical activities, and the biophysics of CCAN proteins, a functional assignment for many subunits, and how they cooperate with one another to carry out the kinetochore functions, is still missing. In particular, how CCAN proteins assemble at the regional centromere in comparison to point centromeres in budding yeast, and thus form a scaffold for the recruitment of the microtubule-binding components of the outer kinetochore, is still uncertain.

### **2.2.2. The outer kinetochore KNL1/MIS12/NDC80 (KMN) network**

One of the key functions of the kinetochore is to sustain the dynamic attachment to depolymerizing microtubules, which must resist the forces exerted by the spindle microtubules during anaphase when the chromosomes segregate. This sophisticated task is fulfilled by the outer layer of the kinetochore. The core of the outer kinetochore is formed by the KMN network, established by the three subcomplexes SPC105c<sup>KNL1</sup>, MTW1c<sup>MIS12</sup>, and NDC80c<sup>NDC80</sup>, presumably at a 1:1:1 ratio (17). Each subcomplex is essential for viability and performs clearly distinct functions. Mis-localization of one of them leads to chromosome segregation defects and either partial or complete detachment of kinetochores from microtubules (57-59).

The MTW1c also referred to as MIND complex is formed by two stable heterodimers Mtw1/Nnf1 and Dsn1/Nsl1. All four proteins are essential and assemble at a 1:1:1:1 stoichiometry (60). Structural analysis revealed a Y- shape like structure showing two globular heads at the end of a coiled-coil shaft (49). Super resolution light microscopy *in vivo* suggested that the complex functions as a bridge and bidirectional linker between inner kinetochore complexes and the rest of the KMN network (61). As already described, in budding yeast COMA binds to the MTW1c via the Ame1 N-terminus (25). Moreover, the inner kinetochore protein Mif2 associates through an N-terminal motif with the Mtw1/Nsl1 heterodimer (49). On the outer part of the MTW1c, connections with the C-terminal RWD domains of the NDC80c subunits Spc24 and Spc25 are established through C-terminal motifs of the Nsl1/Dsn1 heterodimer (62, 63). By a similar noncompetitive binding mechanism, the

Nsl1/Dsn1 heterodimer also recruits the largely unstructured protein Knl1 by binding its C-terminal tandem RWD domains (62, 63). The molecular basis for recruitment of the SPC105c to budding yeast MTW1c remains to be addressed.

In budding yeast, the SPC105 complex is assembled by Spc105 and Kre28 at a 1:2 molar ratio (64). It is mainly required for the recruitment of spindle assembly checkpoint proteins, a surveillance mechanism for establishing bipolar attachment of sister kinetochores. While the C-terminal part of Spc105 is associated with the MTW1c, the N-terminus harbors multiple MELT repeats (Met-Glu-Leu-Thr), which upon phosphorylation by Mps1 kinase serve as assembly platform for the SAC complexes preventing mitotic exit before chromosomes are bioriented at the mitotic spindle (65).

It has been suggested that the SPC105c is part of the interface that directly interacts with microtubules. However, the contribution of SPC105c in establishing microtubule attachment by the kinetochore is unclear as its size makes it a difficult target for *in vitro* studies.

Within the KMN network, microtubule contact is mainly established by the dumbbell shaped tetrameric NDC80 complex. Each subunit contains a globular domain connected to large segments of coiled coils, enabling heterodimerization of Ndc80/Nuf2 and Spc24/Spc25 and subsequently tetramerization (7). During metaphase the complex spans 54 nm, while presumably lack of tension in anaphase triggers an intramolecular conformational switch and the complex length becomes reduced to 34 nm long (61). This stretching/relaxing mechanism has been shown to require a loop interrupting the Ndc80/Nuf2 coiled coils, which exhibits a high degree of evolutionary conservation (66). While the C-terminal domains of the Spc24/25 heterodimer point towards the inner kinetochore and directly interact with the C-termini of the Dsn1/Nsl1 heterodimer of the MTW1c, the N-terminal parts of the Ndc80/Nuf2 heterodimer bind microtubules. In particular, the two interacting calponin homology domains in Ndc80 and Nuf2 and an intrinsically unstructured positively charged N-terminal Ndc80 tail contact the microtubule lattice (67). Compared to human NDC80c, the budding yeast complex displays a lower affinity towards microtubules highlighting the requirement of an additional component to ensure stable kinetochore microtubule attachments (60). This task is fulfilled by the yeast specific 10-subunit DAM1 complex, which assembles as a ring around microtubules (68), thereby enabling the complex to autonomously track growing and shrinking microtubule ends (69). While the structure of NDC80c allows lateral and end-on binding to microtubules (70), DAM1c is only present at microtubule ends, an important difference in the binding properties of the two complexes. In human cells, the spindle and kinetochore-associated (SKA) complex fulfills a similar but not essential function for stabilizing kinetochore-



microtubule attachments (71). The indispensability of the DAM1 complex might be a consequence of only a single kinetochore unit linking the point centromere to a single microtubule in budding yeast. At vertebrate regional centromeres an array of those kinetochore units provides attachment sites for 3 to 30 microtubules (16).

### **2.3. Regulation of kinetochore microtubule attachments**

While the main function of the kinetochore is to provide the physical linkage between the centromeric DNA and the highly dynamic spindle microtubules, it additionally serves as a hub for the regulatory feedback machinery, establishing SAC signaling and error correction. A highly complex interplay between the kinetochore and the involved regulatory proteins aligns the proper kinetochore-microtubule attachment state with cell cycle progression. A prerequisite for faithful chromosome segregation is the attachment of each sister kinetochore to microtubules emanating from one of the opposing spindle poles which is also referred to as amphitelic attachment (72) (Figure 2). The establishment of kinetochore-microtubule attachments is naturally an error prone process. Therefore, monotelic attachments (only one kinetochore is connected to microtubules) or syntelic attachments (both sister kinetochores are connected to microtubules of the same pole) have to be resolved and corrected before the cell cycle continues (6), in order to avoid aneuploidy and genomic instability (8), both, being associated with tumorigenesis, congenital trisomies and aging (73, 74).

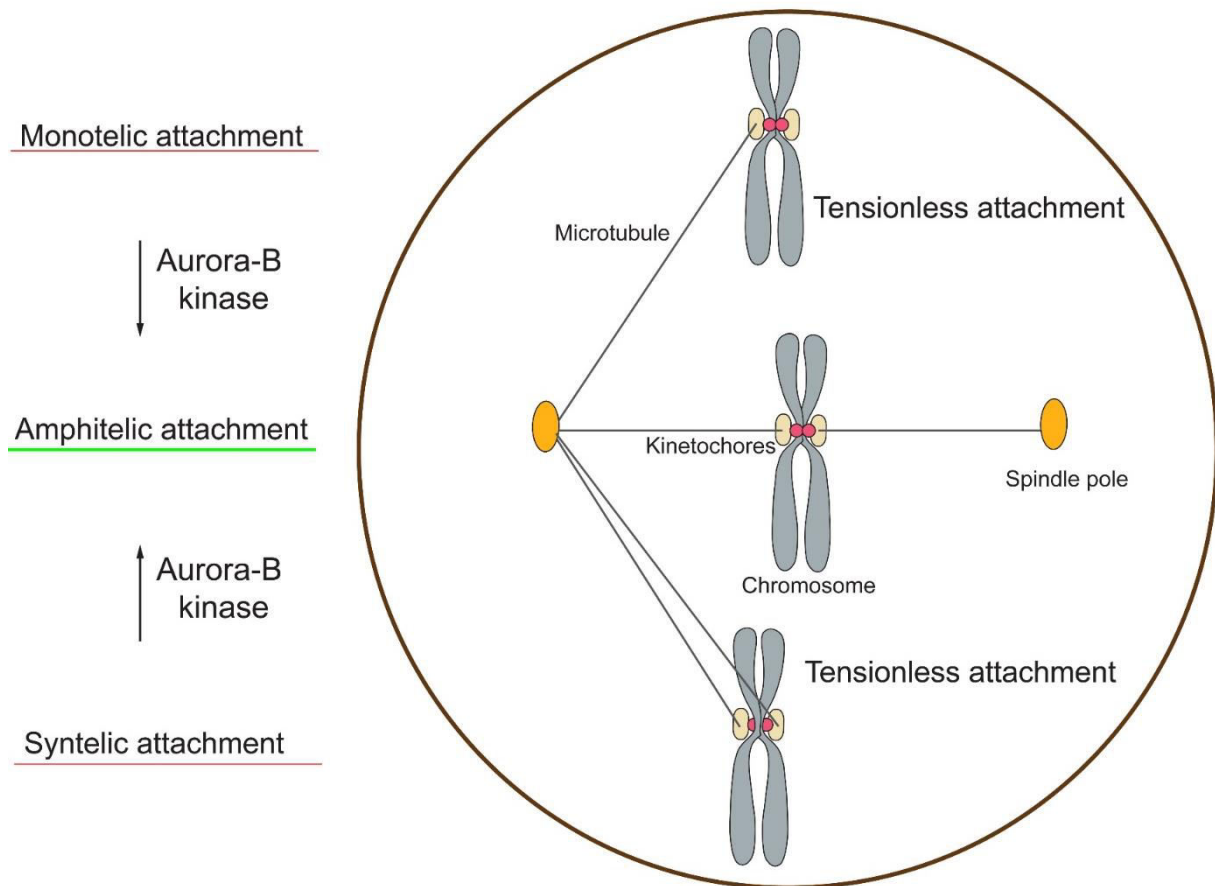


**Figure 2. Different configurations of kinetochore-microtubule attachments in metaphase.** A single sister kinetochore binding to a microtubule from one pole is called monotelic attachment. Both sister kinetochores binding to microtubules from opposite poles are amphitelicly attached. Attachment of sister kinetochores to microtubules from the same pole is termed syntelic attachment. Tension across centromeres upon amphitelic attachment is exerted by the depolymerizing microtubules and leads to intra- and inter-kinetochore stretching. The lack of tension in the monotelic and syntelic attachment state results in phosphorylation of the microtubule binding interface and the recruitment of SAC proteins to the kinetochore.

Several *in vivo* experiments showed that biorientation is sensed by cells via the tension applied across kinetochores (75, 76). A lack of tension results in the phosphorylation of the microtubule binding interface by the CPC and the selective destabilization of incorrect kinetochore microtubule attachments. Unattached kinetochores are subsequently sensed by the SAC to prevent premature mitotic exit (Figure 3). The turnover of kinetochore microtubule attachments increases and consequently the likelihood of the stochastic formation of properly bioriented chromosomes is improved. Intra-kinetochore stretching upon tension prevents phosphorylation of the microtubule binding sites such that these attachments are stably maintained (77).

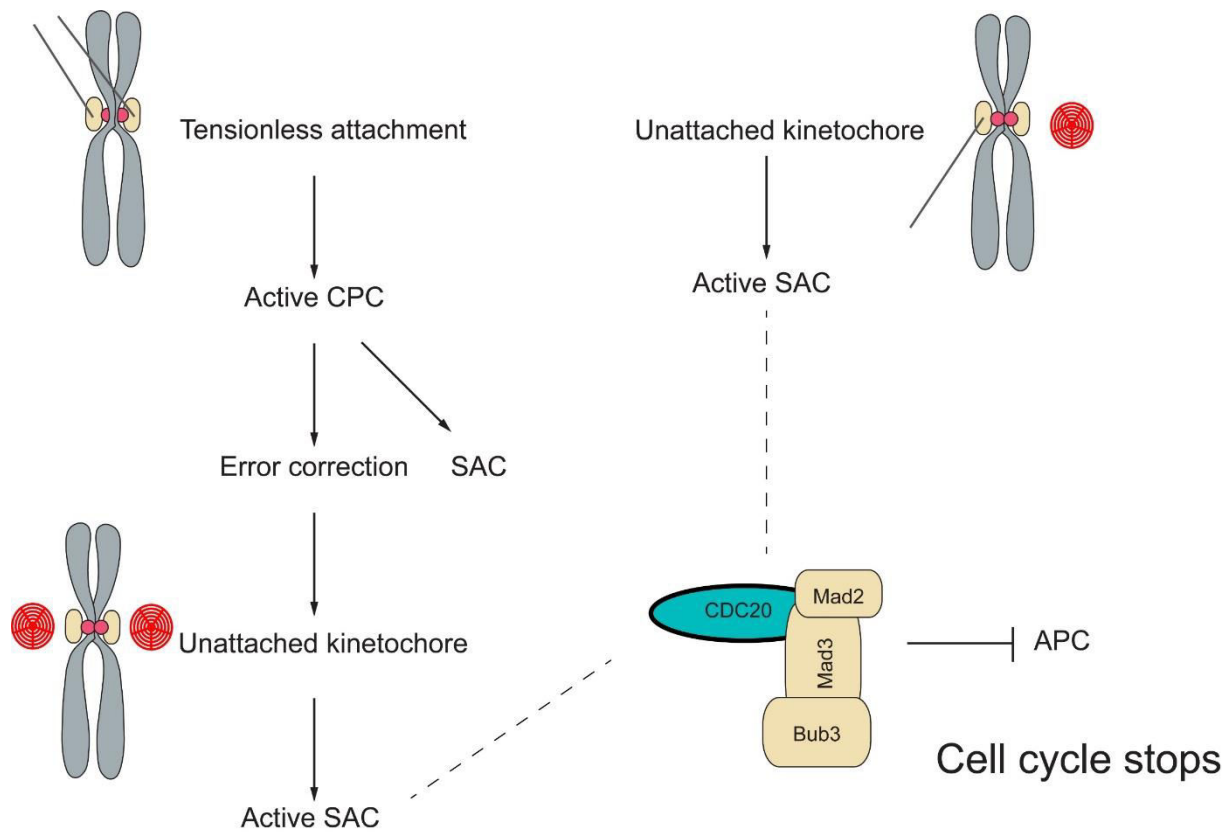


**Figure 3. Feedback control mechanisms activated by incorrect kinetochore-microtubule attachments.** In case of incorrect kinetochore-microtubule attachment states the CPC creates unattached kinetochores that are subsequently sensed by the SAC to prevent premature mitotic exit. SAC signaling halts the cell cycle by generating an inhibitory signal – the mitotic checkpoint complex (MCC) that halts cell cycle progression by inhibiting the activity of the APC/C (78).

### 2.3.1. The chromosomal passenger complex (CPC)

One of the major regulatory components in generating the correct amphitelic kinetochore-microtubule attachment state is the CPC. In early models, the CPC's function was mainly attributed to regulate error correction in early mitosis. However, this view has been progressively revised by identifying the contribution of the complex in a number of additional processes (79).

The CPC is composed of four highly conserved proteins: Ipl1<sup>Aurora-B</sup>, Sli15<sup>INCENP</sup>, Bir1<sup>Survivin</sup> and Nbl1<sup>Borealin</sup> (Figure 4). Bir1<sup>Survivin</sup> and Nbl1<sup>Borealin</sup> together with the N-terminus of Sli15<sup>INCENP</sup> form a three helix bundle (80, 81), which constitutes the CPC localization module required for localization of the effector kinase Ipl1<sup>Aurora-B</sup> to centromeres during early mitosis (82). To date, all known mechanisms for recruitment of the CPC to the budding yeast centromere rely on Bir1, which directly associates with Ndc10 of the CBF3 complex (83). Additionally, fission yeast Bir1 is targeted via Sgo1 to Bub1 phosphorylated histone H2A

(84) (Figure 5A). Human Survivin association with histone H3, phosphorylated at threonine 3 by Haspin kinase, is also implicated in centromere recruitment of the CPC (79, 85). However, knockouts of the Haspin-like genes, *Alk1* and *Alk2*, in yeast do not display any growth defects, suggesting that this mechanism either does not exist, or is simply not required in yeast (86).

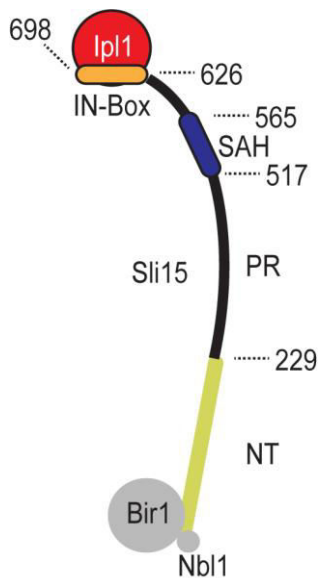


**Figure 4. Model of the chromosomal passenger complex.** The CPC is a four-subunit complex. Sli15 acts as a scaffold interacting with Bir1 and Nbl1 at its N-terminus. In the central region Sli15 harbors a phosphoregulated region (PR) and a single alpha helical domain (SAH), and the C-terminus contains the IN-box which mediates binding of Ipl1 and is required for increasing its kinase activity (87).

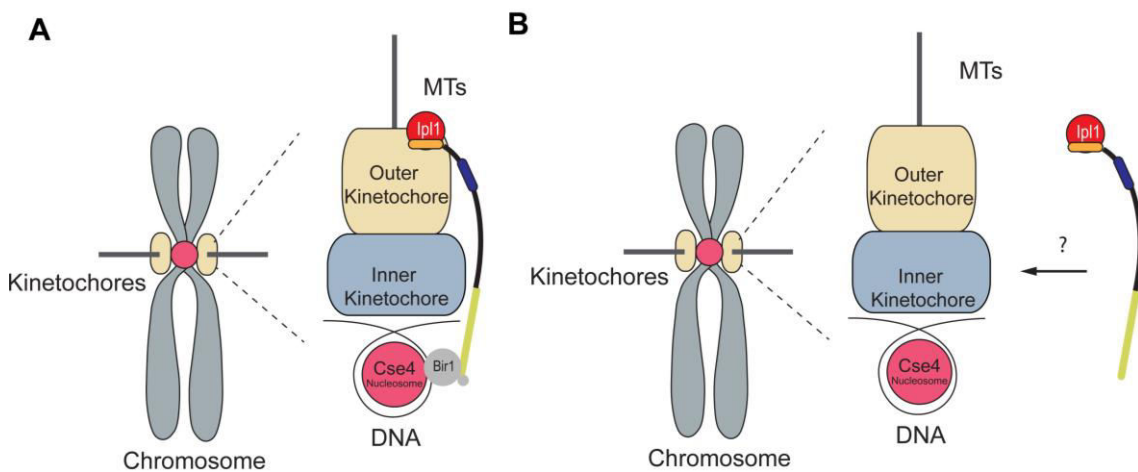


**Figure 5. Kinetochore localization of the CPC.** (A) The CPC is recruited to centromeric nucleosomes by Bir1 mediated pathways. (B) How the CPC interacts with kinetochores in the absence of its targeting domain is unclear.

Sli15<sup>INCENP</sup> is the scaffold protein within the CPC. Besides the N-terminal centromere targeting domain the protein harbors a single  $\alpha$  helix (SAH). In INCENP this region mediates the direct interaction with microtubules *in vitro* (88, 89). In budding yeast the SAH domain is required for chromosome biorientation and viability (90). Adjacent to the SAH domain is a phosphoregulated region (PR) that is implicated in the translocation of the complex to spindle microtubules at anaphase onset (90, 91). The PR is phosphorylated early in mitosis by Ipl1 and Cdk1 and at the onset of anaphase is dephosphorylated by Cdc14. Thus, preventing Sli15 phosphorylation leads to its premature localization to spindle microtubules in metaphase (91). Ipl1 is the effector kinase of the CPC and is bound to the highly conserved IN box at the Sli15 C-terminus (92). Interestingly, the association with the IN-box and the Ipl1 mediated phosphorylation of the IN-box on a Thr-Ser-Ser (TSS) motif as well as Ipl1 autophosphorylation is required for full kinase activation (87, 93, 94). As both phosphorylation events are presumably catalyzed in-trans (94), Ipl1 activation requires high local concentrations of Ipl1, probably established by clustering at distinct locations like the centromeres. In agreement with this, experiments using a FRET-based biosensor (95) showed that the CPC population at the inner centromere is constitutively active and that substrates localized in close proximity to this active pool are phosphorylated.

However, there is also an active CPC pool at the outer kinetochore which dissociates once kinetochores are properly aligned, whereas the pool local to centromeres remains prominent (96). This observation might indicate an important role of the outer kinetochore bound CPC population in error correction, although a comprehensive understanding of how both pools contribute to this pathway is still missing.

Mechanistically, CPC mediates biorientation by selective destabilization of incorrect kinetochore–microtubule attachments via Ipl1 phosphorylation of the microtubule binding interfaces at the outer kinetochore. The DAM1c and NDC80c are the substrates of Ipl1 phosphorylation (6). Phosphorylation of the Ndc80 positively charged N-terminal tail (97) drastically reduces the affinity towards microtubules *in vitro* and in human deletion leads to a complete loss of kinetochore–microtubule attachments (95, 98). Accordingly, Ndc80 phosphomimicking mutants show a lack of stable kinetochore–microtubule attachments (58, 98) resulting in the accumulation of syntelic and merotelic attachments in cells (58, 96). Apart from that, Ipl1 phosphorylation of the DAM1 complex (99) disrupts the simultaneous binding and bridging across two DAM1c via NDC80c (100, 101). Consistent with these

observations, Aurora-B mediated phosphorylation of the spindle and kinetochore-associated (SKA) complex, negatively regulates kinetochore microtubule attachments (102).

Although the substrates of Ipl1<sup>Aurora-B</sup> are well defined, it is unclear, how lack of tension triggers the phosphorylation of outer kinetochore proteins by the CPC. The substrate separation model highlights the distance between centromere-localized CPC and its target proteins at the outer kinetochore (103, 104). In case of bioriented sister kinetochores, the observed intra-kinetochore stretching (61) would spatially separate Ipl1<sup>Aurora-B</sup> from its substrates. The reduction of the local Ipl1 kinase activity would allow counteracting phosphatases, like PP1 (105), to dephosphorylate Ipl1 sites and to stabilize the kinetochore-microtubule attachments. Still, this model does not explain how initial attachments would be established with active Ipl1<sup>Aurora-B</sup> in close proximity. Moreover, a recent study (86) challenged this model by showing that cells expressing a centromere targeting deficient mutant version of the CPC are indistinguishably viable from wildtype cells and display normal chromosome biorientation. Furthermore, the CPC mutant still colocalizes with the outer kinetochore protein Nuf2. These observations suggest that the tension-sensing is intrinsic to the kinetochore and support an alternative model in which the functionally relevant pool of Ipl1<sup>Aurora-B</sup> resides at kinetochores rather than at centromeres (8, 106). The detailed molecular mechanism of how the CPC interacts with kinetochores and how tension-sensing is achieved remains to be elucidated (Figure 5B).

Notably, apart from ensuring proper kinetochore-microtubule attachments and contributing to the SAC signaling, the kinase activity of Ipl1 is also implicated in the assembly of the KMN network on the inner kinetochore. Phosphorylation of Dsn1 by Ipl1 enhances the interaction of the MTW1c with Mif2<sup>CENP-C</sup> (49, 107) by releasing an autoinhibitory mechanism of Dsn1. Furthermore, Mif2 is also phosphorylated by Ipl1 which increases the robustness of kinetochore function (42). Moreover, the CPC is implicated in regulating microtubule dynamics by directing the activity and localization of microtubule-associated proteins (65). These examples highlight the complexity and diverse functionalities of the CPC during early mitosis. A study showed that the temporal inhibition of the CPC in interphase leads to chromosome missegregation in the next mitosis, suggesting even an important role before entry in mitosis (108). In late mitosis the CPC translocates to the spindle midzone and modulates anaphase chromatid compaction and anaphase spindle dynamics (79). Finally, during cytokinesis the CPC is also implicated in contractile ring formation, regulation of furrow ingression and abscission (79). Notably, most studies are focused on the function of the CPC in mediating chromosome biorientation during early mitosis.

### 2.3.2. The spindle assembly checkpoint (SAC)

Besides error correction Ipl1<sup>Aurora-B</sup> is implicated in a second feedback control mechanism, the SAC, which mediates a cell cycle arrest in response to a single unattached kinetochore thereby providing more time to establish the correct amphitelic attachment state (Figure 3). The requirement of Aurora-B for recruitment of SAC components shows that the two pathways are tightly interwoven and interdependent (109). Artificial tethering of Mps1 kinase to the kinetochore bypasses the dependence of Ipl1<sup>Aurora-B</sup> for checkpoint activity in human cells, suggesting that the primary function of the CPC in the SAC is the recruitment of Mps1 to kinetochores (106). Mps1 kinase acts as an upstream regulator of the SAC and in budding yeast, Mps1 is the only essential protein of the SAC complex (6). Subsequent to its kinetochore localization the kinase phosphorylates multiple Met-Glu-Leu-Thr (MELT) repeats in the Spc105<sup>Kn11</sup> N-terminus which provide docking sites for the additional SAC members Bub1 and Bub3 (110, 111). This enables the binding of Mad3<sup>BubR1</sup> in complex with Bub3 to Spc105. Next, Mad1/2 heterodimers localize at the kinetochore (112). The kinetochore bound SAC complexes catalyze the conversion of open state Mad2 (O-Mad2) to closed state Mad2 (C-Mad2) (112). Soluble C-Mad2 bound to Cdc20 in complex with Mad2, Mad3<sup>BubR1</sup>, and Bub3 assemble the active mitotic checkpoint complex (MCC). The MCC delays anaphase onset until all chromosomes are properly aligned at the spindle by inhibiting the anaphase-promoting complex/cyclosome (APC/C), blocking substrate recognition through its regulatory protein Cdc20 (113) (Figure 3, Figure 6). Upon biorientation of all chromosomes, protein phosphatase 1 (PP1) and PP2A<sup>B56</sup> are recruited to Spc105<sup>Kn11</sup> and dephosphorylate the MELT motifs (114, 115). Hence, SAC complexes are not recruited to the kinetochore and SAC arrest is released. Subsequently, free Cdc20 can associate with the APC/C. The APC/C functions as an ubiquitin ligase marking cell cycle proteins for degradation by the proteasome, with Cdc20 and Cdh1 being the essential coactivators. The two key substrates targeted by APC<sup>Cdc20</sup> for degradation are Pds1<sup>Securin</sup>, and clb2<sup>cyclin B</sup> (116). Securin binds the protease separase<sup>Esp1</sup> and blocks cleavage of the cohesin complex by inhibiting its cysteine protease activity. The cohesion ring holds sister chromatids together and resists the microtubule pulling forces and degradation of securin enables the separase-mediated cleavage of the cohesin subunit Scc1 and thus, allows sister chromatids to separate (117, 118). Cyclin B, a member of the cyclin family, is the activator of cyclin dependent kinase 1 (Cdk1). The complex formed by these two proteins is termed mitosis promoting

factor. Ubiquitination and the subsequent proteasomal degradation of cyclin B permits Cdk1 inactivation and mitotic exit.

The SAC pathway is highly sensitive and already a single unattached kinetochore was shown to delay anaphase for many hours (119), while biorientation of all chromosomes immediately silences the checkpoint allowing securin and cyclin B degradation and anaphase onset (120).

Taken together, the macromolecular structure of the kinetochore directly links the DNA of the sister chromatids to the spindle microtubules and integrates the signaling of the feedback control mechanisms of the SAC and error correction. Therefore, it represents a key macromolecular protein complex in mitosis, and its comprehensive molecular description is crucial for understanding the molecular mechanisms that safeguard accurate chromosome segregation.

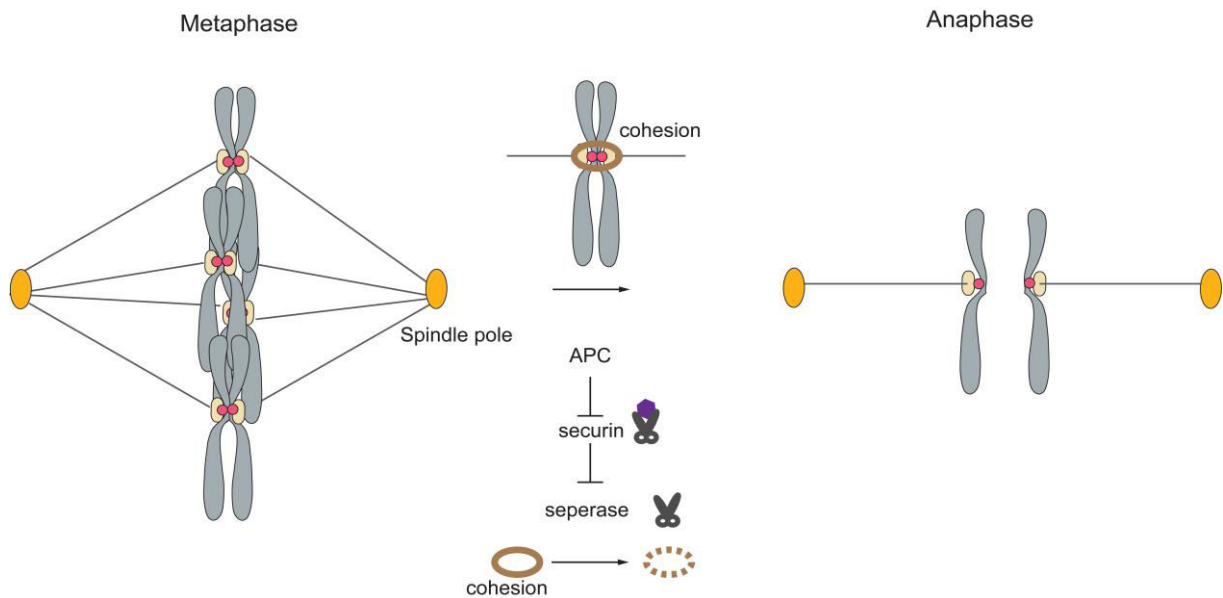


**Figure 6. Metaphase-anaphase transition mediated by the ubiquitin-protein ligase activity of the APC/C.** The APC/C is activated at the entry of mitosis through association with its coactivator Cdc20. Bipolar attachment of all sister kinetochores to the mitotic spindle correctly aligns chromosomes at the spindle midzone and silencing the SAC allows targeting securin and cyclin B by APC/C mediated ubiquitination for degradation. Seperase is released and cuts the cohesin ring that holds sister chromatids together. In anaphase sister chromatids are segregated towards the spindle poles by the pulling forces of depolymerizing microtubules.



## 2.4. Aim of this work

Genetics, biochemistry and light microscopy unraveled the composition of the kinetochore, the organization of proteins in stable subcomplexes, and their conserved hierarchy of assembly from centromeric DNA to the microtubule binding site (8). Moreover, high resolution structures of kinetochore subcomplexes (7) as well as the structure of the budding yeast CCAN by cryo-electron microscopy (35) and the kinetochore *in situ* structure by tomography have been solved (121).

Up to now, a comprehensive topological map of the fully assembled kinetochore displaying the protein connectivities and interfaces is still missing. This is in part attributed to the difficulties to purify the intact kinetochore complex and to the lack of specific structural methods capable of acquiring structural information from heterogeneous protein complexes composed of largely flexible and disordered proteins. In particular, the molecular understanding of the integration of the error correction mechanism and the SAC into the structural framework of the kinetochore is a challenging task and absolutely crucial for the mechanistic understanding of its role in chromosome segregation.

Recent work in budding yeast by Campbell et al. (86) showed that a mutant of Sli15, lacking the N-terminal 228 amino acids (Sli15 $\Delta$ N), which mediate centromere targeting, is viable and capable of performing chromosome biorientation. The molecular basis of how the kinetochore associated Sli15 $\Delta$ N mutant retained its biological function remained elusive. Interestingly, the *sli15 $\Delta$ N* mutant becomes synthetically lethal upon deletion of the CTF19c subunits, Ctf19 or Mcm21.

Based on these observations I started out to address the following questions:

- What is the topology of the budding yeast inner kinetochore and how does it establish a selective and high-affinity binding environment for Cse4<sup>CENP-A</sup> containing nucleosomes?
- Does the CPC directly associate with the kinetochore and if so, how does this interaction contribute to the accuracy of chromosome segregation?
- Does the architecture of the inner kinetochore play a role in mediating error correction?
- Does an interaction of the CPC with inner kinetochore proteins stabilize or position Ipl1 activity at a distinct kinetochore conformation in order to perform tension sensing and error correction?

In this thesis I describe my analysis of the inner kinetochore architecture in budding yeast and its interaction with the CPC using chemical crosslinking combined with mass spectrometry (XLMS). This method aids the identification of protein-protein binding interfaces in endogenous and reconstituted protein complexes. Detection of protein contacts reveals the subunit topology of the kinetochore complexes. To investigate the architecture of native kinetochores I analyzed kinetochore complexes isolated from budding yeast cell extracts, while *in vitro* reconstitution was used to study the association of the inner kinetochore with the CPC and Cse4 containing nucleosomes. Both the *in vitro* reconstitution and mutational analysis were guided by the crosslink-derived distance restraints. Subsequently, the identified interaction motifs were investigated for their biological relevance by performing *in vivo* growth assays using a variety of mutant and fusion proteins.

## **3. Results**

### **3.1. Mass spectrometric analysis of native yeast kinetochores**

Up to now, the complexity of the kinetochore, its sheer size and the predominance of elongated, coiled-coil-rich proteins have limited the structural analysis of this assembly. This is in part attributed to the difficulties to purify entire kinetochore complexes and to the lack of specialized structural methods capable of acquiring structural information from heterogeneous and flexible protein complexes.

To circumvent these limitations and to obtain a comprehensive connectivity map of kinetochores I used XLMS to identify spatial restraints on low abundant native protein complexes (122). Briefly, the subunits of the protein complexes are crosslinked using an isotopically tagged N-hydroxy disuccinimidyl ester (123). Subsequent to the proteolytic digestion the crosslinked peptides are enriched by size exclusion chromatography, the crosslink fractions are analyzed by an Orbitrap Elite mass spectrometer and crosslink spectra are identified using the dedicated search engine xQuest (124). Identification of the linkage sites by mass spectrometry yields distance restraints within a single polypeptide or between subunits of a complex, showing which proteins are in proximity to each other at the level of protein motifs (122).

#### **3.1.1. Quantitative mass spectrometry identified the protein composition of native yeast kinetochore complexes**

In order to purify stable endogenous kinetochore subcomplexes, yeast strains expressing C-terminally tandem affinity tagged kinetochore proteins from native promoters were generated. Prior to investigating the architecture of the inner kinetochore assembly using XLMS (Figure 7B), small scale pilot purifications from 5 grams of yeast cell powder have been successfully carried out (Figure 7A).

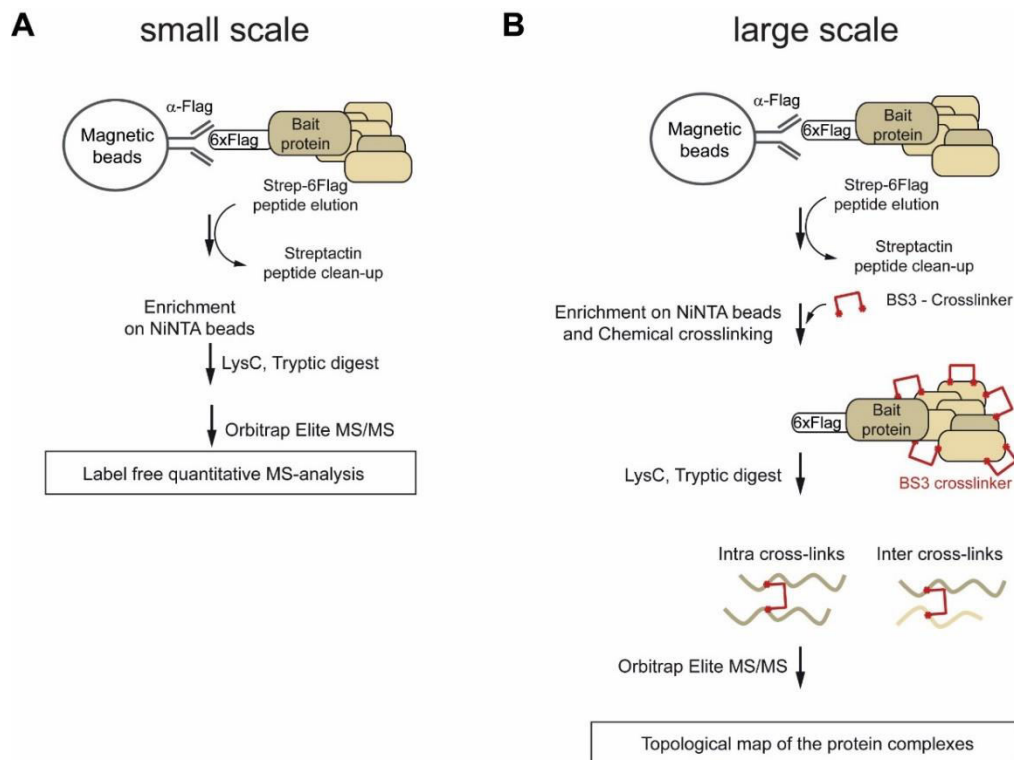


**Figure 7. Mass spectrometric analysis of native kinetochore complexes.** (A) Schematic representation of the workflow used to identify the quantitative protein composition of native kinetochore complexes. (B) XLMS workflow for the analysis of native kinetochore complexes.

To cover the complete set of the stable subcomplexes forming the CCAN, various tagged strains were tested, having the following proteins C-terminally 6xHis-6xFLAG tagged: Wip1, Cnn1, Chl4, Ame1, Ctf3, Mif2, Iml3. Mass spectrometry analysis revealed that the purified samples included all known kinetochore subunits (Figure 1, Figure 8). Moreover, the amount of specific peptides from different subcomplexes discovered in the various pulldowns already provided indications, which subcomplexes might be stably interacting and are in close proximity to each other in the cellular environment. Hence, the higher the number of peptides of a specific protein discovered in the analysis compared to the bait protein, normalized to the sizes, suggests a higher probability of a close association *in vivo*. This assumption was endorsed by the observation, that isolation of a subunit of a kinetochore complex mostly yields proteins of the respective subcomplex followed by proteins of spatially proximal subcomplexes (Figure 8).

### 3.1.1.1. Ame1 associated complexes

The label-free mass spectrometry experiments of Ame1-FLAG eluates detected Okp1 and Nkp1 at the abundance level of 90 % of the bait protein. Okp1 has been shown to form a stable heterodimer with Ame1 (25). The Ctf19/Mcm21 and Ame1/Okp1 heterodimers form

the tetrameric COMA complex which is associated with Nkp1/Nkp2 as it has been shown by previous studies (Figure 8) (34). Among the abundant copurifying proteins histones, especially Cse4, were detected, suggesting that the COMA complex is in close proximity and possibly interacting with the centromeric nucleosome. The observation that none of the known nucleosome binding proteins such as Mif2 was detected at similar abundance level, indicated that COMA itself associates with the centromeric NCP, either by binding to DNA as proposed recently (25) or through direct interaction with Cse4. The list of detected proteins was completed by CTF3c (Ctf3, Mcm21, Mcm16), Chl4/Iml3 and KMN components at a relative abundance of about 8-1 %. The fact that Ctf19/Mcm21 are required for the correct centromeric localization of CTF3c (35) and Chl4/Iml3 (34) already suggested interaction of COMA with the respective proteins. Moreover, the idea that COMA, Nkp1/Nkp2, CTF3c and Chl4/Iml3 are packed closely together in the CCAN structure was supported by a recent EM study using *in vitro* reconstituted proteins (35), showing several interaction surfaces between the respective complexes. Our Ame1-FLAG pulldown data is consistent with the CCAN EM 3D reconstruction.

### **3.1.1.2. Cnn1/Wip1 associated complexes**

Cnn1-FLAG isolation co-purifies components of the CTF3 complex as the most abundant hits, followed by proteins of Chl4/Iml3, COMA and Nkp1/Nkp2 at similar abundance and KMN at levels of ~10 % (Figure 8). In consistence with previous reports, Spc25, which together with Spc24 forms the binding interface for Cnn1 (48) was among the most abundant members of outer kinetochore proteins. Purifications of the bait-protein Wip1, the direct interactor of Cnn1 (32), presented a similar pattern of copurifying kinetochore complexes. Interestingly, in both datasets histone proteins have not been enriched. Histone 4 (Hhf1) was the highest ranked with 6 % relative abundance compared to Cnn1. Therefore, I concluded that despite the presence of histone folds (46) and the notion that Cnn1/Wip1/Mhf1/Mhf2 form a nucleosome-like structure similar to their human orthologues CENP-T/W/S/X (125), Cnn1/Wip1 are not directly incorporated into nucleosomal core particles (NCPs) *in vivo*. Taken together, the results suggest that within the kinetochore Cnn1/Wip1 interact with proteins of the outer and inner kinetochore. Previous studies showed that the Cnn1 N-terminus recruits NDC80c and Cnn1/Wip1 forms a stable five subunit complex with CTF3c (32). According to our findings, the Cnn1/Wip1 interaction with CTF3c might establish a stable association of Cnn1/Wip1 with COMA and Nkp1/Nkp2 which anchors Cnn1 at the centromeric nucleosome.

### 3.1.1.3. CTF3c associated complexes

By pulling on the CTF3c/HIK protein Ctf3 we predominantly detected subunits of the COMA and Nkp1/Nkp2 complexes and Cnn1/Wip1 at similar levels, but less of the outer-kinetochore KMN proteins were co-purified (Figure 8). Hence, our data suggests that KMN association to CTF3c is not direct, but mediated either via COMA and Nkp1/Nkp2 or Cnn1/Wip1, which is in agreement with previous observations (32). Moreover, the high abundance of Chl4/Iml3 in the samples indicates that in yeast similar to humans CTF3c forms a super-complex with Chl4/Iml3 (41). In addition, a recent electron microscopy analysis of the *in vitro* assembled CCAN structure showed Iml3 interacting with Ctf3 (35), consistent with our *in vivo* observation.

### 3.1.1.4. Chl4/Iml3 associated proteins

Together with Chl4-FLAG Iml3 was co-purified at a 1:1 molar ratio (Figure 8) (29). Notably, in most of the performed pulldowns Chl4/Iml3 was obtained at similar levels, indicating that both proteins form a stable heterodimer *in vivo* that survives the purification procedure. Further abundant proteins were subunits of the COMA, Nkp1/Nkp2 and CTF3c complexes, followed by members of the KMN network. Interestingly, the levels of detected histone proteins were ~ 2 % compared to the bait protein Chl4-FLAG. In comparison to the human orthologues, this does not indicate a direct association of Chl4/Iml3 with Cse4 containing NCPs. To obtain a comprehensive map of the proteins associated with Chl4/Iml3 I also performed pull-downs with Iml3-FLAG as bait. However, only few co-purifying kinetochore proteins were detected indicating a possibly poor incorporation of the tagged protein into the kinetochore complexes.

### 3.1.1.5. MS analysis of Mif2 associated proteins

In the Mif2-FLAG pulldowns hardly any CCAN proteins were detected (Figure 8). The known interaction partner Ame1/Okp1 (25), was detected in the 10 % range compared to the bait. Consistent with this result, Mif2 was not detected among the 30 most abundant proteins in other CCAN pulldowns. This result was counterintuitive, as Mif2 is one of the three essential proteins within the CCAN. As a tighter association with other CCAN proteins was expected this suggests that Mif2 establishes a separate pathway linking the centromeric nucleosome to the outer kinetochore.

However, all four histone proteins were discovered in a range between 42 - 116 % compared to the bait, which is in agreement with Mif2 directly associating with the Cse4-NCP, and displays that this interaction is quite stable. Notably, only the histone H3 variant Cse4, present in centromeric NCPs, but not canonical H3 was co-purified, highlighting the binding specificity of Mif2 for Cse4. It should be noted, that prior purification of Mif2 associated complexes, the lysate was incubated with the endonuclease benzonase. Without benzonase treatment Mif2 purifications showed considerably less histones. Moreover, all ten proteins of the outer kinetochore were co-purified in a range of 10 – 30 % relative to the bait. This is consistent with a previous study showing that the Mif2 N-terminus directly interacts with the MTW1c and thereby supports KMN assembly at the kinetochore (25).

In summary, the detected protein compositions of the Ame1, Cnn1/Wip1, Ctf3, Chl4 and Mif2 pulldowns suggest a structural model, in which CTF3c is spatially positioned in-between COMA, Nkp1/Nkp2 and Cnn1/Wip1 at the kinetochore. Apart from that, it seems that COMA and Nkp1/Nkp2 are placed directly at the centromere interface, while Cnn1/Wip1 appears to be positioned more distal within the CCAN and might directly link CTF3c and KMN (32). Furthermore, our data might propose a mechanism of Mif2 linking the centromeric NCP directly with KMN independent of direct interactions with other CCAN proteins. Still, we can not exclude that Mif2 was degraded or interactions were not stably maintained during the purification procedure. Our quantitative MS data of purified native CTF19 complexes is largely in agreement with the literature and confirms many observations that were made *in vitro*.

Finally, we reasoned that our pulldown protocol would allow kinetochore particle purification in the range of microgram quantities sufficient for XLMS, enabling us to gain deeper insights into the protein connectivity of the CCAN complexes at the resolution of protein motifs.

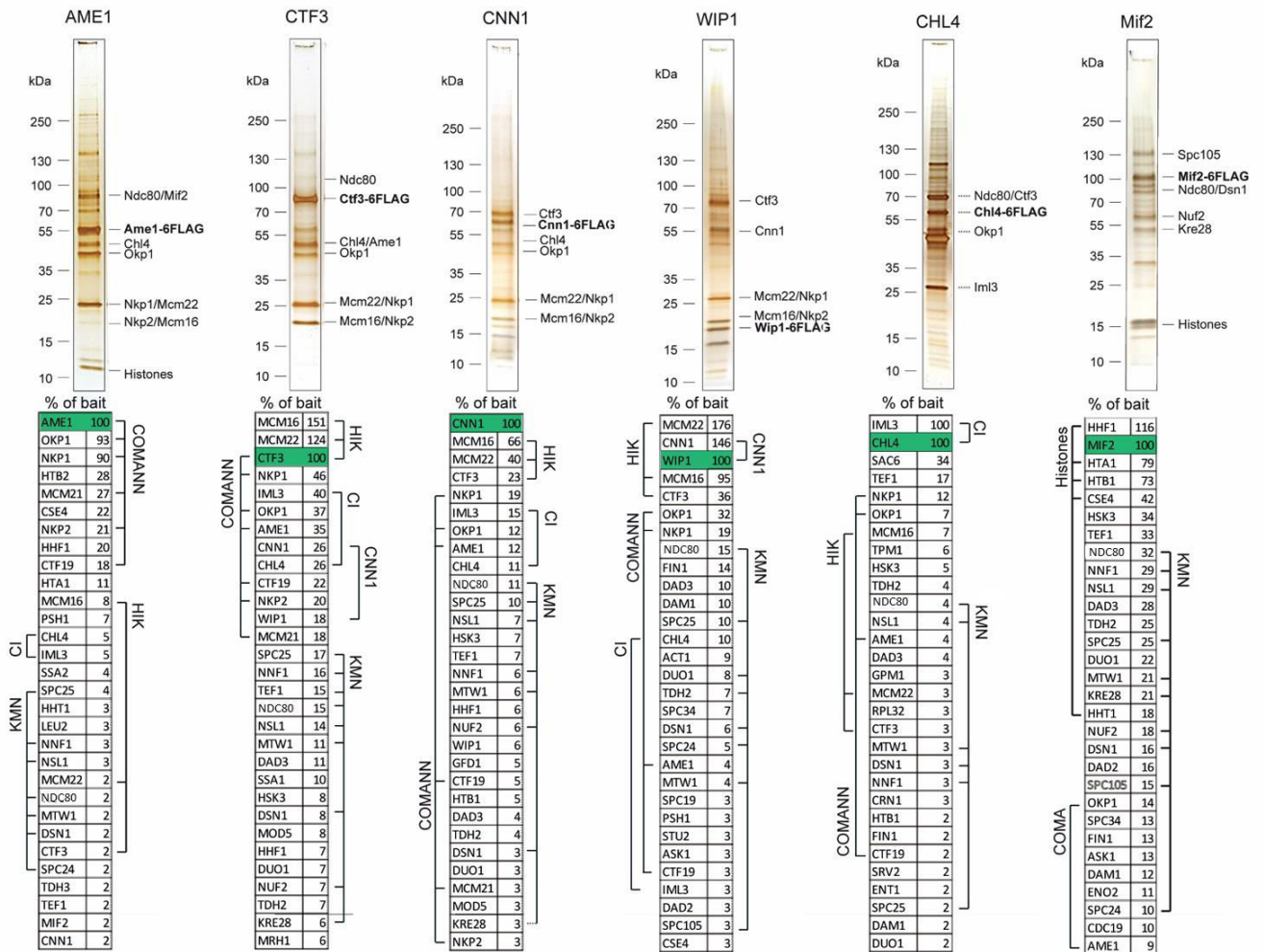


**Figure 8. The quantitative mass spectrometric analysis of native inner and outer kinetochore purifications.** Label-free mass spectrometry quantification of native kinetochore complexes which were purified by pulling on Ame1-, Ctf3-, Cnn1-, Wip1-, Chl4- and Mif2-FLAG. Eluted proteins were visualized by SDS-PAGE followed by silver staining (upper panel) and quantified based on IBAQ protein intensities of the MaxQuant software (lower panel). The 30 most abundant kinetochore subunits normalized to their molecular weights and to the bait intensity (% of bait highlighted in green) are listed.

### 3.1.2. Optimization of the purification protocol to enrich for kinetochore associated regulatory complexes

Besides deciphering connectivities within the CCAN, we aimed to co-purify complexes of the SAC and error correction mechanism. None of the pulldowns showed significant levels of checkpoint proteins. In an attempt to co-purify SAC and CPC complexes we synchronized yeast cells in mitosis. The arrest was performed by applying benomyl or a combination of nocodazole and benomyl (data not shown), which depolymerizes microtubules. Subsequently, unattached kinetochores activate the SAC. This approach did not result in the copurification of the proteins of the SAC (Figure 9).



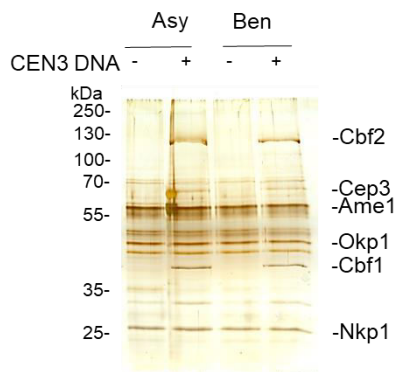


**Figure 9. The copurification of the CBF3c with Ame1 was dependent on centromeric DNA.** Ame1-FLAG pulldowns were performed from extracts of asynchronous (Asy) or benomyl (Ben) arrested yeast cells in the absence or presence of PCR amplified CEN3 DNA (-/+CEN3). Eluted proteins were visualized by SDS-PAGE and silver staining. Proteins of the CBF3 complex were copurified from lysates of asynchronous and mitotic yeast cells supplemented with CEN3 DNA.

An additional strategy to enrich for regulatory proteins was to supplement the lysate of Ame1-FLAG expressing cells with the PCR amplified CEN3 DNA prior to the pull-downs. A previous study reported that the COMA complex can directly bind centromeric DNA and addition of centromeric DNA might be necessary for proper CCAN formation (25). In our experiment CEN3 DNA induced assembly of the entire CBF3 complex with the COMA complex (Figure 9). The addition of CEN3 DNA did not significantly increase the levels of associated regulatory proteins.

In a further attempt to purify stable complexes of kinetochore and regulatory proteins, we affinity-tagged proteins of the SAC and CPC. I generated strains having Bir1 and Sli15 of the CPC and the checkpoint proteins Bub3, Mad3 and Mps1 C-terminally tagged at their endogenous locus.

Bub3-FLAG and Mad3-FLAG co-purified CDC20, Bub1, Bub2, Mad1. However, no kinetochore proteins were detected among the top 30 proteins. In pulldowns using Sli15-FLAG and Bir1-FLAG the levels of copurifying kinetochore proteins were not significant.

Only in Mps1-FLAG purifications we observed enriched kinetochore protein levels. For example, Nsl1 was copurified at 21 % compared to the bait. Ndc80, which interacts with Mps1 through its CH domain (126) was detected at 8 % compared to the bait. Interestingly, Spc105, which is a substrate of Mps1, was only detected at around 4 % of the bait. We did not identify any SAC proteins among the top 30 hits.

Therefore, we concluded that our experimental pulldown approach for studying the interactions of SAC and CPC with the kinetochore complexes was insufficient to isolate these assemblies from budding yeast cell lysates. The transient nature of the interactions between

the structural kinetochore proteins and regulatory proteins did not allow the isolation of stable native complexes.

### **3.1.3. Chemical crosslinking and mass spectrometry (XLMS) analysis of native yeast kinetochore complexes**

Chemical cross-linking in combination with mass spectrometry (XLMS) has become a versatile tool in hybrid structural biology approaches to analyze the connectivity and topology of proteins and their complexes at the level of protein motifs. The method is well established in our laboratory and allows the detection of spatial restraints on low abundant native protein complexes (122). I attempted to generate a topological map of native kinetochore assemblies. I focused on the inner kinetochore complexes that were isolated through Ame1-FLAG, Ctf3-FLAG, Mif2-FLAG, Cnn1-FLAG, Wip1-FLAG, and Chl4-FLAG, which in preliminary experiments yielded the most complete CCAN preparations and used them for large scale pull-down experiments with 200 g yeast pellets as starting material. As for small scale pilot experiments native kinetochore subassemblies were isolated from yeast strains containing FLAG tagged kinetochore proteins at the endogenous loci (Figure 7B). Briefly, the subunits of the purified protein complexes were cross-linked using the isotopically-tagged N-hydroxy disuccinimidyl ester based crosslinker bis(sulfosuccinimidyl)suberate (BS3) (123). After protease digest the cross-linked peptides were enriched by size exclusion chromatography, cross-link fractions were analyzed by an Orbitrap Elite mass spectrometer and cross-link spectra were identified using the dedicated search engine xQuest (124).

The single datasets were combined and resulted in a topological map covering the assembly of the inner kinetochore proteins that delineated their interactions to the outer kinetochore (Figure 10). The majority of the crosslinks within the different subcomplexes COMA, Nkp1/Nkp2, CTF3c, KMN are in agreement with the results of our label free quantification approach and with previous studies (19, 25, 29, 32). While the composition of the stable subcomplexes was already well defined, our topological map displays a more comprehensive arrangement between the different subcomplexes, co-purified under native conditions.

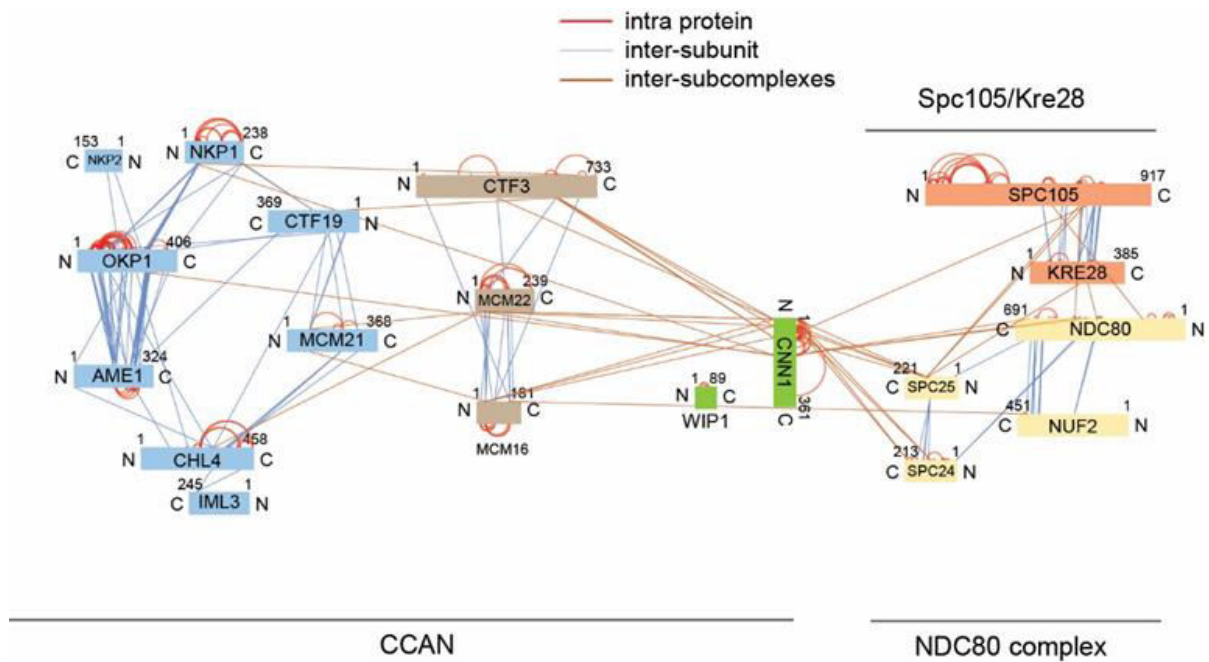


**Figure 10.** XLMS analysis identifies a novel linkage between COMA and microtubule binding proteins bypassing the MTW1c. CCAN kinetochore subcomplexes were purified by Ame1-, Ctf3-, Cnn1-, Wip1-, Chl4- and Mif2-FLAG pulldowns. The topology of the yeast CCAN complexes and their connectivity with the NDC80 and Spc105/Kre28 complexes are depicted by 122 distance restraints obtained by XLMS analysis. Proteins are represented as bars and the protein lengths and linkage sites are scaled to the amino acid sequence. Subunits within a complex are displayed in the same color.

We identified crosslinks between Chl4/Iml3 and all members of COMA (Figure 10), indicating that COMA subunits provide an extensive binding interface for Chl4/Iml3. This observation was confirmed by a recent EM structure of an *in vitro* reconstituted CCAN (35). Consistently in human cells, CENP-OPQUR binds to a joint interface on the CENP-HIKM and CENP-LN complexes (44).

Additionally, we found one crosslink between Chl4 and Mcm22. Crosslinks between Nkp1/Nkp2 and the rest of the CCAN proteins were primarily detected on Ame1/Okp1 which is consistent with a previous study (34). Moreover, we found single crosslinks from Nkp1 to Ctf3 and Cnn1.

Proteins of the COMA complex were in cross-linkable vicinity to the CTF3c proteins. In the Ctf19/Mcm21 heterodimer we identified crosslinks from the N-terminal extension of Mcm21 to the N-termini of Mcm22 and Mcm16 and a crosslink from the Ctf19 N-terminal extension to the C-terminal end of Ctf3, which is in agreement with the recently described CCAN EM-structure. Moreover, we found cross-links between all three subunits of the CTF3c and Cnn1. In particular, there were crosslinks from the entire N-terminal domain of Cnn1 to the N-termini of Mcm22/Mcm16 and the Ctf3 C-terminus. This is confirming the recently reported

formation of a stable Cnn1/Wip1:CTF3c complex *in vitro* (32). Therefore, we assume that CTF3c is spatially positioned in-between COMA and Cnn1/Wip1 and bridges the respective complexes. As shown in a previous study Cnn1 itself was cross-linked to the Spc24/Spc25 heads of the NDC80c (48). The compiled crosslink results indicate a direct COMA-CTF3c-Cnn1-Ndc80c link, anchoring the outer-kinetochore KMN network to the inner-centromere CCAN assembly.

Overall, the data is consistent with the observations of the label free quantitative mass spectrometry analysis and suggests the same hierarchical arrangement of the subcomplexes from inner kinetochore towards the microtubule binding interface. In particular, the results of the Ctf3-FLAG pulldowns resemble the crosslink information. In the pulldowns we predominantly detected proteins of the COMA, Nkp1/2 complexes and Cnn1/Wip1 at similar amounts while KMN proteins were less abundant.

### **3.2. The chromosomal passenger complex directly associates with native kinetochore complexes**

The chromosomal passenger complex has been shown to be recruited to the centromere to fulfill its essential function in establishing correct microtubule kinetochore attachments during pro-metaphase (95, 103). However, deleting the first 228 residues, which harbor the centromere targeting region of Sli15 $\Delta$ N does not affect chromosome biorientation (86). Moreover, deletions of the nonessential COMA complex proteins Ctf19/Mm21 become synthetically lethal in the *sli15 $\Delta$ N* background (86). As Ctf19/Mcm21 are important for cohesin loading and maintenance, the synthetic lethality has led to the hypothesis that centromere located CPC might also play a role in these processes. Apart from that, it was suggested, that the Sli15 $\Delta$ N mutant retains its biological function by clustering at microtubules via the Sli15 microtubule binding domain (86). An alternative model for CPC function is that the functionally relevant pool resides near or at kinetochores (8, 106). Supporting the later model, Amel has been shown to promote Sli15 localization at kinetochores and that the reduced localization of Sli15 in the absence of Amel results in persistent defective attachments (51).

Initially, I aimed to investigate possible interactions between the CPC and kinetochore proteins by co-purifying native kinetochore-CPC complexes using the protocol described in chapter 5.11. Up to now, the isolation protocols of native kinetochore complexes have failed to copurify crosslinkable amounts of CPC with kinetochore complexes. To circumvent these

limitations I established an experimental strategy that used recombinant Sli15 $\Delta$ N/Ipl1 and native kinetochore preparations (Figure 11A), in order to increase the amounts of CPC in the sample and to shift the binding equilibrium of kinetochore proteins.

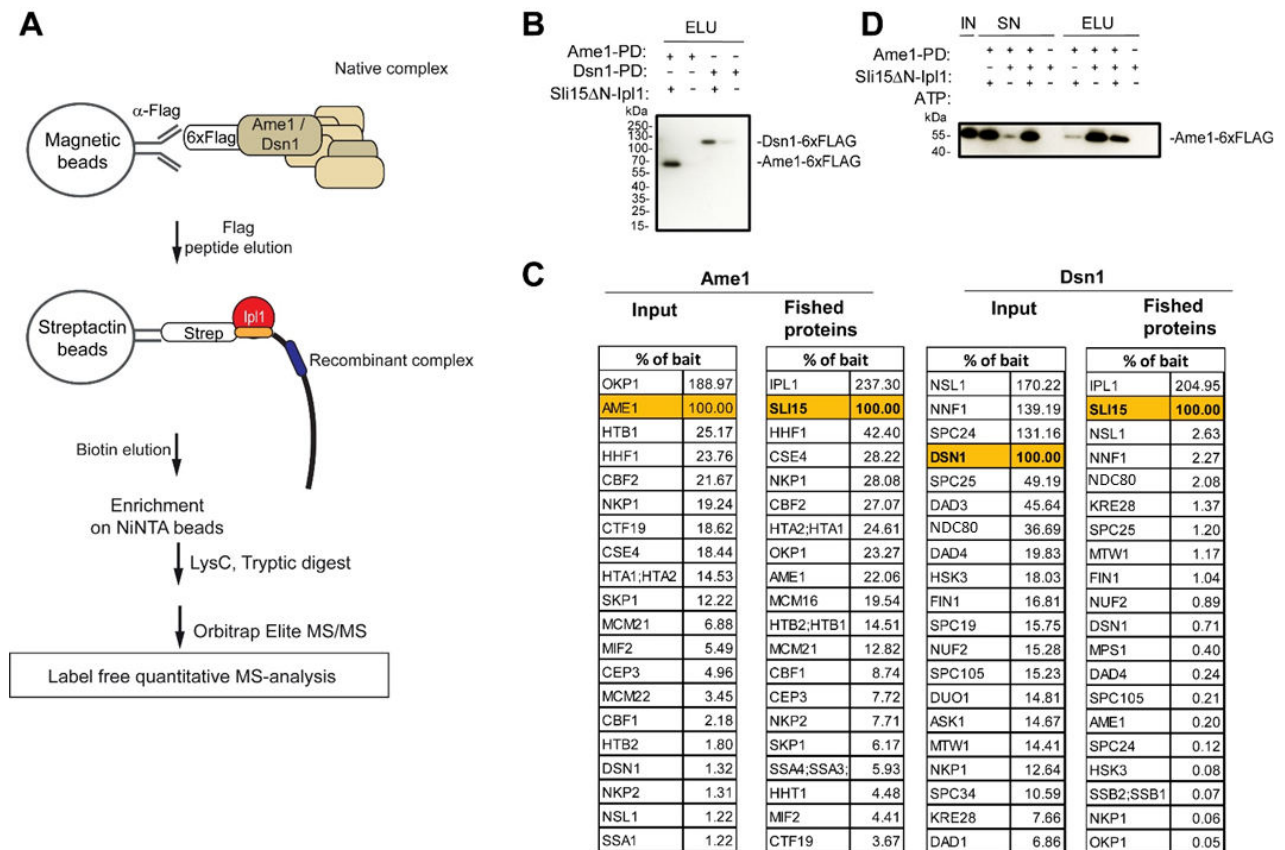


**Figure 11. CPC associates with kinetochore proteins in a Bir1 independent manner.** (A) Sli15 $\Delta$ N/Ipl1 was recombinantly expressed from single viruses in insect cells. Subsequently a single Strep-tag affinity purification was performed. To test its binding ability towards kinetochore subcomplexes the bead bound Sli15 $\Delta$ N/Ipl1 was incubated with purified native kinetochore subcomplexes derived from Ame1-FLAG or Dsn1-FLAG pulldowns. Proteins were eluted and enriched on Ni-NTA beads prior to analyzing the composition via mass spectrometry. (B) Western blot analysis of eluates confirming the association of kinetochore proteins with Sli15 $\Delta$ N/Ipl1. (C) Quantification of inputs and eluted proteins via mass spectrometry. The 20 most abundant proteins are ranked according to the molar percentage relative to the bait. (D) Presence of ATP largely reduces the binding of Ame1-FLAG to Sli15 $\Delta$ N/Ipl1.

To identify kinetochore proteins that associate with the CPC I used the Sli15 $\Delta$ N mutant which is not targeted to centromeres (86). Deletion of the Sli15 N-terminus prevents direct association of Sli15/Ipl1 with the native CBF3 complex assembled at centromeric nucleosomes. To test its ability to associate with kinetochore subcomplexes the recombinantly expressed Sli15 $\Delta$ N/Ipl1 was immobilized on beads and subsequently incubated with purified native outer and inner kinetochore complexes (Figure 11A). Native kinetochore complexes were obtained by immunoprecipitating Ame1-FLAG yielding a large subset of CCAN proteins or Dsn1-FLAG resulting in a nearly stoichiometric KMN super-complex. In this preliminary fishing experiment the specific enrichment of Ame1-FLAG and Dsn1-FLAG

copurifying proteins on Sli15 $\Delta$ N/Ipl1 was observed (Figure 11B/D). The mass spectrometry analysis of the enriched proteins showed similar compositions as detected in the inputs (Figure 11C), indicating that complexes did not dissociate during the fishing procedure. Quantification of CCAN proteins associating with Sli15 $\Delta$ N/Ipl1 identified all members of the COMA complex within the 20 most abundant proteins indicating a direct interaction of COMA with the minimal CPC. Notably, compared to the Ame1-FLAG isolated complexes in the input Mif2 was highly enriched in the fished eluate of inner kinetochore proteins (Figure 11C).

In addition, among the outer kinetochore proteins interacting with Sli15 $\Delta$ N/Ipl1 Kre28, Ndc80 and Mps1 were enriched relative to the levels in the input preparations (Figure 11C). Neither in the input nor in the Sli15 $\Delta$ N/Ipl1 enriched samples we detected peptides of microtubules. This observation further supported a direct CPC interaction with kinetochores that was not mediated through its association with microtubules as previously suggested (86). To elucidate whether phosphorylation affects the association of CCAN proteins with Sli15 $\Delta$ N/Ipl1 the fishing experiment was performed from native CTF19c preparations supplemented with 5 mM ATP. Western blotting of Ame1-FLAG showed a drastically reduced interaction upon ATP addition (Figure 11D), suggesting that the interaction of inner kinetochore proteins with the CPC was perturbed by phosphorylation. To identify potential targets of phosphorylation within the kinetochore proteins we analyzed the unbound fraction (supernatant) of the fishing experiment by mass spectrometry. We did not detect an increase in phosphorylation levels of kinetochore proteins compared to the input (data not shown). We thus assumed that phosphorylation of the CPC itself might affect the binding of the CTF19c. Indeed, I detected elevated phosphorylation levels of certain sites at Sli15 and to a minor degree at Ipl1 compared to the input (Figure 12). In summary, these results suggested that Sli15/Ipl1 autophosphorylation or phosphorylation by a CTF19c associated kinase negatively regulates the interaction with inner kinetochore complexes similar to the effect of Sli15 phosphorylation on its association with microtubules.

To investigate whether Ipl1 or Ame1 copurifying kinases were implicated in Sli15 phosphorylation, I analyzed phosphorylation levels of Sli15 $\Delta$ N/Ipl1 after incubation with ATP in the absence of the Ame1-FLAG isolated kinetochore complexes. The phosphorylation pattern was not significantly altered suggesting that the autophosphorylation of Sli15 $\Delta$ N/Ipl1 affected its binding to the CTF19c.

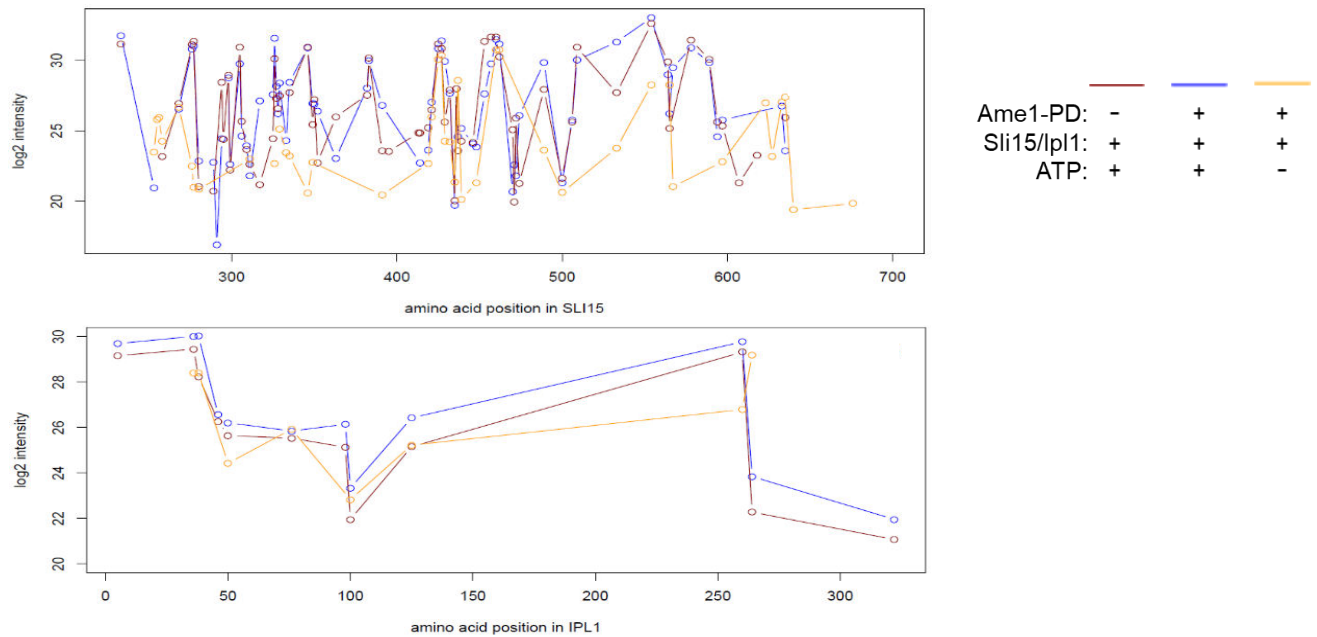


**Figure 12. Mass spectrometric quantification of Sli15ΔN/Ipl1 *in vitro* phosphorylation sites.** The Sli15ΔN/Ipl1 *in vitro* phosphorylation sites were quantified by mass spectrometry and the software MaxQuant (vers. 1.5.2.8) in the presence or absence of ATP and Ame1-FLAG copurifying kinetochore complexes. Protein abundances were estimated as the sum of peptide intensities divided by the peptide counts. The intensities of the phosphorylated peptides were normalized to the respective protein intensities.

### 3.3. *In vitro* reconstitution of inner kinetochore subcomplexes interacting with the chromosomal passenger complex

The previous fishing experiments suggested the association of Sli15ΔN/Ipl1 with CTF19c. To investigate the molecular basis of this interaction and to identify putative binding partners of the CPC a subset of CTF19 complexes was reconstituted.

#### 3.3.1. The core CPC directly interacts with the COMA complex

The centromere-targeting deficient mutant *sli15ΔN* shows synthetic lethality with deletions of Ctf19 or Mcm21 (86). Additionally, a study reported an essential role of the COMA complex in mediating correct localization of the CPC (51). Thus, I asked whether the COMA complex directly interacts with Sli15/Ipl1 *in vitro*. The essential proteins Ame1/Okp1 were purified from *E.coli* as described previously, while Ctf19/Mcm21 was successfully purified from insect cells as homogenous and nearly stoichiometric complex.

XLMS analysis of COMA subunits and Sli15/Ipl1 at stoichiometric ratios identified 98 inter-protein and 69 intra-protein crosslinks (Figure 13). The majority of crosslinks within the

COMA complex are in agreement with previous reports (34, 35). Only one crosslink between Ipl1 and the COMA complex was detected. However, 16 crosslinks targeting COMA were found on Sli15, 15 of which are located in its microtubule binding domain. Notably, 10 of these crosslinks were located in the C-terminal RWD (RWD-C) domain of Ctf19. In addition to that, 4 crosslinks were located in the RWD-C domain of Mcm21 and two in Okp1. Within the COMA complex the two RWD-C domains are in close proximity (50). Moreover, one crosslink detected on lysine 366 of Okp1 is close to the reported Ctf19/Mcm21 binding site of Okp1 (34) and thereby also positioned in vicinity to the RWD-C domains. Collectively the crosslink data suggested that Sli15 provides most of the interaction surface within Sli15/Ipl1. Within the COMA complex several protein regions of more than one protein might contribute in forming an association site, with the Ctf19 C-terminal RWD domain playing a predominant role.

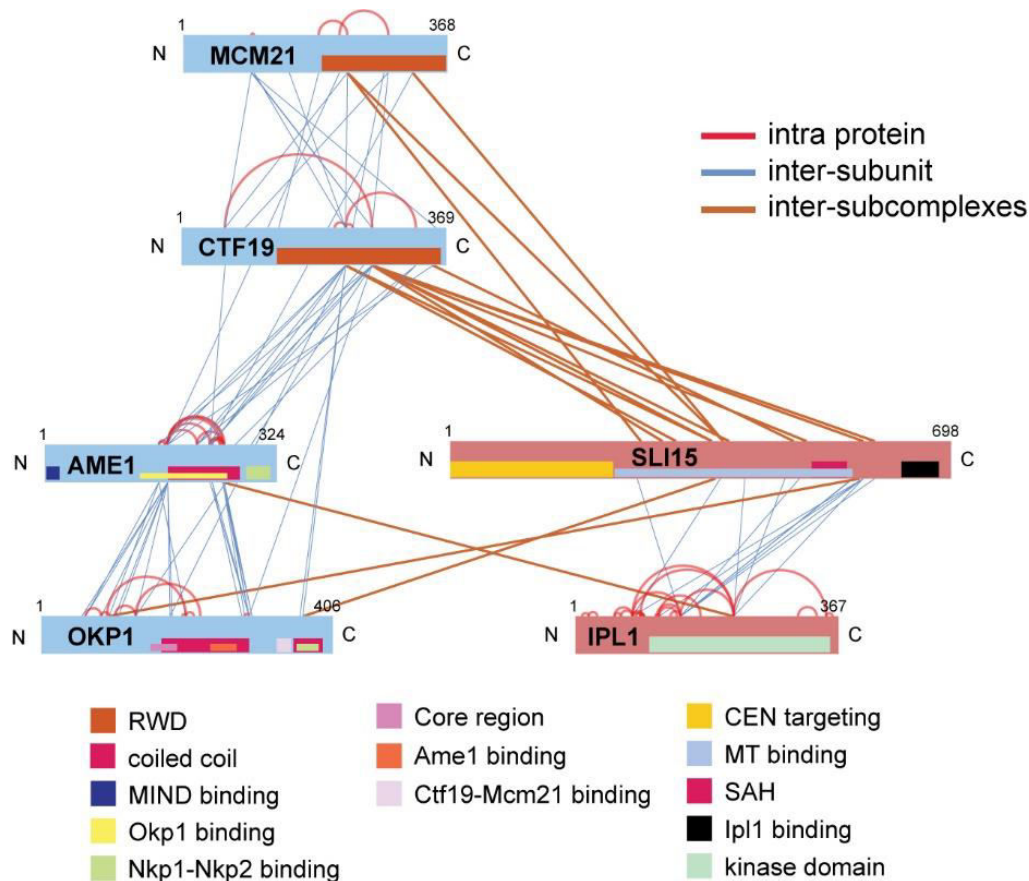


**Figure 13. The crosslinks detected between recombinant Sli15/Ipl1 and the COMA complex display potential binding sites.** Topology map of Sli15/Ipl1 in complex with COMA, based on the 167 restraints obtained by XLMS analysis. Sli15/Ipl1 and Ctf19/Mcm21 were recombinantly expressed from single viruses in insect cells, Ame1/Okp1 was expressed in *E.coli*. Purified complexes were mixed at equimolar amounts prior to crosslinking with BS3. Proteins are represented as bars and the protein lengths and linkage sites correspond to the amino acid sequence. Subunits within a complex are displayed in the same color.



To further elucidate the molecular mechanism of the Sli15/Ipl1:COMA association and to validate the crosslink data I performed *in vitro* binding assays. Sli15/Ipl1 was pre-bound to Streptavidin beads and incubated with heterodimers Ame1/Okp1 and Ctf19/Mcm21 individually or combined. Strikingly, both complexes showed interaction with Sli15/Ipl1 compared to the bead control (Figure 14A). Notably, auto-phosphorylation of Sli15/Ipl1 prior to performing the *in vitro* binding assay abrogated binding of the COMA proteins (Figure 14A), validating the observations of the fishing experiment in which native kinetochore complexes were applied (Figure 11D). Further dephosphorylation by lambda phosphatase treatment did not enrich binding (Figure 14A).

Despite extensive efforts to show stable binding via analytic SEC, I was unable to observe a co-migrating complex. Either Sli15/Ipl1 interacted with the column material and consequently could not be eluted, or no co-migrating complex with COMA subunits was formed under the tested conditions. I next asked whether binding is also established in a more complex environment than represented in the *in vitro* pull down assays. Therefore, I conducted another fishing experiment. Sli15 $\Delta$ N/Ipl1 pre-bound to beads was incubated with insect cell lysates containing either Ame1/Okp1 or Ctf19/Mcm21 expressed from single viruses. Compared to empty beads, a clear increase in association of Ame1 and Ctf19 with Sli15 $\Delta$ N/Ipl1 beads was observed (Figure 15), highlighting the ability of Ame1-FLAG and Ctf19-FLAG to bind Sli15 $\Delta$ N/Ipl1 despite other proteins competing for the binding site.

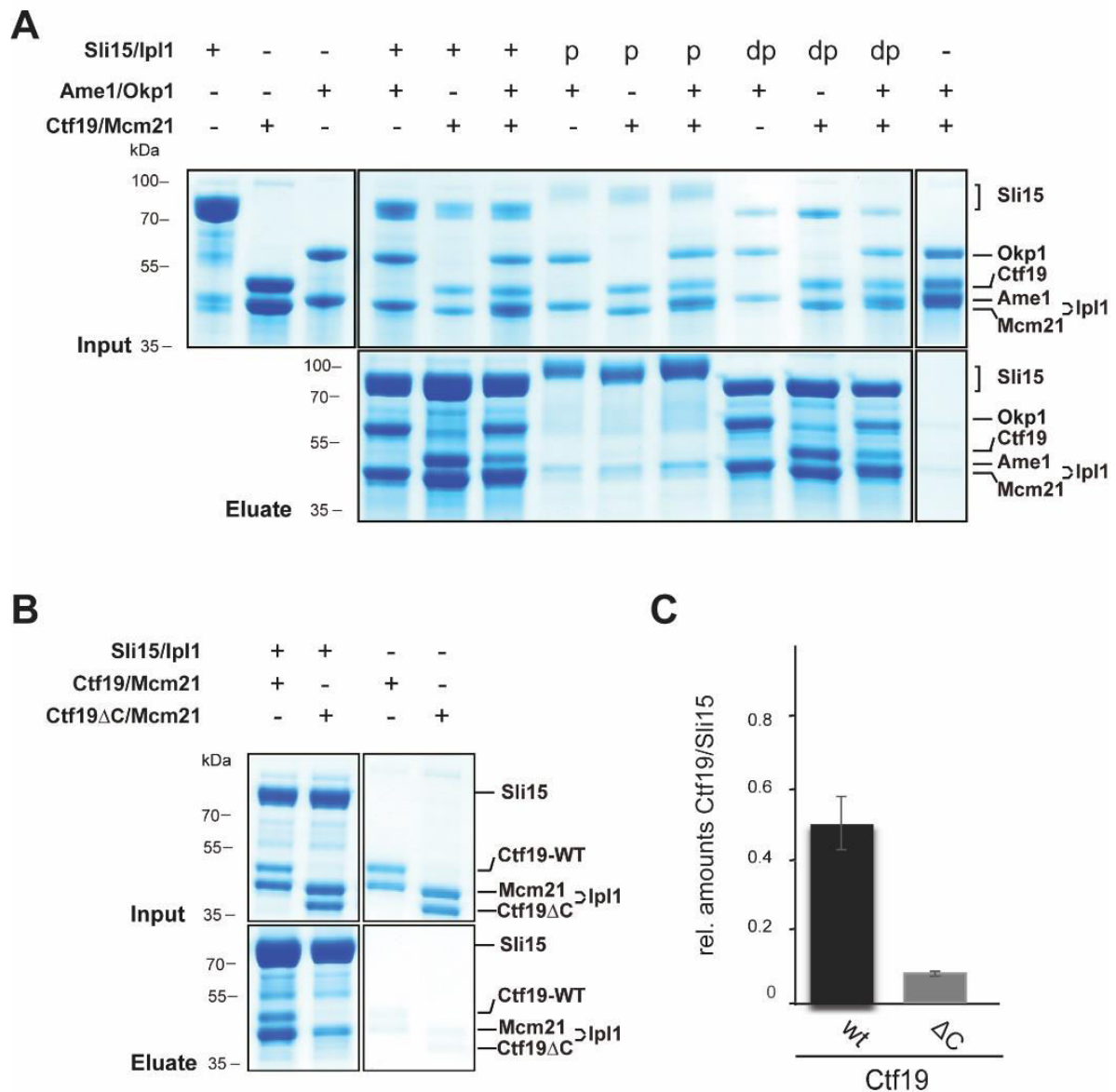


**Figure 14.** Sli15 $\Delta$ N/Ipl1 interacts with Ame1/Okp1 and Ctf19/Mcm21 in a phosphorylation dependent manner, with the Ctf19 C-terminal RWD domain acting as a defined binding site. (A) *In vitro* binding assays showing individual or combined association of Ame1/Okp1 and Ctf19/Mcm21 with Sli15/Ipl1. Sli15/Ipl1 immobilized on Streptavidin beads was either untreated, pre-phosphorylated (p) or dephosphorylated (dp) prior incubation with the respective COMA proteins. Eluted proteins were visualized by SDS-PAGE and coomassie staining. (B) *In vitro* binding assays of Ctf19 $\Delta$ C lacking the last 100 amino acids which form the C-terminal RWD domain, compared to Ctf19 wildtype (WT). (C) Quantification of Figure (B). Intensities of pulled down Ctf19 wildtype or Ctf19 $\Delta$ C protein levels relative to Sli15 protein levels were quantified. Graph depicts mean values and standard deviations obtained from three independent experiments.

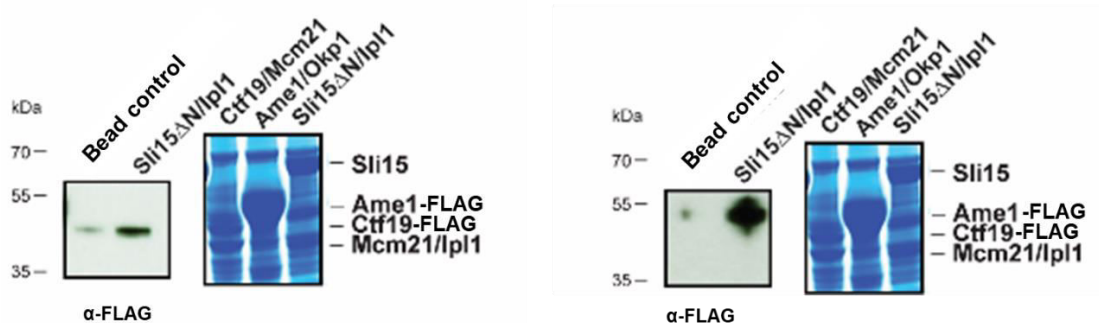


**Figure 15.** Ame1/Okp1 and Ctf19/Mcm21 associate with Sli15ΔN/Ipl1 in a complex environment. Western blot analysis showing Ctf19-FLAG or Ame1-FLAG interaction with Sli15ΔN-Strep/Ipl1 immobilized on Strepavidin beads (left panel). Coomassie stained SDS-PAGE gel of insect cell lysate aliquots showing the expression of Ctf19-FLAG/Mcm21, Ame1-FLAG/Okp1 or Sli15ΔN-Strep/Ipl1.

To further explore whether the Ctf19 C-terminal RWD domain functions as interaction site, I generated a C-terminal RWD deletion mutant, Ctf19Δ270-369 (Ctf19ΔC). The mutant still formed a stoichiometric complex with Mcm21, but was not pulled down with Sli15/Ipl1 (Figure 14B/C). Collectively, the *in vitro* binding assays and XLMS data reveal at least two docking sites for Sli15/Ipl1 within the COMA complex, one of which being the C-terminal RWD domain of Ctf19.

Our crosslink data did not point towards an obvious Sli15/Ipl1 binding site within the Ame1/Okp1 heterodimer for Sli15/Ipl1 binding. However, a recent study provided a structural and functional characterization of Okp1, highlighting the requirement for viability of a coiled coil region ( aa 234-264 ) (34). Interestingly the same region overlapped with the identified minimal region (229-336) required for interaction with the RWD domains of Ctf19/Mcm21. I hypothesized that within the tetrameric COMA complex, the individual Sli15/Ipl1 docking sites of Ame1/Okp1 and Ctf19/Mcm21 might be in close proximity. To test this, I generated two Okp1 mutants lacking all or part of this feature, Okp1ΔCC1 (241-282 aa) and Okp1ΔCC2 (204-271 aa), respectively. One of the two crosslinks of Okp1 to Sli15 was detected close to the single alpha helix (SAH) motif of Sli15. Notably, crosslinks of Ctf19 to Sli15 were also found in that region. I concluded that this alpha helix might interact with the coiled coil region of Okp1. However, *in vitro* binding assays showed that neither the alpha helix of Sli15 nor the coiled coil region of Okp1 were required for interaction (Figure 16). Future experiments will have to address which region in Ame1/Okp1 mediates this interaction. Apart from that, *in vivo* experiments are required to clarify the relevance of the multiple docking sites.

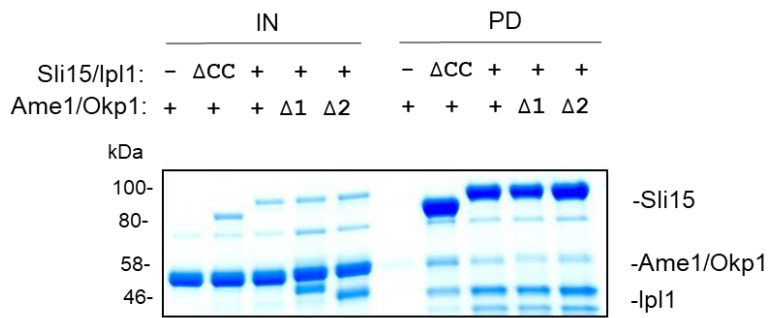


**Figure 16. Sli15ΔN/Ipl1 binding to Ame1/Okp1 does not require certain coiled coil structures.** *In vitro* binding assays showing association of Ame1/Okp1 with Sli15/Ipl1. Sli15/Ipl1 was immobilized on Streptavidin beads prior to incubation with the respective Ame1/Okp1 wildtype or mutant complexes. Eluted proteins were visualized by SDS-PAGE and coomassie staining. Sli15ΔCC lacks amino acids 523-563, which form the SAH domain. Okp1ΔCC1 lacks amino acids 241-282 and Okp1ΔCC2 amino acids 204-271. IN: input, PD: pulldown.

### 3.3.2. The core of the chromosomal passenger complex directly interacts with Mif2, but not with the CTF3c *in vitro*

Mif2 provides a direct link between centromeric NCP and outer kinetochore proteins, and is one of the three essential proteins in the budding yeast CCAN (23). Moreover, Mif2 was one of the proteins enriched in the fishing experiment, hinting towards a close association with CPC proteins (Figure 11C). Therefore, I tested the direct binding of Mif2 to Sli15/Ipl1 via XLMS and *in vitro* binding assays. XLMS analysis did not enable us to pinpoint a possible interaction site, as I detected crosslinks covering most parts of Mif2 and Sli15 (data not shown). Still, *in vitro* binding assays showed a specific interaction, which was phosphorylation dependent (Figure 17).

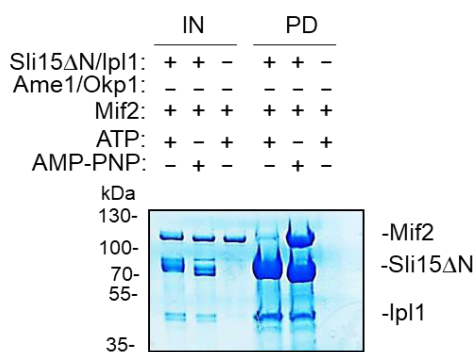


**Figure 17. Sli15ΔN/Ipl1 interacts with Mif2 in a phosphorylation dependent manner.** *In vitro* binding assays showing interaction between Mif2 and Sli15ΔN/Ipl1 in the presence of ATP or the non-hydrolysable analogue AMP-PNP. Sli15ΔN/Ipl1 was immobilized on Streptavidin beads before Mif2 was applied. Eluted proteins were visualized by SDS-PAGE and coomassie staining. IN: input, PD: pulldown.

The fishing experiments and *in vitro* binding assays showed binding of the CPC to kinetochore proteins that are positioned proximal to the centromere. Moreover, I observed

association with more distal complexes like the KMN (Figure 11C), which represents also a target for Ipl1 phosphorylation. Next, I asked whether the CPC interacts with additional complexes, potentially positioned in-between. I speculated that this could facilitate a gradual movement from the centromere to microtubule binding proteins. Therefore, I asked whether CTF3c proteins also directly interact with the CPC. However, *in vitro* binding assays did not show a significant interaction (Figure 18).

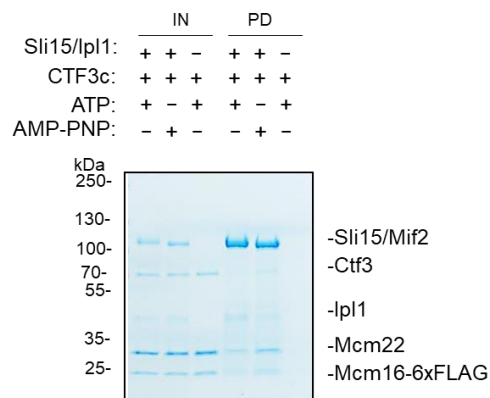


**Figure 18. Sli15 $\Delta$ N/Ipl1 does not interact with the CTF3c.** *In vitro* binding assays analyzing the interaction of Sli15 $\Delta$ N/Ipl1 with the CTF3c in the presence of ATP or the non-hydrolysable analogue AMP-PNP. Sli15 $\Delta$ N/Ipl1 and Ctf3/Mcm22/Mcm16 (HIK/CTF3c) were recombinantly expressed from single viruses in insect cells. Sli15 $\Delta$ N/Ipl1 was immobilized on Streptavidin beads prior to incubation with CTF3c proteins. Eluted proteins were visualized by SDS-PAGE and coomassie staining. IN: input, PD: pulldown.

### 3.3.3. The COMA complex mediates the spatial positioning of Sli15/Ipl1 at the inner kinetochore

The crosslink guided *in vitro* reconstitution identified the COMA complex as a direct interaction partner of Sli15 $\Delta$ N/Ipl1. In addition to that, I observed Mif2 associating with the CPC in *in vitro* pulldown assays. Importantly, an essential role of Ame1 in establishing the proper localization of the CPC at metaphase was already suggested (51). Intriguingly, the centromere-targeting deficient *sli15 $\Delta$ N* mutant is synthetically lethal upon deletion of Ctf19 or Mcm21 (86), though the underlying cause is still unknown. We hypothesized that direct interactions with COMA proteins provide a mechanism for positioning the CPC at inner kinetochores, independent from Bir1 and that the synthetic lethality observed is caused by disturbed CPC positioning. In an attempt to test this hypothesis and thus clarify the functional relevance of the *in vitro* interactions observed, we carried out a variety of yeast viability assays *in vivo*.

First, we reproduced the synthetic lethality reported by applying an anchor-away system (127). We generated a yeast strain in which endogenous Sli15 is replaced by Sli15 $\Delta$ N, and

endogenous Ctf19-FRB can be inducibly depleted from the nucleus upon rapamycin treatment. With this tool in hand we confirmed, that cells expressing Sli15 $\Delta$ N are viable in the presence of Ctf19-FRB, but after Ctf19-FRB depletion, no growth is detected (Figure 19).

### 3.3.4. Cohesin loading defects do not provide a valid explanation for the synthetic lethality of the *ctf19 $\Delta$ /sli15 $\Delta$ N* double mutant

Because Ctf19/Mcm21 also play a role in centromeric cohesin loading (30) a potential role for chromatin-localized CPC in cohesion establishment or maintenance has been suggested (86). Recently, Ctf19 was identified as the receptor of the cohesin loading complex (128). In particular, the first 30 amino acids, comprising essential phosphorylation sites of the Dbf4-dependent kinase (DDK) were shown to be required for the recruitment of the cohesin loading complex Scc2/4 to the centromere (128). Hence, we generated a Ctf19 mutant, lacking the first 30 amino acids (*ctf19 $\Delta$ 2-30*), enabling us to determine whether Sli15 plays an active, essential role in the cohesin loading process. Strikingly, cells expressing Ctf19 $\Delta$ 2-30 in the *sli15 $\Delta$ N* background showed no growth defect upon Ctf19 depletion (Figure 19). This result demonstrates that the synthetic lethality is not caused via a cohesin loading defect and must be accounted to a different cellular process.

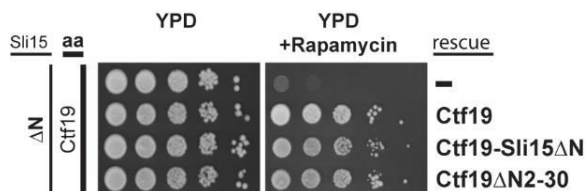


**Figure 19.** The synthetic lethality of a *sli15 $\Delta$ N/ctf19 $\Delta$*  double mutant is independent of the Ctf19 N-terminus containing the cohesin-loader receptor domain. Cell growth assays for analyzing the ability of constructs to rescue synthetic lethality in a *sli15 $\Delta$ N/Ctf19-FRB* double mutants using the anchor-away system. The indicated constructs were ectopically expressed in Ctf19 anchor-away strains carrying *sli15 $\Delta$ N* at the endogenous locus. Yeast growth was monitored in serial dilutions, harboring no (-) or the indicated constructs, on YPD plates in the absence or presence of rapamycin at 30 °C. All tested constructs Ctf19WT, Ctf19 $\Delta$ N2-30 and Ctf19-Sli15 $\Delta$ N are able to restore growth. The displayed spotting assay was carried out by Sylvie Singh.

### 3.3.5. The synthetic lethality of *ctf19 $\Delta$ /sli15 $\Delta$ N* can be rescued by artificial and selective tethering of Sli15 to inner kinetochore proteins

As stated above, we hypothesized that in *ctf19 $\Delta$ /sli15 $\Delta$ N* cells, impaired binding of Sli15 $\Delta$ N to COMA proteins cause the lethal phenotype. In this scenario, repositioning of Sli15 $\Delta$ N to

the inner kinetochore by artificial tethering to inner kinetochore proteins should restore growth. Thus, we generated fusions of Sli15 $\Delta$ N to various inner and outer kinetochore proteins and monitored their ability to restore growth in our anchor away induced *ctf19 $\Delta$ /sli15 $\Delta$ N* double mutant. As expected, fusions to the outer kinetochore proteins Mtw1/Dsn1 and fusions to inner kinetochore proteins Ctf3/Cnn1 did not rescue viability (Figure 20A). However, in accordance with our hypothesis, specific inner kinetochore fusions to the COMA proteins Ame1 and Okp1 conferred viability (Figure 20A), supporting the idea that precise spatial positioning was required. Interestingly, fusing Sli15 $\Delta$ N to Mif2, which also directly interacted with Sli15 in the *in vitro* binding assay, could not restore viability (Figure 20A). We exclude that lack of rescue was caused by a lack of expression of the various protein fusions, as all proteins were detected by western blot analysis (Figure 20B).

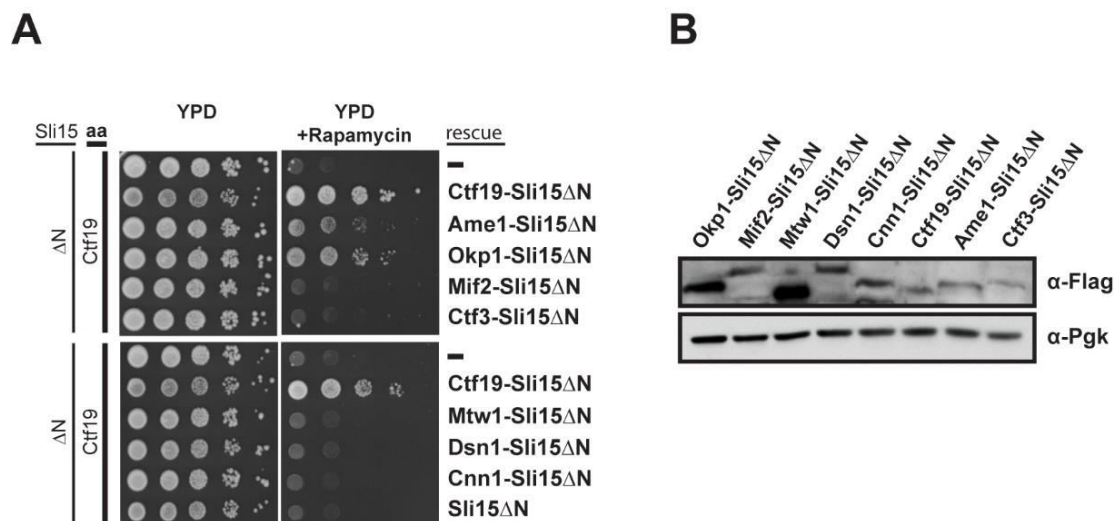


**Figure 20. Artificial and selective tethering of Sli15 $\Delta$ N to Ame1/Okp1 rescues the synthetic lethality in a *sli15 $\Delta$ N/ctf19 $\Delta$*  double mutant.** (A) Cell viability rescue assays were performed as described in Figure 19 in Ctf19 anchor away strains, carrying *sli15 $\Delta$ N* at the endogenous locus. Among the tested fusions to various inner and outer kinetochore proteins (Ctf19-Sli15 $\Delta$ N, Ame1-Sli15 $\Delta$ N, Okp1-Sli15 $\Delta$ N, Mif2-Sli15 $\Delta$ N, Ctf3-Sli15 $\Delta$ N, Mtw1-Sli15 $\Delta$ N, Dsn1-Sli15 $\Delta$ N, Cnn-1-Sli15 $\Delta$ N, Sli15 $\Delta$ N) only the fusions to the COMA proteins Ame1, Okp1 and Ctf19 showed a rescue effect. (B) Amounts of ectopically expressed FLAG tagged fusion constructs used in (A) are displayed via western blot analysis. The displayed experiments were carried out by Sylvie Singh.

### 3.3.6. A functional chromosomal passenger complex tethered at inner kinetochores requires Ipl1 kinase activity

Next, we aimed to determine whether rescue of viability was dependent on Ipl1 kinase activity. Thus, we generated Ame1- and Okp1-Sli15 $\Delta$ N fusion proteins lacking the Ipl1 binding site, referred to as “IN box” (92, 129). As Ame1- and Okp1-Sli15 $\Delta$ N $\Delta$ IN fusions did

not confer viability (Figure 21A), we concluded that Ipl1 kinase activity is required and that the ability to restore growth is not intrinsic to Sli15.

Sli15 harbours a Single Alpha Helix domain (SAH, aa 516-575), which mediates microtubule binding *in vitro* (88, 89). Recently it was proposed, that Sli15 $\Delta$ N is targeted proximal to metaphase kinetochores via this domain and thereby might maintain its biological function (86). To address this assumption and query the role of the SAH domain, we made Ame1- and Okp1-Sli15 $\Delta$ N $\Delta$ SAH fusion constructs. The respective mutants displayed normal growth in the *sli15* $\Delta$ N background (Figure 21A), indicating that the function of the SAH domain is not required for the essential role of the CPC positioned at the inner kinetochores.

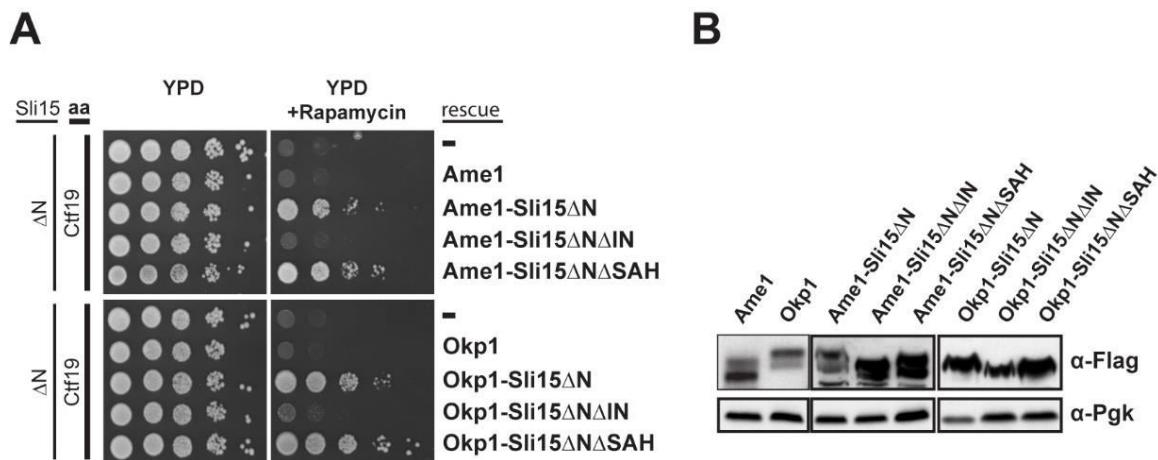


**Figure 21. Rescue effects via Ame1-Sli15 $\Delta$ N or Okp1-Sli15 $\Delta$ N fusion proteins require the Ipl1 binding domain (IN box) of Sli15, whereas its SAH domain is dispensable.** Growth assays applying the anchor away technique were performed as described in Figure 19. The fusion constructs lacking the SAH domain Ame1-Sli15 $\Delta$ N $\Delta$ SAH and Okp1-Sli15 $\Delta$ N $\Delta$ SAH restored growth, while expression of proteins lacking the IN-box, Ame1-Sli15 $\Delta$ N $\Delta$ IN and Okp1-Sli15 $\Delta$ N $\Delta$ IN, did not show a rescue effect. (B) Western blot analysis detecting the C-terminal 7xFLAG tag of the fusion proteins shown in (A). The displayed experiments were carried out by Sylvie Singh.

### 3.3.7. The Ctf19 C-terminal RWD domain mediates the recruitment of Sli15 to inner kinetochores

Finally, since our *in vitro* pulldown experiments identified the C-terminal RWD domain of Ctf19 as essential for Sli15/Ipl1:Ctf19/Mcm21 complex formation (Figure 14B/C), we aimed to verify this observation *in vivo*. However, because the C-terminus of Ctf19 is also required for assembling into the COMA complex (34) (Figure 23), its deletion abrogates Ctf19 kinetochore localization. To circumvent this problem, we tested, whether fusions of Ctf19WT or Ctf19 $\Delta$ C to Ame1 or Okp1 were able to rescue synthetic lethality in a *Ctf19-FRB/sli15* $\Delta$ N background. Consistent with our biochemical data, Ctf19WT- but not Ctf19 $\Delta$ C fusion



constructs were able to restore viability (Figure 22A). All fusion proteins were equally expressed *in vivo*, as indicated by western blot analysis (Figure 22B).

In summary, our data indicate that the Ctf19 C-terminal RWD domain mediates the positioning of Ipl1 kinase activity at the inner kinetochore, thereby ensuring its proper function.

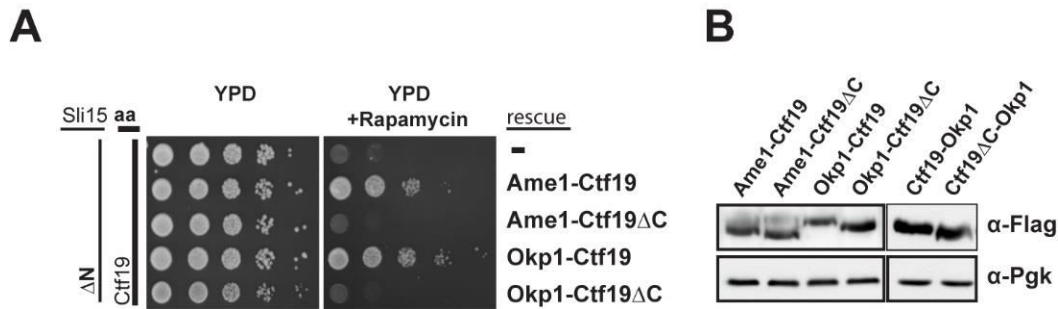


**Figure 22. A functional C-terminal RWD domain of Ctf19 is required for viability in the *sli15ΔN* background.** Rescue experiments applying the anchor away technique were performed as described in Figure 19. The fusion constructs lacking the C-terminal RWD domain of Ctf19, Ame1-Ctf19ΔC and Okp1-Ctf19ΔC fail to restore growth, while the wildtype fusion-proteins Ame1-Ctf19 and Okp1-Ctf19 confer viability. (B) Western blot analysis visualizing the C-terminal FLAG tag of the fusion proteins shown in (A). The displayed experiments were carried out by Sylvie Singh.

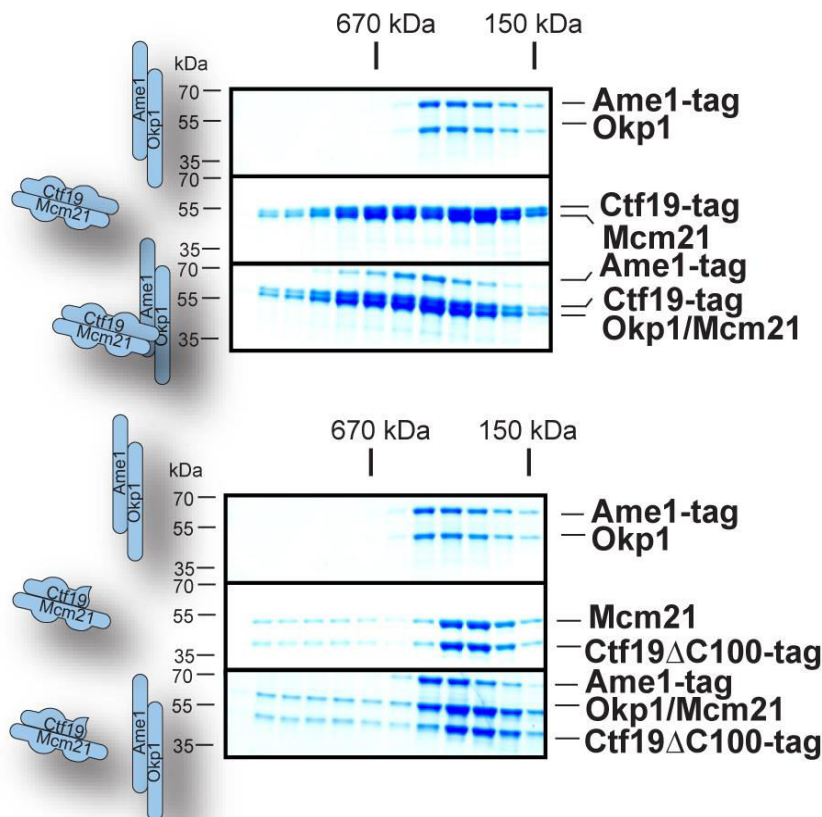


**Figure 23. The C-terminal RWD domain of Ctf19 is required for the formation of the COMA complex in size exclusion experiments.** Ame1/Okp1 association with Ctf19/Mcm21 or Ctf19ΔC/Mcm21 was monitored via size exclusion chromatography. The recombinant protein complexes were applied individually or in combination

at a 1:1 molar ratio. Eluted fractions were analyzed by SDS-PAGE and coomassie staining. Ame1/Okp1 shifted to earlier elution volumes in the presence of Ctf19/Mcm21. No complex formation was detected, when Ame1/Okp1 was combined with Ctf19 $\Delta$ C/Mcm21.

### **3.4. *In vitro* reconstituted KMN interacts with the chromosomal passenger complex**

While the CCAN links the kinetochore to the centromere, the KMN network represents the primary interface between kinetochores and spindle microtubules (57). As such, it has emerged as a critical target of the Aurora-B/Ipl1 kinase mediated error correction. Specifically, the well-defined phosphorylation of the positively charged Ndc80 N-terminus reduces the affinity of kinetochores towards microtubules in response to erroneous attachment states (58, 97). Still, precise knowledge of how incorrect microtubule kinetochore attachments trigger the response of Ipl1 kinase activity is lacking. To date, it is a matter of debate, where the functionally relevant Ipl1 pool that senses and corrects miss-attachments in concert with the KMN network, resides (106). One hypothesis is that the CPC is targeted to centromeres and via dissociation generates a CPC concentration gradient, known as the centromere gradient model (106). Alternative models predict that the active pool is localized at kinetochores, or at microtubules, and that the centromere pool is not strictly required for Ndc80 phosphorylation. Latter models are supported by the observation that the Sli15 $\Delta$ N mutant, lacking the centromere targeting domain, shows normal error correction (86).

Initially, my fishing experiment suggested interactions of the CPC with kinetochore subunits of the inner and outer kinetochore (Figure 11B/C). Most importantly, my crosslink-guided *in vitro* reconstitution identified docking sites of the CPC within the CCAN. Thus, we next investigated whether the CPC also interacts directly with outer kinetochore proteins. For this purpose, I applied crosslink-guided *in vitro* reconstitution.

The KMN consists of three distinct subcomplexes: NDC80c, MTW1c, and Spc105/Kre28. For each subcomplex a single expression vector, harboring the gene-cassettes of all respective proteins, was assembled via the biGBac method (130). By further combination of these constructs, a single expression vector containing all ten KMN subunits was generated and the complex was successfully purified at stoichiometric amounts from insect cells. XLMS analysis of KMN and Sli15/Ipl1 mixed at equimolar amounts yielded 324 inter-protein and 324 intra-protein crosslinks (Figure 24). The inter-crosslinks within the subcomplexes are in agreement with their known structure. For instance, we observed crosslinks between the Ndc80 and Nuf2 coiled coil domains (66), as well as between the Spc24 and Spc25 coiled coil

domains (131). Furthermore, inter crosslinks between Dsn1 and Nsl1, which form a stable heterodimer (60), have been detected. Additionally, the reported connection between the globular C-terminal domain of Spc24-Spc25 and Nsl1 was detected (60). Moreover, numerous crosslinks within the Spc105/Kre28 subcomplex were found. Taken together, the crosslink data validates our experimental approach and confirms that KMN remained intact during the experiment. We found only a single crosslink between Sli15 and the prominent Ipl1 phosphorylation target Ndc80. Strikingly, we detected 19 crosslinks from Sli15 towards Spc105 and 3 towards Kre28. Crosslinks of Ipl1 towards KMN proteins were located exclusively on Kre28. Collectively, this analysis verified known interactions and more importantly, indicated that Spc105/Kre28 provides a docking site for Sli15/Ipl1. To test this observation, I performed *in vitro* binding assays, which indeed showed Sli15/Ipl1 binding to bead-bound Spc105/Kre28 (Figure 25B).

The KMN represents a major target of phosphorylation for regulating its affinity towards microtubules (6). Furthermore, phosphorylation of the Spc105 MELT repeats by Mps1 kinase mediates the recruitment of the SAC machinery (65). In *in vitro* binding assays with CCAN proteins, I observed a reduction of Sli15/Ipl1 binding due to phosphorylation. Therefore, I tested whether phosphorylation influences binding of Sli15/Ipl1 towards the KMN in a similar manner.

The addition of ATP, resulting in auto-phosphorylation of Sli15/Ipl1 and Ipl1 mediated phosphorylation of KMN, abrogated the binding (Figure 25 - lane 5). Still, individual phosphorylation of either Sli15/Ipl1 (Figure 25 - lane 3) or KMN (Figure 25 - lane 4) by Ipl1 did not significantly reduce this interaction. This is in contrast to the finding that Sli15 phosphorylation is sufficient to abrogate association with COMA proteins (Figure 14A). We also tested whether Mps1 phosphorylation has an impact on the observed binding properties. For this purpose we took advantage of a Sli15/Ipl1 kinase dead mutant (D227A) enabling us to specifically differentiate between Mps1 and Ipl1 phosphorylation. Interestingly, phosphorylation of KMN by Mps1 alone was not sufficient to abrogate the interaction with Sli15/Ipl1 (Figure 25 - lane 7). However, as with the observed Ipl1 mediated phosphorylation effect, the additional phosphorylation of Sli15/Ipl1 by Mps1 significantly reduced the amounts of pulled down Sli15/Ipl1 (Figure 25 - lane 8). Thus, we conclude that phosphorylation of both interaction partners, Sli15/Ipl1 and KMN, are required to abrogate complex formation and, that phosphorylation of individual complexes is not sufficient. The precise role of Spc105/Kre28 binding to Sli15/Ipl1 *in vivo* should be the subject of further investigations. Is this interaction relevant for error correction or SAC signaling? Does this

interaction provide a mechanism for positioning active Ipl1 close to its target protein Ndc80, in order to correct false microtubule kinetochore attachment states? How is the interaction regulated *in vivo*? Does phosphorylation play a role?

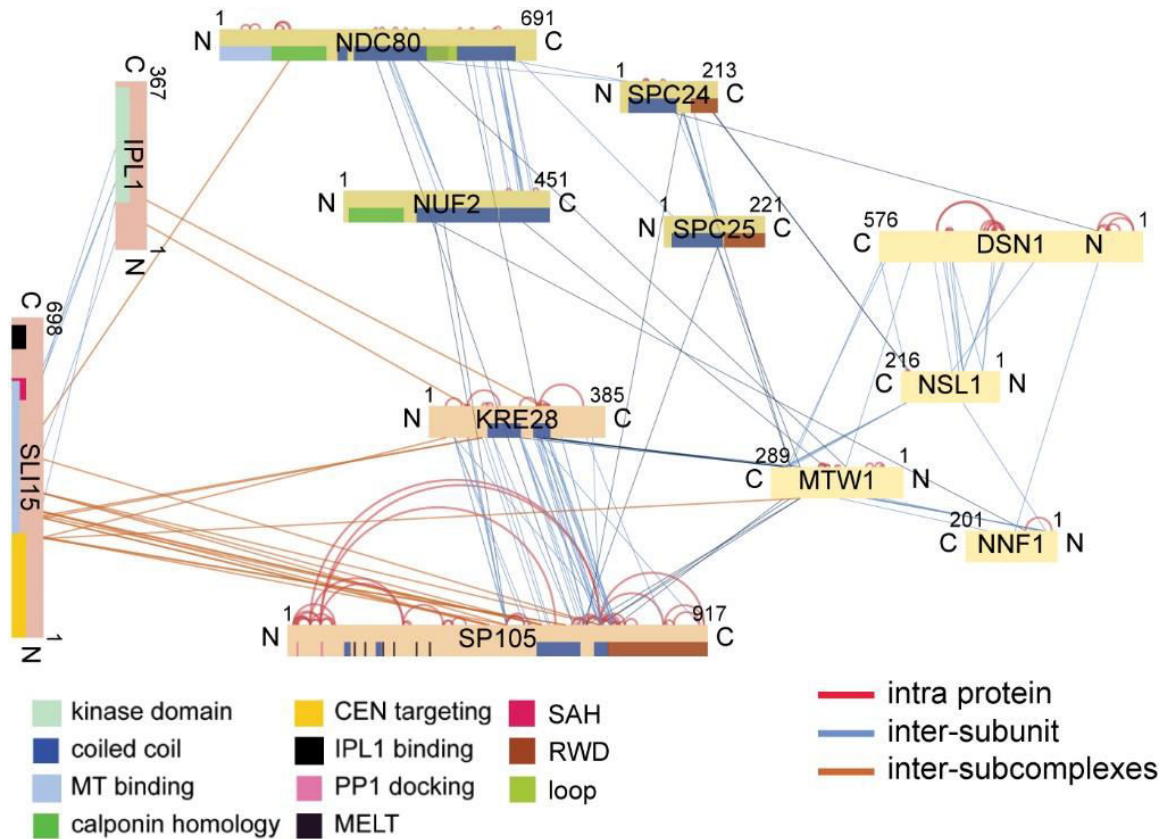


**Figure 24.** XLMS analysis identified the Spc105105/Kre28 complex as a putative docking site for Sli15/Ipl1 at the outer kinetochore. Crosslinking analysis of *in vitro* reconstituted Sli15/Ipl1 with the KMN complexes is visualized as network diagram as described (Figure 13). Sli15/Ipl1 and KMN were recombinantly expressed from single viruses in insect cells. The purified complexes were mixed at equimolar amounts prior crosslinking with BS3.

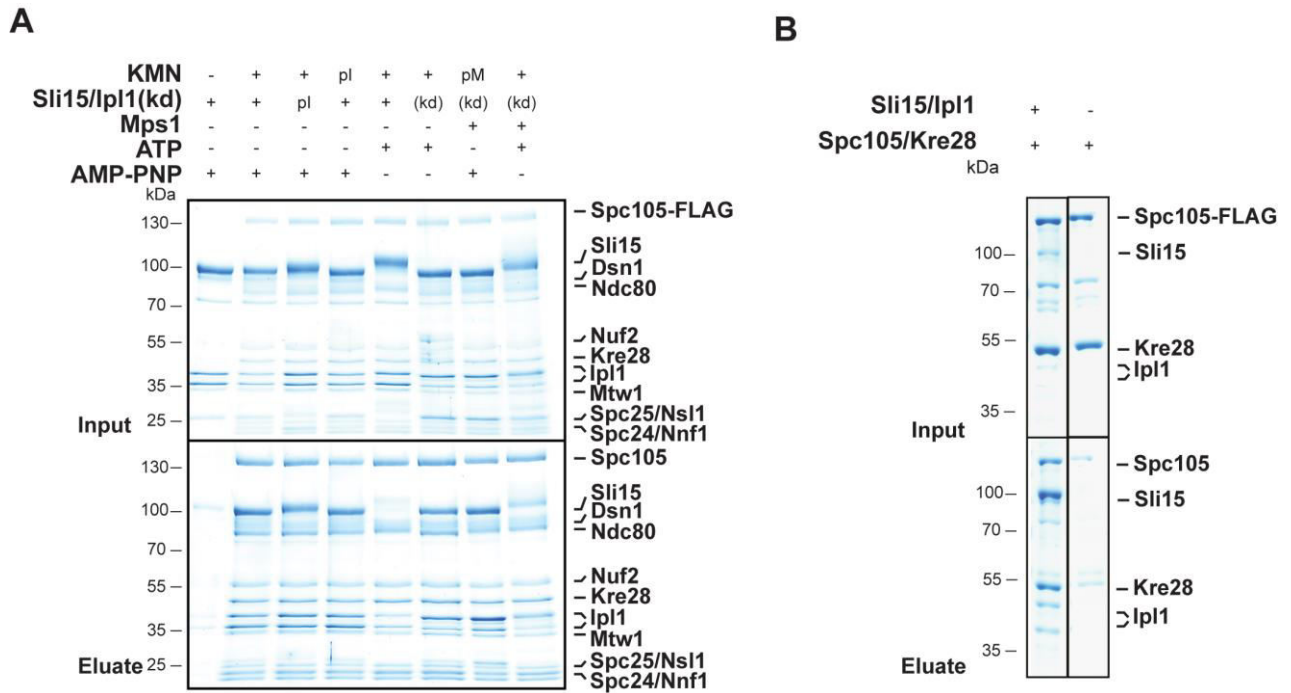


**Figure 25. *In vitro* binding assay showing phosphorylation dependent association of Sli15/Ipl1 with the KMN network.** (A) The KMN network was immobilized via Spc105-FLAG on FLAG-beads prior to incubation with Sli15/Ipl1 or the kinase dead (kd) Sli15/Ipl1 mutant. The KMN proteins and Sli15/Ipl1 were pre-phosphorylated by Ipl1 (pI) or Mps1 (pM), phosphorylated in the incubation mixture or mock-treated with AMP-PNP. (B) Sli15/Ipl1 was immobilized on Streptavidin beads prior incubation with Spc105/Kre28. Eluted proteins were visualized by SDS-PAGE and coomassie staining.

### 3.5. The Ame1/Okp1 heterodimer selectively binds Cse4 containing nucleosomes

To date, only one budding yeast CCAN protein, Mif2, has been identified to directly and specifically associate with Cse4<sup>CENP-A</sup> containing nucleosomes (23). This is in contrast to human, where CENP-N also contributes to the hierarchical assembly by selectively recognizing CENP-A (38). For the budding yeast homologue of CENP-N, Chl4, no direct association has yet been observed. Furthermore, the localization of Chl4 depends on Ctf19/Mcm21 and Mif2 (33, 34). This suggests a more downstream role for Chl4 in the assembly process than in the human system. My label free quantitative mass spectrometry data further supports this idea. In the *in vivo*-pull-downs of Chl4-FLAG the most abundant copurifying proteins were members of COMA- and CTF3 complexes instead of nucleosomal proteins (Figure 8). However, as the budding yeast point centromere is marked by a single Cse4 nucleosome, cooperative stable interactions with CCAN proteins are anticipated to ensure the proper and spatially restricted kinetochore assembly. To screen for further direct

interaction partners of Cse4-NCPs we looked at our label free quantitative mass spectrometry data for candidate proteins. Within the tested CCAN proteins (Ame1/Chl4/Cnn1/Wip1/Ctf3), the highest amounts of Cse4 were co-purified by using Ame1-FLAG as bait protein (Figure 8), indicating a close association of COMA proteins with centromeric nucleosomes. Moreover, we reasoned that Mif2 was not required for this association as the detected amounts of Mif2 in Ame1-FLAG pulldowns were ten times lower than the amounts of Cse4. To assess whether COMA proteins directly interact with Cse4-NCP, I performed an XLMS guided *in vitro* reconstitution approach. I extended the analysis by adding Mif2, to serve as a positive control for association with Cse4. In total 115 inter-subunit crosslinks between the nine proteins were identified (Figure 26). Crosslinks within COMA complex and from the Mif2 signature motif to the Cse4 C-terminus (24) are in agreement with previously described interfaces. Strikingly, we detected numerous crosslinks between Okp1 and Cse4. Apart from that, Okp1, with the exception of a single crosslink between Ame1 and H2A, was the only COMA protein that crosslinked to additional histone proteins. This clearly suggested that in addition to Mif2, the budding yeast protein Okp1 binds directly to Cse4-NCP.

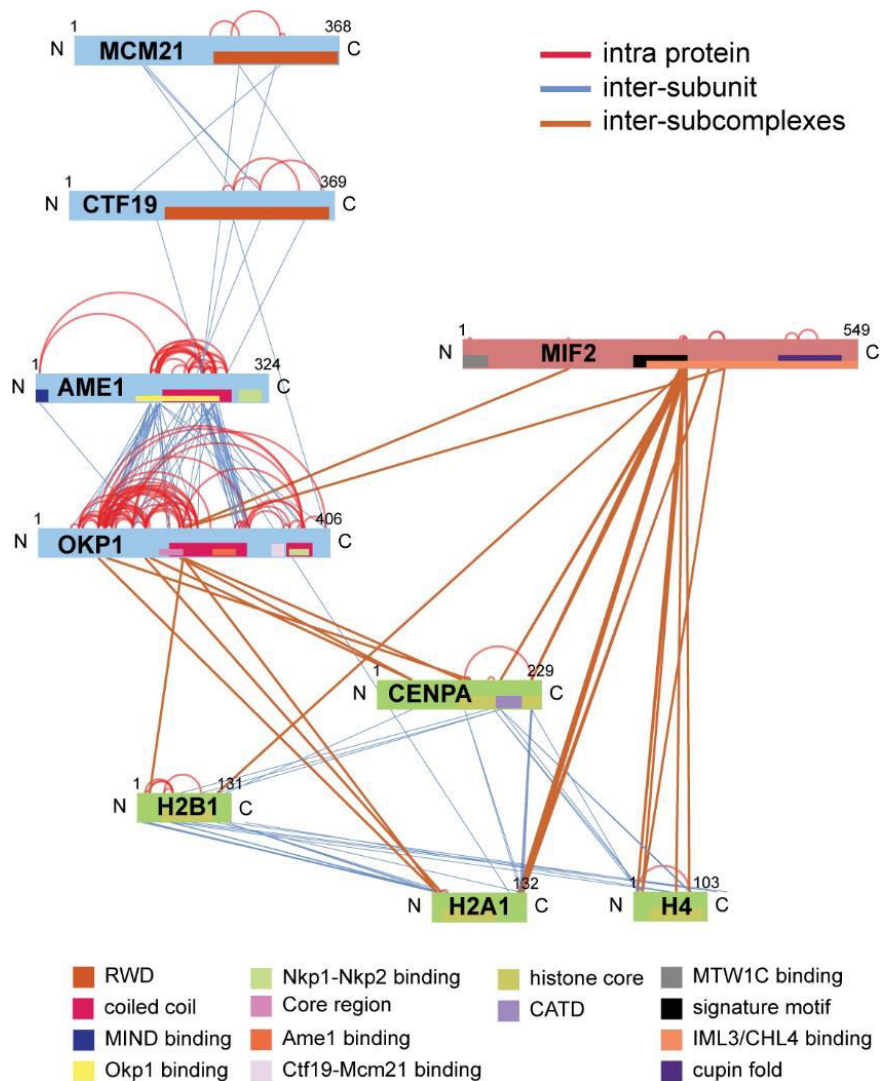


**Figure 26. XLMS analysis identifies Okp1 as a direct binding partner of Cse4-NCPs.** XLMS analysis of the *in vitro* reconstituted Cse4-NCPs together with COMA complex and Mif2. Purified complexes were mixed at equimolar amounts prior to crosslinking with BS3. Detected crosslinks are visualized as network diagram as described (Figure 13).

To validate this observation and further characterize the interaction between the COMA complex and Cse4-NCPs we performed size exclusion chromatography (SEC) studies. As expected, Ame1/Okp1 combined with Cse4-NCPs co-eluted at earlier volumes when compared to the single complex runs (Figure 27). Strikingly, we did not observe a shift towards earlier fractions for Ame1/Okp1 combined with H3-NCP (Figure 27). As Cse4-NCPs and H3-NCPs were reconstituted using the same 601 DNA sequence, we reasoned that the observed interaction is specific towards Cse4-NCP and not mediated solely by the affinity of Ame1 towards AT-rich centromeric DNA, as recently proposed (25). Collectively, the SEC experiments verified our XLMS data and, more importantly, highlighted the selective property of the association.

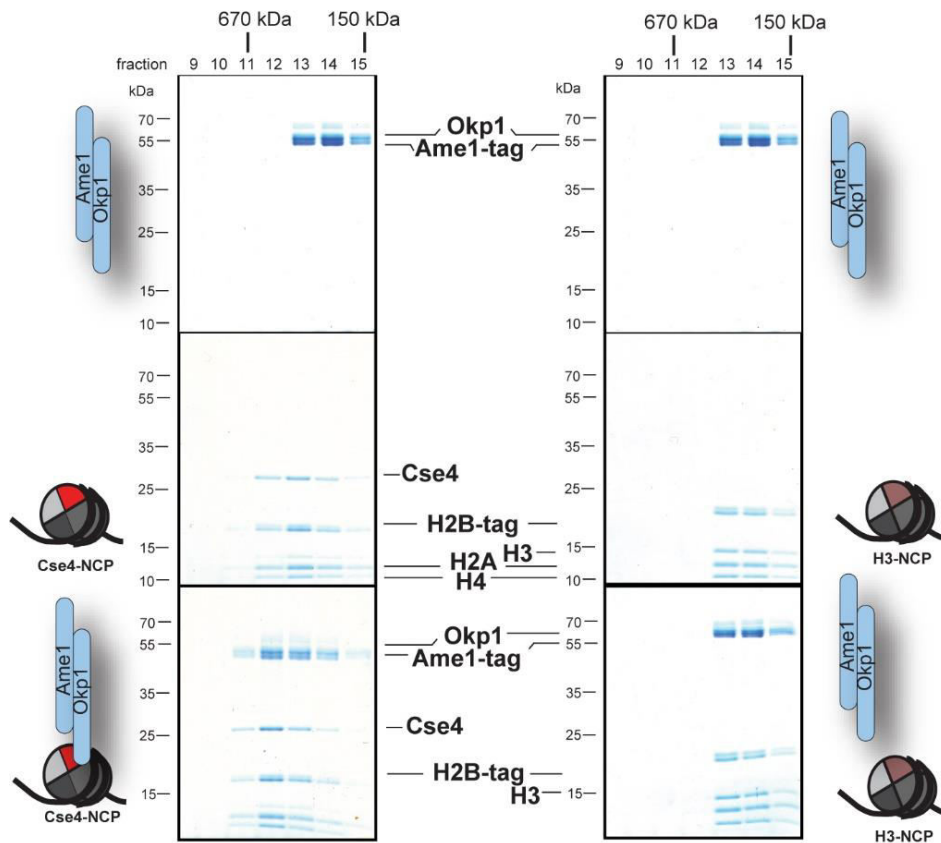


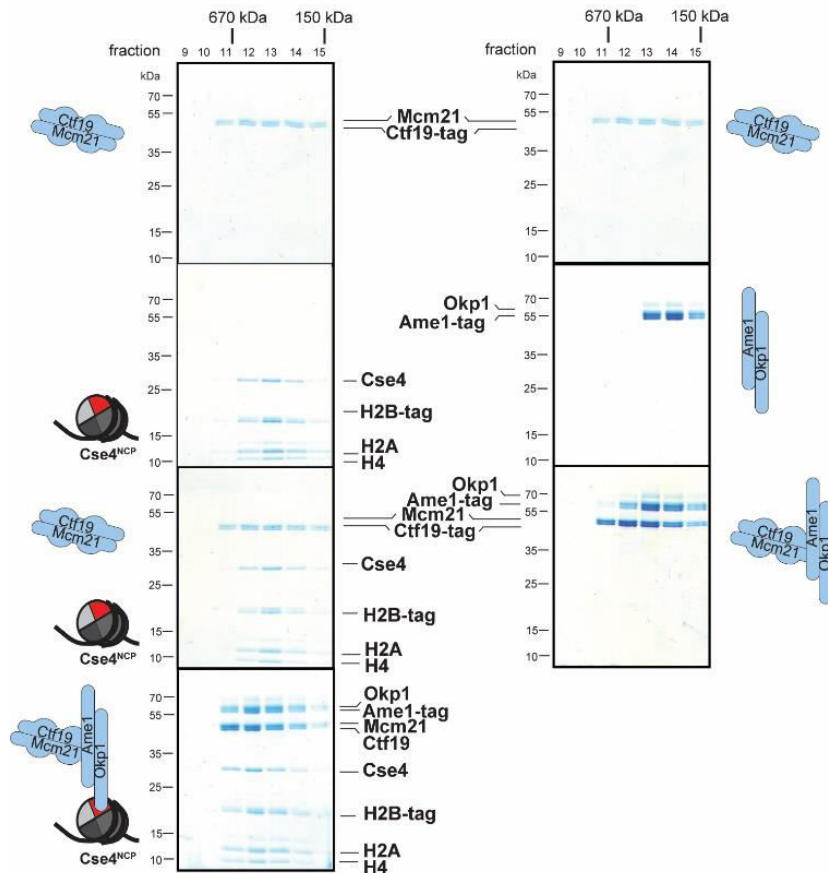
**Figure 27.** The Ame1/Okp1 heterodimer selectively and exclusively interacts with Cse4 containing nucleosomes in size exclusion experiments. Individual recombinant protein complexes or indicated equimolar mixtures were separated by size exclusion chromatography and fractions were analyzed by SDS-PAGE and coomassie staining. Ame1/Okp1 shifted to earlier elution volumes in the presence of Cse4-NCP. No co-migration was detected when Ame1/Okp1 was combined with H3-NCP.

### 3.5.1. The Ame1/Okp1 heterodimer links other kinetochore proteins directly to Cse4 containing nucleosomes

To investigate whether Ame1/Okp1 is able to target other kinetochore proteins to centromeric Cse4-NCPs we performed further SEC analysis including the other COMA complex proteins Ctf19/Mcm21 and MTW1c (25). As expected, Ctf19/Mcm21 did not directly interact with Cse4-NCP in the absence of Ame1/Okp1 (Figure 28A), however, in the presence of Ame1/Okp1 a stable COMA:Cse4-NCP complex was established (Figure 28A). More importantly, we observed the formation of a supramolecular complex between Ame1/Okp1:Cse4-NCP:MTW1c (Figure 28B), suggesting that Ame1/Okp1 provides a direct link for the KMN to the centromeric nucleosome. This is in agreement with a recent study showing that point mutations in the Cse4 N-terminus (Cse4-R37A), which reduce Ame1/Okp1 binding, cause decreased recruitment of Mtw1 to the centromere. Notably, the decreased recruitment could be restored by Okp1 suppressor mutants (132).



A



B

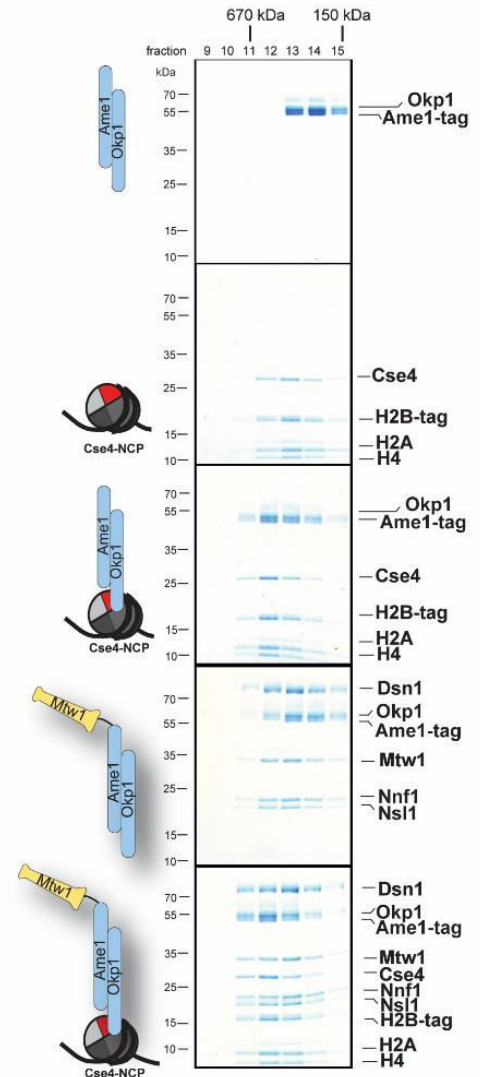
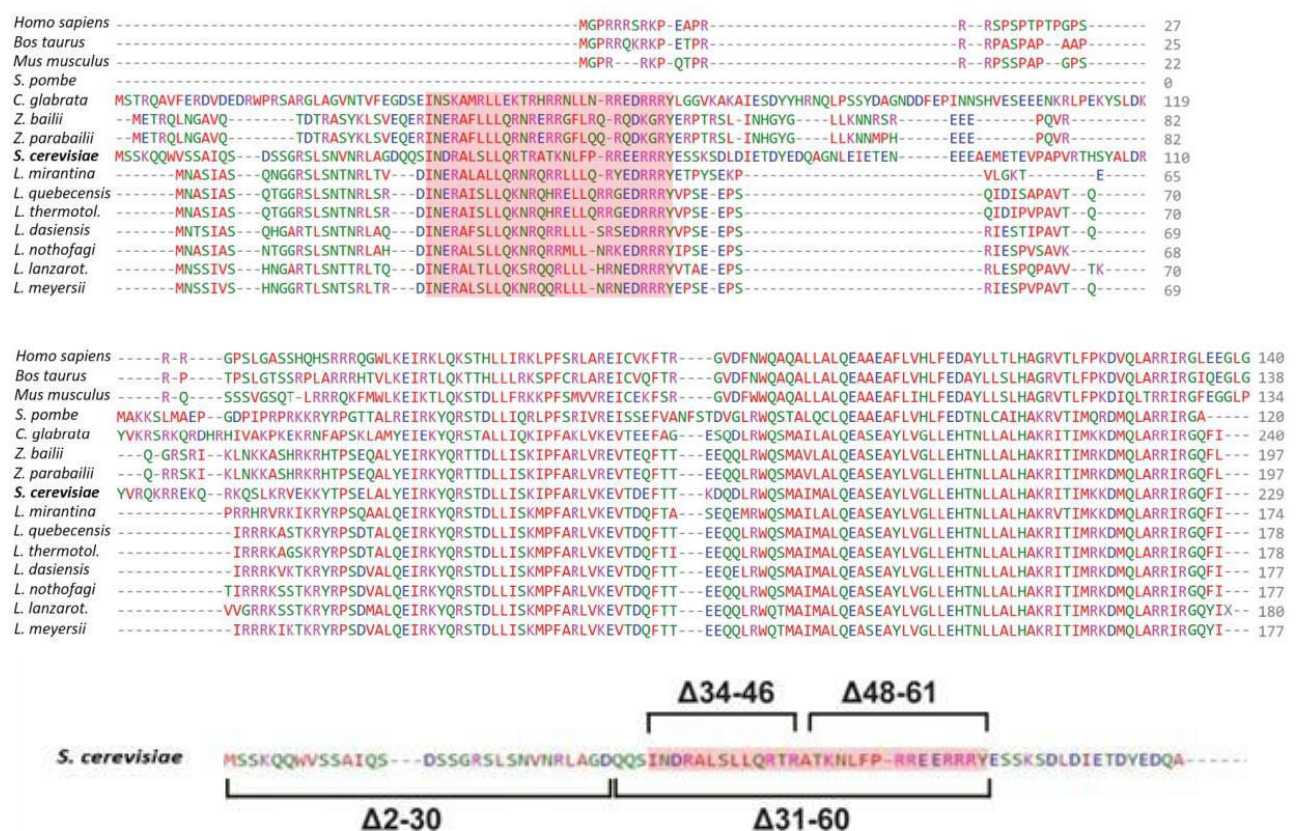


**Figure 28. In complex with Ame1/Okp1 the Ctf19/Mcm21 heterodimer and MTW1c are stably linked to Cse4-NCP in size exclusion experiments.** Individual recombinant protein complexes or indicated equimolar mixtures were separated by size exclusion chromatography and fractions were analyzed by SDS-PAGE and coomassie staining. (A) A distinct shift of Ame1/Okp1 by one fraction to higher molecular weights in the presence of Ctf19/Mcm21 indicated formation of the COMA complex. Cse4-NCP did not directly associate with Ctf19/Mcm21 in the absence of Ame1/Okp1. Co-migration of Ctf19/Mcm21 with Cse4-NCP was observed in the presence of Ame1/Okp1 as seen by the shift of the Ame1/Okp1 and the Ctf19/Mcm21 peak to fractions 11/12. (B) Ame1/Okp1 shifts to earlier fractions when combined either with MTW1c or Cse4-NCP. Combined, the respective proteins form a stable supramolecular complex.

### 3.5.2. A small, essential, N-terminal region in Cse4 is required for binding the Ame1/Okp1 heterodimer

Next, we aimed to elucidate the contributing binding interfaces of Okp1 and Cse4. The binding discrimination observed between H3 and Cse4 containing nucleosomes already indicated that the selective interaction interface resides outside of the histone fold domain

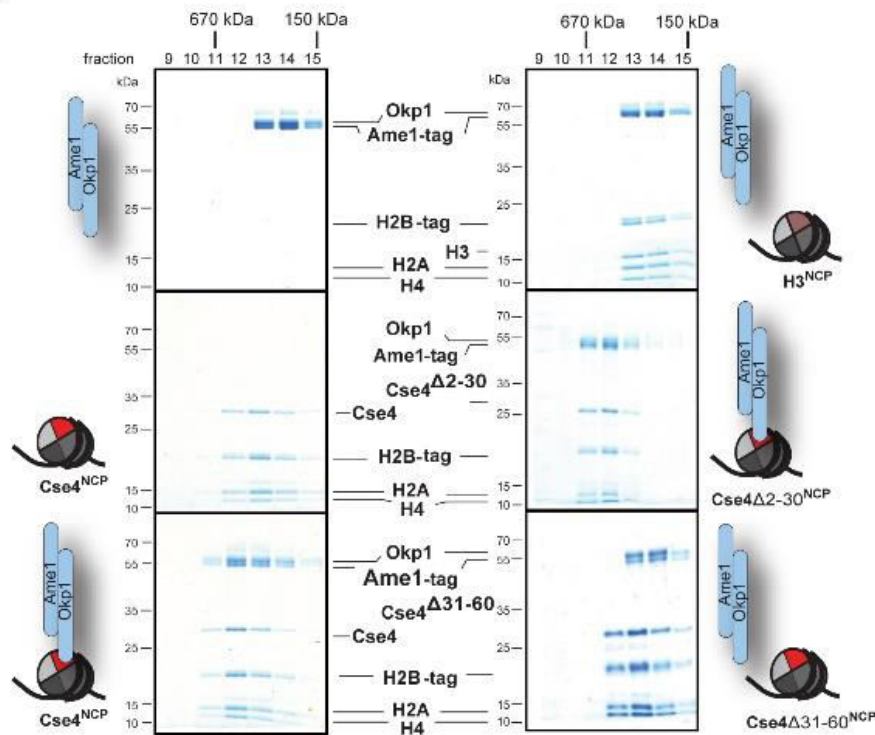
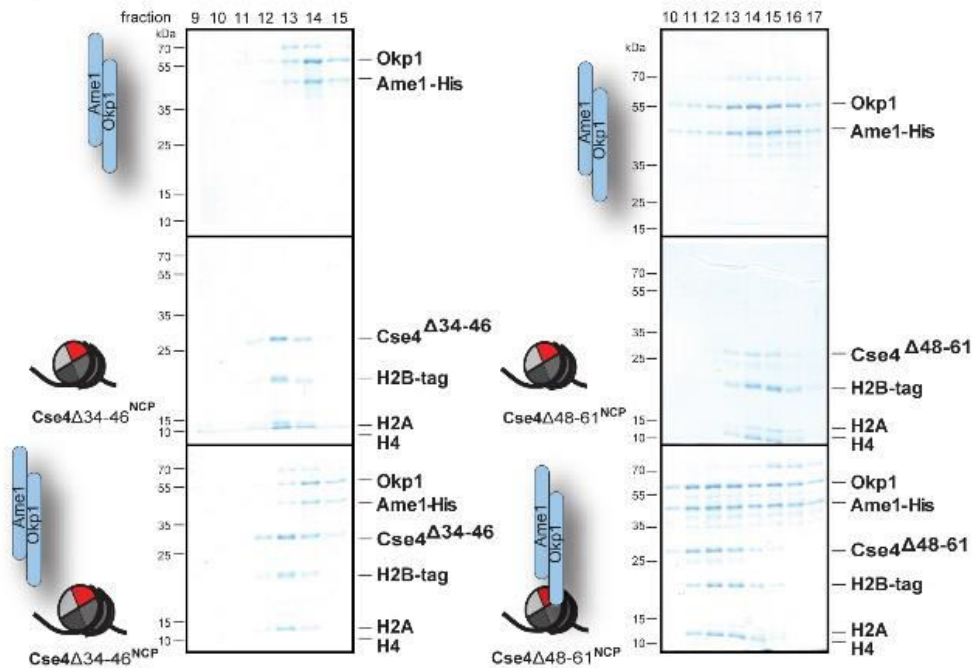
(HFD), which is structurally homologous between the two histone variants. Moreover, we detected two crosslinks between Okp1 and the divergent N-terminus of Cse4 (Figure 24). As Ame1 and Okp1 are essential for viability in budding yeast, we assumed that the respective Cse4 binding interface is conserved among yeast species. Multiple sequence alignment (MSA) including representatives of the budding yeast family (*Saccharomycetaceae*), three mammalian and the *Schizosaccharomyces pombe* CENP-A sequences highlighted a yeast specific conserved region absent in the other species, encompassing amino acids 34-61 of *S. cerevisiae* Cse4 (Figure 29). Yeast genetic experiments have already shown that amino acids 28 to 60 are sufficient to provide the essential function of the Cse4 N-terminus (133), though do not provide an explanation for the mechanistic role of this region.



**Figure 29. Multiple Sequence Alignment (MSA) of Cse4 protein sequences reveals a conserved N-terminal patch in *Saccharomycetaceae*, which is absent in mammalian CENP-A homologs.** (A) A MSA of Cse4 proteins from interrelated budding yeast species was conducted with Clustal W. Protein sequences with the highest similarity to *Saccharomyces cerevisiae* Cse4, determined by a protein BLAST search, the *S. pombe* and three mammalian CENP-A protein sequences were included in the alignment. Within the 135 amino acids long N-terminal tail of Cse4, specific to CENP-A homologs in *Saccharomycetaceae*, we identified a patch including amino acids 34 to 61 (highlighted in pink) as conserved in interrelated yeasts (amino acid color scheme assigned by Clustal W). Scheme of the Cse4 deletion mutants. Two sequential deletions cover the first 90 N-terminal amino acids and two deletions split the conserved patch (highlighted in pink) to narrow down the potential binding site for the Ame1/Okp1 heterodimer.

To confirm our findings and assess whether the unveiled domain mediates the interaction with the Ame1/Okp1 heterodimer, we generated N-terminal deletion mutants of Cse4 for SEC

analysis. As all purified mutants as well as wild type Cse4-NCP display a similar elution profile, we reasoned that stability, folding and incorporation into the nucleosome structure is not impaired. While removing the first 30 N-terminal residues of Cse4 (Cse4 $\Delta$ 2-30) did not affect binding to Ame1/Okp1, deletion of the essential and conserved N-terminal region (Cse4 $\Delta$ 31-60) completely abrogated Ame1/Okp1:Cse4-NCP complex formation (Figure 30A). Next, we tried to further constrain the interaction interface by generating mutants with half of the essential domain deleted, Cse4 $\Delta$ 34-46 and Cse4 $\Delta$ 48-61. Cse4 $\Delta$ 48-61 formed a stable stoichiometric complex with Ame1/Okp1 (Figure 30B), though we did not observe any co-migration in our SEC analysis for Cse4 $\Delta$ 34-46 (Figure 30B). Taken together, the XLMS analysis and the results from SEC suggest that the conserved N-terminal motif is the primary, if not sole site of interaction with Ame1/Okp1. Consistently, recent SEC analysis showed direct interaction between Ame1/Okp1 with a Cse4 N-terminal peptide (aa 21-219) (132).

**A****B**

**Figure 30. Size exclusion experiments reveal the requirement of a short (13 aa) N-terminal region in Cse4 for interaction with the Ame1/Okp1 heterodimer.** Individual recombinant protein complexes or indicated equimolar mixtures were separated by size exclusion chromatography. Eluted complexes were analyzed by SDS-PAGE and coomassie staining. (A) The Ame1/Okp1 heterodimer co-migrates with Cse4 $\Delta$ 2-30-NCPs, no complex formation is observed when combined with Cse4 $\Delta$ 31-60-NCPs. (B) Ame1/Okp1 shifts to earlier volumes when incubated with Cse4 $\Delta$ 34-46-NCPs. In the presence of Cse4 $\Delta$ 48-61-NCPs no shift of Ame1/Okp1 is detected.

### 3.5.3. The small N-terminal region in Cse4, required for binding the Ame1/Okp1 heterodimer *in vitro*, is essential for viability

We hypothesized that the indispensable function of the Cse4 N-terminus in budding yeast is its ability to recruit the essential Ame1/Okp1 heterodimer, thereby enabling proper kinetochore assembly. In this model, the minimal region for disturbing the interaction *in vitro* should also cause a lethal phenotype *in vivo*. To test this, we depleted endogenous Cse4 from the nucleus using the anchor-away technique and performed rescue experiments by ectopically expressing the same Cse4 constructs that were used in the SEC analysis. Indeed the mutants that did not form a stable complex with Ame1/Okp1 *in vitro*, Cse4 $\Delta$ 34-46 and Cse4 $\Delta$ 31-60, could not restore viability, while expression of Cse4 construct Cse4 $\Delta$ 47-61 resulted in normal growth in every dilution tested (Figure 31). The observed correlation between the inability of the Cse4 mutants to restore growth and to stably interact with Ame1/Okp1, supports our model that recruitment of the Ame1/Okp1 heterodimer to Cse4-NCPs, mediated by a defined (13 aa) N-terminal region, is essential for viability.

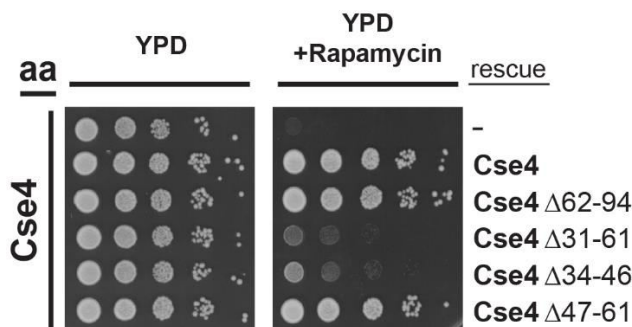


**Figure 31. Rescue experiments reveal the requirement of the short (13 aa) N-terminal patch of Cse4 that mediates Ame1/Okp1 binding for viability.** Growth assay of Cse4-FRB anchor-away (AA) strains carrying constructs for the ectopical expression of wildtype and indicated mutant proteins. Cell growth of serial dilutions (1:10) was analyzed on YPD plates at 30 °C in the absence and presence of rapamycin. Cells expressing Cse4WT, Cse4 $\Delta$ 62-94 or Cse4 $\Delta$ 48-61 show normal growth, while Cse4 $\Delta$ 31-60, Cse4 $\Delta$ 34-46 fail to restore viability. The displayed spotting assay was carried out by Sylvie Singh.

### 3.5.4. The Okp1 core domain is required for Cse4 binding

We next aimed to narrow down the Cse4 binding site in Okp1. Crosslinking analysis pointed towards a region encompassing the previously described Okp1 core domain (aa 166-211) (Figure 26), which is essential for cell growth (34). A multiple sequence alignment analysis of Okp1 reveals that this region overlaps with a conserved stretch (aa 127-184) (Figure 32A). Additionally, secondary structure analysis predicted two alpha helices within this region

(helix1 aa 130-140, helix2 aa 156-188) (Figure 32A). Accordingly, we generated three partly overlapping deletion mutants spanning the conserved patch (Okp1 $\Delta$ 123-147, Okp1 $\Delta$ 140-170, Okp1 $\Delta$ 163-187). All mutants were successfully isolated together with Ame1 as the corresponding Ame1/Okp1 complexes from *E. coli*. Therefore, we concluded that the deletions did not affect Ame1/Okp1 heterodimer formation. To probe the interaction of Ame1/Okp1 wildtype and mutants with Cse4 nucleosomes an EMSA was performed by Mia Potocnjak. While Ame1/Okp1 $\Delta$ 123-147 showed clear interaction with Cse4-NCP comparable to the wildtype Ame1/Okp1 complex, Ame1/Okp1 $\Delta$ 140-170 showed only weak association (Figure 32B). Strikingly, no interaction was detected with Ame1/Okp1 $\Delta$ 163-187, suggesting that Okp1 helix 2 is required for Cse4 binding. To explore whether helix 2 is sufficient for binding I generated a peptide of Okp1 (140-192) encompassing the respective region. In order to detect a significant shift in the EMSA experiment in case of Cse4-NCP binding, the peptide was fused to GFP. However, in my experimental setup no interaction was observed, even when GFP-Okp1-peptide(140-192) was applied in excess (1:10 and 1:100) (Figure 32C). Still, I can not exclude the possibility, that GFP sterically disrupts the interaction. Moreover, the applied peptide might possess a different fold than that represented in full length Okp1. Additionally, other regions in Okp1 or Ame1 could be contributing or stabilizing the interaction with Cse4.

### **3.5.5. The Okp1 core domain required for Cse4 binding is essential for cell growth**

Finally, to further support our model which states that direct recruitment of Ame1/Okp1 by Cse4-NCP is essential in budding yeast, we used our Ame1/Okp1 mutants in rescue experiments applying the anchor away technique as described above. Strikingly, cells expressing Okp1 $\Delta$ 122-147 which interacts with Cse4-NCP in our EMSA, display normal growth (Figure 32D). However, the Cse4-NCP binding deficient mutant, Okp1 $\Delta$ 163-187, fails to restore viability (Figure 32D). Taken together our EMSA and rescue experiments show that Okp1 aa 163-187 are required for mediating association with Cse4-NCP, highlighting again that recognition of Ame1/Okp1 by Cse4-NCP might be essential in budding yeast.

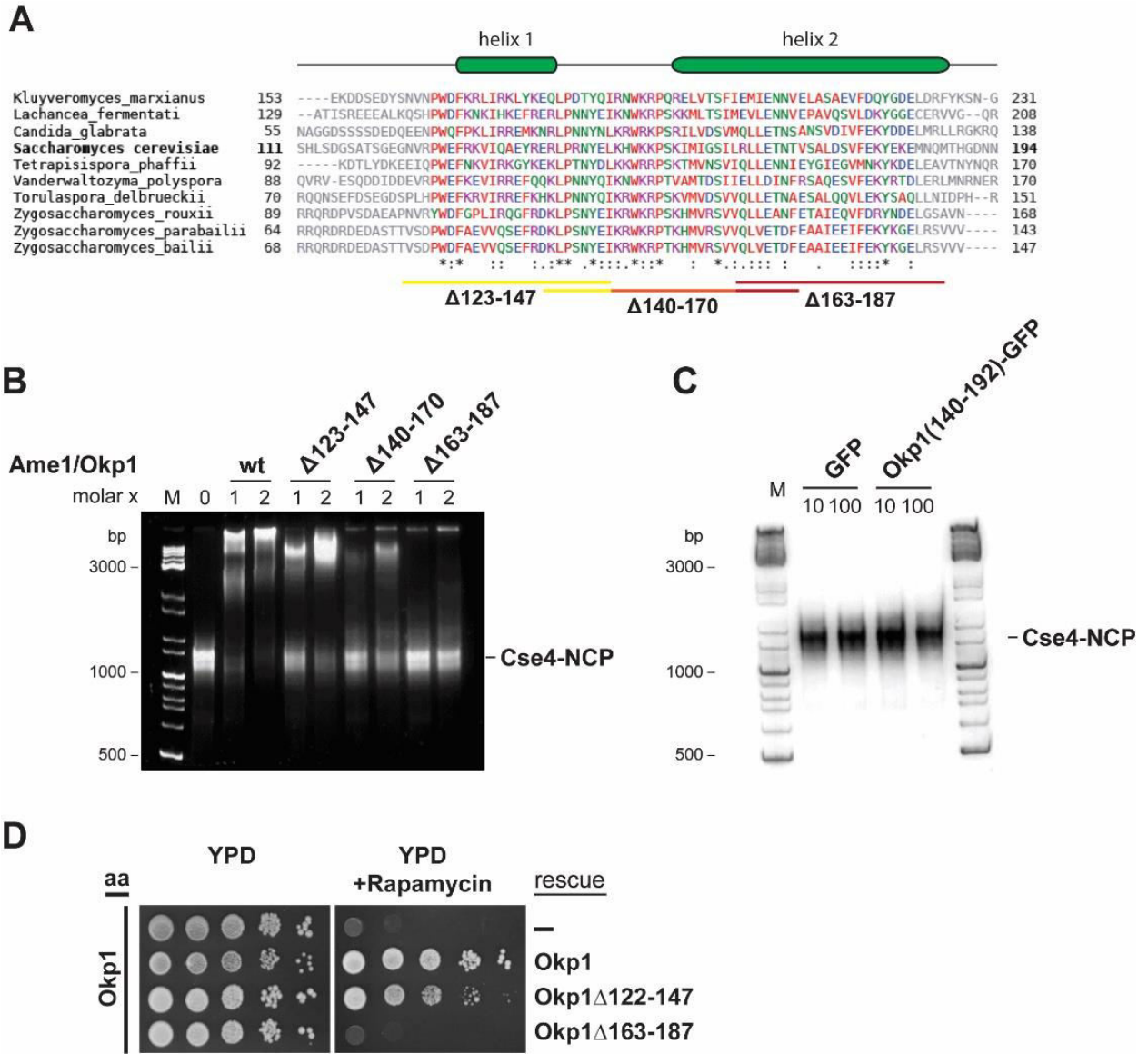


**Figure 32. Ame1/Okp1:Cse4-NCP complex formation requires the Okp1 core domain.** (A) Multiple sequence alignment (MSA) of Okp1 amino acid sequences from related yeast species. Amino acid color scheme was assigned by Clustal W. Alpha helical regions predicted by Jpred are displayed as green bars above the sequences. The overlapping Okp1 deletion mutants are depicted as lines below the alignment. (B) EMSA monitoring binding of wildtype and mutant Ame1/Okp1 proteins to Cse4-NCP. Recombinant complexes were pre-incubated at a 1:1 or 1:2 molar ratio. For visualizing the DNA SYBR Gold was applied. (C) Association of GFP-Okp1(aa 140-192) with Cse4-NCP was tested via EMSA. Recombinant complexes were pre-incubated at a 1:10 or 1:100 molar ratio. For visualizing the DNA SYBR Gold was applied. (D) Growth assay of Okp1-FRB anchor-away strains carrying the indicated ectopical expression constructs. Cell viability of serial dilutions (1:10) was analyzed on YPD plates at 30 °C in the absence and presence of rapamycin. Cells expressing Okp1WT and Okp1Δ122-147 show normal growth, while Okp1Δ163-187 fails to restore viability. The displayed spotting assay was carried out by Sylvie Singh.

Partial results of the work presented in this thesis have been already published in eLife (see appendix). The published work describes the direct interaction between COMA complex and Cse4-NCP and how this interaction positions Sli15/Ipl1 at the budding yeast inner kinetochore.

The published results include the sections 3.3 – 3.3.7 and 3.5-3.5.5. In this thesis the results of these sections are discussed independently of the discussion in the publication.



## 4. Discussion

One main goal of this work was the characterization of the inner kinetochore topology and its linkages to the centromeric nucleosome and the outer kinetochore. Although biochemical reconstitution and protein crystallography and cryo-electron microscopy provided valuable insights into the subcomplexes, a comprehensive map of protein connectivities of the kinetochore complexes was still missing. Chemical cross-linking combined with mass spectrometry had the potential to acquire distance restraints that indicated the protein connectivity within native kinetochore complexes at the level of protein motifs.

### 4.1. The Cnn1/Wip1:CTF3c complex links COMA complex to the NDC80c

A previously identified hub for interactions between inner and outer kinetochore proteins is the MTW1c. The N-terminal Mtw1 head domain provides binding interfaces for the extended N-terminal tails of Mif2 and Ame1 (25, 49). The C-termini of the tetrameric MTW1c mediate the recruitment of the outer kinetochore complexes NDC80c and Spc105/Kre28 (25, 26, 49, 62). Thus, the MTW1c is a hub that links the inner to the outer kinetochore (25). Interestingly, the non-essential histone fold protein Cnn1 establishes an alternative pathway to recruit the NDC80c to the kinetochore. A Cnn1 N-terminal peptide motif interacts with the hydrophobic pocket on the globular Spc24/25 domains and competes with the C-terminus of the MTW1c subunit Dsn1 (48). How Cnn1 itself is tethered at the inner kinetochore and the functional importance of its NDC80c recruitment was unclear at the time. Label free mass-spectrometry showed the relative protein abundancies in the various pulldowns and highlighted some novel dependencies for inter-complex interactions (Figure 8). In Ame1 pulldowns we detected histones, in particular Cse4, among the most abundant copurifying proteins, indicating a close association with centromeric nucleosomes. Ctf3-FLAG isolation co-purified predominantly components of the COMA complex and Cnn1/Wip1 at similar amounts. In Cnn1 pulldowns the most abundant proteins were subunits of the CTF3c followed by the COMA complex and KMN proteins. Taken together the data suggested that Cnn1/Wip1 directly links the COMA complex through CTF3c to KMN components.

Spatial restraints acquired by XLMS supported the initial observation that this pathway could represent a linkage of the microtubule binding NDC80c to the centromeric chromatin independent of MTW1c (Figure 10).

Cnn1 has a central role by interacting with the Spc24/25 heads of NDC80c (48) and CTF3c (32), which may interact with subunits of the COMA complex as indicated by multiple crosslinks (Figure 10). The crosslinks of Cnn1 to Spc24/25 were detected at its N-terminus, which is in agreement with the literature (48). Strikingly, Cnn1 crosslinked to each subunit of the CTF3c (Ctf3, Mcm16, Mcm22) with all crosslinks residing in its N-terminus. In parallel, another group performed biochemical and structural XLMS analysis of reconstituted CTF3c together with Cnn1/Wip1 and NDC80c, revealing a similar crosslink map (32). In our Cnn1/Wip1-FLAG pulldowns the histone fold containing proteins Mhf1/Mhf2 were not co-purified at detectable amounts. Hence, we also did not detect any crosslinks to Mhf1/Mhf2. For this reason, we conclude that these two proteins are not required for establishing the described linkage pathway COMA:CTF3c:Wip/Cnn1:NDC80c. Although we can not exclude that interactions occur under certain cellular conditions, our data provides evidence that in contrast to their human orthologues (125) Cnn1/Wip1:Mhf1/Mhf2 are not primarily assembled through their histone folds into a nucleosome like structure. Supporting this assumption, attempts to show interactions between Cnn1/Wip1:Mhf1/Mhf2 using *in vitro* reconstituted budding yeast proteins were not successful (32).

In Cnn1-FLAG pulldowns the most abundant proteins detected were subunits of the CTF3c at levels of 23 - 66 % compared to the bait (Figure 8). Histone proteins were detected at ~ 5 %. Moreover, the entire N-terminal domain of Cnn1 crosslinked to the N-termini of Mcm22/Mcm16 and the Ctf3 C-terminus (Figure 10). Therefore, we assume that Cnn1/Wip1 are not positioned directly at centromeric nucleosomes. Presumably, kinetochore tethering of Cnn1/Wip1 requires concomitant binding to CTF3c proteins (Figure 10) rather than depending on direct interactions with DNA or nucleosomal proteins. In agreement with this model, the kinetochore recruitment of Cnn1/Wip1 is greatly reduced in a Ctf3 deletion mutant strain (32). Likewise, human orthologues CENP-TW bind directly to CENP-CHIKMLN which is required for kinetochore targeting (44). Taken together our *in vivo* data coincides with studies performed *in vitro* (32) and provides further evidence that cooperative interactions tether the KMN network to the CTF19c and Cse4 containing nucleosomes.

## 4.2. The Ame1/Okp1 heterodimer selectively binds Cse4 containing nucleosomes

Label free quantitative mass spectrometry analysis of native stable subcomplexes derived from Ame1-, Chl4-, Ctf3-, Cnn1-, Wip1- or Mif2 pulldowns enabled us to screen the CTF19c for potential direct interactors of Cse4. We found that in addition to Mif2, Ame1 coprecipitates high levels of Cse4 containing nucleosomes from cell lysates (Figure 8). The low amounts of Mif2 in Ame1-FLAG preparations provided evidence that the recruitment of COMA proteins to Cse4-NCPs is independent of Mif2. By using XLMS and SEC analysis with *in vitro* reconstituted complexes, we revealed that Ame1/Okp1 directly and selectively interacts with Cse4-NCP (Figure 26, Figure 27). Previously, Ame1/Okp1 have been shown to bind DNA *in vitro* (25). However the observed ability of Ame1/Okp1 to clearly discriminate between H3- and Cse4-NCPs suggested that DNA binding is not sufficient for Ame1/Okp1 recruitment.

Earlier yeast two hybrid studies suggested a direct interaction of Ctf19/Mcm21 with Cse4 (55). However, we were unable to detect such an interaction *in vitro*. We showed recruitment of Ctf19/Mcm21 to Cse4-NCPs via Ame1/Okp1 (Figure 28A). This is consistent with the fact that in *ctf19Δ* and *mcm21Δ* cells kinetochore localization of Ame1/Okp1 is not reduced (19). Instead, *ame1-4* and *okp1-5* temperature sensitive mutants display mis-localization of Ctf19 and Mcm21 (51). Hence, our results clearly depict that Ctf19/Mcm21 is linked via Ame1/Okp1 to the Cse4 containing nucleosome.

We further narrowed down the binding interface between Ame1/Okp1 and Cse4, identifying the aa 163-187 of the Okp1 core domain and the aa 34-46 within the essential Cse4 N-terminus to be required for establishing the interaction *in vitro* (Figure 30B, Figure 32B). In agreement with our data, a parallel study showed direct binding of a synthetic Cse4 peptide (aa 33–110) to Ame1/Okp1 (132). The extended (130 aa) yeast specific Cse4 N-terminus harbors a conserved END (aa 28 to 60), which is required for viability (133). In SEC experiments the Cse4 aa 34-46 patch was the minimal motif required for the interaction with Ame1/Okp1 (Figure 30) and was essential for viability (Figure 31). Hence, our findings suggest that the respective interaction is essential in budding yeast. Furthermore, the Cse4-NCP:Ame1/Okp1 complex stably associates with Ctf19/Mcm21 and MTW1c (Figure 28B). Our *in vitro* data agrees with a recent study, which showed that point mutations in the Cse4 N-terminus (Cse4-R37A), reducing Ame1/Okp1 binding, affect the recruitment of Mtw1 to the centromere. Notably, the decreased Mtw1 recruitment could be restored by Okp1

suppressor mutants (132). Taken together, our findings indicate that Ame1/Okp1 provides an essential link for KMN proteins to the centromeric nucleosome. KMN recruitment via Mif2 and Cnn1 are redundant anchoring pathways and only become essential if one is compromised (25, 47).

### **4.3. Ame1/Okp1 represent a centerpiece of kinetochore assembly in budding yeast**

In vertebrates, CENP-LN and CENP-C (24, 36, 41) have been shown to specifically interact with CENP-A. CENP-C binds the divergent C-terminal CENP-A tail and the acidic patches of H2A and H2B (24) and CENP-N associates with the CENP-A centromere targeting domain (CATD) (36). Up to now, in budding yeast only Mif2 was identified as direct binding partner of Cse4. In this study, I revealed the direct and selective binding of Ame1/Okp1 to Cse4-NCP and characterized the sequence motifs mediating this interaction.

Label free mass spectrometry analysis of Chl4-FLAG pull-downs showed that Cse4 copurified at levels just above > 1 % of the bait, indicating that there is no tight association of Chl4/Iml3 with Cse4-NCP (Figure 8). Furthermore, our XLMS data suggested that Chl4/Iml3 is recruited via COMA proteins to the centromere. This is consistent with the fact that proper centromere localization of Chl4/Iml3 requires Ctf19 (33). Moreover, Ame1 and Okp1 are essential while Chl4/Iml3 are dispensable for viability. Therefore, we propose a dominant and upstream role of Ame1/Okp1 in mediating the hierarchical assembly of the kinetochore in budding yeast and suggest Chl4/Iml3 acting further downstream in this process. My crosslinking data of native kinetochore complexes displays possible interaction surfaces between the COMA complex and Chl4/Iml3 (Figure 10) that might facilitate its kinetochore localization.

In humans, the hierarchical order of kinetochore assembly is different. Recruitment of CENP-OPQRU to kinetochores requires a joint interface formed by CENP-HIKM and CENP-LN (44, 52, 53) and loss of the complex does not affect localization of other inner kinetochore proteins. Moreover, while Ame1/Okp1 are essential in budding yeast, CENP-U/Q knockout DT40 cells (21) are viable. Notably, a requirement of CENP-U for viability was observed in mouse embryonic stem cells, but not in mouse fibroblasts (56). Moreover, our data provided an explanation for the essential role of the END in the extended Cse4 N-terminus, and underlined the key role of Ame1/Okp1 within the budding yeast kinetochore. Thus, we reason that Ame1/Okp1 recruitment to the Cse4 N-terminus is a yeast specific feature.

Multiple sequence alignment clearly displayed that the Cse4 N-terminus is unique to inter-related budding yeasts and is not homologous to the N-terminus of CENP-A of metazoans (Figure 29). It will be interesting to determine the precise mechanism of how CENP-UQ is tethered to the inner kinetochore and its role in kinetochore function.

We suggest that the slight differences in composition and function of kinetochore subcomplexes between budding yeast and humans reflect the requirements of increased stability for the single kinetochore unit assembled at point centromeres. In contrast to yeast, higher organisms have evolved regional centromeres spanning up to mega bases of repetitive DNA stretches (134) with interspersed CENP-A and H3-containing nucleosomes (135). Within these regional centromeres an array of kinetochore units may be formed, each providing an attachment site for 3 to 30 microtubules (16). Therefore, regional centromeres may provide the foundation for a more dynamic and less stringent assembly.

#### **4.4. Inner kinetochore subcomplexes support Sli15/Ipl1 localization**

Kinetochore substrate phosphorylation by Ipl1 mediates the destabilization of mis-attached kinetochores and thereby implements correction of erroneous microtubule attachments (82). How the lack of pulling force at mis-attached kinetochores is sensed and how the CPC positions itself at centromeres and kinetochores is still poorly understood. The spatial separation model suggests that outer kinetochore proteins become physically separated from Ipl1 kinase, located at centromeres as tension is exerted across kinetochores (103). However, this model was challenged by the identification of a Sli15 $\Delta$ N mutant which is deficient in centromere targeting, but conferred normal viability and established proper chromosome biorientation (86). An alternative hypothesis is that the functionally relevant pool of Ipl1 resides at microtubules. This is built on the observation that Sli15<sup>INCENP</sup> binds microtubules (88) and Sli15 $\Delta$ N is enriched at pre-anaphase microtubules (86). Yet, another model suggests, that Ipl1 performs its functions located near or at kinetochores (106) which implies that CPC may directly interact with kinetochore subunits. Supporting this theory, a role of Ame1 in recruiting Sli15 proximal to kinetochores has been shown (51). While Ame1/Okp1 are required for viability and crucial for kinetochore assembly at point centromeres as shown in this thesis, the Ctf19/Mcm21 subcomplex is not essential. Nevertheless, deletion mutants of Ctf19 and Mcm21 display chromosome segregation and cohesion defects (30, 55, 128, 136, 137). Strikingly, Ctf19 and Mcm21 deletions become synthetic lethal in case Sli15 is not targeted to the centromere through Bir1 (86). Due to

this finding we hypothesized, that there is a Bir1 independent recruiting mechanism of Sli15/Ipl1 to centromeres or inner kinetochores.

In my fishing experiment followed by *in vitro* reconstitution, crosslinking and binding assays I identified inner kinetochore proteins Ame1/Okp1, Ctf19/Mcm21 and Mif2 as direct interaction partners of Sli15/Ipl1 (Figure 11B, Figure 13, Figure 14, Figure 17). While the binding surfaces of Ame1/Okp1 and Mif2 have not been determined, I successfully identified the C-terminal RWD domain of Ctf19 as Sli15/Ipl1 interaction site within Ctf19/Mcm21 *in vitro* (Figure 14B, Figure 22). Intriguingly, we showed that the synthetic lethality between Ctf19/Mcm21 and the *sli15ΔN* mutant is rescued by fusions of Sli15ΔN to COMA proteins, while fusions to other kinetochore proteins such as Ctf3, Cnn1, Mif2 and the outer kinetochore proteins Mtw1, Dsn1 failed to restore viability (Figure 20A). This led us to the conclusion that interactions of Sli15/Ipl1 with COMA proteins mediate the rescue and that the requirement for this interaction only becomes essential in centromere targeting deficient mutant. Our findings suggest that the COMA complex is placed in close proximity to centromeres by the direct binding of Okp1 to the Cse4 N-terminal region.

As COMA-Sli15ΔN fusion constructs lacking the Ipl1 binding (IN-box) domain of Sli15 failed to rescue in our growth assays (Figure 21A), we suggest that proper localization of Ipl1 kinase by the Sli15-COMA interaction is crucial for restoring viability. A functional SAH domain of Sli15 is important for microtubule binding (88, 89) but was not required within the COMA-Sli15ΔN fusion constructs to rescue synthetic lethality (Figure 21A). Thus, we conclude that the SAH domain is dispensable for Ipl1 function localized at the inner kinetochore. Notably, cells lacking at least one functional SAH allele are not viable (88-90, 129), though the molecular basis of this observation remains elusive. As our assays were executed in a *sli15ΔN* background, the endogenous Sli15ΔN rescued synthetic lethality. Our findings suggest that the SAH domain is dispensable during metaphase, but might have an essential role after pre-anaphase when Sli15 translocates to the spindle microtubules (91).

Our results were supported by a recent study (138) which showed that depletion of Mcm21 and Bir1 affects Ipl1 localization to centromeres. The effects upon Mcm21 and Bir1 depletion were additive indicating that COMA and Bir1 represent independent pathways to localize Ipl1 to the centromere/inner kinetochore (138).

The *ctf19ΔN2-30* mutant lacking the receptor domain for the cohesin loading complex Scc2/Scc4 (128) was viable in the *sli15ΔN* background (Figure 19). This indicates that the synthetic lethality of *ctf19Δ/sli15ΔN* cells is due to a defect in establishing pericentromeric

cohesion. Consistently, mutants (such as *dbf4-myc*) which result in weak pericentromeric cohesion display no additive growth defect combined with Bir1 depletion or Sli15 $\Delta$ N (138).

I demonstrated that the C-terminal RWD domain of Ctf19 is required for *in vitro* association (Figure 14B) and is essential for viability in the *sli15 $\Delta$ N* background (Figure 22). Taken together, these findings suggest that the C-terminal RWD domain of Ctf19 mediates Sli15 binding to the inner kinetochore and may position Sli15/Ipl1 next to the centromeric nucleosome.

A recent study showed that when both Bir1 and COMA mediated recruitment of CPC are perturbed, artificial positioning of Sli15 to the inner kinetochore rescues chromosome biorientation defects (138). While we generated various direct fusion constructs in a *ctf19 $\Delta$ /sli15 $\Delta$ N* background, Garcia-Rodriguez et al. applied the rapamycin induced FKBP12–FRB system to target Sli15 $\Delta$ N to Mif2 in Bir1/Mcm21 double deletion mutants. Using this approach, they could show that rapamycin induced interaction of Mif2-FKBP12 rescued Sli15-FRB inner kinetochore/centromere localization and the frequency of chromosome bi-orientation. Although I found a direct interaction between Mif2 and Sli15/Ipl1 *in vitro* (Figure 17), the Mif2-Sli15 $\Delta$ N fusion construct did not restore viability in *CTF19-FRB/sli15 $\Delta$ N* cells (Figure 20A). Consistent with my data the rapamycin induced Sli15 recruitment to Mif2 by the Tanaka lab (138) did also not restore viability, however, rescued defects in chromosome biorientation. In my experiment Sli15/Ipl1 is constitutively recruited to the inner kinetochore by the Mif2-Sli15 $\Delta$ N fusion throughout the whole cell cycle which may affect the cell cycle at different stages and thus, prevent rescue of the synthetic lethality. The importance of a putative Mif2-Sli15 interaction *in vivo* remains elusive. Notably, Mif2 besides Ame1/Okp1 is the only budding yeast inner kinetochore protein shown to directly bind Cse4-NCP. Therefore, Sli15-Mif2 binding could provide a mechanism of positioning Ipl1 kinase close to the point centromere, similar to the Bir1 and COMA mediated recruitment.

Taken together, our results together with the concomitant study (138) suggest that the COMA complex and Bir1 are implicated in promoting chromosome bi-orientation by independently recruiting Sli15/Ipl1 to inner kinetochores and centromeres, respectively. We hypothesize that the interaction with the inner kinetochore might ensure the precise spatial positioning of Ipl1 kinase towards outer kinetochore substrates like Ndc80 and Dam1 in the tensionless state.

In my *in vitro* binding assays I observed that autophosphorylation of Sli15/Ipl1 abrogated the COMA–Sli15/Ipl1 interactions (Figure 14A). But it is unclear whether this phosphorylation dependency is functionally relevant for chromosome segregation.

It will be interesting to determine if the recruitment of Sli15/Ipl1 by COMA proteins to inner kinetochores is conserved among species. The functions of CENP-OPQUR and COMA in kinetochore assembly and regulatory feedback mechanisms might be quite different as phylogenetic analysis showed that CENP-QUR originated more recently (22).

Similar to Sli1 $\Delta$ N, the human orthologue INCENP $\Delta$ N lacking the Survivin-binding domain still facilitates biorientation (139). Moreover, Survivin mutants, which do not form a complex with Aurora-B, display normal growth in DT 40 cells (140). It was also shown that Aurora-B accumulates at ectopic kinetochores that display no association with CENP-A (141). These observations may indicate that also in vertebrates kinetochore proteins mediate localization of Aurora-B/INCENP to inner kinetochores independently of Survivin.

#### **4.5. The interaction of KMN with Sli15/Ipl1 and its putative functional relevance**

The KMN network constitutes together with the DASH/DAM1 complex the core microtubule binding interfaces of the kinetochore in budding yeast (8). They represent the predominant target of the error correction mechanism through phosphorylation by the kinase Ipl1<sup>Aurora-B</sup>. Phosphorylation of the basic Ndc80 N-terminal tail by Ipl1 reduces its affinity to microtubules (97) and promotes resolution of erroneous kinetochore-microtubule attachments that lack tension.

The *in vitro* reconstitution experiments, crosslinking and binding assays revealed that Sli15/Ipl1 directly and stably interacted with the KMN network, in particular, with its subcomplex Spc105/Kre28 (Figure 24, Figure 25A/B). In contrast to the Ame1/Okp1-Sli15 fusion proteins Sli15 tethered to Dsn1 and Mtw1 did not rescue the synthetic lethality of *ctf19 $\Delta$ /sli15 $\Delta$ N* cells. This may indicate that the constitutive localization of Sli15/Ipl1 and phosphorylation of outer kinetochore substrates might interfere with establishing stable microtubule attachments and cell cycle progression. Presumably, the continuous tethering at outer kinetochores prevents KMN de-phosphorylation (95) which is crucial for stabilizing correct microtubule kinetochore attachments. In agreement with this model, Ipl1 delocalizes from outer kinetochores once bi-orientation is established (142). However, we do not exclude the possibility that a temporally intermediate association of Sli15/Ipl1 with Spc105/Kre28 might facilitate phosphorylation of Ndc80. Supporting this theory KNL1 is required for full



Aurora-B activity at kinetochores (143). KNL1 mediates Bub1 accumulation at kinetochores thereby promoting Aurora-B targeting to phosphorylated histone H2A. However, KNL1 truncation mutants, deficient of mediating Bub1 recruitment to kinetochores, promote partial Aurora-B activity (143). This indicates that KNL1 enhances Aurora-B activity independent of Bub1 (143).

A centromere or inner kinetochore located pool of Ipl1 might facilitate error correction according to the spatial separation model. The transient positioning of the CPC at outer kinetochores might fit into an alternative model, which implies a conformational transition of the kinetochore architecture upon the loss of tension that enables access of Ipl1 to outer kinetochore substrates. Consistent with this theory, Ndc80 switches between stretched and compact states in a tension driven manner (104). Future studies will have to rigorously address the implications of these models to explain tension sensing by the CPC.

Strikingly, phosphorylation of Sli15/Ipl1 and KMN either by Ipl1 or Mps1 drastically reduced their association *in vitro* (Figure 25B). Whether a CPC-KMN interaction is also regulated by phosphorylation *in vivo* remains to be addressed.

Further studies will be required to uncover the molecular basis of the complex interplay between the kinetochore, the CPC and the SAC for ensuring proper chromosome segregation. The work described here for successful generation of a recombinant KMN network complex might provide a valuable tool to further address these questions *in vitro*.

#### **4.6. Summary scheme of the findings**

I successfully uncovered the direct interplay of kinetochore assemblies with the error correction mechanism, thereby contributing to a better understanding of how cells establish proper chromosome biorientation. I suggest the following structural model of the budding yeast kinetochore in concert with the CPC. Okp1 directly interacts with the Cse4 N-terminus thereby targeting the COMA complex directly to Cse4-NCP. The COMA complex is directly linked to KMN components through CTF3c:Cnn1/Wip1. Within the COMA complex the Ctf19 C-terminal RWD domain mediates recruitment of Sli15/Ipl1 to inner kinetochores in a Bir1 independent manner. Therefore, I consider the COMA complex as a centerpiece within the assembly, as it is crucial and most upstream for kinetochore formation and plays an important role in positioning the CPC.

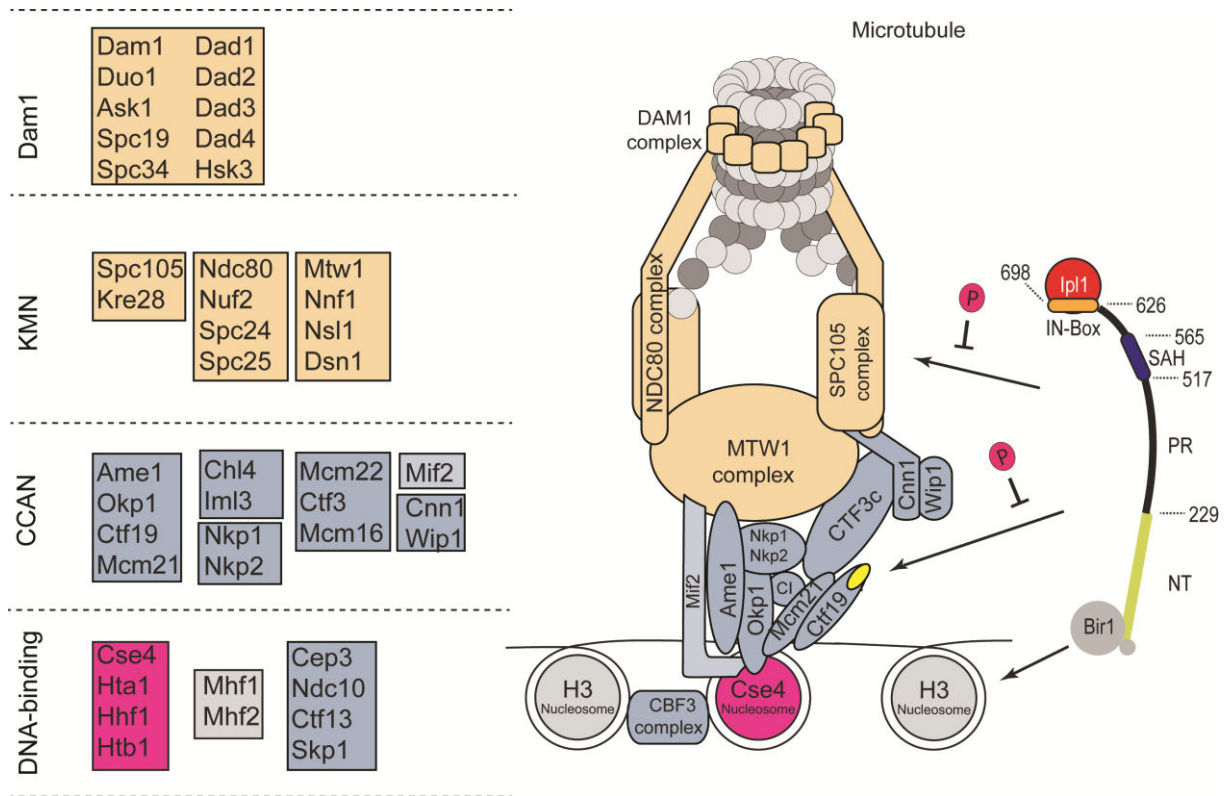


**Figure 33. The molecular architecture of the *S. cerevisiae* kinetochore and its interactions with the chromosomal passenger complex.** The COMA complex directly interacts with the Cse4-N-terminus via Okp1, which is essential for kinetochore assembly and viability in budding yeast. Besides direct association of Ame1 with Mtw1 (25), the COMA complex is linked through the CTF3c:Cnn1/Wip1 to the NDC80c. The Ctf19 C-terminal RWD domain mediates recruitment of Sli15/Ipl1 to inner kinetochores in a Bir1 independent manner. Ame1/Okp1 and Mif2 provide additional inner kinetochore interfaces for the CPC. The outer kinetochore complex Spc105/Kre28 was identified to bind Sli15/Ipl1 *in vitro*. The interactions of Sli15/Ipl1 to both, Ctf19 and Spc105, were shown to be sensitive to Ipl1 phosphorylation.

## 5. Material and Methods

### 5.1. Cloning of baculoviral transfer vectors

In general, open reading frames encoding the respective subunits were amplified from yeast genomic DNA by PCR and cloned into the pLIB or pBIG1/2 vectors according to the biGBac system (130). Primers for amplification carried the sequence overhang 5'--CCACCATCGGGCGCGGATCC (followed by the start codon and gene specific sequences) and a reverse primer that carried the sequence overhang 5'--TCCTCTAGTACTTCTCGACAAGCTT (followed by the reverse complement of stop codon and gene specific sequences). For introducing mutations in expression vectors the Q5® site-directed mutagenesis kit (New England Biolabs) was used. Subsequent to the transformation of the vectors into chemical competent DH5 $\alpha$  cells, the plasmid DNA was extracted using a Mini-prep kit (NucleoSpin®, Macherey-Nagel) and sequenced for verification of the mutants.

### 5.2. Generation of recombinant baculoviruses

Depending on the size of the constructs, they were transformed via heat-shock or electroporation into DH10bac cells. All expression vectors carry the gene for gentamycin resistance and Tn7 elements, meaning that the expression cassettes are flanked by Tn7R and Tn7L sites. The respective *E.coli* cells contain a helper plasmid (tetracycline resistance) coding for the transposase required for Tn7 transposition of the expression cassettes into the baculoviral genome at its mini-attTn7 attachment site. This site is located in the coding region for a lacZ peptide, thereby enabling blue/white selection. After 4 hours incubation at 37°C the transformed cells were plated on LB-agar containing 50  $\mu$ g/ml kanamycin, 7  $\mu$ g/ml gentamycin and 10  $\mu$ g/ml tetracycline as well as 50  $\mu$ g/ml X-galactose and 0.1 mM IPTG for blue/white selection. Subsequent to three days of incubation at 37°C, white colonies were picked and grown for 24 h in 5 ml LB containing 50  $\mu$ g/ml kanamycin, 7  $\mu$ g/ml gentamycin and 10  $\mu$ g/ml tetracycline. For isolation of recombinant bacmid DNA the following procedure was used. Bacterial pellets were resuspended in 250  $\mu$ l P1 buffer (Qiagen) and cells were lysed by adding 250  $\mu$ l P2 buffer (Qiagen). After 2 min of cell lysis the pH was neutralized with 350  $\mu$ l N3 buffer (Qiagen) and cells were centrifuged for 10 min at 20000 g. To the supernatant 750  $\mu$ l isopropanol were added and the solution was incubated at -20°C for 30

min. DNA was precipitated by centrifugation for 15 min at 20000 g, 4°. Pellets were washed by adding 70 % ethanol and were centrifuged again for 15 min at 4°C. After complete removal of ethanol, the pellets were dried at 50°C for 20 minutes. Finally, bacmid constructs were dissolved in 40µl of H<sub>2</sub>O. Adherent SF21 (*Spodoptera frugiperda*) cells were transfected with 1-2 µg of the baculovirus constructs diluted in suspension medium (Sf-900™ III medium, Gibco) using FuGENE® HD transfection reagent (Promega). Virus were upscaled by adding the transfection supernatant to 10 ml of 1x10<sup>6</sup>/ml SF21 cells in suspension medium (Sf-900™ III medium, Gibco) and subsequent incubation for three days at 27°C. The cell suspension was centrifuged at 300 g for 10min and virus were harvested by filtration of the supernatant using the Steriflip® system (Merck Millipore). Viral stocks were stored in the dark at 4°C. Quality of the virus was determined by the number of viable cells, which should be below 2x10<sup>6</sup>/ml after 3 days. Before infecting cells for protein expression the viral stocks (V1) were used for two rounds of upscaling the virus. For each amplification step 50 ml of 0,4x10<sup>6</sup>/ml SF21 cells in suspension medium were infected with 0.5 ml virus and incubated for three days at 27°C. As before, the suspension was centrifuged at 300 g for 10min and the virus were harvested by filtration of the supernatant using the Steriflip® system (Merck Millipore).

### **5.3. Expression of recombinant protein complexes from insect cells**

All proteins or protein complexes were expressed in High Five insect cell suspension (Thermo Scientific) culture using Express Five medium supplemented with 1 % L-glutamine (Gibco) and 1 % pluronic (Invitrogen). Typically 1 l of 1x10<sup>6</sup>/ml HF was infected with 10 ml of the V3 virus and incubated in a 5 l Erlenmeyer flask at 95 rpm, 27°C for three days.

### **5.4. Purification of recombinant protein complexes from insect cells**

C-terminal 6xHis-6xFLAG-tags on Ctf19, Mif2, Dsn1, Mcm16 and C-terminal 2xStrep-tags on Sli15 were used to affinity-purify Ctf19/Mcm21, Mif2, KMN, and Sli15/Ipl1 complexes. Mps1 purification was performed via a C-terminal GST-tag.

#### **5.4.1. Purification of proteins via FLAG-tag**

In general, following the three days of incubation the infected High Five cell suspensions were centrifuged at 1000 g for 10 min at 4°C and the pellets were washed with ice-cold PBS.

Pellets were resuspended in lysis buffer (50 mM Tris pH 7.5, 300 mM NaCl, 5 % glycerol) supplemented with complete EDTA-free protease inhibitors (Roche) and lysed by dounce homogenization. The lysate was centrifuged at 19500 rpm for 25 min at 4°C using a SS34 rotor. Cleared extracts were incubated with equilibrated M2 anti-FLAG agarose (Sigma-Aldrich) for 2 h, rotating at 4°C. The protein bound beads were centrifuged at 800 g for 10 min and washed once with wash buffer (50 mM Tris pH 7.5, 150 mM NaCl, 5 % glycerol), before applying the resin onto Bio-Spin® disposable chromatography columns (Bio-Rad). Following three washing steps using in total five column volumes of wash buffer, proteins were eluted in the same buffer containing 1 mg/ml 3xFLAG peptide. For complexes, which were further used for XLMS, two additional washing steps with Tris-free buffer (50 mM Hepes, pH 7.5, 150 mM NaCl, 5 % glycerol) were applied and the proteins were eluted in the Tris-free buffer containing 1 mg/ml 3xFLAG peptide. FLAG peptide was either removed via PD10 desalting columns (GE-Healthcare) or SEC using a Superdex 200 HiLoad 16/60 column (GE-Healthcare) and isocratic elution in Hepes buffer (50 mM Hepes, pH 7.5, 150 mM NaCl, 5 % glycerol).

#### **5.4.2. Purification of proteins via Strep-tag**

The procedure for purifying Strep-tagged proteins from insect cells was the same as described for FLAG-tagged proteins. However, to lyse High Five cells expressing Strep-tagged Sli15/Ipl1, pellets were resuspended in Strep-buffer (50 mM NaH<sub>2</sub>PO<sub>4</sub> pH 8, 300 mM NaCl, 5% glycerol) supplemented with Complete EDTA-free protease inhibitors (Roche). Subsequent to incubating the cleared lysates with Strep-Tactin Superflow agarose (Qiagen) for 2 h, rotating at 4°C, for the washing steps Strep-buffer with 150 mM NaCl was used. Proteins, which were subsequently used for the *in vitro* binding assays with inner kinetochore complexes, were directly kept on the beads. To elute Sli15/Ipl1 the Strep-buffer was supplemented with 8 mM biotin. For purifying phosphorylated Sli15/Ipl1, protein bound beads were incubated with 5 mM MgCl<sub>2</sub> and 5 mM ATP for 25 min at 25°C before washing with Strep-buffer. Biotin was either removed via PD10 desalting columns (GE-Healthcare) or SEC using a Superdex 200 HiLoad 16/600 column (GE-Healthcare) and isocratic elution in Hepes buffer (50 mM Hepes, pH 7.5, 150 mM NaCl, 5 % glycerol).

#### **5.4.3. Purification of Mps1-GST**

Handling of insect cells expressing Mps1-GST and affinity purification was performed as described for FLAG-tagged proteins with the exception of the following applications. Cells were lysed in GST-buffer (1xPBS, 0.1 % triton, 5 % glycerol) supplemented with Complete EDTA-free protease inhibitors (Roche). Cleared lysates were incubated with glutathione-sepharose (GE Healthcare) for 2 h, rotating at 4°C. Protein bound beads were washed with GST-buffer. For the last washing step the same buffer was supplemented with 400 mM NaCl. Mps1-GST was eluted from the beads with buffer containing 20 mM Glutathione in 50 mM Tris HCl, pH 8 ,150mM NaCl, 5 % glycerol.

### **5.5. Ame1-6xHis/Okp1 expression and purification**

Ame1-6xHis/Okp1 is on a pST39 vector under control of a T7 promoter. The vector was a gift of Stefan Westermann (University Duisburg-Essen). For the synthesis of the Okp1 deletion mutants the Q5® site-directed mutagenesis kit (New England Biolabs) was used. The GFP-6xHis-Okp1(140-192) construct was cloned into the pet28 vector. The plasmids were transformed in *E. coli* cells via heat-shock. Afterwards, the plasmid DNA was extracted with a Mini-prep kit (NucleoSpin®, Macherey-Nagel) and sequenced to verify the mutant constructs. For expression, all Ame1/Okp1 vectors used in this study were transformed via heat-shock into *E.coli* Rosetta cells. Cells harboring the plasmid were grown at 37°C in LB medium containing ampicillin until OD600 of 0.6 and subsequently protein expression was induced by addition of 0.5 mM isopropyl-β-D-thiogalactopyranoside (IPTG). After incubation in the shaker overnight at 18°C, cells were harvested via centrifugation for 15 min at 4000 rpm, at 4°C in a SLC 6000 rotor and washed with icecold water. Pellets from a 500 ml culture were resuspended in 10 ml Lysis buffer (50 mM Hepes pH7.5, 1000 mM NaCl, 30 mM imidazole, 5 % glycerol, 1 mM DTT supplemented with Complete EDTA-free protease inhibitors (Roche)) and subsequently the cells were lysed using a cell disrupter. The lysate was cleared by centrifugation in a SS34 rotor at 19500 rpm for 25 min at 4°C. The supernatant was applied to pre-equilibrated 0.4 ml Ni-NTA resin (Quiagen) on a rotating wheel for 2 h at 4°C. To remove the *E. Coli* DNA that was bound to Ame1/Okp1, beads were washed six times, each time for 10 min at 4°C rotating in wash buffer (50 mM Hepes pH 7.5, 600 mM NaCl, 30 mM imidazole, 5 % glycerol, 1mM DTT). Afterwards, the resin was transferred onto Bio-Spin disposable chromatography columns (Bio-Rad). Proteins were eluted in elution buffer (50 mM Hepes pH7.5, 150 mM NaCl, 300 mM imidazole, 5 % glycerol). Prior to elution, beads were incubated with elution buffer for 5 minutes. Elution

fractions containing Ame1/Okp1 were combined, concentrated in centrifugal filters with 10 kDa MWCO (Amicon® Ultra-15, Millipore) and further purified via SEC.

## **5.6. Preparative size exclusion chromatography (SEC)**

### **5.6.1. Preparative SEC of Ame1/Okp1**

In general, preparative SEC was performed on a ÄKTA pure (GE Healthcare) chromatography system. Ame1/Okp1 complexes were loaded on a HiLoad 16/600 Superdex column. The chromatography was performed in Hepes buffer (30 mM Hepes, pH 7.5, 150 mM NaCl, 5 % glycerol) under isocratic elution conditions applying a flow rate of 1 ml/min and 1 ml fractionation size. Fractions containing Ame1/Okp1 were combined and the proteins were concentrated in centrifugal filters with 10 kDa MWCO (Amicon® Ultra-15, Millipore) by stepwise centrifugation.

### **5.6.2. Preparative SEC of Sli15/Ipl1**

Proteins were purified on a HiLoad 16/600 Superdex column using a Na-phosphat buffer (50 mM NaH<sub>2</sub>PO<sub>4</sub> pH 8, 300 mM NaCl, 5 % glycerol). Isocratic elution conditions at a flow rate of 1.5 ml/min and 1.5 ml fractionation size was applied. Elutions of Sli15/Ipl1 were upconcentrated in centrifugal filters with 10 kDa MWCO (Amicon® Ultra-15, Millipore)

## **5.7. *In vitro* reconstitution of Cse4- and H3-NCPs**

Budding yeast histones were recombinantly expressed in *E.coli* BL21 (DE3) and assembled on a 167 bp DNA stretch containing the 'Widom 601' nucleosome positioning sequence. Octameric Cse4 and H3 containing nucleosomes were *in vitro* reconstituted as described by (144)

## **5.8. Interaction studies using size exclusion chromatography (SEC)**

Analytical SEC experiments were performed using a Superdex 200 Increase 3.2/300 column (GE Healthcare). To detect complex formation, proteins were mixed at equimolar ratios and incubated for 1 h on ice before loading on the column. All SEC interaction studies were conducted under isocratic elution conditions with SEC buffer (50 mM Hepes pH 7.5, 150 mM NaCl, 5 % glycerol) at 4°C and a flowrate of 0.5 ml/min. Elution of proteins was monitored

by absorbance at 280 nm. Fractions of 100  $\mu$ l were collected and analyzed by SDS-PAGE and coomassie staining.

## **5.9. Yeast genetics**

All yeast strains were generated using standard methods and procedures. C-terminal tags and deletions were inserted at the C-terminus of genes at their native loci by PCR based tagging standard approaches as described in Janke et al. (145). If not indicated otherwise yeast strains belong to S288C background. The constructs for the anchor-away rescue experiments were generated by cloning the respective promoters, open reading frames and the tag into the pRS313 vector. In general, open reading frames encoding the respective proteins were amplified from yeast genomic DNA by PCR. Mutations in the constructs were introduced via Q5 site-directed mutagenesis kit (New England Biolabs). The rescue constructs were transformed into the respective anchor-away strains and subsequently cell growth was tested on YPD plates in the absence or presence of rapamycin (1  $\mu$ g/ml). To generate the fusion constructs of Sli15 $\Delta$ N2-228 and the respective kinetochore proteins the individual promoters and open reading frames were amplified via PCR from yeast genomic DNA. After the fusion constructs were assembled and cloned into pRS313 by applying the Gibson assembly reaction, the vectors expressing the constructs were transformed into the respective anchor-away strains.

## **5.10. Growth assays**

For anchor-away rescue experiments with synthetic lethal strains the ribosomal RPL13-FKBP12 anchor was used as previously described (Haruki 2008). Cells of anchor-away strains ectopically expressing wildtype and mutant proteins were grown overnight in YEP with 2 % glucose (YPD) at 30°C. Cell cultures were adjusted to an OD600 of 0.5 and five 1:10 serial dilutions were prepared. Of each dilution 10  $\mu$ l were spotted on YPD-, YPD + rapamycin (1  $\mu$ g/ml)- and YPD + rapamycin + the microtubule destabilizing drug benomyl (15  $\mu$ g/ml) plates. Subsequently plates were incubated at 30°C or 37°C for 3-5 days.

## **5.11. Pulldown of native yeast complexes for Mass spectrometry**

Ame1, Dsn1, Cnn1, Ctf3, Mif2, Chl4, Sli15, Bir1, Mps1, Mad3, Bub3 and Wip1 genes were C-terminally tagged with 6xHis-6xFLAG at the endogenous loci and expression was



confirmed by Western blot. Asynchronous yeast cultures, were grown in YEP + 2 % glucose at 30°C to reach an OD<sub>600</sub> of 1, either shaking in 5 l flasks or in a 50 l fermenter (Bioengineering) for preparative crosslinking. Cells were harvested at 4°C, washed with H<sub>2</sub>O and pellets were resuspended in lysis buffer (25 mM Hepes pH 8.0, 2 mM MgCl<sub>2</sub>, 0.02 % NP-40, 5 % glycerol, 150 mM KCl) supplemented with 1x phosphatase inhibitor (0.4 mM Na<sub>4</sub>P<sub>2</sub>O<sub>7</sub>, 0.25 mM NaN<sub>3</sub>, 0.5 mM NaF, 20 mM Na<sub>3</sub>VO<sub>4</sub>) and 1x protease inhibitor cocktail mix IV (Merck). Pearls of yeast cells were generated by pipetting the viscous cell solution directly into liquid nitrogen and subsequently the yeast cells were lysed by homogenizing the pearls using Freezer Mill (Spex Sampleprep) into powder. All purification steps were performed at 4°C. For quantitative label free analysis of the pulldowns via mass spectrometry 10 g and for XLMS 200 g of yeast powder were used. After resuspending the powder in lysis buffer using a 2:1 ratio (g/ml) either in 50 ml falcon tubes rotating for 30 min or in a beaker with a magnetic stirrer, the lysate was cleared by centrifugation for 30 min at 25000 rpm using a Ti70.1 rotor. The supernatant was applied to pre-equilibrated Protein A Dynabeads (Life Technologies) coupled with anti-FLAG antibody (M2, Sigma) for 2 h rotating. Performance of the beads was tested beforehand using lysate of Dsn1 FLAG-tagged strain. Protein bound beads were collected by using a magnetic rack and washed 2x with lysis buffer. Beads were transferred into 1.5 ml Eppendorf tubes and proteins were eluted 3x with 650 µl 2xStrep-6xFLAG peptide (0.15 mg/ml) by 5 min rotating at 4°C. For small scale purification only 1 elution step with 120 µl was performed. The combined eluates were centrifuged at full speed for 1 min and the supernatant was transferred to a new Eppendorf tube to remove the remaining beads. Excess of the 2xStrep-6xFLAG peptide in the samples was removed by passing the eluate twice over Streptactin beads (Qiagen). The flow-through was subsequently concentrated on 20 µl (for MS analysis) or 120 µl (for XLMS) Ni-NTA slurry (Qiagen) by rotating for 2 h. Complex bound beads were washed 1x with lysis buffer and 2x with lysis buffer without detergent by centrifugation for 3 min at 1200 g in low binding Eppendorf tube (Sarstedt). Finally, 5 µl or 60 µl of Lysis buffer without detergent were added to the beads.

## **5.12. Chemical crosslinking and mass spectrometry of kinetochore complexes**

*In vitro* reconstituted complexes were assembled in solution at equimolar rates while purified native kinetochore complexes were crosslinked on Ni-NTA beads (Qiagen). In general, complexes were crosslinked with bis(sulfosuccinimidyl)suberate (BS3) H12/D12 (Creative

Molecules), in the molar range of 0.25 – 1.5 mM, for 30 min at 30 °C, shaking. The crosslinking reaction was quenched by adding  $\text{NH}_4\text{HCO}_3$  (AMBIC) to a final concentration of 100 mM and further incubation for 10 min at 30°C. Crosslinked complexes were denatured by adding 2 sample volumes of 8 M urea and reduced with 5 mM TCEP (Thermo Scientific). After incubation at 30°C for 15 min the sample was alkylated by application of 10 mM iodoacetamide (Sigma-Aldrich) for 40 min at RT in the dark. Protein digestion with lysyl endopeptidase (Wako) was performed at 35 °C for 2 h (at enzyme-substrate ratio of 1:50 w/w) and was followed by a second protein digestion with trypsin (Promega) at 35°C overnight (at enzyme-substrate ratio 1:50 w/w). Before applying the second protease trypsin, the sample was supplied with 50 mM AMBIC. The volume of added AMBIC equaled 7x the volume of urea used for initial denaturation. Digestion was stopped by adding acetonitrile (ACN) to a final concentration of 3 % and trifluoroacetic acid (TFA) to 1 % final concentration. Acidified peptides were purified by reversed phase chromatography using C18 cartridge columns (Sep-Pak, Waters). After the column was activated by applying 1 ml of 100 % ACN, it was washed 2x with 1 ml of washing buffer (3 % ACN and 0,2 % formic acid (FA)). The acidified peptides were applied to the column, the flow-through was collected and applied again. The column with the bound peptides was washed 2x with washing buffer. Before eluting the peptides, the residual washing buffer was completely removed by applying vacuum. Peptides were eluted twice with 350  $\mu\text{l}$  of 60 % ACN and 0,2 % FA. The eluate was dried by vacuum centrifugation and the peptides were reconstituted in 25 % ACN and 0.1 % TFA, by incubation at 35°C for 20 min, shaking at 1400 rpm. For direct analysis via LC-MS/MS of non crosslinked samples the peptides were dissolved directly in 20  $\mu\text{l}$  3 % ACN and 0.2 % FA by incubation at 35°C for 20 min, shaking at 1400 rpm. After centrifugation at RT for 10 min at 21000 g the supernatant containing the dissolved peptides was transferred into MS vials, air bubbles were removed by centrifugation and the samples were analyzed by liquid chromatography coupled to a tandem mass spectrometer, a hybrid LTQ Orbitrap Elite (Thermo Scientific) instrument. Prior analyzing crosslink samples via MS, reconstituted crosslinked peptides were enriched on a Superdex 3.2/30 column at a flow rate of 25  $\mu\text{l}/\text{min}$  using 23 % ACN and 0.1 % TFA as a mobile phase. Under these conditions crosslinked peptides elute in between the retention volumes 1.0-1.5ml (elutions: +2,+1,0,-1,-2). The respective fractions, each 100  $\mu\text{l}$ , were collected, dried, reconstituted in 3 % ACN and 0.2 % TFA as described before and further analysed by LC-MS/MS.

### **5.13. Mass spectrometry - analysis and settings**

Non crosslinked and enriched crosslinked peptides (fractions: +1, 0, -1 ) were analyzed using an EASY-nLC 1000 liquid chromatography system in combination with a LTQ Orbitrap Elite mass spectrometer (Thermo Fisher Scientific). In general, up to 4  $\mu$ l, equal to  $\sim$  1  $\mu$ g of crosslinked peptide, were used per run. The peptides were separated according to their polarity at a flow rate of 300 nl/minute with a gradient ranging from 5 % to 35 % of mobile phase B (97 % ACN and 0.1 % formic acid). During each MS1 cycle, the 10 most intense peptides possessing a minimum charge of 4 were selected for further fragmentation and MS2 scanning, with an exclusion time set to 30 s. All MS1 spectra were acquired in the orbitrap at 12000 resolution, and MS2 fragment scans at low resolution in the linear ion trap. Fragment ion spectra were measured and crosslinked peptides were identified by the dedicated software xQuest (124). Searched spectra were filtered according to the following parameters:  $\Delta$  score  $\leq$  0.85, MS1 tolerance window of -4 to +4 ppm and score  $\geq$  22. Additionally all filtered crosslink spectra were manually validated before being visualized with respect to the protein lengths using xVis and Network plot (146).

#### **5.14. *In vitro* protein binding assay of Sli15/Ipl1 to inner kinetochore proteins**

For all binding experiments with the inner kinetochore proteins (Ame1/Okp1, Ctf3/Mcm16/Mcm22, Mif2, Ctf19/Mcm21), wildtype or mutant Sli15-2xStrep-HA-6xHis/Ipl1 was immobilized on Strep-Tactin Superflow agarose (Qiagen). All binding tests were performed in protein low binding tubes (Sarstedt). To prephosphorylate Sli15/Ipl1, protein bound beads were incubated at 30 °C for 30 min in the presence of 5 mM MgCl<sub>2</sub> and 5 mM ATP. Samples for non-phosphorylated Sli15/Ipl1 were treated the same way but instead of 5 mM ATP the non-hydrolysable analog AMP-PNP (Santa Cruz Biotechnology) was applied. For removing any basal phosphorylation, Sli15/Ipl1 was incubated with lambda phosphatase (NEB) at 30 °C for 30 min. Before testing the binding to kinetochore proteins the non-phosphorylated, phosphorylated or dephosphorylated Sli15/Ipl1 complexes were washed 3x with binding buffer (50 mM NaH<sub>2</sub>PO<sub>4</sub> pH 8, 120 mM NaCl, 5% glycerol) via centrifugation for 3 min at 4°C and 1200 rpm.

In general, kinetochore proteins were incubated at a molar ratio ranging from 1:1 till 1:2 in binding buffer with Sli15/Ipl1 bound to beads, either in the presence of 5 mM ATP and 5 mM MgCl<sub>2</sub> or 5 mM AMP-PNP and MgCl<sub>2</sub>. As a negative control, kinetochore proteins were applied to Strep-Tactin Superflow agarose (Qiagen), which was pre-incubated with BSA.

After 10 min at RT, 1 h at 4°C and further 10 min at RT constantly shaking in a thermomixer, the unbound proteins were removed by washing 3x with binding buffer. The complexes were either eluted with 8 mM biotin in 50 mM NaH<sub>2</sub>PO<sub>4</sub> pH 8, 500 mM NaCl, 5 % glycerol, or by boiling in 2x SDS loading buffer. For calculating molar ratios between bound protein and the bait protein, SDS page protein band intensities were analyzed with the software Fiji (147).

### **5.15. *In vitro* protein binding assay of KMN to Sli15/Ipl1**

The KMN complex was immobilized on M2 anti-FLAG agarose (Sigma-Aldrich). Prephosphorylation was performed by incubating KMN at 25°C for 25 min in the presence of 5 mM MgCl<sub>2</sub> and 5 mM ATP with Sli15/Ipl1 or Mps1. Samples for non-phosphorylated KMN were handled the same way, but instead of 5 mM ATP the non-hydrolysable analogue AMP-PNP (Santa Cruz Biotechnology) was applied. Subsequently, non-phosphorylated as well as phosphorylated KMN were washed 3x with binding buffer (50 mM Tris pH 7.5, 150 mM NaCl, 5% glycerol) to remove ATP or AMP-PNP. Complex formation was tested by adding unphosphorylated -, prephosphorylated Sli15/Ipl1 or the Sli15/Ipl1(D227A) kinase dead variant to the KMN bound beads. After incubating the Sli15/Ipl1-KMN complexes at 25°C for 25 min in the presence of 5 mM ATP and 5 mM MgCl<sub>2</sub> or 5 mM AMP-PNP and 5 mM MgCl<sub>2</sub>, unbound Sli15-Ipl1 was removed by washing 3x with binding buffer. Bound proteins were eluted with 200 mM glycine pH 1.8. Eluates were analyzed by SDS-PAGE and coomassie staining.

### **5.16. Electrophoretic mobility shift assay**

Reconstituted nucleosomes and Ame1/Okp1 were mixed at a 1:1 molar ratio. For testing the binding of the Okp1(140-192)-GFP fusion construct an excess of the peptide at a 1:100 molar ratio was applied. After incubation for 1 h at 4°C in a buffer containing 20 mM Hepes (pH 7.5), the interaction was analyzed by electrophoresis at 130 V for 90 min on a 6 % native polyacrylamide gel in a buffer containing 25 mM Tris and 25 mM boric acid. DNA was stained with SYBR® Gold (Thermo Fisher).

### **5.17. *In vitro* binding assay using Sli15/Ipl1 and native kinetochore complexes**

Pulldowns of yeast cells expressing either Ame1-6xHis-6xFLAG or Dsn1-6xHis-6xFLAG were performed as described. However, the representative complexes were eluted from the FLAG-beads with 3xFLAG peptide and subsequently immediately incubated for 1 h at 4°C with Sli15-2xStrep-HA-6xHis/Ipl1, which was immobilized on Strep-Tactin Superflow agarose (Qiagen). As a negative control the kinetochore complexes were applied to Strep-Tactin Superflow agarose (Qiagen), which was pre-incubated with BSA. After unbound proteins were removed by washing 3x with washing buffer (25 mM Hepes pH 8.0, 2 mM MgCl<sub>2</sub>, 0,02 % NP-40, 5 % glycerol, 200 mM KCl), bound proteins were eluted with 8 mM biotin in washing buffer. Biotin was removed via PD10 desalting columns (GE-Healthcare) and the samples were either resuspended in SDS sample buffer and analyzed by SDS-PAGE followed by western blotting, or the proteins were digested as described for further analysis by LC-MS/MS.

### **5.18. *In vitro* binding assay using whole cell lysates**

Cleared lysates of High five cells expressing either Ame1/Okp1 or Ctf19/Mcm21 were incubated for 1 h at 4°C with Sli15-2xStrep-HA-6xHis/Ipl1, which was immobilized on Strep-Tactin Superflow agarose (Qiagen). As a negative control the cleared lysates were applied to Strep-Tactin Superflow agarose (Qiagen), which was pre-incubated with BSA. After unbound proteins were removed by washing 3x with binding buffer. The complexes were eluted by boiling in 2x SDS loading buffer. Analysis was performed by SDS-PAGE and western blotting.

### **5.19. Enrichment of phosphorylated peptides**

After digestion and peptide cleanup via reversed phase chromatography using C18 cartridge columns (Sep-Pak, Waters), samples were dried by vacuum centrifugation and reconstituted in 200 µl 60 % CAN and 6 % TFA by 10 minutes of sonication. For enrichment of phosphorylated peptides 0.5 mg TiO<sub>2</sub> beads (GL Sciences) per sample were used. The beads were resuspended in 80 % ACN and 6 % TFA and transferred on top of a C8 (single layer) StageTip. The StageTip was centrifuged for 5 min at 500 g at RT to remove the buffer before the reconstituted samples were applied. After centrifugation at 50 g for 15 minutes, the flowthrough was applied a second time to the resin. Not phosphorylated peptides were removed by washing the beads 3x with 200 µl 60 % ACN and 1 % TFA and 1x with 200 µl 80 % ACN and 0.5 % acetic acid, each time via centrifugation at 500 g for 5min. To the

enriched peptides, which were eluted 2x with 30 µl elution buffer (40 % ACN, 3.75 % NH<sub>4</sub>OH) via centrifugation at 500 g for 5 min, 60 µl of 2 % ACN and 0.3 % TFA was added. Finally, the samples were dried in the vacuum centrifuge, reconstituted in 3 % ACN and 0.2 % TFA as described before and further analyzed by LC-MS/MS.

## **5.20. SDS page analysis**

Proteins were separated according to their size by sodium dodecylsulfate polyacrylamide gel electrophoresis (SDS-PAGE), using homemade (8 - 12 %) or 4 – 20 % precast gradient gels (Mini-PROTEAN® TGX™ Precast Protein Gels, Bio-Rad). Prestained and unstained protein markers were used as size standards. The gels were either stained with coomassie (25 % isopronaol, 10 % acidic acid, 0.005 % brilliant blue) or by silver staining. For silver staining the gels were first briefly washed in fixing solution (45 % methanol, 10 % acidic acid) and subsequently incubated in fixing solution for at least 20 min. After washing the gel 2x 10 min with 50 % EtOH and one time for 10 min with 30 % EtOH, 0.8mM Na<sub>2</sub>S<sub>2</sub>O<sub>3</sub> solution was applied for 1 min to sensitize the gels. Gels were washed 3x 20 sec with water and incubated in a 2 g/l AgNO<sub>3</sub> and 0.026 % formaldehyde solution for 20 minutes. After washing the gels 3x 20 sec with water the developing solution (6 % Na<sub>2</sub>CO<sub>3</sub>, 0.0185 % formaldehyde, 16 µM Na<sub>2</sub>S<sub>2</sub>O<sub>3</sub>) was applied. Staining was stopped by addition of 10 % acidic acid, as soon as the protein bands were nicely visible.

## **5.21. Immunoblotting**

For transferring the proteins to PVDF membranes a wet transfer technique was applied. The transfer was performed for 1 h at 100 V and 4°C using western blotting transfer buffer (25 mM Tris, 192 mM glycine, 10 % methanol). Subsequently the membranes were washed with TBST (50 mM Tris-HCl pH 7.6, 150 mM NaCl, 0.05 % Tween), blocked in TBST supplemented with 5 % milk powder for 1 h at RT and incubated with primary antibody (anti-FLAG M2 (Sigma-Aldrich) diluted 1:5000 in TBST and 5 % w/v milk powder) at 4°C for at least 1 h. The membranes were washed 3x 15 min with TBST and incubated with the HRP-conjugated anti mouse secondary antibody (1:10000, Santa Cruz). After the membranes were again washed as described, Amersham ECL solution (GE Healthcare) and Amersham Hyperfilm (GE Healthcare) were used for developing.

## 5.22. Lists and Tables

### 5.22.1. Plasmids list

Plasmid	description	source
2886	pYCF1/ CEN3.L	
pST44-Cse4	pST44-6xHis-TEV-Flag-H2B-CSE4-H2A-H4	Alwin Köhler (148)
BSW1	pST44-6xHis-TEV-Flag-H2B-CSE4 $\Delta$ 2-30-H2A-H4	this study
BSW2	pST44-6xHis-TEV-Flag-H2B-CSE4 $\Delta$ 31-60-H2A-H4	this study
BSW4	pST44-6xHis-TEV-Flag-H2B-CSE4 $\Delta$ 34-46-H2A-H4	this study
BSW5	pST44-6xHis-TEV-Flag-H2B-CSE4 $\Delta$ 48-61-H2A-H4	this study
pST44-H3	pST44-6xHis-TEV-Flag-H2B-H3-H2A-H4	Alwin Köhler
BJF6	pLIB-MIF2-6xHis-6xFlag	this study
pPH74	pST39-OKP1-AME1-6xHis	Stefan Westermann
BJF26	pST39-OKP1 $\Delta$ 123-147-AME1-6xHis	this study
BJF27	pST39-OKP1 $\Delta$ 140-170-AME1-6xHis	this study
BJF28	pST39-OKP1 $\Delta$ 163-187-AME1-6xHis	this study
pSW661	pST39-CTF19-MCM21-6xHis	Stefan Westermann
BJF25	pST39-CTF19 $\Delta$ C270-369 -MCM21-6xHis	this study
BJF7	pBIG1-MCM21-6xHis-6xFlag/CTF19	this study
BJF47	pBIG1-MCM21-6xHis-6xFlag/CTF19 $\Delta$ C270-369	this study
BJF50	pBIG1-AME1-6xHis-6xFlag-OKP1	this study
BJF51	pBIG1-AME1-6xHis-6xFlag-OKP1 $\Delta$ 241-282	this study
BJF52	pBIG1-AME1-6xHis-6xFlag-OKP1 $\Delta$ 204-271	this study
BJF75	pET28-GFP-6xHis	this study
BJF76	pET28-GFP-6xHis-Okp1(140-192)	this study
BJF10	pBIG1-pHIK-CTF3-MCM16-6xHis-6xFlag-MCM22	this study
BJF4	pBIG1-SLI15 $\Delta$ 2-228-2xStrep-HA-6xHis/IPL1	this study
BJF1	pBIG1-SLI15-2xStrep-HA-6xHis-IPL1	this study
BJF23	pBIG1-Sli15 $\Delta$ 2-228-2xStrep-HA-6xHis-IPL1(kd)	this study
BJF41	pBIG1-Sli15 $\Delta$ 23-563-2xStrep-HA-6xHis-IPL1	this study
BPB1	pBIG2-pKMN-SPC105-6xHis-6xFlag-KRE28-Ndc80 Spc24-Spc25-Nuf2-Mtw1-Dsn1-Nnf1-Nsl1-	this study
BJF53	pBIG1-pKS-SPC105-6xHis-6xFlag-KRE28	this study
BSS93	pRS313-pCSE4-3xFlag-CSE4	this study
BSS94	pRS313-pCSE4-3xFlag-CSE4 $\Delta$ 31-60	this study
BSS95	pRS313-pCSE4-3xFlag-CSE4 $\Delta$ 62-94	this study
BSS96	pRS313-pCSE4-3xFlag-CSE4 $\Delta$ 34-46	this study
BSS97	pRS313-pCSE4-3xFlag-CSE4 $\Delta$ 48-61	this study
BSS134	pRS313-pCTF19-CTF19WT-SLI15 $\Delta$ 2-228-6xHis-7xFlag	this study
BSS146	pRS313-pAME1-AME1-SLI15 $\Delta$ 2-228-6xHis-7xFlag	this study
BSS142	pRS313-pOKP1-OKP1-SLI15 $\Delta$ 2-228-6xHis-7xFlag	this study
BSS145	pRS313-pMIF2-MIF2-SLI15 $\Delta$ 2-228-6xHis-7xFlag	this study

<b>Plasmid</b>	<b>description</b>	<b>source</b>
BSS143	pRS313-pCTF3-CTF3-SLI15Δ2-228-6xHis-7xFlag	this study
BSS144	pRS313-pMTW1-MTW1-SLI15Δ2-228-6xHis-7xFlag	this study
BSS141	pRS313-pDSN1-DSN1-SLI15Δ2-228-6xHis-7xFlag	this study
BSS147	pRS313-pCNN1-CNN1-SLI15Δ2-228-6xHis-7xFlag	this study
BSS1	pRS313-pSLI15-SLI15-6xHis-6xFlag	this study
BSS15	pRS313-pSLI15-SLI15ΔSAH-6xHis-6xFlag	this study
BSS2	pRS313-pSLI15-SLI15Δ2-228-6xHis-6xFlag	this study
BSS16	pRS313-pSLI15-SLI15Δ2-228ΔSAH-6xHis-6xFlag	this study
BSS129	pRS313-pCTF19-CTF19-6xHis-7xFlag	this study
BSS159	pRS313-pCTF19-3xMyc-CTF19Δ2-30-6xHis-7xFlag	this study
BSS76	pRS313-pAME1-AME1-6xHis-7xFlag	this study
BSS169	pRS313-pOKP1-OKP1-6xHis-6xFlag	this study
BSS172	pRS313-pOKP1-OKP1Δ123-147-6xHis-6xFlag	this study
BSS174	pRS313-pOKP1-OKP1Δ163-187-6xHis-6xFlag	this study
BSS165	pRS313-pAME1-AME1-SLI15Δ2-228-ΔINbox(626-698)-6xHis-7xFlag	this study
BSS167	pRS313-pAME1-AME1-SLI15Δ2-228-ΔSAH(516-575)-6xHis-7xFlag	this study
BSS164	pRS313-pOKP1-OKP1-SLI15Δ2-228-ΔINbox(626-698)-6xHis-7xFlag	this study
BSS166	pRS313-pOKP1-OKP1-SLI15Δ2-228-ΔSAH(516-575)-6xHis-7xFlag	this study
BSS175	pRS313-pAME1-AME1-CTF19-6xHis-7xFlag	this study
BSS176	pRS313-pAME1-AME1-CTF19ΔC270-369 -6xHis-7xFlag	this study
BSS177	pRS313-pOKP1-OKP1-CTF19-6xHis-7xFlag	this study
BSS178	pRS313-pOKP1-OKP1-CTF19ΔC270-369 -6xHis-7xFlag	this study

### 5.22.2. Yeast strains

All yeast strains belong to S288C background. Yeast strains were generated by standard procedures

<b>strain</b>	<b>genotype</b>
YSS225	MAT a, tor1-1, fpr1::loxP-Leu2-loxP, RPL13A-2xFKBP12::lox-TRP1-loxP, CSE4-FRB::KanMX
YSS226	MAT a, tor1-1, fpr1::loxP-Leu2-loxP, RPL13A-2xFKBP12::lox-TRP1-loxP, CSE4-FRB::KanMX, pRS313-pCSE4-CSE4
YSS227	MAT a, tor1-1, fpr1::loxP-Leu2-loxP, RPL13A-2xFKBP12::lox-TRP1-loxP, CSE4-FRB::KanMX, pRS313-pCSE4-CSE4Δ62-94
YSS228	MAT a, tor1-1, fpr1::loxP-Leu2-loxP, RPL13A-2xFKBP12::lox-TRP1-loxP, CSE4-FRB::KanMX, pRS313-pCSE4-CSE4Δ31-60
YSS229	MAT a, tor1-1, fpr1::loxP-Leu2-loxP, RPL13A-2xFKBP12::lox-TRP1-loxP, CSE4-FRB::KanMX, pRS313-pCSE4-CSE4Δ34-46



<b>strain</b>	<b>genotype</b>
YSS230	MAT a, tor1-1, fpr1::loxP-Leu2-loxP, RPL13A-2xFKBP12::lox-TRP1-loxP, CSE4-FRB::KanMX, pRS313-pCSE4-CSE4 $\Delta$ 48-61
YSS216	MAT a, tor1-1, fpr1::loxP-Leu2-loxP, RPL13A-2xFKBP12::lox-TRP1-loxP, CTF19-FRB::KanMX, sli15 $\Delta$ 2-228::hphNT1
YSS325	MAT a, tor1-1, fpr1::loxP-Leu2-loxP, RPL13A-2xFKBP12::lox-TRP1-loxP, CTF19-FRB::KanMX, sli15 $\Delta$ 2-228::hphNT1, pRS313-pCTF19-CTF19-6xHis-7xFlag
YSS301	MAT a, tor1-1, fpr1::loxP-Leu2-loxP, RPL13A-2xFKBP12::lox-TRP1-loxP, CTF19-FRB::KanMX, sli15 $\Delta$ 2-228::hphNT1, pRS313-pCTF19-CTF19WT-SLI15 $\Delta$ 2-228-6xHis-7xFlag
YSS348	MAT a, tor1-1, fpr1::loxP-Leu2-loxP, RPL13A-2xFKBP12::lox-TRP1-loxP, CTF19-FRB::KanMX, sli15 $\Delta$ 2-228::hphNT1, pRS313-pCTF19-3xMyc-CTF19 $\Delta$ 2-30-6xHis-7xFlag
YSS334	MAT a, tor1-1, fpr1::loxP-Leu2-loxP, RPL13A-2xFKBP12::lox-TRP1-loxP, CTF19-FRB::KanMX, sli15 $\Delta$ 2-228::hphNT1, pRS313-pAME1-AME1-6xHis-1xFlag
YSS335	MAT a, tor1-1, fpr1::loxP-Leu2-loxP, RPL13A-2xFKBP12::lox-TRP1-loxP, CTF19-FRB::KanMX, sli15 $\Delta$ 2-228::hphNT1, pRS313-pAME1-AME1-SLI15 $\Delta$ 2-228-6xHis-7xFlag
YSS336	MAT a, tor1-1, fpr1::loxP-Leu2-loxP, RPL13A-2xFKBP12::lox-TRP1-loxP, CTF19-FRB::KanMX, sli15 $\Delta$ 2-228::hphNT1, pRS313-pAME1-AME1-SLI15 $\Delta$ 2-228- $\Delta$ INbox(626-698)-6xHis-7xFlag
YSS337	MAT a, tor1-1, fpr1::loxP-Leu2-loxP, RPL13A-2xFKBP12::lox-TRP1-loxP, CTF19-FRB::KanMX, sli15 $\Delta$ 2-228::hphNT1, pRS313-pAME1-AME1-SLI15 $\Delta$ 2-228- $\Delta$ SAH(516-575)-6xHis-7xFlag
YSS342	MAT a, tor1-1, fpr1::loxP-Leu2-loxP, RPL13A-2xFKBP12::lox-TRP1-loxP, CTF19-FRB::KanMX, sli15 $\Delta$ 2-228::hphNT1, pRS313-pOKP1-OKP1-6xHis-1xFlag
YSS351	MAT a, tor1-1, fpr1::loxP-Leu2-loxP, RPL13A-2xFKBP12::lox-TRP1-loxP, OKP1-FRB::KanMX, pRS313-pOKP1-OKP1-6xHis-6xFlag
YSS394	MAT a, tor1-1, fpr1::loxP-Leu2-loxP, RPL13A-2xFKBP12::lox-TRP1-loxP, OKP1-FRB::KanMX, pRS313-pOKP1-OKP1 $\Delta$ 122-147-6xHis-6xFlag
YSS395	MAT a, tor1-1, fpr1::loxP-Leu2-loxP, RPL13A-2xFKBP12::lox-TRP1-loxP, OKP1-FRB::KanMX, pRS313-pOKP1-OKP1 $\Delta$ 163-187-6xHis-6xFlag
YSS343	MAT a, tor1-1, fpr1::loxP-Leu2-loxP, RPL13A-2xFKBP12::lox-TRP1-loxP, CTF19-FRB::KanMX, sli15 $\Delta$ 2-228::hphNT1, pRS313-pOKP1-OKP1-SLI15 $\Delta$ 2-228-6xHis-7xFlag
YSS344	MAT a, tor1-1, fpr1::loxP-Leu2-loxP, RPL13A-2xFKBP12::lox-TRP1-loxP, CTF19-FRB::KanMX, sli15 $\Delta$ 2-228::hphNT1, pRS313-pOKP1-OKP1-SLI15 $\Delta$ 2-228- $\Delta$ INbox(626-698)-6xHis-7xFlag

<b>strain</b>	<b>genotype</b>
YSS345	MAT a, tor1-1, fpr1::loxP-Leu2-loxP, RPL13A-2xFKBP12::lox-TRP1-loxP, CTF19-FRB::KanMX, sli15Δ2-228::hphNT1, pRS313-pOKP1-OKP1-SLI15Δ2-228-ΔSAH(516-575)-6xHis-7xFlag
YSS315	MAT a, tor1-1, fpr1::loxP-Leu2-loxP, RPL13A-2xFKBP12::lox-TRP1-loxP, CTF19-FRB::KanMX, sli15Δ2-228::hphNT1, pRS313-pMIF2-MIF2-SLI15Δ2-228-6xHis-7xFlag
YSS313	MAT a, tor1-1, fpr1::loxP-Leu2-loxP, RPL13A-2xFKBP12::lox-TRP1-loxP, CTF19-FRB::KanMX, sli15Δ2-228::hphNT1, pRS313-pCTF3-CTF3-SLI15Δ2-228-6xHis-7xFlag
YSS314	MAT a, tor1-1, fpr1::loxP-Leu2-loxP, RPL13A-2xFKBP12::lox-TRP1-loxP, CTF19-FRB::KanMX, sli15Δ2-228::hphNT1, pRS313-pMTW1-MTW1-SLI15Δ2-228-6xHis-7xFlag
YSS311	MAT a, tor1-1, fpr1::loxP-Leu2-loxP, RPL13A-2xFKBP12::lox-TRP1-loxP, CTF19-FRB::KanMX, sli15Δ2-228::hphNT1, pRS313-pDSN1-DSN1-SLI15Δ2-228-6xHis-7xFlag
YSS317	MAT a, tor1-1, fpr1::loxP-Leu2-loxP, RPL13A-2xFKBP12::lox-TRP1-loxP, CTF19-FRB::KanMX, sli15Δ2-228::hphNT1, pRS313-pCNN1-CNN1-SLI15Δ2-228-6xHis-7xFlag
YSS366	MAT a, tor1-1, fpr1::loxP-Leu2-loxP, RPL13A-2xFKBP12::lox-TRP1-loxP, CTF19-FRB::KanMX, sli15Δ2-228::hphNT1, pRS313-pSLI15-SLI15Δ2-228-6xHis-6xFlag
YSS399	MAT a, tor1-1, fpr1::loxP-Leu2-loxP, RPL13A-2xFKBP12::lox-TRP1-loxP, CTF19-FRB::KanMX, sli15Δ2-228::hphNT1, pRS313-pAME1-AME1-CTF19-6xHis-7xFlag
YSS400	MAT a, tor1-1, fpr1::loxP-Leu2-loxP, RPL13A-2xFKBP12::lox-TRP1-loxP, CTF19-FRB::KanMX, sli15Δ2-228::hphNT1, pRS313-pAME1-AME1-CTF19ΔC270-369-6xHis-7xFlag
YSS401	MAT a, tor1-1, fpr1::loxP-Leu2-loxP, RPL13A-2xFKBP12::lox-TRP1-loxP, CTF19-FRB::KanMX, sli15Δ2-228::hphNT1, pRS313-pOKP1-OKP1-CTF19-6xHis-7xFlag
YSS402	MAT a, tor1-1, fpr1::loxP-Leu2-loxP, RPL13A-2xFKBP12::lox-TRP1-loxP, CTF19-FRB::KanMX, sli15Δ2-228::hphNT1, pRS313-pOKP1-OKP1-CTF19ΔC270-369-6xHis-7xFlag
YSS366	MAT a, tor1-1, fpr1::loxP-Leu2-loxP, RPL13A-2xFKBP12::lox-TRP1-loxP, CTF19-FRB::KanMX, sli15Δ2-228::hphNT1, pRS313-pSLI15-SLI15Δ2-228-6xHis-6xFlag
YTZ51	MAT a; leu2, ura3-52, trp1, prb1-1122, pep4-3, pre1-451, Ctf3-6xHis-6xFLAG::KanMX
YTZ2	MAT a; leu2, ura3-52, trp1, prb1-1122, pep4-3, pre1-451, Ame1-6xHis-6xFLAG::KanMX
YTZ3	MAT a; leu2, ura3-52, trp1, prb1-1122, pep4-3, pre1-451, Dsn1-6xHis-6xFLAG::KanMX
YTZ52	MAT a; leu2, ura3-52, trp1, prb1-1122, pep4-3, pre1-451, Mif2-6xHis-6xFLAG::KanMX

<b>strain</b>	<b>genotype</b>
YTZ53	MAT a; leu2, ura3-52, trp1, prb1-1122, pep4-3, pre1-451, Mcm16-6×His-6×FLAG::KanMX
YJF2	MAT a; leu2, ura3-52, trp1, prb1-1122, pep4-3, pre1-451, Cnn1-6×His-6×FLAG::KanMX
YJF3	MAT a; leu2, ura3-52, trp1, prb1-1122, pep4-3, pre1-451, Bub3-6×His-6×FLAG::KanMX
YJF4	MAT a; leu2, ura3-52, trp1, prb1-1122, pep4-3, pre1-451, Chl4-6×His-6×FLAG::KanMX
YJF5	MAT a; leu2, ura3-52, trp1, prb1-1122, pep4-3, pre1-451, Wip1-6×His-6×FLAG::KanMX
YJF6	MAT a; leu2, ura3-52, trp1, prb1-1122, pep4-3, pre1-451, Iml3-6×His-6×FLAG::KanMX
YTZ80	MAT a; leu2, ura3-52, trp1, prb1-1122, pep4-3, pre1-451, Mps1-6×His-6×FLAG::KanMX
YTZ57	MAT a; leu2, ura3-52, trp1, prb1-1122, pep4-3, pre1-451, Mad3-6×His-6×FLAG::KanMX
YTZ55	MAT a; leu2, ura3-52, trp1, prb1-1122, pep4-3, pre1-451, Sli15-6×His-6×FLAG::KanMX
YTZ73	MAT a; leu2, ura3-52, trp1, prb1-1122, pep4-3, pre1-451, Bir1-6×His-6×FLAG::KanMX

### 5.22.3. Predicted and experimentally annotated protein domains and motifs depicted in protein crosslink networks

Native and recombinant protein complexes were prepared and crosslinked as described.

Detected inter- and intra-protein crosslinks are represented as protein network diagrams in

Figure 10, Figure 13, Figure 24 and Figure 26.

Protein	Domain/Motif	Start	End	Reference
AME1	coiled coil	177	272	MARCOIL prediction
AME1	MIND binding	1	15	(25)
AME1	Okp1 binding	129	247	(34)
AME1	Nkp1-Nkp2 binding	268	292	(34)
CENPA/ CSE4	histone core	113	227	(149)
CENPA/ CSE4	CATD	166	201	(149)
CHL4	IML3 binding	361	458	(29)
CNN1	histone fold	271	335	(20)
CTF19	RWD	134	361	Sequence alignment model /Psipred structure prediction

Protein	Domain/Motif	Start	End	Reference
H2A	histone core	14	90	(150)
H2B	histone core	34	105	(150)
H3	histone core	63	132	(150)
H4	histone core	24	96	(150)
IML3	dimerization	169	198	(29)
IPL1	kinase domain	104	355	Sequence alignment model
MCM21	RWD	156	368	Sequence alignment model /Pspired strcuture prediction
MIF2	MTW1C binding	1	35	(25)
MIF2	signature motif	238	312	(25)
MIF2	IML3/CHL4 binding	256	549	(29)
MIF2	cupin fold	439	526	(25)
NDC80	MT binding	1	113	(60)
NDC80	calponin homology	114	233	(67)
NDC80	coiled coil	258	279	MARCOIL prediction
NDC80	coiled coil	294	499	MARCOIL prediction
NDC80	loop	453	520	(151)
NDC80	coiled coil	519	645	MARCOIL prediction
NUF2	calponin homology	13	132	(152)
NUF2	coiled coil	161	338	MARCOIL prediction
NUF2	coiled coil	341	450	MARCOIL prediction
OKP1	Core region	166	211	(34)
OKP1	coiled coil	183	290	MARCOIL prediction
OKP1	Ame1 binding	234	264	(34)
OKP1	Ctf19-Mcm21 binding	321	329	(34)
OKP1	coiled coil	346	381	MARCOIL prediction
OKP1	Nkp1-Nkp2	357	375	(34)
SLI15	CEN targeting	1	227	(86)
SLI15	MT binding	228	559	(90)
SLI15	SAH	517	565	(90)
SLI15	IPL1 binding	630	681	(92, 129)
SPC105	PP1 docking	21	24	(153)
SPC105	PP1 docking	74	78	(153)
SPC105	coiled coil	125	138	MARCOIL prediction
SPC105	MELT	146	149	(114)
SPC105	MELT	169	172	(114)
SPC105	coiled coil	194	206	MARCOIL prediction
SPC105	MELT	208	211	(114)
SPC105	MELT	232	235	(114)
SPC105	MELT	281	284	(114)
SPC105	MELT	310	313	(114)
SPC105	coiled coil	545	639	MARCOIL prediction
SPC105	coiled coil	670	700	MARCOIL prediction
SPC105	RWD	700	917	HHpred
SPC24	coiled coil	19	123	MARCOIL prediction
SPC24	RWD	155	213	(131)
SPC25	coiled coil	18	129	MARCOIL prediction
SPC25	RWD	133	221	(131)
WIP1	histone fold	1	89	Sequence alignment model
KRE28	coiled coil	129	201	MARCOIL prediction
KRE28	coiled coil	229	265	MARCOIL prediction

## 6. References

1. Barnum KJ, O'Connell MJ. Cell cycle regulation by checkpoints. *Methods Mol Biol.* 2014;1170:29-40.
2. Sullivan M, Morgan DO. Finishing mitosis, one step at a time. *Nat Rev Mol Cell Biol.* 2007;8(11):894-903.
3. Uhlmann F, Nasmyth K. Cohesion between sister chromatids must be established during DNA replication. *Current biology : CB.* 1998;8(20):1095-101.
4. Sivakumar S, Gorbsky GJ. Spatiotemporal regulation of the anaphase-promoting complex in mitosis. *Nat Rev Mol Cell Biol.* 2015;16(2):82-94.
5. Thornton BR, Toczyski DP. Securin and B-cyclin/CDK are the only essential targets of the APC. *Nat Cell Biol.* 2003;5(12):1090-4.
6. Biggins S. The composition, functions, and regulation of the budding yeast kinetochore. *Genetics.* 2013;194(4):817-46.
7. Musacchio A, Desai A. A Molecular View of Kinetochore Assembly and Function. *Biology (Basel).* 2017;6(1).
8. Santaguida S, Musacchio A. The life and miracles of kinetochores. *The EMBO journal.* 2009;28(17):2511-31.
9. Furuyama S, Biggins S. Centromere identity is specified by a single centromeric nucleosome in budding yeast. *Proc Natl Acad Sci U S A.* 2007;104(37):14706-11.
10. Bodor DL, Mata JF, Sergeev M, David AF, Salimian KJ, Panchenko T, et al. The quantitative architecture of centromeric chromatin. *Elife.* 2014;3:e02137.
11. Fitzgerald-Hayes M, Clarke L, Carbon J. Nucleotide sequence comparisons and functional analysis of yeast centromere DNAs. *Cell.* 1982;29(1):235-44.
12. Hasson D, Panchenko T, Salimian KJ, Salman MU, Sekulic N, Alonso A, et al. The octamer is the major form of CENP-A nucleosomes at human centromeres. *Nat Struct Mol Biol.* 2013;20(6):687-95.
13. Cai M, Davis RW. Yeast centromere binding protein CBF1, of the helix-loop-helix protein family, is required for chromosome stability and methionine prototrophy. *Cell.* 1990;61(3):437-46.
14. Lechner J, Carbon J. A 240 kd multisubunit protein complex, CBF3, is a major component of the budding yeast centromere. *Cell.* 1991;64(4):717-25.
15. Heun P, Erhardt S, Blower MD, Weiss S, Skora AD, Karpen GH. Mislocalization of the *Drosophila* centromere-specific histone CID promotes formation of functional ectopic kinetochores. *Dev Cell.* 2006;10(3):303-15.
16. Walczak CE, Cai S, Khodjakov A. Mechanisms of chromosome behaviour during mitosis. *Nat Rev Mol Cell Biol.* 2010;11(2):91-102.
17. Joglekar AP, Bouck DC, Molk JN, Bloom KS, Salmon ED. Molecular architecture of a kinetochore-microtubule attachment site. *Nat Cell Biol.* 2006;8(6):581-5.
18. Zinkowski RP, Meyne J, Brinkley BR. The centromere-kinetochore complex: a repeat subunit model. *J Cell Biol.* 1991;113(5):1091-110.
19. De Wulf P, McAinsh AD, Sorger PK. Hierarchical assembly of the budding yeast kinetochore from multiple subcomplexes. *Genes Dev.* 2003;17(23):2902-21.
20. Westermann S, Schleiffer A. Family matters: structural and functional conservation of centromere-associated proteins from yeast to humans. *Trends Cell Biol.* 2013;23(6):260-9.
21. Hori T, Okada M, Maenaka K, Fukagawa T. CENP-O class proteins form a stable complex and are required for proper kinetochore function. *Mol Biol Cell.* 2008;19(3):843-54.
22. van Hooff JJ, Tromer E, van Wijk LM, Snel B, Kops GJ. Evolutionary dynamics of the kinetochore network in eukaryotes as revealed by comparative genomics. *EMBO Rep.* 2017;18(9):1559-71.

23. Xiao H, Wang F, Wisniewski J, Shaytan AK, Ghirlando R, FitzGerald PC, et al. Molecular basis of CENP-C association with the CENP-A nucleosome at yeast centromeres. *Genes Dev.* 2017;31(19):1958-72.
24. Kato H, Jiang J, Zhou BR, Rozendaal M, Feng H, Ghirlando R, et al. A conserved mechanism for centromeric nucleosome recognition by centromere protein CENP-C. *Science.* 2013;340(6136):1110-3.
25. Hornung P, Troc P, Malvezzi F, Maier M, Demianova Z, Zimniak T, et al. A cooperative mechanism drives budding yeast kinetochore assembly downstream of CENP-A. *J Cell Biol.* 2014;206(4):509-24.
26. Screpanti E, De Antoni A, Alushin GM, Petrovic A, Melis T, Nogales E, et al. Direct binding of Cenp-C to the Mis12 complex joins the inner and outer kinetochore. *Current biology : CB.* 2011;21(5):391-8.
27. Przewloka MR, Venkei Z, Bolanos-Garcia VM, Debski J, Dadlez M, Glover DM. CENP-C is a structural platform for kinetochore assembly. *Current biology : CB.* 2011;21(5):399-405.
28. Cohen RL, Espelin CW, De Wulf P, Sorger PK, Harrison SC, Simons KT. Structural and functional dissection of Mif2p, a conserved DNA-binding kinetochore protein. *Mol Biol Cell.* 2008;19(10):4480-91.
29. Hinshaw SM, Harrison SC. An Iml3-Chl4 heterodimer links the core centromere to factors required for accurate chromosome segregation. *Cell Rep.* 2013;5(1):29-36.
30. Fernius J, Marston AL. Establishment of cohesion at the pericentromere by the Ctf19 kinetochore subcomplex and the replication fork-associated factor, Csm3. *PLoS Genet.* 2009;5(9):e1000629.
31. Natsume T, Muller CA, Katou Y, Retkute R, Gierlinski M, Araki H, et al. Kinetochores coordinate pericentromeric cohesion and early DNA replication by Cdc7-Dbf4 kinase recruitment. *Mol Cell.* 2013;50(5):661-74.
32. Pekgoz Altunkaya G, Malvezzi F, Demianova Z, Zimniak T, Litos G, Weissmann F, et al. CCAN Assembly Configures Composite Binding Interfaces to Promote Cross-Linking of Ndc80 Complexes at the Kinetochore. *Current biology : CB.* 2016;26(17):2370-8.
33. Pot I, Measday V, Snyderman B, Cagney G, Fields S, Davis TN, et al. Chl4p and iml3p are two new members of the budding yeast outer kinetochore. *Mol Biol Cell.* 2003;14(2):460-76.
34. Schmitzberger F, Richter MM, Gordiyenko Y, Robinson CV, Dadlez M, Westermann S. Molecular basis for inner kinetochore configuration through RWD domain-peptide interactions. *The EMBO journal.* 2017.
35. Hinshaw SM, Harrison SC. The structure of the Ctf19c/CCAN from budding yeast. *Elife.* 2019;8.
36. Carroll CW, Silva MC, Godek KM, Jansen LE, Straight AF. Centromere assembly requires the direct recognition of CENP-A nucleosomes by CENP-N. *Nat Cell Biol.* 2009;11(7):896-902.
37. Guse A, Carroll CW, Moree B, Fuller CJ, Straight AF. In vitro centromere and kinetochore assembly on defined chromatin templates. *Nature.* 2011;477(7364):354-8.
38. Pentakota S, Zhou K, Smith C, Maffini S, Petrovic A, Morgan GP, et al. Decoding the centromeric nucleosome through CENP-N. *Elife.* 2017;6.
39. Chittori S, Hong J, Saunders H, Feng H, Ghirlando R, Kelly AE, et al. Structural mechanisms of centromeric nucleosome recognition by the kinetochore protein CENP-N. *Science.* 2018;359(6373):339-43.
40. Tian T, Li X, Liu Y, Wang C, Liu X, Bi G, et al. Molecular basis for CENP-N recognition of CENP-A nucleosome on the human kinetochore. *Cell Res.* 2018;28(3):374-8.

41. Weir JR, Faesen AC, Klare K, Petrovic A, Basilico F, Fischbock J, et al. Insights from biochemical reconstitution into the architecture of human kinetochores. *Nature*. 2016;537(7619):249-53.
42. Westermann S, Cheeseman IM, Anderson S, Yates JR, 3rd, Drubin DG, Barnes G. Architecture of the budding yeast kinetochore reveals a conserved molecular core. *J Cell Biol*. 2003;163(2):215-22.
43. McKinley KL, Sekulic N, Guo LY, Tsinman T, Black BE, Cheeseman IM. The CENP-L-N Complex Forms a Critical Node in an Integrated Meshwork of Interactions at the Centromere-Kinetochore Interface. *Mol Cell*. 2015;60(6):886-98.
44. Pesenti ME, Prumbaum D, Auckland P, Smith CM, Faesen AC, Petrovic A, et al. Reconstitution of a 26-Subunit Human Kinetochore Reveals Cooperative Microtubule Binding by CENP-OPQUR and NDC80. *Mol Cell*. 2018;71(6):923-39 e10.
45. Hori T, Amano M, Suzuki A, Backer CB, Welburn JP, Dong Y, et al. CCAN makes multiple contacts with centromeric DNA to provide distinct pathways to the outer kinetochore. *Cell*. 2008;135(6):1039-52.
46. Schleiffer A, Maier M, Litos G, Lampert F, Hornung P, Mechtler K, et al. CENP-T proteins are conserved centromere receptors of the Ndc80 complex. *Nature cell biology*. 2012;14(6):604-13.
47. Lang J, Barber A, Biggins S. An assay for de novo kinetochore assembly reveals a key role for the CENP-T pathway in budding yeast. *Elife*. 2018;7.
48. Malvezzi F, Litos G, Schleiffer A, Heuck A, Mechtler K, Clausen T, et al. A structural basis for kinetochore recruitment of the Ndc80 complex via two distinct centromere receptors. *The EMBO journal*. 2013;32(3):409-23.
49. Dimitrova YN, Jenni S, Valverde R, Khin Y, Harrison SC. Structure of the MIND Complex Defines a Regulatory Focus for Yeast Kinetochore Assembly. *Cell*. 2016;167(4):1014-27 e12.
50. Schmitzberger F, Harrison SC. RWD domain: a recurring module in kinetochore architecture shown by a Ctf19-Mcm21 complex structure. *EMBO Rep*. 2012;13(3):216-22.
51. Knockleby J, Vogel J. The COMA complex is required for Sli15/INCENP-mediated correction of defective kinetochore attachments. *Cell Cycle*. 2009;8(16):2570-7.
52. Foltz DR, Jansen LE, Black BE, Bailey AO, Yates JR, 3rd, Cleveland DW. The human CENP-A centromeric nucleosome-associated complex. *Nat Cell Biol*. 2006;8(5):458-69.
53. Okada M, Cheeseman IM, Hori T, Okawa K, McLeod IX, Yates JR, 3rd, et al. The CENP-H-I complex is required for the efficient incorporation of newly synthesized CENP-A into centromeres. *Nat Cell Biol*. 2006;8(5):446-57.
54. Meluh PB, Koshland D. Budding yeast centromere composition and assembly as revealed by in vivo cross-linking. *Genes Dev*. 1997;11(24):3401-12.
55. Ortiz J, Stemmann O, Rank S, Lechner J. A putative protein complex consisting of Ctf19, Mcm21, and Okp1 represents a missing link in the budding yeast kinetochore. *Genes Dev*. 1999;13(9):1140-55.
56. Kagawa N, Hori T, Hoki Y, Hosoya O, Tsutsui K, Saga Y, et al. The CENP-O complex requirement varies among different cell types. *Chromosome Res*. 2014;22(3):293-303.
57. Cheeseman IM, Desai A. Molecular architecture of the kinetochore-microtubule interface. *Nature reviews Molecular cell biology*. 2008;9(1):33-46.
58. DeLuca JG, Gall WE, Ciferri C, Cimini D, Musacchio A, Salmon ED. Kinetochore microtubule dynamics and attachment stability are regulated by Hec1. *Cell*. 2006;127(5):969-82.

59. Kline SL, Cheeseman IM, Hori T, Fukagawa T, Desai A. The human Mis12 complex is required for kinetochore assembly and proper chromosome segregation. *J Cell Biol.* 2006;173(1):9-17.
60. Lampert F, Westermann S. A blueprint for kinetochores - new insights into the molecular mechanics of cell division. *Nature reviews Molecular cell biology.* 2011;12(7):407-12.
61. Joglekar AP, Bloom K, Salmon ED. In vivo protein architecture of the eukaryotic kinetochore with nanometer scale accuracy. *Current biology : CB.* 2009;19(8):694-9.
62. Petrovic A, Pasqualato S, Dube P, Krenn V, Santaguida S, Cittaro D, et al. The MIS12 complex is a protein interaction hub for outer kinetochore assembly. *J Cell Biol.* 2010;190(5):835-52.
63. Petrovic A, Mosalaganti S, Keller J, Mattiuzzo M, Overlack K, Krenn V, et al. Modular assembly of RWD domains on the Mis12 complex underlies outer kinetochore organization. *Mol Cell.* 2014;53(4):591-605.
64. Pagliuca C, Draviam VM, Marco E, Sorger PK, De Wulf P. Roles for the conserved spc105p/kre28p complex in kinetochore-microtubule binding and the spindle assembly checkpoint. *PLoS One.* 2009;4(10):e7640.
65. Foley EA, Kapoor TM. Microtubule attachment and spindle assembly checkpoint signalling at the kinetochore. *Nature reviews Molecular cell biology.* 2013;14(1):25-37.
66. Wang HW, Long S, Ciferri C, Westermann S, Drubin D, Barnes G, et al. Architecture and flexibility of the yeast Ndc80 kinetochore complex. *J Mol Biol.* 2008;383(4):894-903.
67. Wei RR, Al-Bassam J, Harrison SC. The Ndc80/HEC1 complex is a contact point for kinetochore-microtubule attachment. *Nat Struct Mol Biol.* 2007;14(1):54-9.
68. Westermann S, Avila-Sakar A, Wang HW, Niederstrasser H, Wong J, Drubin DG, et al. Formation of a dynamic kinetochore- microtubule interface through assembly of the Dam1 ring complex. *Mol Cell.* 2005;17(2):277-90.
69. Grishchuk EL, Spiridonov IS, Volkov VA, Efremov A, Westermann S, Drubin D, et al. Different assemblies of the DAM1 complex follow shortening microtubules by distinct mechanisms. *Proc Natl Acad Sci U S A.* 2008;105(19):6918-23.
70. Wilson-Kubalek EM, Cheeseman IM, Yoshioka C, Desai A, Milligan RA. Orientation and structure of the Ndc80 complex on the microtubule lattice. *J Cell Biol.* 2008;182(6):1055-61.
71. Helgeson LA, Zelter A, Riffle M, MacCoss MJ, Asbury CL, Davis TN. Human Ska complex and Ndc80 complex interact to form a load-bearing assembly that strengthens kinetochore-microtubule attachments. *Proc Natl Acad Sci U S A.* 2018;115(11):2740-5.
72. Tanaka TU. Kinetochore-microtubule interactions: steps towards bi-orientation. *The EMBO journal.* 2010;29(24):4070-82.
73. Baker DJ, Chen J, van Deursen JM. The mitotic checkpoint in cancer and aging: what have mice taught us? *Current opinion in cell biology.* 2005;17(6):583-9.
74. Pfau SJ, Amon A. Chromosomal instability and aneuploidy in cancer: from yeast to man. *EMBO Rep.* 2012;13(6):515-27.
75. Tanaka TU, Rachidi N, Janke C, Pereira G, Galova M, Schiebel E, et al. Evidence that the Ipl1-Sli15 (Aurora kinase-INCENP) complex promotes chromosome bi-orientation by altering kinetochore-spindle pole connections. *Cell.* 2002;108(3):317-29.
76. Dewar H, Tanaka K, Nasmyth K, Tanaka TU. Tension between two kinetochores suffices for their bi-orientation on the mitotic spindle. *Nature.* 2004;428(6978):93-7.
77. Nicklas RB. How cells get the right chromosomes. *Science.* 1997;275(5300):632-7.
78. Kitagawa M, Lee SH. The chromosomal passenger complex (CPC) as a key orchestrator of orderly mitotic exit and cytokinesis. *Frontiers in cell and developmental biology.* 2015;3:14.



79. Carmena M, Wheelock M, Funabiki H, Earnshaw WC. The chromosomal passenger complex (CPC): from easy rider to the godfather of mitosis. *Nature reviews Molecular cell biology*. 2012;13(12):789-803.
80. Klein UR, Nigg EA, Gruneberg U. Centromere targeting of the chromosomal passenger complex requires a ternary subcomplex of Borealin, Survivin, and the N-terminal domain of INCENP. *Mol Biol Cell*. 2006;17(6):2547-58.
81. Jeyaprakash AA, Klein UR, Lindner D, Ebert J, Nigg EA, Conti E. Structure of a Survivin-Borealin-INCENP core complex reveals how chromosomal passengers travel together. *Cell*. 2007;131(2):271-85.
82. van der Horst A, Lens SM. Cell division: control of the chromosomal passenger complex in time and space. *Chromosoma*. 2014;123(1-2):25-42.
83. Cho US, Harrison SC. Ndc10 is a platform for inner kinetochore assembly in budding yeast. *Nat Struct Mol Biol*. 2011;19(1):48-55.
84. Kawashima SA, Yamagishi Y, Honda T, Ishiguro K, Watanabe Y. Phosphorylation of H2A by Bub1 prevents chromosomal instability through localizing shugoshin. *Science*. 2010;327(5962):172-7.
85. Wang F, Dai J, Daum JR, Niedzialkowska E, Banerjee B, Stukenberg PT, et al. Histone H3 Thr-3 phosphorylation by Haspin positions Aurora B at centromeres in mitosis. *Science*. 2010;330(6001):231-5.
86. Campbell CS, Desai A. Tension sensing by Aurora B kinase is independent of survivin-based centromere localization. *Nature*. 2013;497(7447):118-21.
87. Bishop JD, Schumacher JM. Phosphorylation of the carboxyl terminus of inner centromere protein (INCENP) by the Aurora B Kinase stimulates Aurora B kinase activity. *J Biol Chem*. 2002;277(31):27577-80.
88. Samejima K, Platani M, Wolny M, Ogawa H, Vargiu G, Knight PJ, et al. The Inner Centromere Protein (INCENP) Coil Is a Single alpha-Helix (SAH) Domain That Binds Directly to Microtubules and Is Important for Chromosome Passenger Complex (CPC) Localization and Function in Mitosis. *J Biol Chem*. 2015;290(35):21460-72.
89. van der Horst A, Vromans MJ, Bouwman K, van der Waal MS, Hadders MA, Lens SM. Inter-domain Cooperation in INCENP Promotes Aurora B Relocation from Centromeres to Microtubules. *Cell Rep*. 2015;12(3):380-7.
90. Fink S, Turnbull K, Desai A, Campbell CS. An engineered minimal chromosomal passenger complex reveals a role for INCENP/Slh15 spindle association in chromosome biorientation. *J Cell Biol*. 2017;216(4):911-23.
91. Pereira G, Schiebel E. Separase regulates INCENP-Aurora B anaphase spindle function through Cdc14. *Science*. 2003;302(5653):2120-4.
92. Adams RR, Wheatley SP, Gouldsworthy AM, Kandels-Lewis SE, Carmena M, Smythe C, et al. INCENP binds the Aurora-related kinase AIRK2 and is required to target it to chromosomes, the central spindle and cleavage furrow. *Current biology : CB*. 2000;10(17):1075-8.
93. Honda R, Korner R, Nigg EA. Exploring the functional interactions between Aurora B, INCENP, and survivin in mitosis. *Mol Biol Cell*. 2003;14(8):3325-41.
94. Sessa F, Mapelli M, Ciferri C, Tarricone C, Areces LB, Schneider TR, et al. Mechanism of Aurora B activation by INCENP and inhibition by hesperadin. *Mol Cell*. 2005;18(3):379-91.
95. Liu D, Vader G, Vromans MJ, Lampson MA, Lens SM. Sensing chromosome bi-orientation by spatial separation of aurora B kinase from kinetochore substrates. *Science*. 2009;323(5919):1350-3.
96. DeLuca KF, Lens SM, DeLuca JG. Temporal changes in Hec1 phosphorylation control kinetochore-microtubule attachment stability during mitosis. *Journal of cell science*. 2011;124(Pt 4):622-34.

97. Cheeseman IM, Chappie JS, Wilson-Kubalek EM, Desai A. The conserved KMN network constitutes the core microtubule-binding site of the kinetochore. *Cell*. 2006;127(5):983-97.
98. Guimaraes GJ, Dong Y, McEwen BF, Deluca JG. Kinetochore-microtubule attachment relies on the disordered N-terminal tail domain of Hec1. *Curr Biol*. 2008;18(22):1778-84.
99. Tien JF, Umbreit NT, Gestaut DR, Franck AD, Cooper J, Wordeman L, et al. Cooperation of the Dam1 and Ndc80 kinetochore complexes enhances microtubule coupling and is regulated by aurora B. *J Cell Biol*. 2010;189(4):713-23.
100. Lampert F, Mieck C, Alushin GM, Nogales E, Westermann S. Molecular requirements for the formation of a kinetochore-microtubule interface by Dam1 and Ndc80 complexes. *The Journal of cell biology*. 2013;200(1):21-30.
101. Kim JO, Zelter A, Umbreit NT, Bollozos A, Riffle M, Johnson R, et al. The Ndc80 complex bridges two Dam1 complex rings. *eLife*. 2017;6.
102. Chan YW, Jeyaprakash AA, Nigg EA, Santamaria A. Aurora B controls kinetochore-microtubule attachments by inhibiting Ska complex-KMN network interaction. *J Cell Biol*. 2012;196(5):563-71.
103. Lampson MA, Cheeseman IM. Sensing centromere tension: Aurora B and the regulation of kinetochore function. *Trends Cell Biol*. 2011;21(3):133-40.
104. Maresca TJ, Salmon ED. Welcome to a new kind of tension: translating kinetochore mechanics into a wait-anaphase signal. *Journal of cell science*. 2010;123(Pt 6):825-35.
105. Francisco L, Wang W, Chan CS. Type 1 protein phosphatase acts in opposition to IpL1 protein kinase in regulating yeast chromosome segregation. *Mol Cell Biol*. 1994;14(7):4731-40.
106. Krenn V, Musacchio A. The Aurora B Kinase in Chromosome Bi-Orientation and Spindle Checkpoint Signaling. *Front Oncol*. 2015;5:225.
107. Akiyoshi B, Nelson CR, Biggins S. The aurora B kinase promotes inner and outer kinetochore interactions in budding yeast. *Genetics*. 2013;194(3):785-9.
108. Hayashi-Takanaka Y, Yamagata K, Nozaki N, Kimura H. Visualizing histone modifications in living cells: spatiotemporal dynamics of H3 phosphorylation during interphase. *J Cell Biol*. 2009;187(6):781-90.
109. Santaguida S, Vernieri C, Villa F, Ciliberto A, Musacchio A. Evidence that Aurora B is implicated in spindle checkpoint signalling independently of error correction. *The EMBO journal*. 2011;30(8):1508-19.
110. Yamagishi Y, Yang CH, Tanno Y, Watanabe Y. MPS1/Mph1 phosphorylates the kinetochore protein KNL1/Spc7 to recruit SAC components. *Nat Cell Biol*. 2012;14(7):746-52.
111. Shepperd LA, Meadows JC, Sochaj AM, Lancaster TC, Zou J, Buttrick GJ, et al. Phosphodependent recruitment of Bub1 and Bub3 to Spc7/KNL1 by Mph1 kinase maintains the spindle checkpoint. *Current biology : CB*. 2012;22(10):891-9.
112. London N, Biggins S. Signalling dynamics in the spindle checkpoint response. *Nat Rev Mol Cell Biol*. 2014;15(11):736-47.
113. Musacchio A, Salmon ED. The spindle-assembly checkpoint in space and time. *Nat Rev Mol Cell Biol*. 2007;8(5):379-93.
114. London N, Ceto S, Ranish JA, Biggins S. Phosphoregulation of Spc105 by Mps1 and PP1 regulates Bub1 localization to kinetochores. *Curr Biol*. 2012;22(10):900-6.
115. Espert A, Uluocak P, Bastos RN, Mangat D, Graab P, Gruneberg U. PP2A-B56 opposes Mps1 phosphorylation of Knl1 and thereby promotes spindle assembly checkpoint silencing. *The Journal of cell biology*. 2014;206(7):833-42.
116. Kim S, Yu H. Mutual regulation between the spindle checkpoint and APC/C. *Semin Cell Dev Biol*. 2011;22(6):551-8.

117. Buschhorn BA, Peters JM. How APC/C orders destruction. *Nat Cell Biol.* 2006;8(3):209-11.
118. Ciosk R, Zachariae W, Michaelis C, Shevchenko A, Mann M, Nasmyth K. An ESP1/PDS1 complex regulates loss of sister chromatid cohesion at the metaphase to anaphase transition in yeast. *Cell.* 1998;93(6):1067-76.
119. Rieder CL, Schultz A, Cole R, Sluder G. Anaphase onset in vertebrate somatic cells is controlled by a checkpoint that monitors sister kinetochore attachment to the spindle. *J Cell Biol.* 1994;127(5):1301-10.
120. Rieder CL, Cole RW, Khodjakov A, Sluder G. The checkpoint delaying anaphase in response to chromosome monoorientation is mediated by an inhibitory signal produced by unattached kinetochores. *J Cell Biol.* 1995;130(4):941-8.
121. McIntosh JR, O'Toole E, Zhudenkov K, Morphey M, Schwartz C, Ataulakhanov FI, et al. Conserved and divergent features of kinetochores and spindle microtubule ends from five species. *The Journal of cell biology.* 2013;200(4):459-74.
122. Herzog F, Kahraman A, Boehringer D, Mak R, Bracher A, Walzthoeni T, et al. Structural probing of a protein phosphatase 2A network by chemical cross-linking and mass spectrometry. *Science.* 2012;337(6100):1348-52.
123. Seebacher J, Mallick P, Zhang N, Eddes JS, Aebersold R, Gelb MH. Protein cross-linking analysis using mass spectrometry, isotope-coded cross-linkers, and integrated computational data processing. *J Proteome Res.* 2006;5(9):2270-82.
124. Walzthoeni T, Claassen M, Leitner A, Herzog F, Bohn S, Forster F, et al. False discovery rate estimation for cross-linked peptides identified by mass spectrometry. *Nature methods.* 2012;9(9):901-3.
125. Nishino T, Takeuchi K, Gascoigne KE, Suzuki A, Hori T, Oyama T, et al. CENP-T-W-S-X forms a unique centromeric chromatin structure with a histone-like fold. *Cell.* 2012;148(3):487-501.
126. Ji Z, Gao H, Yu H. CELL DIVISION CYCLE. Kinetochore attachment sensed by competitive Mps1 and microtubule binding to Ndc80C. *Science.* 2015;348(6240):1260-4.
127. Haruki H, Nishikawa J, Laemmli UK. The anchor-away technique: rapid, conditional establishment of yeast mutant phenotypes. *Mol Cell.* 2008;31(6):925-32.
128. Hinshaw SM, Makrantonis V, Harrison SC, Marston AL. The Kinetochore Receptor for the Cohesin Loading Complex. *Cell.* 2017;171(1):72-84 e13.
129. Kang J, Cheeseman IM, Kallstrom G, Velmurugan S, Barnes G, Chan CS. Functional cooperation of Dam1, Ipl1, and the inner centromere protein (INCENP)-related protein Sli15 during chromosome segregation. *J Cell Biol.* 2001;155(5):763-74.
130. Weissmann F, Petzold G, VanderLinden R, Huis In 't Veld PJ, Brown NG, Lampert F, et al. biGBac enables rapid gene assembly for the expression of large multisubunit protein complexes. *Proc Natl Acad Sci U S A.* 2016;113(19):E2564-9.
131. Wei RR, Schnell JR, Larsen NA, Sorger PK, Chou JJ, Harrison SC. Structure of a central component of the yeast kinetochore: the Spc24p/Spc25p globular domain. *Structure.* 2006;14(6):1003-9.
132. Anedchenko EA, Samel-Pommerencke A, Tran Nguyen TM, Shahnejat-Bushehri S, Popsel J, Lauster D, et al. The kinetochore module Okp1(CENP-Q)/Ame1(CENP-U) is a reader for N-terminal modifications on the centromeric histone Cse4(CENP-A). *The EMBO journal.* 2019;38(1).
133. Chen Y, Baker RE, Keith KC, Harris K, Stoler S, Fitzgerald-Hayes M. The N terminus of the centromere H3-like protein Cse4p performs an essential function distinct from that of the histone fold domain. *Mol Cell Biol.* 2000;20(18):7037-48.
134. Burrack LS, Berman J. Neocentromeres and epigenetically inherited features of centromeres. *Chromosome Res.* 2012;20(5):607-19.

135. Blower MD, Sullivan BA, Karpen GH. Conserved organization of centromeric chromatin in flies and humans. *Dev Cell*. 2002;2(3):319-30.
136. Hyland KM, Kingsbury J, Koshland D, Hieter P. Ctf19p: A novel kinetochore protein in *Saccharomyces cerevisiae* and a potential link between the kinetochore and mitotic spindle. *J Cell Biol*. 1999;145(1):15-28.
137. Poddar A, Roy N, Sinha P. MCM21 and MCM22, two novel genes of the yeast *Saccharomyces cerevisiae* are required for chromosome transmission. *Mol Microbiol*. 1999;31(1):349-60.
138. Garcia-Rodriguez LJ, Kasciukovic T, Denninger V, Tanaka TU. Aurora B-INCENP Localization at Centromeres/Inner Kinetochores Is Required for Chromosome Bi-orientation in Budding Yeast. *Current biology : CB*. 2019;29(9):1536-44 e4.
139. Hengeveld RCC, Vromans MJM, Vleugel M, Hadders MA, Lens SMA. Inner centromere localization of the CPC maintains centromere cohesion and allows mitotic checkpoint silencing. *Nature communications*. 2017;8:15542.
140. Yue Z, Carvalho A, Xu Z, Yuan X, Cardinale S, Ribeiro S, et al. Deconstructing Survivin: comprehensive genetic analysis of Survivin function by conditional knockout in a vertebrate cell line. *The Journal of cell biology*. 2008;183(2):279-96.
141. Hori T, Shang WH, Takeuchi K, Fukagawa T. The CCAN recruits CENP-A to the centromere and forms the structural core for kinetochore assembly. *The Journal of cell biology*. 2013;200(1):45-60.
142. Tanaka K, Mukae N, Dewar H, van Breugel M, James EK, Prescott AR, et al. Molecular mechanisms of kinetochore capture by spindle microtubules. *Nature*. 2005;434(7036):987-94.
143. Caldas GV, DeLuca KF, DeLuca JG. KNL1 facilitates phosphorylation of outer kinetochore proteins by promoting Aurora B kinase activity. *The Journal of cell biology*. 2013;203(6):957-69.
144. Turco E, Gallego LD, Schneider M, Kohler A. Monoubiquitination of histone H2B is intrinsic to the Bre1 RING domain-Rad6 interaction and augmented by a second Rad6-binding site on Bre1. *J Biol Chem*. 2015;290(9):5298-310.
145. Janke C, Magiera MM, Rathfelder N, Taxis C, Reber S, Maekawa H, et al. A versatile toolbox for PCR-based tagging of yeast genes: new fluorescent proteins, more markers and promoter substitution cassettes. *Yeast*. 2004;21(11):947-62.
146. Grimm M, Zimniak T, Kahraman A, Herzog F. xVis: a web server for the schematic visualization and interpretation of crosslink-derived spatial restraints. *Nucleic Acids Res*. 2015;43(W1):W362-9.
147. Schindelin J, Arganda-Carreras I, Frise E, Kaynig V, Longair M, Pietzsch T, et al. Fiji: an open-source platform for biological-image analysis. *Nature methods*. 2012;9(7):676-82.
148. Tan S, Kern RC, Selleck W. The pST44 polycistronic expression system for producing protein complexes in *Escherichia coli*. *Protein Expr Purif*. 2005;40(2):385-95.
149. Zhou Z, Feng H, Zhou BR, Ghirlando R, Hu K, Zwolak A, et al. Structural basis for recognition of centromere histone variant CenH3 by the chaperone Scm3. *Nature*. 2011;472(7342):234-7.
150. Wang F, Li G, Altaf M, Lu C, Currie MA, Johnson A, et al. Heterochromatin protein Sir3 induces contacts between the amino terminus of histone H4 and nucleosomal DNA. *Proc Natl Acad Sci U S A*. 2013;110(21):8495-500.
151. Maure JF, Komoto S, Oku Y, Mino A, Pasqualato S, Natsume K, et al. The Ndc80 loop region facilitates formation of kinetochore attachment to the dynamic microtubule plus end. *Current biology : CB*. 2011;21(3):207-13.
152. Ciferri C, Pasqualato S, Screpanti E, Varetti G, Santaguida S, Dos Reis G, et al. Implications for kinetochore-microtubule attachment from the structure of an engineered Ndc80 complex. *Cell*. 2008;133(3):427-39.

153. Rosenberg JS, Cross FR, Funabiki H. KNL1/Spc105 recruits PP1 to silence the spindle assembly checkpoint. *Current biology* : CB. 2011;21(11):942-7.

## **7. Appendix**

**Publication: The COMA complex interacts with Cse4 and positions Sli15/Ipl1 at the budding yeast inner kinetochore (Fischboeck-Halwachs et al., eLife, 2019)**



# The COMA complex interacts with Cse4 and positions Sli15/Ipl1 at the budding yeast inner kinetochore

Josef Fischböck-Halwachs<sup>1,2†</sup>, Sylvia Singh<sup>1,2†</sup>, Mia Potocnjak<sup>1,2†</sup>, Götz Hagemann<sup>1,2</sup>, Victor Solis-Mezarino<sup>1,2</sup>, Stephan Woike<sup>1,2</sup>, Medini Ghodgaonkar-Steger<sup>1,2</sup>, Florian Weissmann<sup>3</sup>, Laura D Gallego<sup>4</sup>, Julie Rojas<sup>5</sup>, Jessica Andreani<sup>6</sup>, Alwin Köhler<sup>4</sup>, Franz Herzog<sup>1,2\*</sup>

<sup>1</sup>Gene Center Munich, Department of Biochemistry, Ludwig-Maximilians-Universität München, Munich, Germany; <sup>2</sup>Department of Biochemistry, Ludwig-Maximilians-Universität München, Munich, Germany; <sup>3</sup>Research Institute of Molecular Pathology (IMP), Vienna Biocenter (VBC), Vienna, Austria; <sup>4</sup>Max F Perutz Laboratories, Medical University of Vienna, Vienna, Austria; <sup>5</sup>Laboratory of Chromosome Biology, Max Planck Institute of Biochemistry, Martinsried, Germany; <sup>6</sup>Institute for Integrative Biology of the Cell (I2BC), CEA, CNRS, Université Paris-Sud, Université Paris-Saclay, Gif-sur-Yvette, France

**Abstract** Kinetochores are macromolecular protein complexes at centromeres that ensure accurate chromosome segregation by attaching chromosomes to spindle microtubules and integrating safeguard mechanisms. The inner kinetochore is assembled on CENP-A nucleosomes and has been implicated in establishing a kinetochore-associated pool of Aurora B kinase, a chromosomal passenger complex (CPC) subunit, which is essential for chromosome biorientation. By performing crosslink-guided *in vitro* reconstitution of budding yeast kinetochore complexes we showed that the Ame1/Okp1<sup>CENP-U/Q</sup> heterodimer, which forms the COMA complex with Ctf19/Mcm21<sup>CENP-P/O</sup>, selectively bound Cse4<sup>CENP-A</sup> nucleosomes through the Cse4 N-terminus. The Sli15/Ipl1<sup>INCENP/Aurora-B</sup> core-CPC interacted with COMA *in vitro* through the Ctf19 C-terminus whose deletion affected chromosome segregation fidelity in Sli15 wild-type cells. Tethering Sli15 to Ame1/Okp1 rescued synthetic lethality upon Ctf19 depletion in a Sli15 centromere-targeting deficient mutant. This study shows molecular characteristics of the point-centromere kinetochore architecture and suggests a role for the Ctf19 C-terminus in mediating CPC-binding and accurate chromosome segregation.

DOI: <https://doi.org/10.7554/eLife.42879.001>

\*For correspondence:  
herzog@genzentrum.lmu.de

†These authors contributed  
equally to this work

**Competing interests:** The  
authors declare that no  
competing interests exist.

**Funding:** See page 22

**Received:** 16 October 2018

**Accepted:** 20 May 2019

**Published:** 21 May 2019

**Reviewing editor:** Jennifer G  
DeLuca, Colorado State  
University, United States

© Copyright Fischböck-Halwachs et al. This article is distributed under the terms of the [Creative Commons Attribution License](https://creativecommons.org/licenses/by/4.0/), which permits unrestricted use and redistribution provided that the original author and source are credited.

## Introduction

Kinetochores enable the precise distribution of chromosomes during the eukaryotic cell division to avoid aneuploidy (*Santaguida and Musacchio, 2009*) which is associated with tumorigenesis, congenital trisomies and aging (*Baker et al., 2005; Pfau and Amon, 2012*). Faithful segregation of the duplicated sister chromatids relies on their exclusive attachment to spindle microtubules emerging from opposite spindle poles (*Foley and Kapoor, 2013*). The physical link between chromosomal DNA and microtubules is the kinetochore, a macromolecular protein complex that mediates the processive binding to depolymerizing microtubules driving the sister chromatids apart into the two emerging cells (*Biggins, 2013; Musacchio and Desai, 2017*). Kinetochore assembly is restricted to centromeres, chromosomal domains that are marked by the presence of the histone H3 variant Cse4<sup>CENP-A</sup> (human ortholog names are superscripted if appropriate) (*Earnshaw and Rothfield,*

1985; Fukagawa and Earnshaw, 2014). In humans, regional centromeres span megabases of DNA embedding up to 200 CENP-A containing nucleosomal core particles (NCPs) (Bodor et al., 2014; Musacchio and Desai, 2017). In contrast, *Saccharomyces cerevisiae* has point centromeres, which are characterized by a specific ~125 bp DNA sequence wrapped around a single Cse4-containing histone octamer (Fitzgerald-Hayes et al., 1982; Camahort et al., 2009; Hasson et al., 2013).

The budding yeast kinetochore is composed of about 45 core subunits which are organized in different stable complexes (De Wulf et al., 2003; Westermann et al., 2003) of which several are present in multiple copies (Joglekar et al., 2006). The kinetochore proteins are evolutionary largely conserved between yeast and humans (Westermann and Schleiffer, 2013; van Hooff et al., 2017) and share a similar hierarchy of assembly from DNA to the microtubule binding interface (De Wulf et al., 2003). The centromere proximal region is established by proteins of the Constitutive Centromere Associated Network (CCAN), also known as the CTF19 complex (CTF19c) in budding yeast. The CTF19c comprises the Chl4/Iml3<sup>CENP-N/L</sup>, Mcm16/Ctf3/Mcm22<sup>CENP-H/I/K</sup>, Cnn1/Wip1<sup>CENP-T/W</sup>, Mhf1/Mhf2<sup>CENP-S/X</sup> and Ctf19/Okp1/Mcm21/Ame1<sup>CENP-P/Q/O/U</sup> (COMA) complexes plus Mif2<sup>CENP-C</sup> (Cheeseman et al., 2002; Westermann et al., 2003; Biggins, 2013; Musacchio and Desai, 2017) and the budding-yeast specific Nkp1/Nkp2 heterodimer. Another yeast inner kinetochore complex, the CBF3 (Ndc10/Cep3/Ctf13/Skp1) complex, has been identified as sequence-specific binder of the centromeric DNA sequence CDEIII (Ng and Carbon, 1987; Lechner and Carbon, 1991). The CTF19c<sup>CCAN</sup> provides a cooperative high-affinity binding environment for the Cse4<sup>CENP-A</sup>-NCP (Weir et al., 2016), where distinct subunits selectively recognize Cse4<sup>CENP-A</sup> specific features. Across different species the CENP-C signature motif interacts with divergent hydrophobic residues of the CENP-A C-terminal tail (Musacchio and Desai, 2017). Electron microscopy studies have recently resolved the interaction of CENP-N with the CENP-A centromere-targeting domain (CATD) in vertebrates (Carroll et al., 2009; Guse et al., 2011; Pentakota et al., 2017; Chittori et al., 2018; Tian et al., 2018). For budding yeast Cse4, a direct interaction has so far only been demonstrated with Mif2 (Westermann et al., 2003; Xiao et al., 2017). Apart from Mif2, the only essential CTF19c<sup>CCAN</sup> proteins are Ame1 and Okp1 (Meluh and Koshland, 1997; Ortiz et al., 1999; De Wulf et al., 2003), with the N-terminus of Ame1 binding the N-terminal domain of Mtw1 and thus serving as docking site for the outer kinetochore KMN network (KNL1<sup>SPC105</sup>-/MIS12<sup>MTW1</sup>-/NDC80<sup>NDC80</sup>-complexes) (Hornung et al., 2014; Dimitrova et al., 2016).

The kinetochore is also a hub for feedback control mechanisms that ensure high fidelity of sister chromatid separation by relaying the microtubule attachment state to cell cycle progression, known as spindle assembly checkpoint (SAC), and by destabilizing improper kinetochore-microtubule attachments and selectively stabilizing the correct bipolar attachments, referred to as error correction mechanism (Foley and Kapoor, 2013; Krenn and Musacchio, 2015). A major effector of both regulatory feedback loops is the kinase Ipl1<sup>Aurora B</sup>, a subunit of the evolutionary conserved tetrameric chromosomal passenger complex (CPC) which associates close to the centromere from G1 until anaphase (Biggins and Murray, 2001; Widlund et al., 2006; Carmena et al., 2012). The kinase subunit Ipl1<sup>Aurora B</sup> binds to the C-terminal IN-box domain (Adams et al., 2000; Kaitna et al., 2000) of the scaffold protein Sli15<sup>INCENP</sup>, and Nbl1<sup>Borealin</sup> and Bir1<sup>Survivin</sup> form a three-helix bundle with the Sli15 N-terminus (Klein et al., 2006; Jeyaprakash et al., 2007). All known mechanisms for recruitment of the CPC to the yeast centromere rely on Bir1, which directly associates with Ndc10 (Cho and Harrison, 2011) and is recruited through Sgo1 to histone H2A phosphorylated at S121 by Bub1 which so far has only been established in fission yeast (Kawashima et al., 2010). Based on previous reports we refer to the CPC recruited through Ndc10 or H2A-P as centromere-targeted CPC pool, notwithstanding that the centromere-targeted Sli15<sup>INCENP</sup> scaffold may extend to, and Ipl1<sup>Aurora B</sup> may operate at, the kinetochore structure. CPC lacking the centromere-targeting domain (CEN) of Sli15<sup>INCENP</sup> is indicated as inner kinetochore-localized CPC (Knockleby and Vogel, 2009; Musacchio and Desai, 2017).

During early mitosis incorrect microtubule attachment states are resolved by Ipl1<sup>Aurora B</sup> which phosphorylates Ndc80 and Dam1 sites within the microtubule binding interface and thereby reduces their affinity towards microtubules (Cheeseman et al., 2002; Miranda et al., 2005; Westermann et al., 2005; Cheeseman et al., 2006; DeLuca et al., 2006; Santaguida and Musacchio, 2009). The selective destabilization promotes the establishment of a correctly bi-oriented kinetochore configuration at the mitotic spindle, referred to as amphitelic attachment (Tanaka et al., 2002). The spatial separation model for establishing biorientation (Krenn and Musacchio, 2015)

implies that centromere-targeting of Sli15 allows substrate phosphorylation by Ipl1<sup>Aurora B</sup> within the span of the Sli15<sup>INCENP</sup> scaffold and that tension dependent intra-kinetochore stretching (Joglekar *et al.*, 2009) pulls the microtubule binding interface out of reach of Ipl1<sup>Aurora B</sup> resulting in dephosphorylation of outer kinetochore substrates and stabilization of amphitelic kinetochore-microtubule attachments (Liu *et al.*, 2009; Lampson and Cheeseman, 2011).

A recent study challenged this model by showing that a Sli15 mutant lacking the centromere-targeting domain, Sli15 $\Delta$ N2-228 (Sli15 $\Delta$ N), suppressed the deletion phenotypes of Bir1, Nbl1, Bub1 and Sgo1 that mediate recruitment of the CPC to the centromere (Campbell and Desai, 2013). In contrast to wild-type Sli15, which localized between sister kinetochore clusters, Sli15 $\Delta$ N showed weak localization overlapping with Nuf2 at kinetochores (Campbell and Desai, 2013). Apart from the altered localization, Sli15 $\Delta$ N was indistinguishably viable from wild-type and displayed no significant chromosome segregation defects (Campbell and Desai, 2013; Hengeveld *et al.*, 2017). Similarly, a survivin mutant in chicken DT40 cells that failed to localize INCENP and Aurora B to centromeres from prophase to metaphase displayed normal growth kinetics (Yue *et al.*, 2008). These findings suggest that centromere-targeting of Sli15/Ipl1 is largely dispensable for error correction and SAC signaling. But a molecular understanding of how the inner kinetochore-localized Sli15 $\Delta$ N/Ipl1 retains its biological function is missing.

We describe here the use of chemical crosslinking and mass spectrometry (XLMS) (Herzog *et al.*, 2012) together with biochemical reconstitution to characterize the CTF19c<sup>CCAN</sup> subunit connectivity and the protein interfaces that establish a selective Cse4-NCP binding environment. Subunits of the COMA complex were previously implicated in CPC function at kinetochores (De Wulf *et al.*, 2003; Knockleby and Vogel, 2009) and the Sli15 $\Delta$ N mutant showed synthetic lethality with deletions of Ctf19 or Mcm21 (Campbell and Desai, 2013). Thus, we investigated whether the COMA complex directly associates with Sli15/Ipl1. We demonstrate that the Cse4-N-terminus (Chen *et al.*, 2000) binds Ame1/Okp1 through the Okp1 core domain (Schmitzberger *et al.*, 2017) and that dual recognition of budding yeast Cse4-NCP is established through selective interactions of the essential CTF19c<sup>CCAN</sup> proteins Mif2 and Ame1/Okp1 with distinct Cse4 motifs. We further show that Sli15/Ipl1 interacts with the Ctf19 C-terminus and that synthetic lethality upon Ctf19 depletion in the *sli15 $\Delta$ N* background is rescued by fusing Sli15 $\Delta$ N to the COMA complex. Our findings show contacts important for CTF19c<sup>CCAN</sup> architecture assembled at budding yeast point centromeres and indicate that the interaction of CPC and COMA is important for faithful chromosome segregation.

## Results

### The Ame1/Okp1 heterodimer selectively binds Cse4 containing nucleosomes

To screen for direct interaction partners of Cse4-NCPs we reconstituted the individual CTF19c<sup>CCAN</sup> subcomplexes (Mif2, Ame1/Okp1, Ctf19/Mcm21, Chl4/Iml3, Mcm16/Ctf3/Mcm22, Cnn1/Wip1, Nkp1/Nkp2, Mhf1/Mhf2) with Cse4- or H3-NCPs in vitro. The CTF19c<sup>CCAN</sup> complexes were purified either from bacteria or insect cells as homogenous and nearly stoichiometric complexes (Figure 1B). Consistent with a recent study (Xiao *et al.*, 2017), using electrophoretic mobility shift assays (EMSA), we observed that Mif2 selectively interacted with Cse4-NCPs and not with H3-NCPs (Figure 1A). We also found that Ame1/Okp1 bound specifically to Cse4-NCPs (Figure 1A). The lack of interaction with H3-NCPs, which were reconstituted using the same 601 DNA sequence (Tachiwana *et al.*, 2011), suggests that Ame1/Okp1 directly and selectively binds Cse4 and that the interaction does not require AT-rich DNA sequences as previously proposed (Hornung *et al.*, 2014). In contrast to the EMSA titration of human CCAN complexes with CENP-A-NCP (Weir *et al.*, 2016) using 10 nM NCP mixed with up to 20-fold excess of the respective subcomplexes, we could not detect Cse4-NCP band shifts with Chl4/Iml3, the orthologs of human CENP-NL, and with Mcm16/Ctf3/Mcm22, the orthologs of human CENP-HIK (no *S. cerevisiae* ortholog of CENP-M has been identified) using 500 nM NCP incubated with a twofold excess of the complexes. Ctf19/Mcm21, Cnn1/Wip1, Nkp1/Nkp2 and Mhf1/Mhf2 did also not form distinct complexes with either Cse4- or H3-NCPs in the EMSA indicating that Mif2 and Ame1/Okp1 possess a higher relative binding affinity to Cse4-NCPs than the other CTF19c subcomplexes (Figure 1A).



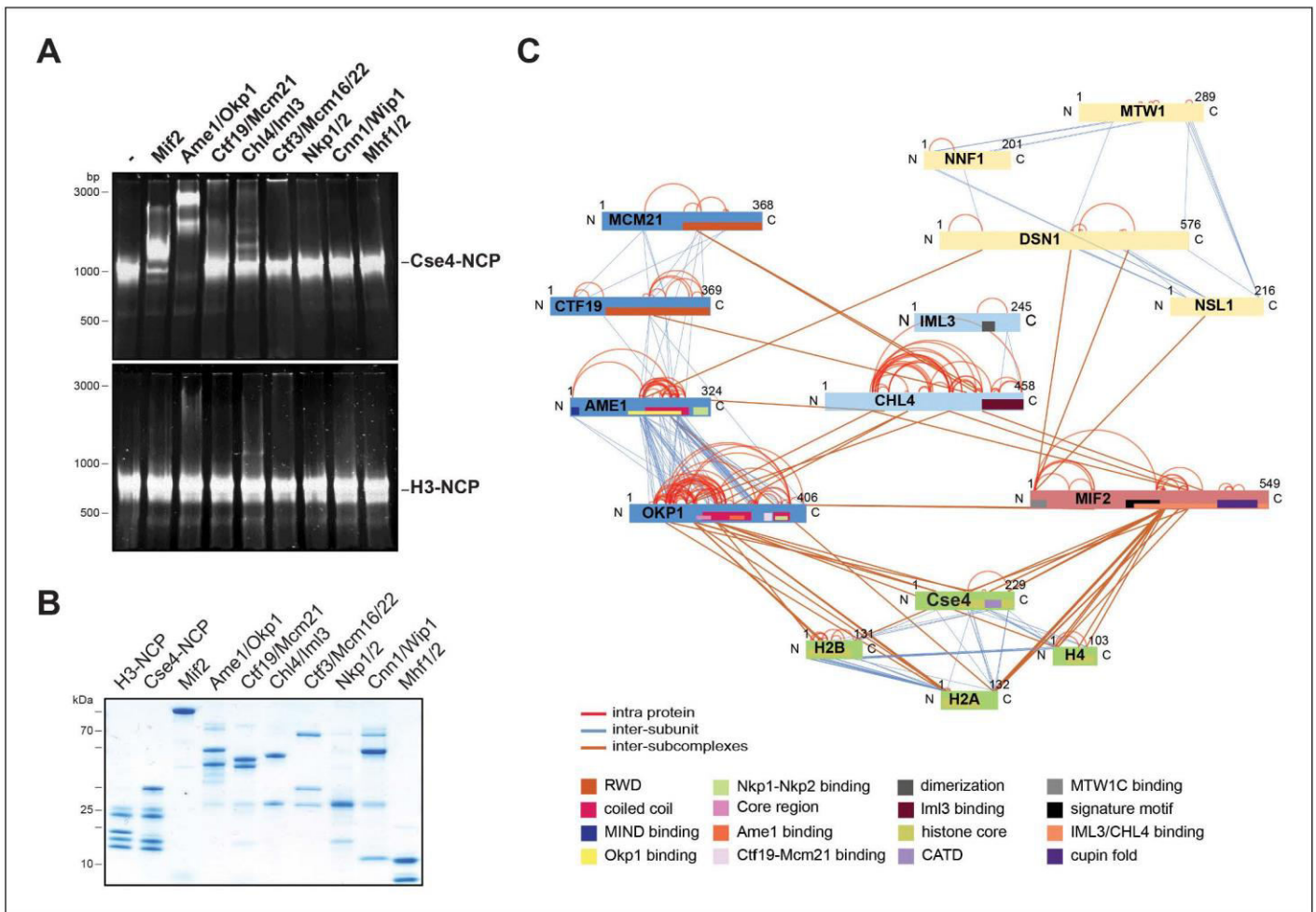


**Figure 1.** The heterodimeric Ame1/Okp1 complex directly and selectively binds the Cse4-NCP. (A) Electrophoretic mobility shift assays (EMSA) of the indicated Ctf19<sup>CCAN</sup> subunits and subcomplexes mixed in a 2:1 molar ratio with either Cse4- or H3-NCPs. DNA/protein complexes were separated on a 6% native polyacrylamide gel. The DNA is visualized by SYBR Gold staining. (B) Coomassie stained gel of the individual inner kinetochore components, recombinantly purified from *E. coli*, used in the EMSA in (A). (C) XLMS analysis of the in vitro reconstituted Cse4-NCP:Mif2:COMA:Chl4/Iml3:MTW1c complex. Proteins are represented as bars indicating domains (**Supplementary file 3**) according to the color scheme in the legend. Subunits of a complex are represented in the same color and protein lengths and cross-link sites are scaled to the amino acid sequence.

DOI: <https://doi.org/10.7554/eLife.42879.002>

The following figure supplement is available for figure 1:

**Figure supplement 1.** Size exclusion chromatography (SEC) of the in vitro reconstituted Ctf19/Mcm21/Ame1/Okp1 (COMA):Chl4/Iml3:Mif2:MTW1c: Cse4-NCP complex.

DOI: <https://doi.org/10.7554/eLife.42879.003>

To identify the binding interfaces of the Ame1/Okp1:Cse4-NCP complex we performed XLMS analysis. We reconstituted a complex on Cse4-NCP composed of Ame1/Okp1, Mif2, Ctf19/Mcm21, Chl4/Iml3 and the MTW1c which links the KMN network to the inner kinetochore receptors Ame1 and Mif2 (Przewlaka et al., 2011; Screpanti et al., 2011; Hornung et al., 2014). Size-exclusion chromatography (SEC) analysis showed that MTW1c forms a complex with Ame1/Okp1, Mif2, Ctf19/Mcm21 and Chl4/Iml3 and the peak fraction shifted to a higher molecular weight upon addition of Cse4-NCPs depicting nearly stoichiometric protein levels of all subunits (Figure 1—figure supplement 1). In all in vitro reconstitution and XLMS experiments we used wild-type MTW1c lacking the phosphorylation mimicking mutations of Dsn1 S240 and S250, which have been shown to stabilize the interaction with Mif2<sup>CENP-C</sup> and Ame1<sup>CENP-U</sup> (Akiyoshi et al., 2013; Dimitrova et al., 2016), but were not required for complex formation on SEC columns (Figure 2C, Figure 1—figure supplement



## Figure 2 continued

according to the ClustalW color and annotation codes (S.: *Schizosaccharomyces*, C.: *Candida*, Z.: *Zygosaccharomyces*, L.: *Lachancea*). Residues that are identical among aligned protein sequences (\*), conserved substitutions (:), and semiconserved substitutions (.) are indicated. (B) Scheme of the deletion mutants within the Cse4 N-terminus used in the SEC experiments in (C) and (D) and in the cell viability assays in (E). The conserved region (aa 34–61) is highlighted in pink. (C) SEC analysis of the indicated mixtures of recombinant Ame1/Okp1 (AO) and MTW1c and reconstituted H3-, Cse4-, Cse4 $\Delta$ 2–30- or Cse4 $\Delta$ 31–60-NCPs. Ame1/Okp1, MTW1c and the Cse4 proteins were mixed equimolar. Eluted proteins were visualized by SDS-PAGE and Coomassie staining. (D) SEC analysis of Ame1/Okp1 (AO) preincubated with Cse4 $\Delta$ 34–46- or Cse4 $\Delta$ 48–61-NCPs. Eluted complexes were analyzed by SDS-PAGE and Coomassie staining. (E) Left panel: Cell growth assay of Cse4 mutants in budding yeast using the anchor-away system. The Cse4 wild-type and indicated mutant proteins were ectopically expressed in a Cse4 anchor-away strain (Cse4-FRB) and cell growth was monitored by plating 1:10 serial dilutions on YPD medium at 30°C in the absence or presence of 1  $\mu$ g/ml rapamycin. Right panel: Western blot analysis of the ectopically expressed Cse4 wild-type and mutant protein levels in the yeast strains shown on the left. Pgk1 levels are shown as loading control.

DOI: <https://doi.org/10.7554/eLife.42879.004>

1). In total 349 inter-subunit crosslinks between the fifteen proteins were identified (Figure 1C, Supplementary file 1). The majority of the crosslinks detected within the different subcomplexes MTW1c, COMA, Chl4/Iml3, and Cse4-NCP are in agreement with previous studies validating our crosslink map (De Wulf et al., 2003; Hinshaw and Harrison, 2013; Hornung et al., 2014). Moreover, crosslinks from the Mif2 N-terminus to the MTW1c (Przewloka et al., 2011; Screpanti et al., 2011), from the Mif2 Chl4/Iml3-binding domain to Chl4 (Hinshaw and Harrison, 2013), and from the Mif2 signature motif to the Cse4 C-terminus (Figure 1C, Supplementary file 1) (Kato et al., 2013) are consistent with previously described interfaces. Crosslinks between Ame1/Okp1 and Cse4 occur exclusively between Okp1 and Cse4, suggesting that Okp1 is the direct binding partner of Cse4. Furthermore, Okp1 was the only COMA subunit that crosslinked to the three canonical histones H2A, H2B and H4 with the exception of one crosslink between Ame1 and H2A. Our analysis indicated a close association between Chl4/Iml3 and all COMA subunits. A direct interaction between COMA and Chl4 was reported previously and the Ctf19/Mcm21 heterodimer was found to be required for the kinetochore localization of Chl4 and Iml3 (Schmitzberger et al., 2017).

### The essential N-terminal domain of Cse4 is required for Okp1 binding

To further characterize the interaction between Ame1/Okp1 and Cse4-NCPs we aimed to identify the binding interface of the Ame1/Okp1:Cse4-NCP complex. Two crosslinks were detected between Okp1 and the essential Cse4 N-terminus (Figure 1C, Supplementary file 1). A multiple sequence alignment (MSA) of Cse4<sup>CENP-A</sup> protein sequences (Figure 2A) detected a conserved region (ScCse4 aa 34–61), unique to Cse4 proteins of interrelated yeasts, which is almost identical to the so-called 'essential N-terminal domain' (END), aa 28–60, shown to be required for the essential function of the Cse4 N-terminus and for recruiting the 'Mcm21p/Ctf19p/Okp1p complex' to minichromosomes (Keith et al., 1999; Ortiz et al., 1999; Chen et al., 2000).

To assess whether the Cse4 END mediates the interaction with Ame1/Okp1 we tested binding of recombinant Ame1/Okp1 to reconstituted wild-type and deletion mutants (Figure 2B) of Cse4- and to H3-NCPs by SEC (Figure 2C). Wild-type Cse4-NCP but not H3-NCP formed a stoichiometric complex with Ame1/Okp1 (Figure 2C) which is consistent with our EMSA and XLMS analyses (Figure 1A,C). In addition, Ame1/Okp1 bound to a Cse4-NCP retained the ability to interact with the MTW1c (Hornung et al., 2014), forming a direct link between the KMN network and the centromeric nucleosome (Figure 2C). Truncation of the first 30 N-terminal residues of Cse4 neither affected its ability to bind Ame1/Okp1, nor was it essential for viability (Figure 2C) (Chen et al., 2000). However, the Cse4 $\Delta$ 31–60 mutant abrogated Ame1/Okp1:Cse4-NCP complex formation (Figure 2C). To further narrow down the interface, two deletion mutants splitting the END in half, Cse4 $\Delta$ 34–46 and Cse4 $\Delta$ 48–61 (Figure 2B), were tested in SEC experiments. While Cse4 $\Delta$ 48–61 associated with Ame1/Okp1, deletion of amino acids 34–46 completely disrupted the interaction (Figure 2D). All Cse4 N-terminal mutant and wild-type NCPs eluted at similar retention times from the SEC column indicating that the Cse4 N-terminal deletions did not affect Cse4 incorporation and stability of the nucleosomes (Figure 2C,D).

The crosslink-derived distance restraints as well as SEC analysis identified a conserved Cse4 peptide motif of amino acids 34–46 which is necessary for Ame1/Okp1 interaction. To test whether this motif is essential for cell viability, we depleted endogenous Cse4 from the nucleus using the anchor-

away technique and performed rescue experiments by ectopically expressing the Cse4 mutants Cse4 $\Delta$ 34–46 and Cse4 $\Delta$ 48–61. Indeed, deletion of amino acids 34–46 was lethal, whereas the Cse4 $\Delta$ 48–61 mutant displayed wild-type growth rates (Figure 2E). The observation that deletion of the minimal Ame1/Okp1 interacting Cse4 motif (aa 34–46) correlates with the loss of cell viability, whereas the C-terminal half of the END (aa 48–61) is neither essential for viability nor required for Ame1/Okp1 association suggests that binding of the Ame1/Okp1 heterodimer to Cse4 residues 34–46 is essential for yeast growth. The Mif2 signature motif (Xiao et al., 2017) and Ame1/Okp1 recognize distinct motifs at the Cse4 C- and N-terminus (Figure 1C), respectively, and both are essential for viability (Hornung et al., 2014).

### The Okp1 core domain interacts with Cse4

To characterize the Cse4 binding site in Okp1 we applied crosslink-derived restraints to narrow down the putative interface to amino acids 95–202 of Okp1 (Figure 1C, Supplementary file 1). Based on MSA analysis of Okp1 sequences, this region harbors a conserved stretch (aa 127–184), including part of the previously described Okp1 core domain (aa 166–211) which is essential for cell growth and whose function is still elusive (Schmitzberger et al., 2017) (Figure 3A). Furthermore, a secondary structure analysis predicted two alpha helices within the conserved domain (helix1 aa 130–140, helix2 aa 156–188) (Figure 3A). Thus, we designed three deletion mutants (Okp1 $\Delta$ 123–147, Okp1 $\Delta$ 140–170, Okp1 $\Delta$ 163–187) and purified all Okp1 mutant proteins in complex with Ame1 from *E. coli*. In EMSAs Ame1/Okp1 $\Delta$ 123–147 bound to Cse4-NCPs as well as did the wild-type Ame1/Okp1 complex, whereas Ame1/Okp1 $\Delta$ 140–170 associated only weakly and Ame1/Okp1 $\Delta$ 163–187 failed to associate with Cse4-NCPs (Figure 3B). These results are consistent with monitoring protein complex formation by SEC (Figure 3—figure supplement 1). In addition, analysis of the Okp1 deletion mutants  $\Delta$ 123–147 and  $\Delta$ 163–187 in cell viability assays showed a tight correlation between their requirement for the interaction with Cse4 and being essential for yeast growth (Figure 3C) (Schmitzberger et al., 2017). This finding further supports the notion that the recognition of the Cse4 nucleosome by Ame1/Okp1 is essential in budding yeast.

### The COMA complex interacts with Sli15/Ipl1 through the Ctf19 C-terminus

The COMA complex is composed of two essential, Ame1/Okp1, and two non-essential, Ctf19/Mcm21, subunits (Ortiz et al., 1999; Cheeseman et al., 2002). Both, Ctf19 and Mcm21 contain C-terminal tandem-RWD (RING finger and WD repeat containing proteins and DEAD-like helicases) domains forming a rigid heterodimeric Y-shaped scaffold whose respective N-terminal RWDs of the tandems pack together as shown by a crystal structure of the *K. lactis* complex (Schmitzberger and Harrison, 2012). The *ctf19 $\Delta$*  or *mcm21 $\Delta$*  mutants become synthetically lethal in a *sli15 $\Delta$ N* background (Campbell and Desai, 2013). Furthermore, Ame1 has been suggested to have a role in Sli15 localization close to kinetochores independently of Bir1 (Knockleby and Vogel, 2009). To investigate whether Sli15/Ipl1 associates with the COMA complex, in vitro reconstitution and XLMS analysis detected 98 inter-protein and 69 intra-protein crosslinks (Figure 4A, Supplementary file 2). In particular, there were 10 crosslinks from the C-terminal RWD (RWD-C) domain of Ctf19 and 4 crosslinks from the Mcm21 RWD-C domain to the microtubule binding domain of Sli15 (aa 229–565) (Figure 4A, Supplementary file 2, 3). In the Ame1/Okp1 heterodimer, we identified crosslinks from Sli15 to Okp1 and from Ipl1 to Ame1. The crosslink detected to lysine 366 of Okp1 is located near the identified Ctf19/Mcm21 binding site within Okp1 ('segment 1' aa 321–329) (Schmitzberger et al., 2017) and thus is close to the RWD-C domains of Ctf19 and Mcm21. We verified the interaction of Sli15 and the Ctf19 RWD-C domain by in vitro binding assays. Sli15-2xStrep/Ipl1 was immobilized on Streptavidin beads and incubated with a 2-fold molar excess of either Ame1/Okp1 and Ctf19/Mcm21 using wild-type Ctf19 protein or a C-terminal deletion mutant Ctf19 $\Delta$ 270–369 (Ctf19 $\Delta$ C). Ame1/Okp1 and Ctf19/Mcm21 were both pulled down with Sli15/Ipl1 either as individual complexes or in combination (Figure 4B). In agreement with previous findings (Schmitzberger et al., 2017), recombinant Ctf19 $\Delta$ C formed a stoichiometric complex with Mcm21, but lost its ability to bind Sli15/Ipl1 indicating that the RWD-C of Ctf19 is required for Sli15/Ipl1 interaction in vitro (Figure 4C). Autophosphorylation of Sli15/Ipl1 abrogated its interaction with Ame1/Okp1 and Ctf19/Mcm21 indicating that like the phosphorylation-regulated binding to



Figure 3 continued

DOI: <https://doi.org/10.7554/eLife.42879.005>

The following figure supplement is available for figure 3:

**Figure supplement 1.** Identification of the Cse4 binding site on Okp1.

DOI: <https://doi.org/10.7554/eLife.42879.006>

microtubules, phosphorylation of Sli15 by Ipl1 may prevent and regulate its binding to the COMA complex (**Figure 4B**).

In summary, crosslink-derived restraints identified the Ctf19 RWD-C domain as a Sli15/Ipl1 docking site within the COMA complex, a conclusion supported by the loss of interaction upon deletion of the Ctf19 C-terminus in vitro.

### Tethering Sli15 $\Delta$ N selectively to COMA rescues the synthetic lethality of a *sli15 $\Delta$ N* mutant upon Ctf19 depletion

As deletions of Ctf19 or Mcm21 were synthetically lethal in a *sli15 $\Delta$ N* background (**Campbell and Desai, 2013**) and Sli15 associated with the Ctf19 RWD-C in vitro (**Figure 4**), we investigated the relevance of this interaction by performing yeast viability assays. First, we reproduced the reported synthetic lethality by anchoring-away Ctf19-FRB in a yeast strain, in which the endogenous *SLI15* copy was replaced by *sli15 $\Delta$ N* (**Haruki et al., 2008**). We found that in the presence of Ctf19-FRB, cells expressing Sli15 $\Delta$ N are viable, but display synthetic lethality on rapamycin containing medium, consistent with previous findings (**Campbell and Desai, 2013**) (**Figure 5A**).

Recently, the Ctf19 N-terminus has been identified as the receptor domain of the cohesin loading complex Scc2/4 in late G1 phase (**Hinshaw et al., 2017**). To address whether Sli15/Ipl1 has an active role in this process, we deleted 30 amino acids of Ctf19 (Ctf19 $\Delta$ N2-30) which have been shown to contain phosphorylation sites of the Dbf4-dependent kinase required for Scc2/4 recruitment to the centromere (**Hinshaw et al., 2017**). Cells expressing Ctf19 $\Delta$ N2-30 in the *sli15 $\Delta$ N* background were just as viable upon depletion of Ctf19-FRB as those expressing intact Ctf19 (**Figure 5A**), demonstrating that the synthetic lethality is independent of the Ctf19 N-terminus and its role in cohesin loading.

If the synthetic effect is associated with the loss of interaction between Sli15 $\Delta$ N and COMA, artificial tethering of Sli15 $\Delta$ N to the kinetochore should restore growth. We generated fusions of Sli15 $\Delta$ N to various inner and outer kinetochore proteins and investigated whether growth was restored in a *CTF19-FRB/sli15 $\Delta$ N* background. Ectopic expression of Sli15 $\Delta$ N fusions to the outer kinetochore subunits Mtw1 or Dsn1 and to the inner kinetochore subunits Mif2, Ctf3 or Cnn1 did not rescue viability (**Figure 5B**). But selectively tethering Sli15 $\Delta$ N to Ame1 or Okp1 restored growth (**Figure 5B**).

We further tested whether the rescue of synthetic lethality depended on the Sli15 single alpha helix domain (SAH, aa 516–575) (**Samejima et al., 2015; van der Horst et al., 2015; Fink et al., 2017**) and the Ipl1 binding domain (IN-box, aa 626–698) (**Adams et al., 2000; Kang et al., 2001**). Both domains are essential for cell growth in the Sli15 wild-type or the *sli15 $\Delta$ N* background (**Figure 5C**) (**Kang et al., 2001**). Cells ectopically expressing the Sli15 $\Delta$ N mutant protein grew like wild-type, but displayed sensitivity to 15  $\mu$ g/ml benomyl which contrasted the previous observation that cells carrying the endogenous *sli15 $\Delta$ N* allele were not sensitive to 12.5  $\mu$ g/ml benomyl (**Campbell and Desai, 2013**). These deviating observations may be a result of different experimental conditions. To distinguish the requirement of one domain from that of the other in the context of inner kinetochore-localized Sli15/Ipl1, we generated Ame1- and Okp1-Sli15 $\Delta$ N fusion constructs in which either the IN-box or the SAH domain of Sli15 $\Delta$ N had been deleted. While expression of Ame1- or Okp1-Sli15 $\Delta$ N $\Delta$ SAH proteins rescued cell growth in the *sli15 $\Delta$ N* background upon Ctf19 depletion, Ame1- and Okp1-Sli15 $\Delta$ N $\Delta$ IN fusions did not, indicating that Ipl1 kinase activity is required (**Figure 5D**). Since the ectopically expressed fusion proteins were tested in the *sli15 $\Delta$ N* background, the result indicates that Ipl1 activity associated with endogenous Sli15 $\Delta$ N could not rescue synthetic lethality and that tethering Ipl1 activity to COMA subunits is crucial. In contrast, deletion of the SAH domain in Ame1- and Okp1-Sli15 $\Delta$ N $\Delta$ SAH fusions was not lethal and was presumably rescued by the SAH domain of the endogenous Sli15 $\Delta$ N protein (**Figure 5D**) suggesting that the SAH domain is not required for the function of the inner kinetochore-localized CPC pool.

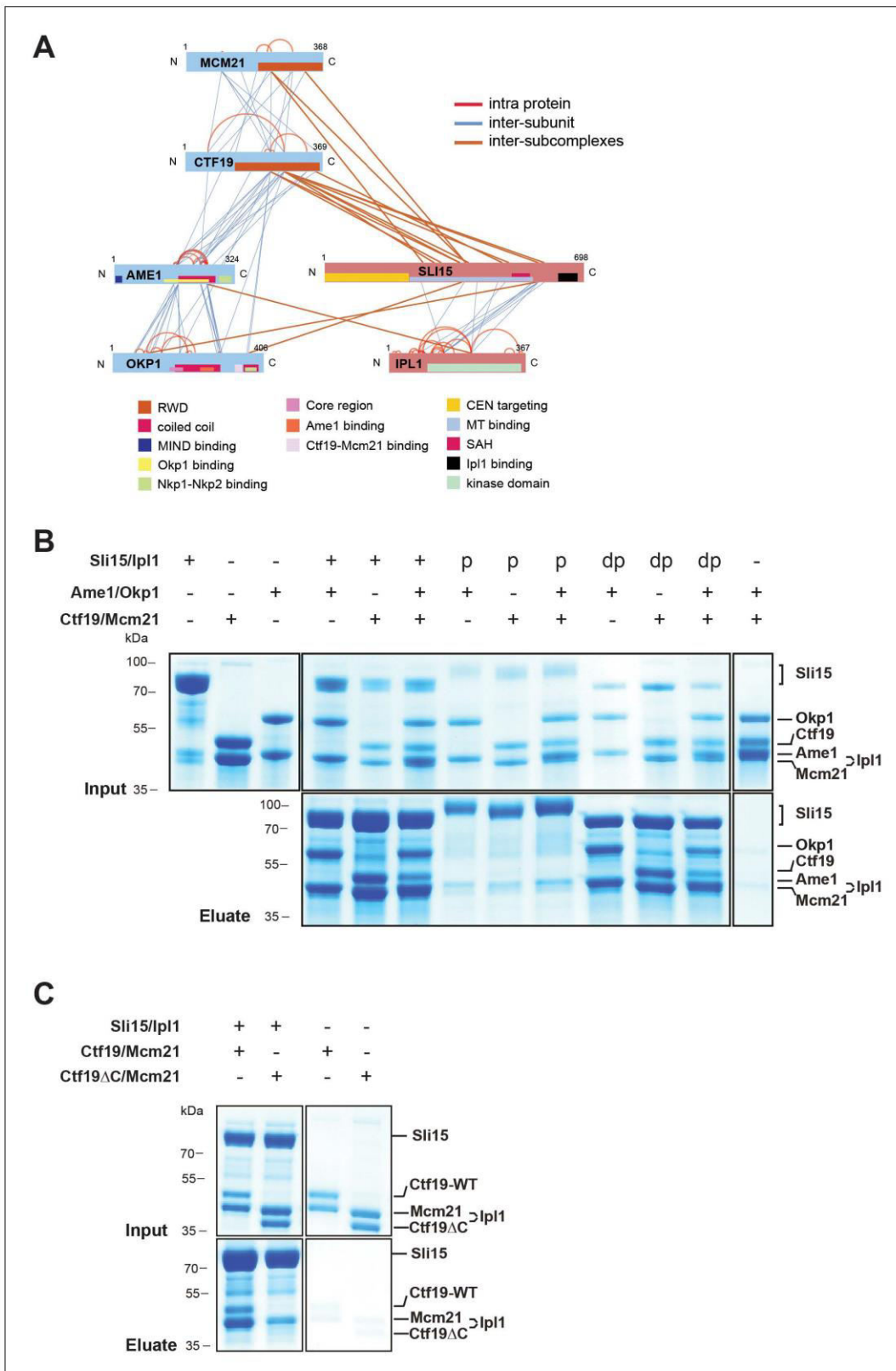


**Figure 4.** The core-CPC Sli15/Ipl1 associates with the COMA complex through the Ctf19 C-terminal RWD domain in vitro. (A) Network representation of lysine-lysine cross-links identified on recombinant Sli15/Ipl1 in complex with COMA. Proteins are represented as bars indicating annotated domains (*Supplementary file 3*) according to the color scheme in the legend. Subunits of a complex are represented in the same color. Protein lengths and cross-link sites are scaled to the amino acid sequence. (B) In vitro binding assay analyzing the interaction of Sli15/Ipl1 with the COMA complex. *Figure 4 continued on next page*

Figure 4 continued

Recombinant Sli15-2xStrep/Ipl1 was immobilized on Streptavidin beads and incubated with Ctf19/Mcm21, Ame1/Okp1 or Ame1/Okp1/Ctf19/Mcm21. Autophosphorylation (p) of Sli15/Ipl1 largely reduced bound protein levels. Dephosphorylation (dp) of Sli15/Ipl1 did not alter the bound proteins levels, which were visualized by SDS-PAGE and Coomassie staining. (C) In vitro binding assay analyzing the interaction of Sli15/Ipl1 with Ctf19/Mcm21 or Ctf19 $\Delta$ C/Mcm21. Ctf19 $\Delta$ C lacks the last 100 amino acids which form the C-terminal RWD domain. This panel is representative of three independent experiments.

DOI: <https://doi.org/10.7554/eLife.42879.007>

### Ame1- or Okp1-Ctf19 fusion proteins require the Ctf19 RWD-C domain to rescue synthetic lethality of a *sli15 $\Delta$ N* mutant strain upon Ctf19 depletion

Since the RWD-C domain of Ctf19 was required for association with Sli15/Ipl1 in vitro (Figure 4C), we asked whether its deletion would cause synthetic lethality with *sli15 $\Delta$ N*. As recently described, the Ctf19 C-terminus is involved in formation of the COMA complex through binding to Okp1 (Schmitzberger et al., 2017) and consequently, its deletion abrogates kinetochore localization of Ctf19 (Figure 6—figure supplement 1). To circumvent loss of Ctf19 from kinetochores, we tested whether Ame1 or Okp1 fusions to wild-type Ctf19 or Ctf19 $\Delta$ C were able to rescue synthetic lethality in the *sli15 $\Delta$ N*/CTF19-FRB background. Fusions to both, the N- or C-terminus, of wild-type Ctf19 restored viability, whereas fusions to Ctf19 $\Delta$ C resulted in synthetic lethality (Figure 6A) suggesting that recruitment of Ipl1 activity to the inner kinetochore mediated by the Ctf19 C-terminus is important for CPC function.

### Deletion of the Ctf19 RWD-C domain causes a chromosome segregation defect in the Sli15 wild-type background

Since Ctf19 mutants display normal growth, but have chromosome segregation defects (Hyland et al., 1999), we tested whether the Ctf19 C-terminus is important for this function using the minichromosome loss assay (Hieter et al., 1985). The Ctf19 anchor-away strain was transformed simultaneously with the various Ctf19 rescue constructs and a centromeric plasmid carrying the *SUP11* gene as a marker which indicated loss of the minichromosome by red pigmentation (Hieter et al., 1985). Depletion of Ctf19 from the nucleus resulted in a severe chromosome segregation defect that was not observed by growing cells on medium lacking rapamycin which showed 4% red/sectored colonies (Figure 6B). Ectopic expression of the Ctf19 wild-type protein decreased the segregation defect to 19% red/sectored colonies (Figure 6B, Figure 6B—source data 1) and fusion of Okp1 to the C-terminus of wild-type Ctf19 reduced the red/sectored colonies to 32%. But the fusion of Okp1 to the Ctf19 N-terminus (Okp1-Ctf19 and Okp1-Ctf19 $\Delta$ C) did not rescue the segregation defect (Figure 6—figure supplement 2, Figure 6B—source data 1), indicating that the function of the Ctf19 N-terminus is compromised by fusing it to Okp1 (Figure 6B, Figure 6B—source data 1). Thus, the Ctf19-Okp1 fusion rescued the segregation defect, albeit to a slightly lesser extent than the Ctf19 wild-type protein. In contrast, Ctf19 $\Delta$ C-Okp1, which was localized at the kinetochore (Figure 6C), was unable to rescue the segregation defect (Figure 6B, Figure 6B—source data 1) suggesting that the Ctf19 C-terminus has a role in mediating accurate chromosome segregation.

## Discussion

### The Ame1/Okp1 heterodimer directly links Cse4 nucleosomes to the outer kinetochore

We investigated the subunit connectivity of the inner kinetochore assembled at budding yeast point centromeres at the domain level using in vitro reconstitution and XLMS. We found that in addition to Mif2 (Xiao et al., 2017), the Ame1/Okp1 heterodimer of the COMA complex is a direct and selective interactor of Cse4-NCPs. We identified the conserved motifs aa 163–187 of the Okp1 core domain (Figure 3B,C) (Schmitzberger et al., 2017) and aa 34–46 (Figure 2D,E) of the Cse4 END to establish the interaction. Although, we did not address whether the Cse4 residues 34–46 are required for the Ame1/Okp1 kinetochore recruitment, the notion that the essential function of the



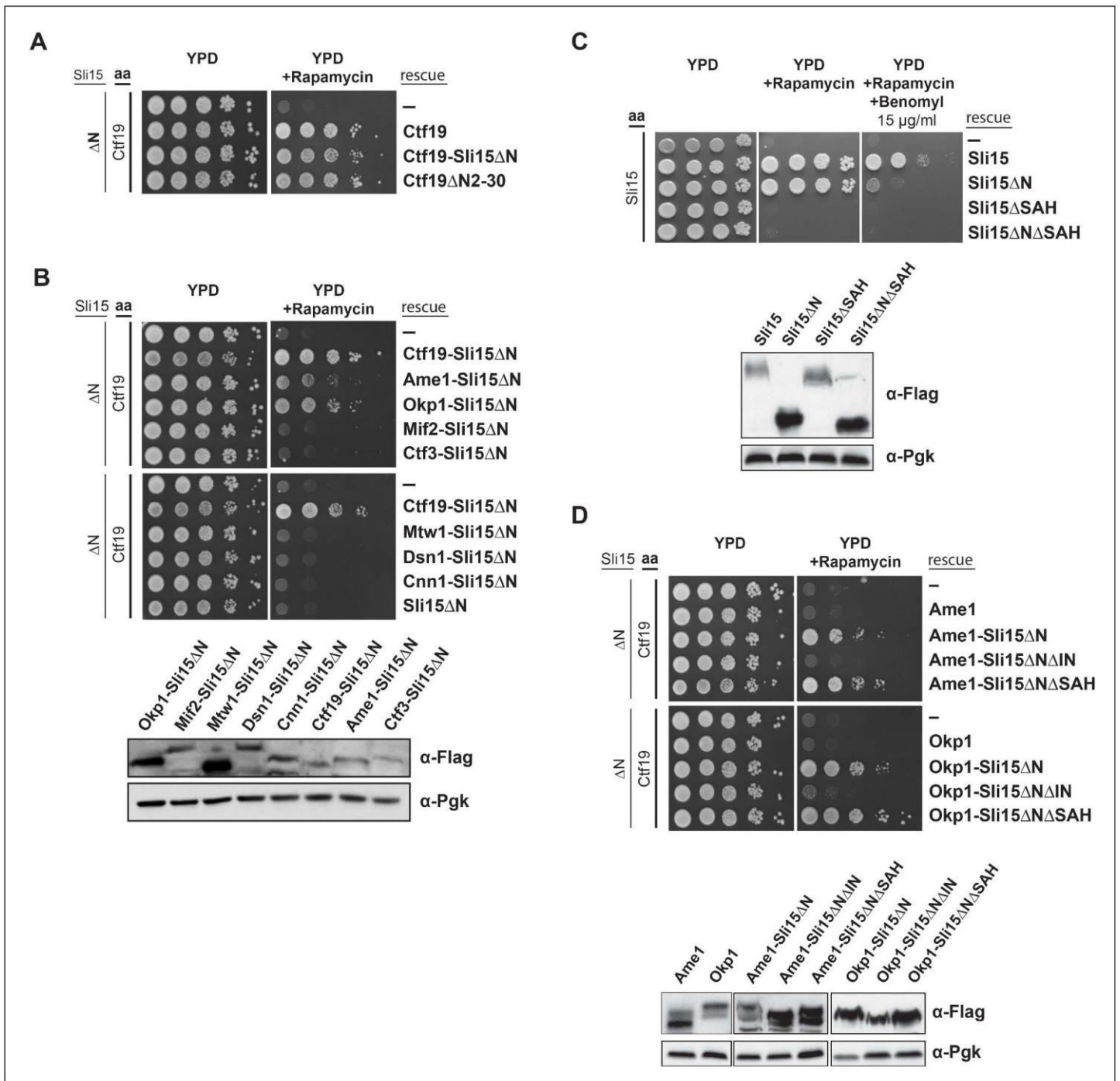


**Figure 5.** Synthetic lethality of Sli15ΔN and Ctf19 depletion is rescued by fusing Sli15ΔN to Ame1/Okp1 and is independent of Ctf19's role in cohesin loading. (A)–(D) Cell viability assays studying the rescue of synthetic lethality of a *sli15ΔN/CTF19-FRB* strain using the anchor-away system. The indicated constructs were transformed into a Ctf19 anchor-away (aa) strain (Ctf19-FRB) carrying *sli15ΔN* (ΔN) at the endogenous locus (A, B, D), or into a Sli15 anchor-away strain (Sli15-FRB) (C). Yeast growth was tested in serial dilutions either untransformed (-) or transformed with the indicated rescue constructs on YPD medium in the absence or presence of 1 μg/ml rapamycin at 30°C. The lower panels in (B), (C) and (D) show western blot analysis of the ectopically expressed protein levels. Pgk1 levels are shown as loading control. (A) Deletion of the Ctf19 N-terminus (Ctf19ΔN2-30) does not affect cell viability in a *sli15ΔN* background. (B) Artificial tethering of Sli15ΔN to Ame1 or Okp1 rescued synthetic lethality of *sli15ΔN* cells upon Ctf19-FRB depletion from the nucleus. (C) Growth phenotypes of Sli15 wild-type, Sli15ΔSAH, Sli15ΔN, and Sli15ΔNΔSAH tested in a Sli15-FRB anchor-away strain. (D) Rescue of cell growth by ectopic Ame1-Sli15ΔN or Okp1-Sli15ΔN fusion proteins is dependent on the Sli15 Ipl1-binding domain (IN-box), whereas the SAH domain is dispensable.

DOI: <https://doi.org/10.7554/eLife.42879.008>

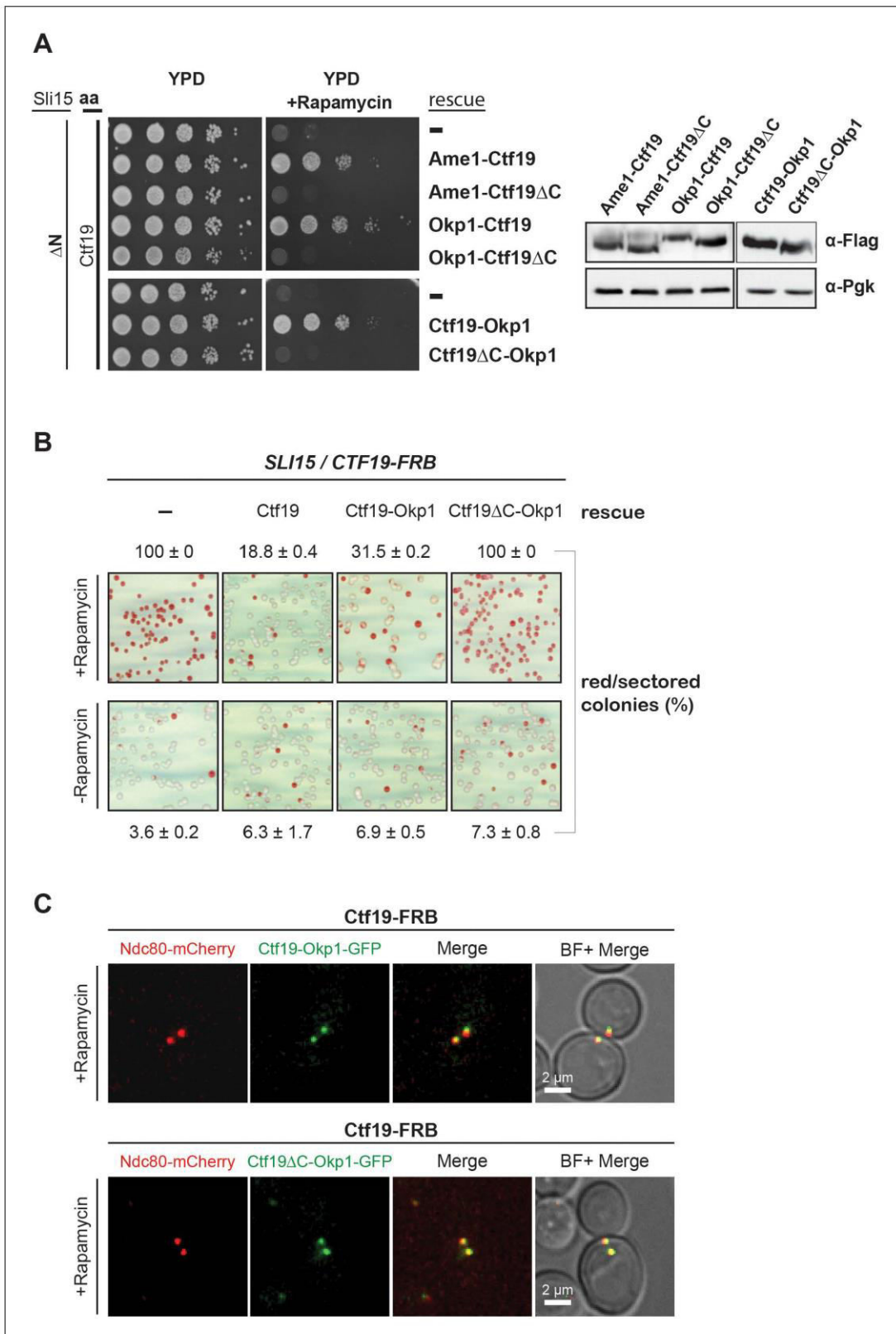


**Figure 6.** The Ctf19 C-terminus is important for chromosome segregation in the Sli15 wild-type background. (A) Left panel: Growth assay of the *sli15ΔN/CTF19-FRB* strain expressing Ame1-Ctf19, Ame1-Ctf19ΔC, Okp1-Ctf19, Okp1-Ctf19ΔC, Ctf19-Okp1 and Ctf19ΔC-Okp1 fusion proteins from the rescue plasmid. Right panel: Western blot analysis visualizing the levels of the ectopically expressed, C-terminally 7xFLAG-tagged fusion proteins. Pgk1 levels are shown as loading control. (aa: Anchor-away) (B) Minichromosome loss assay. Chromosome segregation fidelity was determined in the Ctf19

Figure 6 continued on next page

Figure 6 continued

anchor-away (*SLI15/CTF19-FRB*) strain, containing a minichromosome, either untransformed (-) or transformed with the indicated rescue constructs in the absence or presence of 1  $\mu\text{g/ml}$  rapamycin. The percentage and standard error of red/red sector colonies to the total colony number (white plus red/red sector) of three biological replicates is shown. The results of 100% red colonies may be indicative of non-optimal conditions for the chromosome loss assay in combination with the anchor-away technique. (C) Localisation of ectopically expressed Ctf19-Okp1-GFP and Ctf19 $\Delta\text{C}$ -Okp1-GFP fusion proteins in the Ctf19 anchor-away strain (*SLI15/CTF19-FRB*) in the presence of 1  $\mu\text{g/ml}$  rapamycin. Live cell fluorescence microscopy was performed 3 hr after rapamycin addition. Ndc80-mCherry was used as kinetochore marker. Merged mCherry and GFP signals are shown on the right. (BF: brightfield).

DOI: <https://doi.org/10.7554/eLife.42879.009>

The following source data and figure supplements are available for figure 6:

**Source data 1.** Quantification of the minichromosome loss assay in a *SLI15/CTF19-FRB* strain.

DOI: <https://doi.org/10.7554/eLife.42879.012>

**Figure supplement 1.** Ctf19 $\Delta\text{C}$ -GFP does not localize to kinetochores.

DOI: <https://doi.org/10.7554/eLife.42879.010>

**Figure supplement 2.** The N-terminal fusion protein of Ctf19 with Okp1 does not rescue chromosome segregation defects upon nuclear depletion of Ctf19 in the *Sl15* wild-type background.

DOI: <https://doi.org/10.7554/eLife.42879.011>

Cse4 N-terminus and the binding interface for Ame1/Okp1 are mediated by the same 13 amino acid motif (Figure 2) suggests that Ame1/Okp1 is an essential link between centromeric nucleosomes and the outer kinetochore (Hornung et al., 2014).

Recent studies have identified the same Cse4 region to interact with Ame1/Okp1 (Anedchenko et al., 2019; Hinshaw and Harrison, 2019). Anedchenko et al. found that the affinity of Cse4 N-terminal peptides to Ame1/Okp1 increases with the peptide length up to the low nanomolar range and that methylation of Cse4 R37 and acetylation of Cse4 K49 significantly reduces the binding affinity. Similarly, this region is regulated by Ipl1 phosphorylation in vivo and phosphorylation-mimicking mutants have been found to suppress temperature-sensitive Ipl1 and phosphorylation-deficient Dam1 and Ndc80 mutations (Boeckmann et al., 2013), and to decrease the affinity of a Cse4 peptide to Ame1/Okp1 (Hinshaw and Harrison, 2019). This observation has interesting implications on the regulation of kinetochore assembly by Ipl1 destabilizing the Cse4-Ame1/Okp1 interaction in a cell cycle regulated manner. Moreover, weakening the interaction of Ame1/Okp1 with Cse4 may have a role in the tension sensing and error correction mechanisms (Boeckmann et al., 2013).

### Dual recognition of Cse4 at point centromeres by a CTF19<sup>CCAN</sup> architecture distinct from vertebrate regional centromeres

In vertebrates, CENP-NL and CENP-C, interact directly and specifically with CENP-A. CENP-C binds divergent hydrophobic residues at the CENP-A C-terminus, whereas CENP-N associates with the CENP-A CATD (Carroll et al., 2009; Carroll et al., 2010; Guse et al., 2011; Kato et al., 2013; Weir et al., 2016; Pentakota et al., 2017). Recently, electron microscopy reconstructions of human CENP-A nucleosomes in complex with CENP-N/L identified the RG motif in the L1 loops of the CATD (Zhou et al., 2011) as the CENP-N interaction site in CENP-A (Pentakota et al., 2017; Chittori et al., 2018; Tian et al., 2018). We did not detect complex formation of Chl4/Iml3 with Cse4-NCPs in our EMSA (Figure 1A). Whether this observation can be attributed to the lack of conservation of the RG motif in the corresponding Cse4 sequences in related budding yeasts (Figure 2A), and whether this reflects a different role of Chl4/Iml3 in Cse4 recognition and kinetochore assembly remains to be determined. Our crosslink-derived restraints are also in good agreement with a recent cryo-electron microscopy structure of a 13-subunit budding yeast inner kinetochore complex lacking the Cse4-NCP and Mif2 (Hinshaw and Harrison, 2019) showing for instance crosslinks between the C-terminal domain of Chl4 and central regions of Ctf19 and Mcm21.

Similarly in humans, recruitment of the CENP-OPQRU complex to kinetochores requires a joint interface formed by CENP-HIKM and CENP-LN (Foltz et al., 2006; Okada et al., 2006; Pesenti et al., 2018), but loss of the complex does not affect localization of other inner kinetochore proteins. Differences between vertebrate and budding yeast inner kinetochores are reflected by the physiological importance of the involved proteins, as Ame1/Okp1 together with Mif2 are the

essential Ctf19<sup>c<sup>CCAN</sup></sup> proteins in budding yeast, whereas knockouts of CENP-U/Q in DT40 cells are viable (Hori et al., 2008).

## The Ctf19 C-terminus is required for Sli15/Ipl1 binding in vitro and has a role in accurate chromosome segregation

Although the Ctf19/Mcm21 heterodimer is not essential, *ctf19Δ* and *mcm21Δ* mutants have chromosome segregation and cohesion defects (Hyland et al., 1999; Ortiz et al., 1999; Poddar et al., 1999; Fernius and Marston, 2009; Hinshaw et al., 2017). Moreover, Ctf19 and Mcm21 become essential when centromere-targeting of the CPC is lost in a *sli15ΔN* mutant. This observation has led to the hypothesis that centromere-targeted Sli15 might be involved in cohesin loading or in cohesin maintenance (Campbell and Desai, 2013). An alternative model posits that COMA is required for the localization and positioning of Sli15/Ipl1 at the kinetochore (Knockleby and Vogel, 2009).

Our work showed that COMA interacts directly with Sli15/Ipl1 and identified the Ctf19 RWD-C domain as the primary docking site (Figure 4A,C). Synthetic lethality upon Ctf19 or Mcm21 depletion in a *sli15ΔN* background was rescued by fusions of Sli15ΔN to COMA subunits, whereas fusions to other inner or outer kinetochore proteins did not (Figure 5B). This observation suggests that positioning Sli15/Ipl1 proximal to Ame1/Okp1 is important in vivo. Because of the requirement of a functional Ipl1-binding IN-box on Sli15 for restoring viability we assume that the observed synthetic lethality is due to mislocalized Ipl1 kinase (Figure 5D). Tethering Sli15 to the inner kinetochore might ensure the spatial positioning of Ipl1 kinase activity towards outer kinetochore substrates (Akiyoshi et al., 2013; Foley and Kapoor, 2013; Krenn and Musacchio, 2015), required for correcting erroneous kinetochore-microtubule attachments (Figure 7). COMA-Sli15ΔN fusions lacking the SAH domain rescued growth, indicating that this domain is dispensable for CPC function at the inner kinetochore. Because the SAH domain is required for binding to spindle microtubules and critical for cell survival (Samejima et al., 2015; van der Horst et al., 2015; Fink et al., 2017), we infer that the observed rescue was mediated by the SAH domain of endogenous Sli15ΔN (Figure 5D).

We also showed that deletion of the Ctf19 RWD-C domain was sufficient to cause synthetic lethality with Sli15ΔN (Figure 6A) and that recombinant Ctf19ΔC in complex with Mcm21 (Figure 4C) does not interact with Sli15. Moreover, assessing the initially proposed model for the synthetic growth defect of Ctf19/Mcm21 deletion in a *sli15ΔN* background (Campbell and Desai, 2013), we observed that deletion of the Ctf19 N-terminus did not cause a synthetic effect in *sli15ΔN* mutant cells. This result indicated that the synthetic growth defect is mediated by a Ctf19 domain distinct from its N-terminus and its role in cohesin loading.

Apart from the synthetic condition we addressed whether the Ctf19 C-terminus is required for chromosome segregation in Sli15 wild-type cells by monitoring missegregation in a minichromosome loss assay (Hieter et al., 1985). We showed that loss of the centromeric plasmid upon Ctf19 depletion was rescued to 70% by the ectopic expression of Ctf19-Okp1 and this rescue was abrogated upon deletion of the Ctf19 RWD-C domain in the fusion protein (Figure 6B). Similar observations have been obtained in a concomitant study (García-Rodríguez et al., 2019) using a complementary approach. By performing a 'centromere re-activation' assay (Tanaka et al., 2005) the Tanaka lab showed that Bir1 deletion, and to a lesser extent Mcm21 depletion, reduced localization of Ipl1 at the centromere which was synergistic upon removal of both and the effect on Ipl1 localization correlated with the establishment of chromosome biorientation. This is consistent with our finding that the Ctf19 C-terminus has a role in accurate chromosome segregation and indicates that the Sli15-Ctf19 interaction contributes to the localization and stabilization of the CPC at the inner kinetochore (Figure 7).

Our findings also agree with the observations that the functionally active Aurora B pool is associated with the kinetochore rather than the centromere (DeLuca et al., 2011; Bekier et al., 2015; Krenn and Musacchio, 2015; Hindriksen et al., 2017). A recent study in humans demonstrated that a kinetochore-localized CPC pool lacking the INCENP CEN domain is sufficient to carry out error correction and biorientation, if cohesin removal, which was attributed to the loss of the CEN domain, is prevented (Hengeveld et al., 2017). Furthermore, retaining the human CPC at centromeres in anaphase resulted in the untimely recruitment of Bub1 and BubR1 (Vázquez-Novelle and Petronczki, 2010; Vázquez-Novelle et al., 2014) which suggests that centromere-localization of the CPC is required, and microtubule-association may not be sufficient, for fulfilling its function in the spindle assembly checkpoint and chromosome biorientation. The human CENP-OPQUR complex

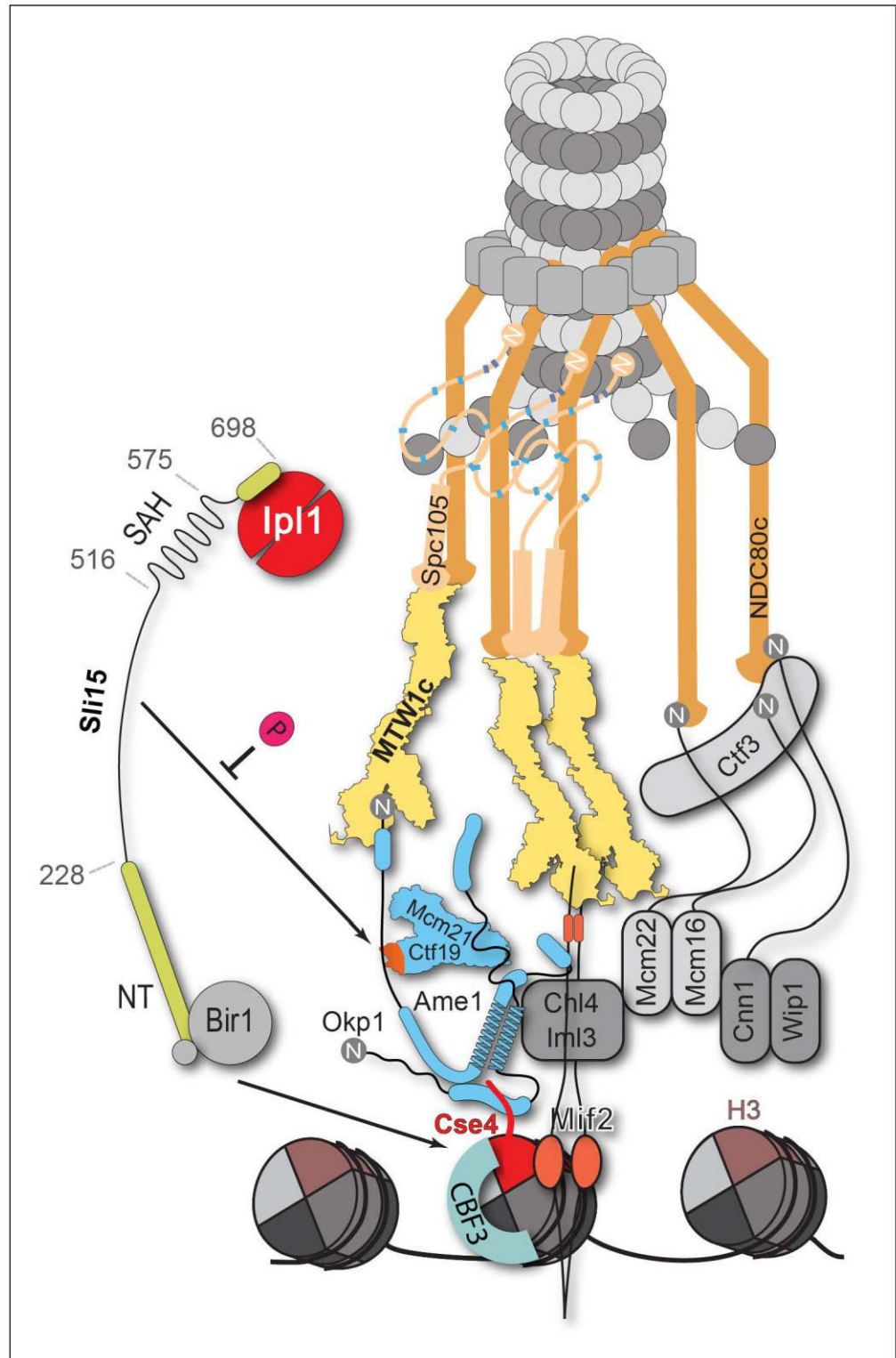


**Figure 7.** Schematic model of the budding yeast kinetochore subunit architecture. The Okp1 core domain directly binds the essential motif of the Cse4 END suggesting that in contrast to humans, the dual recognition of Cse4-NCPs in *S. cerevisiae* is established by the essential inner kinetochore subunits Ame1/Okp1 and Mif2 through interaction with distinct Cse4 motifs. Together with the observation that Ctf19 associates with Sli15/Ipl1, further CPC interactions with the inner and outer kinetochore could be part of a kinetochore conformation that is dependent on Sli15<sup>INCENP</sup>. In line with the observed benomyl sensitivity of cells expressing Sli15 $\Delta$ N as the only nuclear copy (Figure 5C), a recent study in *Xenopus* egg extracts found that CPC lacking the CEN domain of Figure 7 continued on next page

Figure 7 continued

INCENP affected the correction of erroneous kinetochore-microtubule attachments (**Haase et al., 2017**). Centromere-targeting deficient CPC resulted in an imperfect inner kinetochore composition that failed to sense tension-loss and in intermediate Ndc80 phosphorylation levels that indicated the incapability of establishing a sharp phosphorylation gradient according to the spatial separation model. Flat Ndc80 phosphorylation levels could be sufficient for the non-selective turnover of erroneous kinetochore attachments, especially at budding yeast kinetochores which are attached to a single microtubule, unless cells are challenged by microtubule poisons. DOI: <https://doi.org/10.7554/eLife.42879.013>

has recently been shown to promote accurate chromosome alignment by interaction with microtubules (**Pesenti et al., 2018**). If the observed interaction between the CPC and COMA is conserved in higher eukaryotes or is facilitated by other kinetochore proteins remains to be addressed.

In the spatial separation model the CPC is anchored at the centromere and substrate access of the Ipl1<sup>Aurora B</sup> kinase is regulated by tension-dependent intra-kinetochore stretching upon the biorientation of sister kinetochores. Whether the Ctf19-Sli15 interaction is required for CPC stabilization or for the precise positioning of Ipl1 activity at a distinct kinetochore conformation, competent for tension sensing and error correction, poses an interesting future question (**Figure 7**). Our findings place COMA at the center of kinetochore assembly in budding yeast and contribute to the molecular understanding of the fundamental process of how cells establish correct chromosome biorientation at the mitotic spindle.

## Materials and methods

### Key resources table

Reagent type (species) or resource	Designation	Source or reference	Identifiers	Additional information
Gene ( <i>S. cerevisiae</i> )	See <b>Supplementary file 5</b>			
Strain, strain background ( <i>S. cerevisiae</i> )	S288c			
Strain, strain background ( <i>E. coli</i> )	BL21 (DE3)	New England Biolabs	C2527	
Strain, strain background ( <i>E. coli</i> )	DH10Bac	ThermoFisher	10361012	
Cell line ( <i>S. frugiperda</i> )	SF21; <i>Spodoptera frugiperda</i>	ThermoFisher	11497013	
Cell line ( <i>Trichoplusia ni</i> )	High five; <i>Trichoplusia ni</i>	ThermoFisher	B85502	
Genetic reagent ( <i>S. cerevisiae</i> )	See <b>Supplementary file 5</b>			
Antibody	Anti-FLAG M2 (mouse monoclonal)	Sigma-Aldrich	F1804 RRID:AB_262044	1:5000
Antibody	Anti-PGK1 (mouse monoclonal)	Invitrogen	22C5D8 RRID:AB_2532235	1:10000
Antibody	goat anti-mouse IgG-HRP	Santa Cruz Biotechnology	sc-2005 RRID:AB_631736	1:10000
Recombinant DNA reagent	See <b>Supplementary file 4</b>			

Continued on next page

Continued

Reagent type (species) or resource	Designation	Source or reference	Identifiers	Additional information
Peptide, recombinant protein	3xFLAG peptide	Ontores		
Peptide, recombinant protein	lambda phosphatase	New England Biolabs	P0753S	
Commercial assay or kit	Q5 Site-Directed Mutagenesis Kit	New England Biolabs	E0552S	
Chemical compound, drug	BS3-H12/D12 cross-linker	Creative Molecules	001SS	
Chemical compound, drug	Iodoacetamide	Sigma-Aldrich	I6125	
Chemical compound, drug	Lysyl Endopeptidase	FUJIFILM Wako Pure Chemical Corporation	125-05061	
Chemical compound, drug	Trypsin Sequencing Grade Modified	Promega	V5111	
Chemical compound, drug	SYBR Gold	ThermoFisher	S11494	
Chemical compound, drug	AMP-PNP	Santa Cruz Biotechnology	CAS 72957-42-7	
Chemical compound, drug	Rapamycin	Invitrogen	PHZ1235	
Chemical compound, drug	Concanavalin A from <i>Canavalia ensiformis</i>	Sigma-Aldrich	C2010	
Chemical compound, drug	FuGENE HD Transfection Reagent	Sigma-Aldrich	E2311	
Chemical compound, drug	cOmplete ULTRA EDTA-free Protease Inhibitor Cocktail	Roche	5892953001	
Chemical compound, drug	Ni-NTA Agarose	Qiagen	30210	
Chemical compound, drug	Strep-Tactin Superflow Plus Agarose	Qiagen	30004	
Chemical compound, drug	M2 anti-FLAG agarose	Sigma-Aldrich	A4596	
Other	Sep-Pak tC18 cartridges	Waters	WAT054960	
Other	PD-10 Desalting Columns	GE Healthcare	17085101	
Other	$\mu$ -Slide 8 Well	Ibidi	80826	
Software, algorithm	xQuest	(Walzthoeni et al., 2012)		
Software, algorithm	xVis	(Grimm et al., 2015)		
Software, algorithm	Fiji	(Schindelin et al., 2012)		
Software, algorithm	Clustal Omega	(Sievers et al., 2011)		
Software, algorithm	SoftWoRx	GE Healthcare		

## Chemical cross-linking and mass spectrometry of kinetochore complexes

The complex containing Cse4-NCP, Mif2, Ame1/Okp1, Ctf19/Mcm21, Chl4/Iml3 and MTW1c was assembled in solution. It was cross-linked using an equimolar mixture of isotopically light (hydrogen) and heavy (deuterium) labeled bis[sulfosuccinimidyl]suberate (BS3, H12/D12) (Creative Molecules) at a final concentration of 0.25–0.5 mM at 10°C for 30 min. The reaction was quenched by adding ammonium bicarbonate to a final concentration of 100 mM for 10 min at 10°C. The sample was subjected to SEC on a Superose 6 Increase 10/300 GL column (GE Healthcare) and the fractions corresponding to the cross-linked complex were selected for the subsequent protein digest and mass spectrometry (see below).

The complex of Sli15-2xStrep-HA-6xHis/Ipl1 with Ame1/Okp1 and Ctf19/Mcm21 was assembled on Strep-Tactin Superflow agarose (Qiagen) by incubation at room temperature (RT), 1000 rpm for 1 hr in a thermomixer (Eppendorf). Unbound proteins were removed by washing three times with binding buffer [50 mM NaH<sub>2</sub>PO<sub>4</sub>(pH 8.0), 500 mM NaCl, 5% glycerol] and the complex was eluted in binding buffer containing 8 mM biotin. The eluted complex was re-isolated on Ni-NTA beads (Qiagen), washed twice with binding buffer and then cross-linked by resuspending the protein bound beads in BS3 cross-linker at a final concentration of 0.25–0.5 mM at 30°C for 30 min. The cross-linking reaction was stopped by adding ammonium bicarbonate to a final concentration of 100 mM for 20 min at 30°C.

Cross-linked samples were denatured by adding two sample volumes of 8 M urea, reduced with 5 mM TCEP (ThermoFisher) and alkylated by the addition of 10 mM iodoacetamide (Sigma-Aldrich) for 40 min at RT in the dark. Proteins were digested with Lys-C (1:50 (w/w), FUJIFILM Wako Pure Chemical Corporation) at 35°C for 2 hr, diluted with 50 mM ammonium bicarbonate, and digested with trypsin (1:50 w/w, Promega) overnight. Peptides were acidified with trifluoroacetic acid (TFA) at a final concentration of 1% and purified by reversed phase chromatography using C18 cartridges (Sep-Pak, Waters). Cross-linked peptides were enriched on a Superdex Peptide PC 3.2/30 column using water/acetonitrile/TFA (75/25/0.1, v/v/v) as mobile phase at a flow rate of 50 µl/min and were analyzed by liquid chromatography coupled to tandem mass spectrometry (LC-MS/MS) using an Orbitrap Elite instrument (ThermoFisher). Fragment ion spectra were searched and cross-links were identified by the dedicated software xQuest (Walzthoeni *et al.*, 2012). The results were filtered according to the following parameters:  $\Delta$ score  $\leq$  0.85, MS1 tolerance window of –4 to 4 ppm and score  $\geq$  22. The quality of all cross-link spectra passing the filter was manually validated and cross-links were visualized as network plots using the webserver xVis (Grimm *et al.*, 2015).

## Electrophoretic mobility shift assay

Reconstituted nucleosomes (0.5 µM) were mixed in a 1:2 molar ratio with the respective protein complexes in a buffer containing 20 mM Hepes (pH 7.5) and incubated for 1 hr on ice. The interaction was analyzed by electrophoresis at 130 V for 70–90 min on a 6% native polyacrylamide gel in a buffer containing 25 mM Tris and 25 mM boric acid. After electrophoresis, gels were stained with SYBR Gold (ThermoFisher).

## Analytical size exclusion chromatography for interaction studies

Analytical SEC experiments were performed on a Superdex 200 Increase 3.2/300 or a Superose 6 Increase 3.2/300 column (GE Healthcare). To detect the formation of a complex, proteins were mixed at equimolar ratios and incubated for 1 hr on ice before SEC. All samples were eluted under isocratic conditions at 4°C in SEC buffer [50 mM HEPES (pH 7.5), 150 mM NaCl, 5% glycerol]. Elution of proteins was monitored by absorbance at 280 nm. 100 µl fractions were collected and analyzed by SDS-PAGE and Coomassie staining.

## In vitro protein binding assay of Sli15/Ipl1 to Ame1/Okp1 and/or Ctf19/Mcm21

Phosphorylated or non-phosphorylated wild-type or mutant Sli15-2xStrep-HA-6xHis/Ipl1 was immobilized on Strep-Tactin Superflow agarose (Qiagen). For prephosphorylation, Sli15/Ipl1 was incubated at 30°C for 30 min in the presence of 3 mM MgCl<sub>2</sub> and 3 mM ATP. Samples for non-phosphorylated Sli15/Ipl1 were treated the same way, but instead of 3 mM ATP the non-



hydrolysable analog AMP-PNP (Santa Cruz Biotechnology) was applied. To remove basal phosphorylation, Sli15/Ipl1 was treated with lambda phosphatase (New England Biolabs) at 30°C for 30 min. Subsequently, non-phosphorylated as well as phosphorylated or dephosphorylated Sli15/Ipl1 complexes were washed three times with binding buffer [50 mM NaH<sub>2</sub>PO<sub>4</sub>(pH 8), 120 mM NaCl, 5% glycerol].

Testing of binding between Ame1/Okp1, Ctf19/Mcm21 and Sli15/Ipl1 was performed in binding buffer at 4°C, 1000 rpm for 1 hr in a thermomixer (Eppendorf). Unbound proteins were removed by washing three times with binding buffer. The complexes were either eluted with 8 mM biotin in 50 mM NaH<sub>2</sub>PO<sub>4</sub>(pH 8), 500 mM NaCl, 5% glycerol or by boiling in 2x SDS loading buffer.

To quantify the ratios of bound proteins to the bait protein SDS page band intensities were analyzed by using the Fiji software (*Schindelin et al., 2012*).

### Amino acid sequence alignment

Multiple sequence alignment of Cse4 or Okp1 protein sequences from interrelated budding yeast species was conducted with Clustal Omega (*Sievers et al., 2011*). Only protein sequences with the highest similarity to *S. cerevisiae* Cse4 or *S. cerevisiae* Okp1 as determined by a protein BLAST search were included in the search. In addition three mammalian and the *Schizosaccharomyces pombe* homologous CENP-A protein sequences were included in the Cse4 alignment.

### Yeast strains and methods

All plasmids and yeast strains used in this study are listed in *Supplementary file 4* and *Supplementary file 5*, respectively. Yeast strains were created in the S288c background. The generation of yeast strains and yeast methods were performed by standard procedures. The anchor-away technique was performed as previously described (*Haruki et al., 2008*).

For anchor-away rescue experiments, the respective promoters and coding sequences were PCR amplified from yeast genomic DNA and cloned into the vector pRS313 either via the Gibson assembly or the restriction/ligation method. In order to artificially target Sli15ΔN2-228 to the kinetochore, the individual promoters and genes were PCR amplified and the respective gene fusions [CTF19, AME1, OKP1, CTF3, CNN1, MIF2, DSN1, MTW1]-[SLI15ΔN2-228]-[6xHis-7xFLAG] (*Supplementary file 4*) were generated and cloned into pRS313 using the Gibson assembly reaction. The same strategy was applied in order to generate the CTF19 or CTF19ΔC gene fusions to AME1 or OKP1, respectively (*Supplementary file 4*).

The individual deletion mutants were generated using the Q5 site-directed mutagenesis kit (New England Biolabs). The rescue constructs were transformed into Cse4-, Ctf19-, Okp1-, or Sli15 anchor-away strains (*Supplementary file 5*) and cell growth was tested in 1:10 serial dilutions on YPD plates in the absence or presence of rapamycin (1 μg/ml) at 30°C for 3 days.

### Minichromosome loss assay

The Ctf19 anchor-away strain containing a minichromosome (pYCF1/CEN3.L) (*Spencer et al., 1990*) and the Ctf19 anchor-away strains containing a minichromosome (pYCF1/CEN3.L) and the respective rescue plasmid were grown overnight in selective medium (-Ura selecting for the minichromosome, or -His/-Ura selecting for the rescue plasmid and the minichromosome) and then diluted into YPD medium and cultured for 4 hr. The yeast cultures were then plated onto synthetic medium containing rapamycin (1 μg/ml) and low (6 μg/ml) adenine to enhance the red pigmentation (*Hieter et al., 1985*) and incubated for 3 days at 30°C. Colonies retaining the minichromosome are white, and loss events result in the formation of red/red sector colonies. The minichromosome loss frequency was quantified by determining the percentage of red/red sector colonies in relation to the total colony number (white and red/red sector) of three biological replicates.

### Western blot analysis

For western blot analysis an equivalent of 10 OD<sub>600</sub> of cells logarithmically grown in liquid culture was collected by centrifugation at 3140 x g for 5 min at RT and the pellet was washed once with aqua dest. For protein extraction, the pellet was resuspended in 1 ml ice-cold 10% trichloroacetic acid and incubated on ice for 1 hr. Samples were pelleted at 20000x g for 10 min, 4°C and washed twice with ice-cold 95% ethanol. Pellets were air-dried and resuspended in 100 μl 1x SDS-PAGE

sample buffer containing 75 mM Tris (pH 8.8). Samples were boiled (10 min, 95°C) and centrifuged at 10800 x g for 3 min at RT and supernatants were separated on 10% or 15% (Cse4 containing samples) SDS-PAGE gels. Immunoblotting was performed with the following antibodies: Anti-FLAG M2 (Sigma-Aldrich), Anti-PGK1 (ThermoFisher) and visualized by HRP-conjugated anti-mouse secondary antibodies (Santa Cruz).

### Live cell microscopy

For localisation analysis of endogenously tagged Ctf19-GFP and Ctf19 $\Delta$ C-GFP proteins, cells were grown in synthetic medium without tryptophan at 30°C. For localisation analysis of ectopically expressed Ctf19-Okp1-GFP and Ctf19 $\Delta$ C-Okp1-GFP proteins in the Ctf19-anchor-away (Ctf19-FRB) strain, cells were grown in selective medium (-His/-Trp) until OD<sub>600</sub> ~0.4, then rapamycin (1  $\mu$ g/ml) was added and cells were grown for another 3 hr at 30°C. For imaging cells were immobilized on concanavalin-A (Sigma-Aldrich) coated slides (Ibidi). Microscopy was performed using a DeltaVision microscopy system (Applied precision) with a Olympus IX71 microscope controlled by softWoRx software (GE Healthcare). Images were processed using Fiji (*Schindelin et al., 2012*).

### Protein expression and purification

Expression constructs for 6xHis-Chl4/Iml3, 6xHis-Cnn1/Wip1-1xFlag, 6xHis-Nkp1/Nkp2 and Mhf1/Mhf2-1xStrep were created by amplification of genomic DNA and cloned into pETDuet-1 vector (Novagen). Expression was performed in BL21 (DE3) cells (New England Biolabs). Cells were grown at 37°C until OD<sub>600</sub> 0.6, followed by induction with 0.5 mM IPTG for Chl4/Iml3 or 0.2 mM IPTG for all other protein expressions. Protein expression was induced overnight at 18°C, or for 3 hr at 23°C, respectively.

Cells were lysed using a French Press in lysis buffer [50 mM Hepes (pH 7.5), 400 mM NaCl, 3% glycerol, 0.01% Tween20 and cOmplete ULTRA EDTA-free Protease Inhibitor Cocktail (Roche)]. 6xHis-tagged proteins were purified using Ni-NTA agarose (Qiagen), whereby 30 mM imidazole were added to the lysis buffer in the washing step, followed by protein elution in 50 mM Hepes pH 7.5, 150 mM NaCl, 300 mM imidazole, and 5% glycerol. Strep-tag purification was performed using Strep-Tactin Superflow agarose (Qiagen) and eluted in a buffer containing 50 mM Hepes (pH 7.5), 150 mM NaCl, 8 mM biotin and 5% glycerol.

Buffer exchange into a buffer containing 50 mM Hepes (pH 7.5), 150 mM NaCl and 5% glycerol was performed using a Superdex 200 HiLoad 16/60 column (GE Healthcare) for Chl4/Iml3 and Cnn1/Wip1 or using a PD10 desalting column (GE Healthcare) for Nkp1/2 and Mhf1/2 protein complexes.

### Ame1/Okp1 expression and purification

Ame1-6xHis/Okp1 wild-type and mutant protein expression and purification in *E. coli* was performed as described previously (*Hornung et al., 2014*).

### In vitro reconstitution of Cse4- and H3-NCPs

Octameric Cse4 and H3 containing nucleosomes were *in vitro* reconstituted from budding yeast histones which were recombinantly expressed in *E. coli* BL21 (DE3) and assembled on 167 bp of the 'Widom 601' nucleosome positioning sequence according to a modified protocol (*Turco et al., 2015*).

### Affinity-purification of recombinant protein complexes from insect cells

C-terminal 6xHis-6xFLAG-tags on Mcm21, Mif2, Dsn1, Mcm16 and C-terminal 2xStrep- tags on Sli15 were used to affinity-purify Ctf19/Mcm21, Mif2, MTW1c, CTF3c and Sli15/Ipl1 complexes. Open reading frames encoding the respective subunits were amplified from yeast genomic DNA and cloned into the pBIG1/2 vectors according to the biGBac system (*Weissmann et al., 2016*). The pBIG1/2 constructs were used to generate recombinant baculoviral genomes by Tn7 transposition into the DH10Bac *E. coli* strain (ThermoFisher) (*Vijayachandran et al., 2011*). Viruses were generated by transfection of Sf21 insect cells (ThermoFisher) with the recombinant baculoviral genome using FuGENE HD transfection reagent (Promega). Viruses were amplified by adding transfection supernatant to Sf21 suspension cultures. Protein complexes were expressed in High Fiveinsect cell (ThermoFisher) suspension cultures.

For purification of FLAG-tagged kinetochore complexes, insect cells were extracted in lysis buffer [50 mM Tris (pH 7.5), 150 mM NaCl, 5% glycerol] supplemented with cOmplete ULTRA EDTA-free Protease Inhibitor Cocktail (Roche) using a Dounce homogenizer. Cleared extracts were incubated with M2 anti-FLAG agarose (Sigma-Aldrich) for 2 hr, washed three times with lysis buffer and eluted in lysis buffer containing 1 mg/ml 3xFLAG peptide (Ontores).

High Five cells expressing Strep-tagged Sli15/lpl1 were lysed in 50 mM NaH<sub>2</sub>PO<sub>4</sub>(pH 8.0), 300 mM NaCl, 5% glycerol supplemented with cOmplete ULTRA EDTA-free Protease Inhibitor Cocktail (Roche). Subsequent to incubating the cleared lysates with Strep-Tactin Superflow agarose (Qiagen), protein bound beads were washed three times with lysis buffer and the bound protein complex was eluted in lysis buffer containing 8 mM biotin. FLAG peptide or biotin was either removed via PD10 desalting columns (GE Healthcare) or SEC using a Superdex 200 HiLoad 16/60 column (GE Healthcare) and isocratic elution in lysis buffer.

## Acknowledgements

We are grateful to Andrea Musacchio (MPI Dortmund) and Stefan Westermann (University of Essen) for discussions and sharing reagents. We thank Wolfgang Zachariae (MPI Munich) for help with fluorescence microscopy. JFH and GH were funded by the Graduate School (GRK 1721) and MP and VS were funded by the Graduate School (Quantitative Biosciences Munich) of the German Research Foundation (DFG). LDG was a recipient of a DOC Fellowship of the Austrian Academy of Sciences and AK was funded by ERC Grant 281354 (NPC GENEXPRESS). FH was supported by the European Research Council (ERC-StG no. 638218), the Human Frontier Science Program (RGP0008/2015), by the Bavarian Research Center of Molecular Biosystems and by an LMU excellent junior grant.

## Additional information

### Funding

Funder	Grant reference number	Author
Deutsche Forschungsgemeinschaft	Graduate School Quantitative Biosciences Munich	Mia Potocnjak Victor Solis-Mezarino
Deutsche Forschungsgemeinschaft	Graduate School GRK 1721	Götz Hagemann Franz Herzog
Austrian Academy of Sciences	DOC Fellowship	Laura D Gallego
European Research Council	281354 (NPC GENEXPRESS)	Alwin Köhler
European Research Council	ERC-StG MolStruKT, no. 638218	Franz Herzog
Human Frontier Science Program	RGP0008/2015	Franz Herzog
Bavarian Research Center for Molecular Biosystems		Franz Herzog
Ludwig-Maximilians-Universität München	Excellent Junior grant	Franz Herzog

The funders had no role in study design, data collection and interpretation, or the decision to submit the work for publication.

### Author contributions

Josef Fischböck-Halwachs, Sylvia Singh, Formal analysis, Investigation, Methodology, Writing—original draft; Mia Potocnjak, Formal analysis, Methodology; Götz Hagemann, Victor Solis-Mezarino, Formal analysis, Investigation; Stephan Woike, Formal analysis, Investigation, Methodology; Medini Ghodgaonkar-Steger, Jessica Andreani, Formal analysis; Florian Weissmann, Laura D Gallego, Julie Rojas, Alwin Köhler, Methodology; Franz Herzog, Conceptualization, Funding acquisition, Writing—original draft

**Author ORCIDs**Jessica Andreani  <https://orcid.org/0000-0003-4435-9093>Franz Herzog  <https://orcid.org/0000-0001-8270-1449>**Decision letter and Author response**Decision letter <https://doi.org/10.7554/eLife.42879.025>Author response <https://doi.org/10.7554/eLife.42879.026>**Additional files****Supplementary files**

- Supplementary file 1. Inter- and intra-protein cross-links detected on in vitro reconstituted Cse4 containing nucleosomes interacting with the kinetochore complexes Ame1/Okp1, Ctf19/Mcm21, Mif2, Chl4/Iml3 and MTW1c.

DOI: <https://doi.org/10.7554/eLife.42879.014>

- Supplementary file 2. Inter- and intra-protein cross-links detected on in vitro reconstituted Sli15/Ipl1 interacting with the inner kinetochore proteins Ctf19, Okp1, Ame1 and Mcm21 (COMA).

DOI: <https://doi.org/10.7554/eLife.42879.015>

- Supplementary file 3. Predicted and experimentally annotated protein domains and motifs depicted in protein cross-link networks.

DOI: <https://doi.org/10.7554/eLife.42879.016>

- Supplementary file 4. Plasmids used in this study.

DOI: <https://doi.org/10.7554/eLife.42879.017>

- Supplementary file 5. Yeast strains used in this study.

DOI: <https://doi.org/10.7554/eLife.42879.018>

- Transparent reporting form

DOI: <https://doi.org/10.7554/eLife.42879.019>**Data availability**

The mass spectrometry raw data was uploaded to the PRIDE Archive and is publicly available through the following identifiers: PXD011235 (COMA-Sli15/Ipl1); PXD011236 (CCAN).

The following datasets were generated:

Author(s)	Year	Dataset title	Dataset URL	Database and Identifier
Josef Fischböck-Halwachs, Sylvia Singh, Mia Potocnjak, Götz Hagemann, Victor Solis-Mezarino, Stephan Woike, Medini Ghodgaonkar-Steiger, Florian Weissmann, Laura D. Gallego, Julie Rojas, Jessica Andreani, Alwin Köhler, Franz Herzog	2019	COMA-CPC	<a href="https://www.ebi.ac.uk/pride/archive/projects/PXD011235">https://www.ebi.ac.uk/pride/archive/projects/PXD011235</a>	PRIDE, PXD011235
Josef Fischböck-Halwachs, Sylvia Singh, Mia Potocnjak, Götz Hagemann, Victor Solis-Mezarino, Stephan Woike, Medini Ghodgaonkar-Steiger, Florian Weissmann, Laura D.	2019	CCAN	<a href="https://www.ebi.ac.uk/pride/archive/projects/PXD011236">https://www.ebi.ac.uk/pride/archive/projects/PXD011236</a>	PRIDE, PXD011236

Gallego, Julie Rojas,  
Jessica Andreani,  
Alwin Köhler, Franz  
Herzog

## References

- Adams RR, Wheatley SP, Gouldsworthy AM, Kandels-Lewis SE, Carmena M, Smythe C, Gerloff DL, Earnshaw WC. 2000. INCENP binds the Aurora-related kinase AIRK2 and is required to target it to chromosomes, the central spindle and cleavage furrow. *Current Biology* **10**:1075–1078. DOI: [https://doi.org/10.1016/S0960-9822\(00\)00673-4](https://doi.org/10.1016/S0960-9822(00)00673-4), PMID: 10996078
- Akiyoshi B, Nelson CR, Biggins S. 2013. The aurora B kinase promotes inner and outer kinetochore interactions in budding yeast. *Genetics* **194**:785–789. DOI: <https://doi.org/10.1534/genetics.113.150839>, PMID: 23636741
- Anedchenko EA, Samel-Pommerencke A, Tran Nguyen TM, Shahnejat-Bushehri S, Pöpsel J, Lauster D, Herrmann A, Rappsilber J, Cuomo A, Bonaldi T, Ehrenhofer-Murray AE. 2019. The kinetochore module Okp1<sup>CENP-O</sup>/Ame1<sup>CENP-U</sup> is a reader for N-terminal modifications on the centromeric histone Cse4<sup>CENP-A</sup>. *The EMBO Journal* **38**:e98991. DOI: <https://doi.org/10.15252/embj.201898991>, PMID: 30389668
- Baker DJ, Chen J, van Deursen JM. 2005. The mitotic checkpoint in cancer and aging: what have mice taught us? *Current Opinion in Cell Biology* **17**:583–589. DOI: <https://doi.org/10.1016/j.ceb.2005.09.011>, PMID: 16226453
- Bekier ME, Mazur T, Rashid MS, Taylor WR. 2015. Borealin dimerization mediates optimal CPC checkpoint function by enhancing localization to centromeres and kinetochores. *Nature Communications* **6**:6775. DOI: <https://doi.org/10.1038/ncomms7775>, PMID: 25854549
- Biggins S. 2013. The composition, functions, and regulation of the budding yeast kinetochore. *Genetics* **194**:817–846. DOI: <https://doi.org/10.1534/genetics.112.145276>, PMID: 23908374
- Biggins S, Murray AW. 2001. The budding yeast protein kinase Ipl1/Aurora allows the absence of tension to activate the spindle checkpoint. *Genes & Development* **15**:3118–3129. DOI: <https://doi.org/10.1101/gad.934801>, PMID: 11731476
- Bodor DL, Mata JF, Sergeev M, David AF, Salimian KJ, Panchenko T, Cleveland DW, Black BE, Shah JV, Jansen LE. 2014. The quantitative architecture of centromeric chromatin. *eLife* **3**:e02137. DOI: <https://doi.org/10.7554/eLife.02137>, PMID: 25027692
- Boeckmann L, Takahashi Y, Au WC, Mishra PK, Choy JS, Dawson AR, Szeto MY, Waybright TJ, Heger C, McAndrew C, Goldsmith PK, Veenstra TD, Baker RE, Basrai MA. 2013. Phosphorylation of centromeric histone H3 variant regulates chromosome segregation in *Saccharomyces cerevisiae*. *Molecular Biology of the Cell* **24**:2034–2044. DOI: <https://doi.org/10.1091/mbc.e12-12-0893>, PMID: 23637466
- Camahort R, Shivaraju M, Mattingly M, Li B, Nakanishi S, Zhu D, Shilatifard A, Workman JL, Gerton JL. 2009. Cse4 is part of an octameric nucleosome in budding yeast. *Molecular Cell* **35**:794–805. DOI: <https://doi.org/10.1016/j.molcel.2009.07.022>, PMID: 19782029
- Campbell CS, Desai A. 2013. Tension sensing by aurora B kinase is independent of survivin-based centromere localization. *Nature* **497**:118–121. DOI: <https://doi.org/10.1038/nature12057>, PMID: 23604256
- Carmena M, Wheelock M, Funabiki H, Earnshaw WC. 2012. The chromosomal passenger complex (CPC): from easy rider to the godfather of mitosis. *Nature Reviews Molecular Cell Biology* **13**:789–803. DOI: <https://doi.org/10.1038/nrm3474>, PMID: 23175282
- Carroll CW, Silva MC, Godek KM, Jansen LE, Straight AF. 2009. Centromere assembly requires the direct recognition of CENP-A nucleosomes by CENP-N. *Nature Cell Biology* **11**:896–902. DOI: <https://doi.org/10.1038/ncb1899>, PMID: 19543270
- Carroll CW, Milks KJ, Straight AF. 2010. Dual recognition of CENP-A nucleosomes is required for centromere assembly. *The Journal of Cell Biology* **189**:1143–1155. DOI: <https://doi.org/10.1083/jcb.201001013>, PMID: 20566683
- Cheeseman IM, Anderson S, Jwa M, Green EM, Kang J, Yates JR, Chan CS, Drubin DG, Barnes G. 2002. Phospho-regulation of kinetochore-microtubule attachments by the Aurora kinase Ipl1p. *Cell* **111**:163–172. DOI: [https://doi.org/10.1016/S0092-8674\(02\)00973-X](https://doi.org/10.1016/S0092-8674(02)00973-X), PMID: 12408861
- Cheeseman IM, Chappie JS, Wilson-Kubalek EM, Desai A. 2006. The conserved KMN network constitutes the core microtubule-binding site of the kinetochore. *Cell* **127**:983–997. DOI: <https://doi.org/10.1016/j.cell.2006.09.039>, PMID: 17129783
- Chen Y, Baker RE, Keith KC, Harris K, Stoler S, Fitzgerald-Hayes M. 2000. The N terminus of the centromere H3-like protein Cse4p performs an essential function distinct from that of the histone fold domain. *Molecular and Cellular Biology* **20**:7037–7048. DOI: <https://doi.org/10.1128/MCB.20.18.7037-7048.2000>, PMID: 10958698
- Chittori S, Hong J, Saunders H, Feng H, Ghirlando R, Kelly AE, Bai Y, Subramaniam S. 2018. Structural mechanisms of centromeric nucleosome recognition by the kinetochore protein CENP-N. *Science* **359**:339–343. DOI: <https://doi.org/10.1126/science.aar2781>, PMID: 29269420
- Cho US, Harrison SC. 2011. Ndc10 is a platform for inner kinetochore assembly in budding yeast. *Nature Structural & Molecular Biology* **19**:48–55. DOI: <https://doi.org/10.1038/nsmb.2178>, PMID: 22139014
- De Wulf P, McAinsh AD, Sorger PK. 2003. Hierarchical assembly of the budding yeast kinetochore from multiple subcomplexes. *Genes & Development* **17**:2902–2921. DOI: <https://doi.org/10.1101/gad.1144403>, PMID: 14633972

- DeLuca JG, Gall WE, Ciferri C, Cimini D, Musacchio A, Salmon ED. 2006. Kinetochore microtubule dynamics and attachment stability are regulated by Hec1. *Cell* **127**:969–982. DOI: <https://doi.org/10.1016/j.cell.2006.09.047>, PMID: 17129782
- DeLuca KF, Lens SM, DeLuca JG. 2011. Temporal changes in Hec1 phosphorylation control kinetochore-microtubule attachment stability during mitosis. *Journal of Cell Science* **124**:622–634. DOI: <https://doi.org/10.1242/jcs.072629>, PMID: 21266467
- Dimitrova YN, Jenni S, Valverde R, Khin Y, Harrison SC. 2016. Structure of the MIND complex defines a regulatory focus for yeast kinetochore assembly. *Cell* **167**:1014–1027. DOI: <https://doi.org/10.1016/j.cell.2016.10.011>
- Drozdetskiy A, Cole C, Procter J, Barton GJ. 2015. JPred4: a protein secondary structure prediction server. *Nucleic Acids Research* **43**:W389–W394. DOI: <https://doi.org/10.1093/nar/gkv332>, PMID: 25883141
- Earnshaw WC, Rothfield N. 1985. Identification of a family of human centromere proteins using autoimmune sera from patients with scleroderma. *Chromosoma* **91**:313–321. DOI: <https://doi.org/10.1007/BF00328227>, PMID: 2579778
- Fernius J, Marston AL. 2009. Establishment of cohesion at the pericentromere by the Ctf19 kinetochore subcomplex and the replication fork-associated factor, Csm3. *PLoS Genetics* **5**:e1000629. DOI: <https://doi.org/10.1371/journal.pgen.1000629>, PMID: 19730685
- Fink S, Turnbull K, Desai A, Campbell CS. 2017. An engineered minimal chromosomal passenger complex reveals a role for INCENP/Sli15 spindle association in chromosome biorientation. *The Journal of Cell Biology* **216**:911–923. DOI: <https://doi.org/10.1083/jcb.201609123>, PMID: 28314741
- Fitzgerald-Hayes M, Clarke L, Carbon J. 1982. Nucleotide sequence comparisons and functional analysis of yeast centromere DNAs. *Cell* **29**:235–244. DOI: [https://doi.org/10.1016/0092-8674\(82\)90108-8](https://doi.org/10.1016/0092-8674(82)90108-8), PMID: 7049398
- Foley EA, Kapoor TM. 2013. Microtubule attachment and spindle assembly checkpoint signalling at the kinetochore. *Nature Reviews Molecular Cell Biology* **14**:25–37. DOI: <https://doi.org/10.1038/nrm3494>, PMID: 23258294
- Foltz DR, Jansen LE, Black BE, Bailey AO, Yates JR, Cleveland DW. 2006. The human CENP-A centromeric nucleosome-associated complex. *Nature Cell Biology* **8**:458–469. DOI: <https://doi.org/10.1038/ncb1397>, PMID: 16622419
- Fukagawa T, Earnshaw WC. 2014. The centromere: chromatin foundation for the kinetochore machinery. *Developmental Cell* **30**:496–508. DOI: <https://doi.org/10.1016/j.devcel.2014.08.016>, PMID: 25203206
- García-Rodríguez LJ, Kasčiukovic T, Denninger V, Tanaka TU. 2019. Aurora B-INCENP localization at centromeres/Inner kinetochores is required for chromosome Bi-orientation in budding yeast. *Current Biology* **29**:1536–1544. DOI: <https://doi.org/10.1016/j.cub.2019.03.051>, PMID: 31006569
- Grimm M, Zimniak T, Kahraman A, Herzog F. 2015. xVis: a web server for the schematic visualization and interpretation of crosslink-derived spatial restraints. *Nucleic Acids Research* **43**:W362–W369. DOI: <https://doi.org/10.1093/nar/gkv463>, PMID: 25956653
- Guse A, Carroll CW, Moree B, Fuller CJ, Straight AF. 2011. In vitro centromere and kinetochore assembly on defined chromatin templates. *Nature* **477**:354–358. DOI: <https://doi.org/10.1038/nature10379>, PMID: 21874020
- Haase J, Bonner MK, Halas H, Kelly AE. 2017. Distinct roles of the chromosomal passenger complex in the detection of and response to errors in Kinetochore-Microtubule attachment. *Developmental Cell* **42**:640–654. DOI: <https://doi.org/10.1016/j.devcel.2017.08.022>
- Haruki H, Nishikawa J, Laemmli UK. 2008. The anchor-away technique: rapid, conditional establishment of yeast mutant phenotypes. *Molecular Cell* **31**:925–932. DOI: <https://doi.org/10.1016/j.molcel.2008.07.020>, PMID: 18922474
- Hasson D, Panchenko T, Salimian KJ, Salman MU, Sekulic N, Alonso A, Warburton PE, Black BE. 2013. The octamer is the major form of CENP-A nucleosomes at human centromeres. *Nature Structural & Molecular Biology* **20**:687–695. DOI: <https://doi.org/10.1038/nsmb.2562>, PMID: 23644596
- Hengeveld RCC, Vromans MJM, Vleugel M, Hadders MA, Lens SMA. 2017. Inner centromere localization of the CPC maintains centromere cohesion and allows mitotic checkpoint silencing. *Nature Communications* **8**:15542. DOI: <https://doi.org/10.1038/ncomms15542>, PMID: 28561035
- Herzog F, Kahraman A, Boehringer D, Mak R, Bracher A, Walzthoeni T, Leitner A, Beck M, Hartl FU, Ban N, Malmström L, Aebersold R. 2012. Structural probing of a protein phosphatase 2A network by chemical cross-linking and mass spectrometry. *Science* **337**:1348–1352. DOI: <https://doi.org/10.1126/science.1221483>, PMID: 22984071
- Hieter P, Mann C, Snyder M, Davis RW. 1985. Mitotic stability of yeast chromosomes: a colony color assay that measures nondisjunction and chromosome loss. *Cell* **40**:381–392. DOI: [https://doi.org/10.1016/0092-8674\(85\)90152-7](https://doi.org/10.1016/0092-8674(85)90152-7), PMID: 3967296
- Hindriksen S, Lens SMA, Hadders MA. 2017. The ins and outs of aurora B inner centromere localization. *Frontiers in Cell and Developmental Biology* **5**:112. DOI: <https://doi.org/10.3389/fcell.2017.00112>, PMID: 29312936
- Hinshaw SM, Makrantonis V, Harrison SC, Marston AL. 2017. The kinetochore receptor for the cohesin loading complex. *Cell* **171**:72–84. DOI: <https://doi.org/10.1016/j.cell.2017.08.017>, PMID: 28938124
- Hinshaw SM, Harrison SC. 2013. An Iml3-Chl4 heterodimer links the core centromere to factors required for accurate chromosome segregation. *Cell Reports* **5**:29–36. DOI: <https://doi.org/10.1016/j.celrep.2013.08.036>, PMID: 24075991

- Hinshaw SM, Harrison SC. 2019. The structure of the Ctf19c/CCAN from budding yeast. *eLife* **8**:e44239. DOI: <https://doi.org/10.7554/eLife.44239>, PMID: 30762520
- Hori T, Okada M, Maenaka K, Fukagawa T. 2008. CENP-O class proteins form a stable complex and are required for proper kinetochore function. *Molecular Biology of the Cell* **19**:843–854. DOI: <https://doi.org/10.1091/mbc.07-06-0556>, PMID: 18094054
- Hornung P, Troc P, Malvezzi F, Maier M, Demianova Z, Zimniak T, Litos G, Lampert F, Schleiffer A, Brunner M, Mechtler K, Herzog F, Marlovits TC, Westermann S. 2014. A cooperative mechanism drives budding yeast kinetochore assembly downstream of CENP-A. *The Journal of Cell Biology* **206**:509–524. DOI: <https://doi.org/10.1083/jcb.201403081>, PMID: 25135934
- Hyland KM, Kingsbury J, Koshland D, Hieter P. 1999. Ctf19p: A novel kinetochore protein in *Saccharomyces cerevisiae* and a potential link between the kinetochore and mitotic spindle. *The Journal of Cell Biology* **145**:15–28. DOI: <https://doi.org/10.1083/jcb.145.1.15>, PMID: 10189365
- Jeyaprakash AA, Klein UR, Lindner D, Ebert J, Nigg EA, Conti E. 2007. Structure of a Survivin-Borealin-INCENP core complex reveals how chromosomal passengers travel together. *Cell* **131**:271–285. DOI: <https://doi.org/10.1016/j.cell.2007.07.045>, PMID: 17956729
- Joglekar AP, Bouck DC, Molk JN, Bloom KS, Salmon ED. 2006. Molecular architecture of a kinetochore-microtubule attachment site. *Nature Cell Biology* **8**:581–585. DOI: <https://doi.org/10.1038/ncb1414>, PMID: 16715078
- Joglekar AP, Bloom K, Salmon ED. 2009. In vivo protein architecture of the eukaryotic kinetochore with nanometer scale accuracy. *Current Biology* **19**:694–699. DOI: <https://doi.org/10.1016/j.cub.2009.02.056>, PMID: 19345105
- Kaitna S, Mendoza M, Jantsch-Plunger V, Glotzer M. 2000. Incenp and an aurora-like kinase form a complex essential for chromosome segregation and efficient completion of cytokinesis. *Current Biology* **10**:1172–1181. DOI: [https://doi.org/10.1016/S0960-9822\(00\)00721-1](https://doi.org/10.1016/S0960-9822(00)00721-1), PMID: 11050385
- Kang J, Cheeseman IM, Kallstrom G, Velmurugan S, Barnes G, Chan CS. 2001. Functional cooperation of Dam1, Ipl1, and the inner centromere protein (INCENP)-related protein Sli15 during chromosome segregation. *The Journal of Cell Biology* **155**:763–774. DOI: <https://doi.org/10.1083/jcb.200105029>, PMID: 11724818
- Kato H, Jiang J, Zhou BR, Rozendaal M, Feng H, Ghirlando R, Xiao TS, Straight AF, Bai Y. 2013. A conserved mechanism for centromeric nucleosome recognition by centromere protein CENP-C. *Science* **340**:1110–1113. DOI: <https://doi.org/10.1126/science.1235532>, PMID: 23723239
- Kawashima SA, Yamagishi Y, Honda T, Ishiguro K, Watanabe Y. 2010. Phosphorylation of H2A by Bub1 prevents chromosomal instability through localizing shugoshin. *Science* **327**:172–177. DOI: <https://doi.org/10.1126/science.1180189>, PMID: 19965387
- Keith KC, Baker RE, Chen Y, Harris K, Stoler S, Fitzgerald-Hayes M. 1999. Analysis of primary structural determinants that distinguish the centromere-specific function of histone variant Cse4p from histone H3. *Molecular and Cellular Biology* **19**:6130–6139. DOI: <https://doi.org/10.1128/MCB.19.9.6130>, PMID: 10454560
- Klein UR, Nigg EA, Gruneberg U. 2006. Centromere targeting of the chromosomal passenger complex requires a ternary subcomplex of Borealin, Survivin, and the N-terminal domain of INCENP. *Molecular Biology of the Cell* **17**:2547–2558. DOI: <https://doi.org/10.1091/mbc.e05-12-1133>, PMID: 16571674
- Knockleby J, Vogel J. 2009. The COMA complex is required for Sli15/INCENP-mediated correction of defective kinetochore attachments. *Cell Cycle* **8**:2570–2577. DOI: <https://doi.org/10.4161/cc.8.16.9267>, PMID: 19597337
- Krenn V, Musacchio A. 2015. The aurora B kinase in chromosome Bi-Orientation and spindle checkpoint signaling. *Frontiers in Oncology* **5**:225. DOI: <https://doi.org/10.3389/fonc.2015.00225>, PMID: 26528436
- Lampson MA, Cheeseman IM. 2011. Sensing centromere tension: aurora B and the regulation of kinetochore function. *Trends in Cell Biology* **21**:133–140. DOI: <https://doi.org/10.1016/j.tcb.2010.10.007>, PMID: 21106376
- Lechner J, Carbon J. 1991. A 240 kd multisubunit protein complex, CBF3, is a major component of the budding yeast centromere. *Cell* **64**:717–725. DOI: [https://doi.org/10.1016/0092-8674\(91\)90501-O](https://doi.org/10.1016/0092-8674(91)90501-O), PMID: 1997204
- Liu D, Vader G, Vromans MJ, Lampson MA, Lens SM. 2009. Sensing chromosome bi-orientation by spatial separation of aurora B kinase from kinetochore substrates. *Science* **323**:1350–1353. DOI: <https://doi.org/10.1126/science.1167000>, PMID: 19150808
- Meluh PB, Koshland D. 1997. Budding yeast centromere composition and assembly as revealed by in vivo cross-linking. *Genes & Development* **11**:3401–3412. DOI: <https://doi.org/10.1101/gad.11.24.3401>, PMID: 9407032
- Miranda JJ, De Wulf P, Sorger PK, Harrison SC. 2005. The yeast DASH complex forms closed rings on microtubules. *Nature Structural & Molecular Biology* **12**:138–143. DOI: <https://doi.org/10.1038/nsmb896>, PMID: 15640796
- Musacchio A, Desai A. 2017. A molecular view of kinetochore assembly and function. *Biology* **6**:5. DOI: <https://doi.org/10.3390/biology6010005>
- Ng R, Carbon J. 1987. Mutational and in vitro protein-binding studies on centromere DNA from *Saccharomyces cerevisiae*. *Molecular and Cellular Biology* **7**:4522–4534. DOI: <https://doi.org/10.1128/MCB.7.12.4522>, PMID: 2830498
- Okada M, Cheeseman IM, Hori T, Okawa K, McLeod IX, Yates JR, Desai A, Fukagawa T. 2006. The CENP-H-I complex is required for the efficient incorporation of newly synthesized CENP-A into centromeres. *Nature Cell Biology* **8**:446–457. DOI: <https://doi.org/10.1038/ncb1396>, PMID: 16622420
- Ortiz J, Stemmann O, Rank S, Lechner J. 1999. A putative protein complex consisting of Ctf19, Mcm21, and Okp1 represents a missing link in the budding yeast kinetochore. *Genes & Development* **13**:1140–1155. DOI: <https://doi.org/10.1101/gad.13.9.1140>, PMID: 10323865

- Pentakota S**, Zhou K, Smith C, Maffini S, Petrovic A, Morgan GP, Weir JR, Vetter IR, Musacchio A, Luger K. 2017. Decoding the centromeric nucleosome through CENP-N. *eLife* **6**:e33442. DOI: <https://doi.org/10.7554/eLife.33442>
- Pesenti ME**, Prumbaum D, Auckland P, Smith CM, Faesen AC, Petrovic A, Erent M, Maffini S, Pentakota S, Weir JR, Lin Y-C, Raunser S, McAinsh AD, Musacchio A. 2018. Reconstitution of a 26-Subunit human kinetochore reveals cooperative microtubule binding by CENP-OPQR and NDC80. *Molecular Cell* **71**:923–939. DOI: <https://doi.org/10.1016/j.molcel.2018.07.038>
- Pfau SJ**, Amon A. 2012. Chromosomal instability and aneuploidy in cancer: from yeast to man. *EMBO Reports* **13**:515–527. DOI: <https://doi.org/10.1038/embor.2012.65>, PMID: 22614003
- Poddar A**, Roy N, Sinha P. 1999. MCM21 and MCM22, two novel genes of the yeast *Saccharomyces cerevisiae* are required for chromosome transmission. *Molecular Microbiology* **31**:349–360. DOI: <https://doi.org/10.1046/j.1365-2958.1999.01179.x>, PMID: 9987135
- Przewlaka MR**, Venkei Z, Bolanos-Garcia VM, Debski J, Dadlez M, Glover DM. 2011. CENP-C is a structural platform for kinetochore assembly. *Current Biology* **21**:399–405. DOI: <https://doi.org/10.1016/j.cub.2011.02.005>, PMID: 21353555
- Samejima K**, Platani M, Wolny M, Ogawa H, Vargiu G, Knight PJ, Peckham M, Earnshaw WC. 2015. The inner centromere protein (INCENP) Coil is a single  $\alpha$ -Helix (SAH) Domain that binds directly to microtubules and is important for chromosome passenger complex (CPC) Localization and function in mitosis. *Journal of Biological Chemistry* **290**:21460–21472. DOI: <https://doi.org/10.1074/jbc.M115.645317>, PMID: 26175154
- Santaguida S**, Musacchio A. 2009. The life and miracles of kinetochores. *The EMBO Journal* **28**:2511–2531. DOI: <https://doi.org/10.1038/emboj.2009.173>, PMID: 19629042
- Schindelin J**, Arganda-Carreras I, Frise E, Kaynig V, Longair M, Pietzsch T, Preibisch S, Rueden C, Saalfeld S, Schmid B, Tinevez JY, White DJ, Hartenstein V, Eliceiri K, Tomancak P, Cardona A. 2012. Fiji: an open-source platform for biological-image analysis. *Nature Methods* **9**:676–682. DOI: <https://doi.org/10.1038/nmeth.2019>, PMID: 22743772
- Schmitzberger F**, Richter MM, Gordiyenko Y, Robinson CV, Dadlez M, Westermann S. 2017. Molecular basis for inner kinetochore configuration through RWD domain-peptide interactions. *The EMBO Journal* **36**:3458–3482. DOI: <https://doi.org/10.15252/emboj.201796636>, PMID: 29046335
- Schmitzberger F**, Harrison SC. 2012. RWD domain: a recurring module in kinetochore architecture shown by a Ctf19-Mcm21 complex structure. *EMBO Reports* **13**:216–222. DOI: <https://doi.org/10.1038/embor.2012.1>, PMID: 22322944
- Screpanti E**, De Antoni A, Alushin GM, Petrovic A, Melis T, Nogales E, Musacchio A. 2011. Direct binding of Cenp-C to the Mis12 complex joins the inner and outer kinetochore. *Current Biology* **21**:391–398. DOI: <https://doi.org/10.1016/j.cub.2010.12.039>, PMID: 21353556
- Sievers F**, Wilm A, Dineen D, Gibson TJ, Karplus K, Li W, Lopez R, McWilliam H, Remmert M, Söding J, Thompson JD, Higgins DG. 2011. Fast, scalable generation of high-quality protein multiple sequence alignments using clustal omega. *Molecular Systems Biology* **7**:539. DOI: <https://doi.org/10.1038/msb.2011.75>, PMID: 21988835
- Spencer F**, Gerring SL, Connelly C, Hieter P. 1990. Mitotic chromosome transmission fidelity mutants in *saccharomyces cerevisiae*. *Genetics* **124**:237–249. PMID: 2407610
- Tachiwana H**, Kagawa W, Shiga T, Osakabe A, Miya Y, Saito K, Hayashi-Takanaka Y, Oda T, Sato M, Park SY, Kimura H, Kurumizaka H. 2011. Crystal structure of the human centromeric nucleosome containing CENP-A. *Nature* **476**:232–235. DOI: <https://doi.org/10.1038/nature10258>, PMID: 21743476
- Tanaka TU**, Rachidi N, Janke C, Pereira G, Galova M, Schiebel E, Stark MJ, Nasmyth K. 2002. Evidence that the Ipl1-Sli15 (Aurora kinase-INCENP) complex promotes chromosome bi-orientation by altering kinetochore-spindle pole connections. *Cell* **108**:317–329. DOI: [https://doi.org/10.1016/S0092-8674\(02\)00633-5](https://doi.org/10.1016/S0092-8674(02)00633-5), PMID: 11853667
- Tanaka K**, Mukae N, Dewar H, van Breugel M, James EK, Prescott AR, Antony C, Tanaka TU. 2005. Molecular mechanisms of kinetochore capture by spindle microtubules. *Nature* **434**:987–994. DOI: <https://doi.org/10.1038/nature03483>, PMID: 15846338
- Tian T**, Li X, Liu Y, Wang C, Liu X, Bi G, Zhang X, Yao X, Zhou ZH, Zang J. 2018. Molecular basis for CENP-N recognition of CENP-A nucleosome on the human kinetochore. *Cell Research* **28**:374–378. DOI: <https://doi.org/10.1038/cr.2018.13>, PMID: 29350209
- Turco E**, Gallego LD, Schneider M, Köhler A. 2015. Monoubiquitination of histone H2B is intrinsic to the Bre1 RING domain-Rad6 interaction and augmented by a second Rad6-binding site on Bre1. *Journal of Biological Chemistry* **290**:5298–5310. DOI: <https://doi.org/10.1074/jbc.M114.626788>, PMID: 25548288
- van der Horst A**, Vromans MJ, Bouwman K, van der Waal MS, Hadders MA, Lens SM. 2015. Inter-domain cooperation in INCENP promotes aurora B relocation from centromeres to microtubules. *Cell Reports* **12**:380–387. DOI: <https://doi.org/10.1016/j.celrep.2015.06.038>, PMID: 26166576
- van Hooff JJ**, Tromer E, van Wijk LM, Snel B, Kops GJ. 2017. Evolutionary dynamics of the kinetochore network in eukaryotes as revealed by comparative genomics. *EMBO Reports* **18**:1559–1571. DOI: <https://doi.org/10.15252/embr.201744102>, PMID: 28642229
- Vázquez-Novelle MD**, Sansregret L, Dick AE, Smith CA, McAinsh AD, Gerlich DW, Petronczki M. 2014. Cdk1 inactivation terminates mitotic checkpoint surveillance and stabilizes kinetochore attachments in anaphase. *Current Biology* **24**:638–645. DOI: <https://doi.org/10.1016/j.cub.2014.01.034>, PMID: 24583019



## 8. Curriculum Vitae

### Personal data

---

Name: Josef Fischböck-Halwachs

Date of birth: 02.03.1988

Place of birth: Vöcklabruck

Gender: male

### Education

---

2014 – 2019 PhD-thesis: Laboratory of Dr. Franz Herzog; Genecenter; faculty of chemistry and pharmacy; LMU Munich

2011 – 2014 Master of Science: molecular biology; passed with distinction; elective module: biochemistry; university of Vienna

2008 – 2011 Bachelor of Science: biology; elective module: microbiology and genetics; university of Vienna

2006 Matura; BRG Gmunden

## 9. Acknowledgement

I want to thank Dr. Franz Herzog for giving me the chance to work on such an interesting project and for all his support over the years. Thank you very much.

I am grateful towards all group members of the Herzog lab for generating a great working atmosphere and lots of fruitful discussions. I really enjoyed spending time with all of you.

First of all, I want to thank Sylvie Singh for her smart ideas, her constant and incredible effort in performing the *in vivo* assays. I also want to thank Mia Potocnjak for helping with her biochemical expertise. I want to thank Victor Solis for helping with the informatics and data analysis. I want to thank Peter Busslehner for his help on the KMN project and Stephan Woike for his work with the Cse4-mutants. I want to thank Götz Hagemann for his input and constant support.